

# Evaluation of building envelope energy performance through extensive simulation and parametrical analysis

## ***Citation for published version (APA):***

Pernigotto, G. (2013). *Evaluation of building envelope energy performance through extensive simulation and parametrical analysis*. [Phd Thesis 4 Research NOT TU/e / Graduation NOT TU/e], Free University of Bozen-Bolzano]. Free University of Bozen Bolzano.

## ***Document status and date:***

Published: 01/01/2013

## ***Document Version:***

Accepted manuscript including changes made at the peer-review stage

## ***Please check the document version of this publication:***

- A submitted manuscript is the version of the article upon submission and before peer-review. There can be important differences between the submitted version and the official published version of record. People interested in the research are advised to contact the author for the final version of the publication, or visit the DOI to the publisher's website.
- The final author version and the galley proof are versions of the publication after peer review.
- The final published version features the final layout of the paper including the volume, issue and page numbers.

[Link to publication](#)

## ***General rights***

Copyright and moral rights for the publications made accessible in the public portal are retained by the authors and/or other copyright owners and it is a condition of accessing publications that users recognise and abide by the legal requirements associated with these rights.

- Users may download and print one copy of any publication from the public portal for the purpose of private study or research.
- You may not further distribute the material or use it for any profit-making activity or commercial gain
- You may freely distribute the URL identifying the publication in the public portal.

If the publication is distributed under the terms of Article 25fa of the Dutch Copyright Act, indicated by the "Taverne" license above, please follow below link for the End User Agreement:

[www.tue.nl/taverne](http://www.tue.nl/taverne)

## ***Take down policy***

If you believe that this document breaches copyright please contact us at:

[openaccess@tue.nl](mailto:openaccess@tue.nl)

providing details and we will investigate your claim.



UNIVERSITÀ  
DEGLI STUDI  
DI PADOVA

University of Padova  
Department of Management and Engineering

---

**DOCTORAL SCHOOL IN INDUSTRIAL ENGINEERING**

Curriculum: Mechatronics and Industrial Systems

Cycle: XXV

**Evaluation of building envelope energy performance  
through extensive simulation and parametrical analysis**

*Head of the Doctoral School:* Prof. Paolo Colombo

*Curriculum coordinator:* Prof. Alberto Trevisani

*Supervisor:* Prof. Andrea Gasparella

*Co-Supervisor:* Prof. Jan Hensen

*Promovendus:* Giovanni Pernigotto

This research has been realized thanks to the support of  
FSU, Fondazione Studi Universitari Vicenza.

*To my family*





# Acknowledgements

I want to express my gratitude to my supervisor, prof Andrea Gasparella, for the help in the development of my research and to the whole group for the support and encouragement during the three years of the Ph.D. period. In particular, I would like to thank prof. P. Baggio, prof P. Romagnoni, Marco and Francesca for their contributions and for the time and attention dedicated to the research work. My thankfulness goes also to Alessandro, Francesco, Dario, Paola and to all those who have helped in my work in this period.

I would like to thank my co-supervisor, prof Hensen, for his hospitality at the Eindhoven University of Technology, and all the Ph.D. students of the BPS group.

An acknowledgement goes also to my office mates during these years and to the other colleagues of the Doctoral School.

Finally, special thanks to my family for being supportive every day and helping me to complete this path.



# Abstract

More than 30% of the final energy uses in the European Union are due to the building energy consumptions. In order to reduce their energy impact and improve their efficiency, the design activity has been given a large importance, both for new buildings or refurbishment projects. Moreover, besides these goals, during the last years the indoor comfort conditions have assumed a more and more relevant significance for professionals in the building design. That required the development of properly detailed instruments of analysis, such as building energy simulation tools (BES). Generally, the more complex a tool, the higher the number of required inputs but not all of them are always available in the early design stages. For this reason, BES codes have been used also to elaborate simpler models.

This research analyses the possibilities given by an extensive use of the BES for the evaluation of the building envelope energy performance and some of the different issues related to BES. The first topic discussed is related to the external boundary conditions in BES, in particular the definition of a representative weather file for the description of the external environment and of the modelling of the heat transfer through the ground. The second topic analyses the problems of the validation of the results provided by BES tools and the relative accuracy introduced by the choice of a specific code. The comparison between BES software is carried out both considering the outputs of a whole thermal zone, such as heating and cooling energy needs and peak loads and the time of their occurrences, and the response of a single component (i.e., opaque walls and glazings). Finally, the coherence between the energy needs elaborated by means of BES tools and those by the quasi-steady state model presented in the technical Standard EN ISO 13790:2008 is studied and some correction factors are proposed for this simplified method.



# Sommario

Più del 30% degli impieghi finali di energia nell'Unione Europea è dovuto ai consumi energetici degli edifici. Al fine di ridurre il loro impatto energetico e migliorare la loro efficienza, è stata data una sempre maggiore importanza all'attività di progettazione, sia in merito ai nuovi edifici sia per gli interventi di riqualificazione. Inoltre, in aggiunta a questi obiettivi, durante gli ultimi anni le condizioni di comfort nell'ambiente confinato hanno assunto una sempre maggiore significatività per i progettisti edili. Ciò ha richiesto lo sviluppo di strumenti di analisi adeguatamente dettagliati, come i simulatori dinamici dell'edificio. In generale, più è complesso uno strumento, maggiore è il numero di input richiesti ma non tutti sono sempre disponibili nelle fasi iniziali della progettazione. Per questa ragione, i codici di simulazione dinamica sono stati impiegati anche per sviluppare modelli semplificati.

Questa ricerca analizza le possibilità date da un uso estensivo della simulazione dinamica per la valutazione delle prestazioni energetiche dell'involucro edilizio e alcune problematiche relative ad essa. Il primo argomento discusso riguarda le condizioni al contorno nella simulazione dinamica, in particolare la definizione di un file climatico rappresentativo per la descrizione dell'ambiente esterno e la modellazione dello scambio di calore attraverso il terreno. Il secondo argomento analizza i problemi della validazione dei risultati forniti dagli strumenti di simulazione dinamica e l'accuratezza introdotta dalla scelta di uno specifico codice. Il confronto tra i software di simulazione dinamica è condotto sia a livello degli output di un'intera zona termica, quali i fabbisogni di riscaldamento e raffrescamento, i carichi di picco e l'istante in cui si verificano, e la risposta di un singolo componente (i.e., le pareti opache e quelle vetrate). Infine, viene studiata la coerenza tra i fabbisogni energetici elaborati dagli strumenti di simulazione dinamica e quelli ottenuti tramite il modello semi-stazionario presentato nella normativa EN ISO 13790:2008 e vengono proposti alcuni fattori correttivi per questo metodo semplificato.



# Table of contents

<b>Chapter 1: Introduction and literature review</b>	<b>1</b>
<b>1.1 Introduction</b>	<b>3</b>
<b>1.2 Weather data and external conditions in BES</b>	<b>6</b>
1.2.1 Literature review: Weather data for BES	7
1.2.2 Literature review: Heat transfer by components in touch with the ground	9
<b>1.3 BES validation and comparison</b>	<b>11</b>
1.3.1 Literature review	12
<b>1.4 Building envelope characterization with BES</b>	<b>15</b>
1.4.1 Literature review	15
<b>1.5 BES and simplified models</b>	<b>18</b>
1.5.1 Literature review	19
1.5.1.1 Thermal losses	19
1.5.1.2 Thermal gains	20
<b>1.6 Statistical approach</b>	<b>22</b>
1.6.1 Design of Experiments	22
<b>Chapter 2: Weather data and external conditions in BES</b>	<b>25</b>
<b>Part a: Weather data files for BES</b>	<b>29</b>
<b>2a.1 Method</b>	<b>29</b>
2a.1.1 TRY calculation in accordance with the EN ISO 15927-4:2005	29
2a.1.2 Selection and analysis of the weather data of the multi-year series	31
2a.1.3 Analysis of the TRY <sub>EN</sub> weather files representativeness	32
2a.1.3.1 Set of reference buildings	32
2a.1.4 Statistics analysis	34
<b>2a.2 Results</b>	<b>36</b>
2a.2.1 Average monthly data	36
2a.2.2 Annual energy needs and peak loads	40
2a.2.3 Statistics analysis	44



<b>2a.3 Discussion</b>	<b>46</b>
2a.3.1 Average monthly data	46
2a.3.2 Annual energy needs and peak loads	47
2a.3.2.1 Annual energy needs and peak loads: North Italy locations	47
2a.3.2.2 Annual energy needs and peak loads: De Bilt	48
2a.3.3 Statistics analysis	49
<b>2a.4 Main findings</b>	<b>51</b>
 <b>Part b: Boundary conditions for walls and floors in touch with the ground in BES</b>	 <b>53</b>
<b>2b.1 Method</b>	<b>53</b>
2b.1.1 Tested slab on ground cases and boundary conditions	53
2b.1.2 EN ISO 13370:2007 method	55
2b.1.3 Finite elements modelling	57
<b>2b.2 Results</b>	<b>59</b>
2b.2.1 Steady-state conditions: FEM and EN 13370:2007 models	59
2b.2.2 Periodic sinusoidal regime	60
<b>2b.3 Discussion</b>	<b>63</b>
2b.3.1 Steady-state conditions: FEM and EN 13370:2007 models	63
2b.3.2 Periodic sinusoidal regime	64
<b>2b.4 Main findings</b>	<b>66</b>
 <b>Chapter 3: BES validation and comparison</b>	 <b>67</b>
<b>3.1 Methods</b>	<b>71</b>
3.1.1 ANSI/ASHRAE 140:2011 - BESTEST	71
3.1.2 Extensive comparison	73
3.1.2.1 Reference building module and set of configurations	74
3.1.2.2 Assumptions for the simulation	78
3.1.2.2 Statistical analysis	82
<b>3.2 Results</b>	<b>84</b>
3.2.1 BESTEST cases	84
3.2.2 Alignment in the BESTEST cases	85
3.2.3 Simulation plan results	88
3.2.3.1 Statistical analysis results	94

<b>3.3 Discussion</b>	<b>96</b>
3.3.1 <i>BESTEST cases</i>	96
3.3.2 <i>Alignment in the BESTEST cases</i>	97
3.3.3 <i>Simulation plan results</i>	98
3.3.3.1 <i>Statistical Analysis</i>	100
<b>3.4 Main Findings</b>	<b>102</b>
 <b>Chapter 4: Building envelope characterization with BES</b>	 <b>105</b>
<b>Part a: Characterization of the building envelope behaviour by BES</b>	<b>109</b>
<b>4a.1 Method</b>	<b>109</b>
4a.1.1 <i>EN ISO 13786:2007 method</i>	109
4a.1.2 <i>The Fourier series analysis and the EN ISO 13786:2007 method</i>	111
4a.1.3 <i>Transfer functions approach</i>	115
4a.1.4 <i>The Finite Difference Method</i>	115
4a.1.4 <i>Tested walls and boundary conditions</i>	116
<b>4a.2 Results</b>	<b>119</b>
<b>4a.3 Discussion</b>	<b>125</b>
<b>4a.4 Main findings</b>	<b>127</b>
 <b>Part b: Glazings and adiabatic surface temperatures</b>	 <b>129</b>
<b>4b.1 Methods</b>	<b>129</b>
<b>4b.2 Results</b>	<b>131</b>
4b.2.1 <i>Sample of cases with the original glazings</i>	131
4b.2.2 <i>Sample of cases with glazings with unitary emissivity</i>	142
<b>4b.3 Discussion</b>	<b>144</b>
4b.3.1 <i>Sample of cases with the original glazings</i>	144
4b.3.2 <i>Sample of cases with glazings with unitary emissivity</i>	145
<b>4b.4 Main findings</b>	<b>146</b>

<b>Chapter 5: BES and simplified models</b>	<b>147</b>
<b>Part a: Assessment of the quasi-steady state method with the BESTEST cases</b>	<b>151</b>
5a.1 Method	151
5a.2 Results and Discussion	152
5a.3 Main findings	154
<b>Part b: Comparison between the thermal losses by BES and by EN ISO 13790:2008 quasi-steady state method</b>	<b>155</b>
5b.1 Methods	155
5b.1.1 EN ISO 13790:2008 model	155
5b.1.2 Thermal losses calculation procedure with the dynamic simulation approach	156
5b.1.3 Reference building model and set of configurations	158
5b.2 Results	161
5b.2.1 Transmission heat losses and effects of the ventilation rate	161
5b.2.2 Setpoint correction factor for the calculation of thermal losses by transmission	164
5b.3 Discussion	166
5b.3.1 Transmission heat losses	166
5b.3.2 Effects of the ventilation rate	167
5b.3.2 Setpoint correction factor for the calculation of thermal losses by transmission	168
5b.4 Main findings	170
<b>Part c: Comparison between the thermal gains by BES and by EN ISO 13790:2008 quasi-steady state method</b>	<b>171</b>
5c.1 Methods	171
5c.1.1 EN ISO 13790:2008 model	171
5c.1.2 Effective solar transmittance by Oliveti et al.	173
5c.1.3 Thermal gains calculation procedure with the dynamic simulation approach	175
5c.1.4 Reference building model and set of configurations	177
5c.2 Results	180
5c.2.1 Entering solar heat gains	180
5c.2.2 Solar heat gains by transmission	181
5c.2.3 Internal gains	181
5c.2.4 Infrared extra flow towards the sky vault	181
5c.3 Discussion	185
5c.3.1 Entering solar heat gains	185
5c.3.2 Solar heat gains by transmission	185
5c.3.3 Internal gains	186

5c.3.4 Infrared extra flow towards the sky vault	186
5c.3.5 Assessment of the proposed correction factor with some BESTEST cases	186
5c.4 Main findings	188
<b>Part d: Comparison between BES and EN ISO 13790:2008 quasi-steady state method</b>	<b>189</b>
5d.1 Methods	189
5d.1.1 EN ISO 13790:2008 model	189
5d.2 Results	192
5d.2.1 BESTEST cases	192
5d.2.2 Extensive simulation plan	194
5d.3 Discussion	197
5d.4 Main findings	198
<b>Chapter 6: Conclusions</b>	<b>199</b>
<b>Chapter 7: Bibliography</b>	<b>207</b>
<b>Annexes</b>	<b>221</b>



# List of Figures

## Chapter 1

1.1	<i>Relations between the different variables according to Guan (2009)</i>	8
1.2	<i>Correlation between user's needs and availability of validate BES tools</i>	11

## Chapter 2

2a.1	<i>Cumulative probability for the first 3 years of the series of De Bilt for the dry bulb temperature (a), the solar irradiance (b) and the relative humidity (c)</i>	30
2a.2	<i>(a) Average monthly temperature (b) average daily horizontal global radiation and (c) average monthly relative humidity for Trento. The red dots represent the <math>TRY_{EN}</math> monthly values, the external dotted lines represent the maximum and the minimum for the multi-year series, the internal dotted lines the first and the third quartile (<math>Q_1</math> and <math>Q_3</math>), while the continuous line is the median.</i>	37
2a.3	<i>(a) Average monthly temperature (b) average daily horizontal global radiation and (c) average monthly relative humidity for De Bilt. The red dots represent the <math>TRY_{EN}</math> monthly values, the external dotted lines represent the maximum and the minimum for the multi-year series, the internal dotted lines the first and the third quartile (<math>Q_1</math> and <math>Q_3</math>), while the continuous line is the median</i>	38
2a.4	<i>Heating (left) and cooling (right) energy needs: average energy needs (dots) and annual results in the multi-year series respect to the <math>TRY_{EN}</math> values</i>	41
2a.5	<i>Heating (left) and cooling (right) peak loads: average peak loads (dots) and annual results in the multi-year series respect to the <math>TRY_{EN}</math> values</i>	42
2a.6	<i>Heating (left) and cooling (right) energy needs: average energy needs (dots) and annual results in the multi-year series respect to the <math>TRY_{EN}</math> values for De Bilt</i>	43
2a.7	<i>Heating (left) and cooling (right) peak loads: average peak loads (dots) and annual results in the multi-year series respect to the <math>TRY_{EN}</math> values for De Bilt</i>	43
2a.8	<i>Correlations of the building envelope characteristics and the deviations of the annual heating energy needs (a) and annual cooling energy needs (b), evaluated by means of Pearson's index (left) and Spearman's index (right)</i>	44
2a.9	<i>Correlations of the building envelope characteristics and the deviations of the annual heating peak loads (a) and annual cooling peak loads (b), evaluated by means of Pearson's index (left) and Spearman's index (right)</i>	45
2b.1	<i>3-dimensional model (left) and 2-dimensional model (right) according to EN ISO 10211:2007</i>	58
2b.2	<i>Example of FEM model geometry and mesh</i>	58

2b.3	<i>Specific equal heat flux curves [<math>\text{W m}^{-2}</math>] (a, on the top) and ground heat flow share curves [%] (b, on the bottom) computed by the FEM model as a function of ground and floor slab thermal properties: thermal insulation layer either on the external (left) or on internal (right) side (continuous lines refer to 1:4 aspect ratio and dashed line to 4:4 aspect ratio)</i>	59
2b.4	<i>Absolute percentage deviations between the specific heat flux at the ground computed by means of the finite elements model (steady state regime) and by means of the EN ISO 13370:2007 procedure as a function of floor slab thermal conductance, aspect ratios (on the left) or ground type (on the right). Dashed lines represent the envelope curves relevant either to the maximum or the minimum values for the limit aspect ratios (4:4 and 1:4).</i>	60
2b.5	<i>Daily variation of the temperatures and heat flows: comparison of the FEM model in dynamic regime with the steady state approach (rock soil, uninsulated floor slab and 4:4 aspect ratio)</i>	61
2b.6	<i>Yearly variation of the external temperature <math>\theta_{\text{air}}</math> (black dotted lines) for an uninsulated floor slab, 4:4 aspect ratio and clay soil: the temperature on the bottom of the slab-on-ground floor <math>\theta_{\text{slab}}</math> (red solid line) and internal heat flow <math>\Phi</math> (blue solid line) calculated by the FEM simulation</i>	62
2b.7	<i>Virtual temperatures calculated starting from different monthly heat flow rate (rock soil, uninsulated floor slab and 4:4 aspect ratio)</i>	62

### **Chapter 3**

3.1	<i>Conceptual view of the base module</i>	75
3.2	<i>Percentage deviations in the annual heating (a) and cooling (b) energy needs calculations with respect to the normalized BESTEST ranges and percentage deviations in the heating (c) and cooling (d) energy needs sensitivity with respect to the normalized sensitivity BESTEST ranges for TRNSYS and EnergyPlus</i>	84
3.3	<i>Percentage deviations in the annual heating (a) and cooling (b) peak loads calculations with respect to the normalized BESTEST ranges and percentage deviations in the heating (c) and cooling (d) energy needs sensitivity with respect to the normalized sensitivity BESTEST ranges for TRNSYS and EnergyPlus</i>	85
3.4	<i>Monthly differences for the heating (a) and cooling (b) energy needs (on the left) and monthly hourly peak loads (on the right) between EnergyPlus and TRNSYS with respect to TRNSYS energy needs and peak loads results for the BESTEST cases in the reference climatic conditions of Denver</i>	86
3.5	<i>Percentage deviations in the annual heating (a) and cooling (b) energy needs calculations with respect to the normalized BESTEST ranges and percentage deviations in the heating (c) and cooling (d) energy needs sensitivity with respect to the normalized sensitivity BESTEST ranges for TRNSYS and EnergyPlus after the alignment</i>	86
3.6	<i>Percentage deviations in the annual heating (a) and cooling (b) peak loads calculations with respect to the normalized BESTEST ranges and percentage deviations in the heating (c) and cooling (d) energy needs sensitivity with respect to the normalized sensitivity BESTEST ranges for TRNSYS and EnergyPlus after the alignment</i>	87

3.7	<i>Monthly differences for the heating and cooling energy needs for Milan between the two simulation codes with respect to TRNSYS results for BESTEST cases (BT) and for different glazing type (S = single; DH = Double with high SHGC; DL = Double with low SHGC; TH = Triple with high SHGC; TL = Triple with low SHGC) and for different ratios S/V</i>	88
3.8	<i>Monthly differences for the heating and cooling energy needs for Messina between the two simulation codes with respect to TRNSYS results for BESTEST cases (BT) and for different glazing type (S = single; DH = Double with high SHGC; DL = Double with low SHGC; TH = Triple with high SHGC; TL = Triple with low SHGC) and for different ratios S/V</i>	89
3.9	<i>Monthly differences for the heating and cooling peak loads for Milan between the two simulation codes with respect to TRNSYS results for BESTEST cases (BT) and for different glazing type (S = single; DH = Double with high SHGC; DL = Double with low SHGC; TH = Triple with high SHGC; TL = Triple with low SHGC) and for different ratios S/V</i>	91
3.10	<i>Monthly differences for the heating and cooling peak loads for Messina between the two simulation codes with respect to TRNSYS results for BESTEST cases (BT) and for different glazing type (S = single; DH = Double with high SHGC; DL = Double with low SHGC; TH = Triple with high SHGC; TL = Triple with low SHGC) and for different ratios S/V</i>	92
3.11	<i>Frequency distribution of the differences for the occurrence time of heating (on the top) and cooling (on the bottom) monthly peak loads between the two simulation codes for different glazing type (S = single; DH = Double with high SHGC; DL = Double with low SHGC; TH = Triple with high SHGC; TL = Triple with low SHGC)</i>	93
3.12	<i>Standardized coefficients of the regression models for the energy need deviations (a) and the peak load deviations (b)</i>	94

#### **Chapter 4**

4a.1	<i>Fast Fourier Transform (FFT) carried out on the sol-air temperature derived from the measured data of Rome (West oriented vertical wall)</i>	113
4a.2	<i>Average hourly profiles of the dry bulb temperature and the global horizontal solar irradiance of the chosen climates for the month of July</i>	117
4a.3	<i>Periodic thermal transmittances in [<math>W m^{-2} K^{-1}</math>] (left) and time shifts in [h] (right) for the conditions of Rome for the South, North and Horizontal walls respect to the reference FFT parameters. Dotted lines represent the <math>\pm 20\%</math> range</i>	123
4a.4	<i>Periodic thermal transmittances in [<math>W m^{-2} K^{-1}</math>] (left) and time shifts in [h] (right) for the conditions of Rome for the East and West-oriented walls respect to the reference FFT parameters. Dotted lines represent the <math>\pm 20\%</math> range</i>	124
4b.1	<i>Winter (from 14/01 till 21/01) surface temperatures in Milan for the different glazings with <math>S/V=0.3</math> and <math>S/V=0.97</math></i>	132
4b.2	<i>Winter (from 14/01 till 21/01) surface temperatures in Messina for the different glazings with <math>S/V=0.3</math> and <math>S/V=0.97</math></i>	133
4b.3	<i>Summer (from 14/07 till 21/07) surface temperatures in Milan for the different glazings with <math>S/V=0.3</math> and <math>S/V=0.97</math></i>	134



4b.4	<i>Summer (from 14/07 till 21/07) surface temperatures in Messina for the different glazings with <math>S/V=0.3</math> and <math>S/V=0.97</math></i>	135
4b.5	<i>Winter (from 14/01 till 21/01) surface temperatures in Milan and Messina for the different glazings with <math>S/V=1.07</math></i>	136
4b.6	<i>Summer (from 14/07 till 21/07) surface temperatures in Milan and Messina for the different glazings with <math>S/V=1.07</math></i>	137
4b.7	<i>Distribution of the deviations between the surface temperatures of the adiabatic walls in EnergyPlus and TRNSYS in Milan</i>	138
4b.8	<i>Distribution of the deviations between the surface temperatures of the adiabatic walls in EnergyPlus and TRNSYS in Messina</i>	139
4b.9	<i>Distribution of the deviations between the surface temperatures of the glazings in EnergyPlus and TRNSYS in Milan</i>	140
4b.10	<i>Distribution of the deviations between the surface temperatures of the glazings in EnergyPlus and TRNSYS in Messina</i>	141
4b.11	<i>Distribution of the deviations between the surface temperatures of the glazings in EnergyPlus (<math>\epsilon_{gl}=1</math>) and TRNSYS in Milan</i>	142
4b.12	<i>Distribution of the deviations between the surface temperatures of the glazings in EnergyPlus (<math>\epsilon_{gl}=1</math>) and TRNSYS in Messina.</i>	143

## Chapter 5

5a.1	<i>Quasi-steady state method assessed with the BESTEST cases 600, 620, 900, 920 for the location of Milan: annual heating (a) and cooling (b) energy needs. The dotted lines delimitate the confidence interval</i>	152
5a.2	<i>Quasi-steady state method assessed with the BESTEST cases 600, 620, 900, 920 for the location of Messina: annual heating (a) and cooling (b) energy needs. The dotted lines delimitate the confidence interval</i>	153
5b.1	<i>Simulated thermal losses with air temperature setpoint (on the left) and operative setpoint (on the right), without ventilation for the different <math>S/V</math>. Insulated cases in lighter colours</i>	162
5b.2	<i>Percentage deviation of the simulated thermal losses with air temperature setpoint (on the left) and operative setpoint (on the right) of 20 °C respect to the losses calculated with the quasi steady state approach for different air change rates and <math>S/V</math> ratios</i>	163
5b.3	<i>Percentage deviation of the simulated thermal losses with air temperature setpoint (on the left) and operative setpoint (on the right) of 26 °C respect to the losses calculated with the quasi steady state approach for different air change rates and <math>S/V</math> ratios</i>	164
5b.4	<i>Comparison between the corrected EN ISO 13790 method and the air temperature setpoint simulations</i>	168
5b.5	<i>Thermal losses with a setpoint of 20 °C (a) and 27 °C (b), calculated by means of the EN ISO 13790:2008 method (dark colour) and with the correction factor (light colour)</i>	169

5c.1	<i>EN ISO 13790:2008 entering solar gains (a), transmitted solar gains (b) and internal gains (c), calculated according to the Standard (on the left) and using the correction coefficients (right) compared to the simulated gains. Insulated cases in lighter colours</i>	183
5c.2	<i>EN ISO 13790:2008 entering solar gains, calculated according to the Standard considering the procedure by Oliveti et al. for the evaluation of the effective solar heat gain coefficient (on the left) and using the correction coefficients (right) compared to the simulated gains. Insulated cases in lighter colours</i>	184
5c.3	<i>EN ISO 13790:2008 infrared extra flow towards the sky vault, calculated according to the Standard (on the left) and using the correction coefficients (right) compared to the simulated gains. Insulated cases in lighter colours</i>	184
5c.4	<i>Thermal gains calculated by means of the EN ISO 13790:2008 method with the effective global solar heat gain coefficient (dark colour) and with the correction factor (light colour)</i>	187
5d.1	<i>Quasi-steady state method with correction factor assessed with the BESTEST cases 600, 620, 900, 920 for the location of Milan: annual heating (a) and cooling (b) energy needs. The dotted lines delimitate the confidence interval</i>	192
5d.2	<i>Quasi-steady state method with correction factor assessed with the BESTEST cases 600, 620, 900, 920 for the location of Messina: annual heating (a) and cooling (b) energy needs. The dotted lines delimitate the confidence interval</i>	193
5d.3	<i>EN ISO 13790:2008 monthly heating energy needs and TRNSYS heating energy needs considering the thermal flows according to the Standard (case a) and the corrected ones (case b)</i>	194
5d.4	<i>EN ISO 13790:2008 monthly cooling energy needs and TRNSYS cooling energy needs considering the thermal flows according to the Standard (case a) and the corrected ones (case b)</i>	195
5d.5	<i>EN ISO 13790:2008 monthly heating energy needs and TRNSYS heating energy needs considering simulated heat gains and losses in the Standard calculation (case c)</i>	196
5d.6	<i>EN ISO 13790:2008 monthly cooling energy needs and TRNSYS cooling energy needs considering simulated heat gains and losses in the Standard calculation (case c)</i>	196

## **Annexes**

A.1	<i>Absence of interaction between the thermal transmittance of the envelope and the convective internal gains (left) and presence of interaction between the thermal transmittance of the envelope and its dispersing area (right) for the determination of the heating energy needs by BES</i>	224
A.2	<i>2<sup>2</sup> Plan</i>	228
A.3	<i>Pearson's and Spearman's indexes</i>	230
B.1	<i>(a) Average monthly temperature (b) average daily horizontal global radiation and (c) average monthly relative humidity for Aosta. The red dots represent the TRY<sub>EN</sub> monthly values, the external dotted lines represent the maximum and the minimum for the multi-year series, the internal dotted lines the first and the third quartile (<math>Q_1</math> and <math>Q_3</math>), while the continuous line is the median</i>	238

B.2	(a) Average monthly temperature (b) average daily horizontal global radiation and (c) average monthly relative humidity for Bergamo. The red dots represent the $TRY_{EN}$ monthly values, the external dotted lines represent the maximum and the minimum for the multi-year series, the internal dotted lines the first and the third quartile ( $Q_1$ and $Q_3$ ), while the continuous line is the median	239
B.3	(a) Average monthly temperature (b) average daily horizontal global radiation and (c) average monthly relative humidity for Monza. The red dots represent the $TRY_{EN}$ monthly values, the external dotted lines represent the maximum and the minimum for the multi-year series, the internal dotted lines the first and the third quartile ( $Q_1$ and $Q_3$ ), while the continuous line is the median	240
B.4	(a) Average monthly temperature (b) average daily horizontal global radiation and (c) average monthly relative humidity for Trento. The red dots represent the $TRY_{EN}$ monthly values, the external dotted lines represent the maximum and the minimum for the multi-year series, the internal dotted lines the first and the third quartile ( $Q_1$ and $Q_3$ ), while the continuous line is the median	241
B.5	(a) Average monthly temperature (b) average daily horizontal global radiation and (c) average monthly relative humidity for Varese. The red dots represent the $TRY_{EN}$ monthly values, the external dotted lines represent the maximum and the minimum for the multi-year series, the internal dotted lines the first and the third quartile ( $Q_1$ and $Q_3$ ), while the continuous line is the median	242
B.6	(a) Average monthly temperature (b) average daily horizontal global radiation and (c) average monthly relative humidity for De Bilt. The red dots represent the $TRY_{EN}$ monthly values, the external dotted lines represent the maximum and the minimum for the multi-year series, the internal dotted lines the first and the third quartile ( $Q_1$ and $Q_3$ ), while the continuous line is the median	243
C.1	Periodic thermal transmittances in [ $W m^{-2} K^{-1}$ ] (left) and time shifts in [h] (right) for the conditions of Milan for the South, North and Horizontal walls respect to the reference FFT parameters. Dotted lines represent the $\pm 20\%$ range	249
C.2	Periodic thermal transmittances in [ $W m^{-2} K^{-1}$ ] (left) and time shifts in [h] (right) for the conditions of Milan for the East and West-oriented walls respect to the reference FFT parameters. Dotted lines represent the $\pm 20\%$ range	250
C.3	Periodic thermal transmittances in [ $W m^{-2} K^{-1}$ ] (left) and time shifts in [h] (right) for the conditions of Rome for the South, North and Horizontal walls respect to the reference FFT parameters. Dotted lines represent the $\pm 20\%$ range	254
C.4	Periodic thermal transmittances in [ $W m^{-2} K^{-1}$ ] (left) and time shifts in [h] (right) for the conditions of Rome for the East and West-oriented walls respect to the reference FFT parameters. Dotted lines represent the $\pm 20\%$ range	255
C.5	Periodic thermal transmittances in [ $W m^{-2} K^{-1}$ ] (left) and time shifts in [h] (right) for the conditions of Palermo for the South, North and Horizontal walls respect to the reference FFT parameters. Dotted lines represent the $\pm 20\%$ range	259
C.6	Periodic thermal transmittances in [ $W m^{-2} K^{-1}$ ] (left) and time shifts in [h] (right) for the conditions of Palermo for the East and West-oriented walls respect to the reference FFT parameters. Dotted lines represent the $\pm 20\%$ range	260
D.1	Simulated thermal losses with 20 °C air temperature setpoint (on the left) and 20 °C operative setpoint (on the right), without ventilation for the different S/V. Insulated cases in lighter colours	262

D.2	<i>Simulated thermal losses with 20 °C air temperature setpoint (on the left) and 20 °C operative setpoint (on the right), with 0.3 ach/h of ventilation rate for the different S/V. Insulated cases in lighter colours</i>	263
D.3	<i>Simulated thermal losses with 20 °C air temperature setpoint (on the left) and 20 °C operative setpoint (on the right), with 0.6 ach/h of ventilation rate for the different S/V. Insulated cases in lighter colours</i>	264
D.4	<i>Simulated thermal losses with 20 °C air temperature setpoint (on the left) and 20 °C operative setpoint (on the right), with 0.9 ach/h of ventilation rate for the different S/V. Insulated cases in lighter colours</i>	265
D.5	<i>Simulated thermal losses with 26 °C air temperature setpoint (on the left) and 26 °C operative setpoint (on the right), without ventilation for the different S/V. Insulated cases in lighter colours</i>	266
D.6	<i>Simulated thermal losses with 26 °C air temperature setpoint (on the left) and 26 °C operative setpoint (on the right), with 0.3 ach/h of ventilation rate for the different S/V. Insulated cases in lighter colours</i>	267
D.7	<i>Simulated thermal losses with 26 °C air temperature setpoint (on the left) and 26 °C operative setpoint (on the right), with 0.6 ach/h of ventilation rate for the different S/V. Insulated cases in lighter colours</i>	268
D.8	<i>Simulated thermal losses with 26 °C air temperature setpoint (on the left) and 26 °C operative setpoint (on the right), with 0.9 ach/h of ventilation rate for the different S/V. Insulated cases in lighter colours</i>	269



# List of Tables

## Chapter 1

1.1	<i>Contents Table. In italic and grey other topics present in literature related to the ones discussed in this research work and to the accuracy</i>	5
-----	--	---

## Chapter 2

2a.1	<i>Materials thermal properties</i>	33
2a.2	<i>Monthly average variables of the <math>TRY_{EN}</math> (white columns) compared with the UNI 10349:1994 ones (grey columns)</i>	39
2a.3	<i>Selected months for the <math>TRY_{EN}</math></i>	40
2a.4	<i>Monthly average variables, monthly deviations (in grey column) with the monthly median values of the weather data series and selected year of the <math>TRY_{EN}</math></i>	40
2b.1	<i>Thermal properties of the soil and thermal conductance of the considered floors</i>	53
2b.2	<i>Size and external dimensions of the floor</i>	54

## Chapter 3

3.1	<i>BESTEST qualification cases</i>	72
3.2	<i>Opaque Envelope thermal properties</i>	75
3.3	<i>Variables (factors) and alternatives (levels) in the simulation plan</i>	77
3.4	<i>Mean percentage differences and corresponding standard deviations between EnergyPlus and TRNSYS with respect to TRNSYS results for different kind of glazing. Results with energy needs under 3.6 MJ or peak loads under 50 W are not considered</i>	90
3.5	<i>Mean differences and corresponding standard deviations between EnergyPlus and TRNSYS with respect to TRNSYS results for different kind of glazing. Results with energy needs under 3.6 MJ or peak loads under 50 W are not considered</i>	90
3.6	<i>Regression models for the deviation of the heating and cooling monthly energy needs expressed and for heating and cooling monthly hourly peak loads</i>	95

## Chapter 4

4a.1	<i>Analysed walls</i>	116
4a.2	<i>Periodic thermal transmittance according to the conventional EN ISO 13786:2007 one, the FFT and the DRF approaches, with percentage differences between DRF and FFT values for the different orientations in the case of Rome. All values in <math>[W m^{-2} K^{-1}]</math></i>	120
4a.3	<i>Time shift (in the range -24 to 0 hours) according to the conventional EN ISO 13786:2007 one, the FFT and the DRF approaches, with absolute differences between DRF and FFT values for the different orientations in the case of Rome. All values in [h]</i>	120

4a.4	<i>Periodic thermal transmittance according to the conventional EN ISO 13786:2007 one, the FFT and the SS approaches, with percentage differences between SS and FFT values for the different orientations in the case of Rome. All values in <math>[W m^{-2} K^{-1}]</math></i>	121
4a.5	<i>Time shift (in the range -24 to 0 hours) according to the conventional EN ISO 13786:2007 one, the FFT and the SS approaches, with absolute differences between SS and FFT values for the different orientations in the case of Rome. All values in [h]</i>	121
4a.6	<i>Periodic thermal transmittance according to the conventional EN ISO 13786:2007 one, the FFT and the FDM approaches, with percentage differences between FDM and FFT values for the different orientations in the case of Rome. All values in <math>[W m^{-2} K^{-1}]</math></i>	122
4a.7	<i>Time shift (in the range -24 to 0 hours) according to the conventional EN ISO 13786:2007 one, the FFT and the FDM approaches, with absolute differences between FDM and FFT values for the different orientations in the case of Rome. All values in [h]</i>	122

## **Chapter 5**

5b.1	<i>Factors and levels in the simulation plan for thermal losses</i>	160
5b.2	<i>Regression coefficients for the correction factor for the thermal losses</i>	165
5c.1	<i>Properties of the considered glazing systems</i>	179
5c.2	<i>Effective solar heat gain coefficients</i>	179
5c.3	<i>Regression coefficients for the determination of the correction factors for thermal gains</i>	182

## **Annexes**

C.1	<i>Periodic thermal transmittance according to the conventional EN ISO 13786, the FFT and the DRF approaches, with percentage differences between DRF and FFT values for the different orientations in the case of Milan. All values in <math>[W m^{-2} K^{-1}]</math></i>	246
C.2	<i>Time shift (in the range -24 to 0 hours) according to the conventional EN ISO 13786, the FFT and the DRF approaches, with absolute differences between DRF and FFT values for the different orientations in the case of Milan. All values in [h]</i>	246
C.3	<i>Periodic thermal transmittance according to the conventional EN ISO 13786, the FFT and the SS approaches, with percentage differences between SS and FFT values for the different orientations in the case of Milan. All values in <math>[W m^{-2} K^{-1}]</math></i>	247
C.4	<i>Time shift (in the range -24 to 0 hours) according to the conventional EN ISO 13786, the FFT and the SS approaches, with absolute differences between SS and FFT values for the different orientations in the case of Milan. All values in [h]</i>	247
C.5	<i>Periodic thermal transmittance according to the conventional EN ISO 13786, the FFT and the FDM approaches, with percentage differences between FDM and FFT values for the different orientations in the case of Milan. All values in <math>[W m^{-2} K^{-1}]</math></i>	248

C.6	<i>Time shift (in the range -24 to 0 hours) according to the conventional EN ISO 13786, the FFT and the FDM approaches, with absolute differences between FDM and FFT values for the different orientations in the case of Milan. All values in [h]</i>	248
C.7	<i>Periodic thermal transmittance according to the conventional EN ISO 13786, the FFT and the DRF approaches, with percentage differences between DRF and FFT values for the different orientations in the case of Rome. All values in [<math>\text{W m}^{-2} \text{K}^{-1}</math>]</i>	251
C.8	<i>Time shift (in the range -24 to 0 hours) according to the conventional EN ISO 13786, the FFT and the DRF approaches, with absolute differences between DRF and FFT values for the different orientations in the case of Rome. All values in [h]</i>	251
C.9	<i>Periodic thermal transmittance according to the conventional EN ISO 13786, the FFT and the SS approaches, with percentage differences between SS and FFT values for the different orientations in the case of Rome. All values in [<math>\text{W m}^{-2} \text{K}^{-1}</math>]</i>	252
C.10	<i>Time shift (in the range -24 to 0 hours) according to the conventional EN ISO 13786, the FFT and the SS approaches, with absolute differences between SS and FFT values for the different orientations in the case of Rome. All values in [h]</i>	252
C.11	<i>Periodic thermal transmittance according to the conventional EN ISO 13786, the FFT and the FDM approaches, with percentage differences between FDM and FFT values for the different orientations in the case of Rome. All values in [<math>\text{W m}^{-2} \text{K}^{-1}</math>]</i>	253
C.12	<i>Time shift (in the range -24 to 0 hours) according to the conventional EN ISO 13786, the FFT and the FDM approaches, with absolute differences between FDM and FFT values for the different orientations in the case of Rome. All values in [h]</i>	253
C.13	<i>Periodic thermal transmittance according to the conventional EN ISO 13786, the FFT and the DRF approaches, with percentage differences between DRF and FFT values for the different orientations in the case of Palermo. All values in [<math>\text{W m}^{-2} \text{K}^{-1}</math>]</i>	256
C.14	<i>Time shift (in the range -24 to 0 hours) according to the conventional EN ISO 13786, the FFT and the DRF approaches, with absolute differences between DRF and FFT values for the different orientations in the case of Palermo. All values in [h]</i>	256
C.15	<i>Periodic thermal transmittance according to the conventional EN ISO 13786, the FFT and the SS approaches, with percentage differences between SS and FFT values for the different orientations in the case of Palermo. All values in [<math>\text{W m}^{-2} \text{K}^{-1}</math>]</i>	257
C.16	<i>Time shift (in the range -24 to 0 hours) according to the conventional EN ISO 13786, the FFT and the SS approaches, with absolute differences between SS and FFT values for the different orientations in the case of Palermo. All values in [h]</i>	257



C.17	<i>Periodic thermal transmittance according to the conventional EN ISO 13786, the FFT and the FDM approaches, with percentage differences between FDM and FFT values for the different orientations in the case of Palermo. All values in <math>[W m^{-2} K^{-1}]</math></i>	258
C.18	<i>Time shift (in the range -24 to 0 hours) according to the conventional EN ISO 13786, the FFT and the FDM approaches, with absolute differences between FDM and FFT values for the different orientations in the case of Palermo. All values in <math>[h]</math></i>	258

# List of Symbols

## Symbols

$a_H a_C$	dimensionless numeric parameter (-)
$A$	area ( $\text{m}^2$ )
$b$	adjustment factor (-)
$B'$	floor aspect ratio (m)
$BES$	Building Energy Simulation
$c$	specific heat capacity ( $\text{J kg}^{-1} \text{K}^{-1}$ )
$C_a$	heat capacity of the internal air ( $\text{J K}^{-1}$ )
$C_m$	internal heat capacity of the building ( $\text{J K}^{-1}$ )
$CDD$	equivalent Cooling Degree Days ( $\text{K d}$ )
$CI$	confidence interval (-)
$d_t$	total equivalent thickness (m)
$DH$	double glazing with high SHGC
$DL$	double glazing with low SHGC
$DRF$	Direct-Root Finding
$f$	decrement factor (-)
$F$	cumulative distribution function of weather parameters, months, years, days (ch. 2) or view factor (-)
$F_w$	correction factor for non-scattering glazings (-)
$FDM$	Finite Difference Methods
$FEM$	Finite Element Modelling
$FFT$	Fast Fourier Technique
$h$	heat transfer coefficient ( $\text{W m}^{-2} \text{K}^{-1}$ )
$H/\hat{H}$	solar radiation / peak of cumulative solar radiation ( $\text{MJ m}^{-2}$ ) or global heat transfer coefficient ( $\text{W m}^{-2} \text{K}^{-1}$ )
$HDD$	equivalent Heating Degree Days ( $\text{K d}$ )
$J/K$	ranking orders
$k$	regression coefficient

$i$	day
$I$	solar irradiance ( $\text{W m}^{-2}$ )
$m$	month
$N/n$	total number (of days in the whole series of months/in a specific month)
$p$	weather parameter
$\bar{p}$	daily average value of a weather parameter $p$
$P$	perimeter (m)
$q \ \bar{q} \ \hat{q} \ \tilde{q}$	thermal flux / steady state thermal flux component / thermal flux peak / dynamic thermal flux component ( $\text{W m}^{-2} \text{K}^{-1}$ )
$q_i \ q_e$	secondary internal/external radiative-convective heat transfer factors (-)
$Q$	quartile or energy (MJ)
$R$	thermal resistance ( $\text{m}^2 \text{K W}^{-1}$ )
$R^2 \ R_{adj}^2$	index of determination
$s$	thickness (of a layer) (m)
$S$	dispersing surface ( $\text{m}^2$ ) or single glazing
$SHGC \ g$	Solar Heat Gain Coefficient / g-factor (-)
$SS$	Space State Method
$t$	time (s)
$T$	absolute temperature (K)
$TH$	triple glazing with high SHGC
$TL$	triple glazing with low SHGC
$TFM$	Transfer Function Methods
$TRY$	Test Reference Year
$U$	thermal transmittance ( $\text{W m}^{-2} \text{K}^{-1}$ )
$V \ \dot{V}$	thermal zone volume ( $\text{m}^3$ ) or volume rate ( $\text{m}^3 \text{s}^{-1}$ )
$w$	thickness the external walls (m)
$x$	envelope fraction (-)
$y$	year
$Y$	periodic thermal transmittance ( $\text{W m}^{-2} \text{K}^{-1}$ )
$Z$	element of the heat transfer matrix

## Greeks

$\alpha$	solar absorptance (-)
$\alpha_{cav}$	cavity absorption coefficient (-)
$\beta$	time lag (month) (ch. 2) correction factor of radiative exchanges for tilted surfaces (-) (ch. 3, 4)
$\gamma$	heat balance ratio (-)
$\delta$	periodic penetration depth (m)
$\Delta$	difference/deviation
$\Delta_g$	ground heat flow share (%)
$\Delta t$	time shift (h)
$\varepsilon$	emissivity (-)
$\eta$	utilization factor (-)
$\theta \ \bar{\theta} \ \hat{\theta} \ \tilde{\theta}$	temperature / average temperature / peak temperature / temperature harmonics (K)
$\kappa$	area specific heat capacity ( $\text{kJ m}^{-2} \text{K}^{-1}$ )
$\lambda$	thermal conductivity ( $\text{W m}^{-1} \text{K}^{-1}$ )
$\Lambda$	thermal conductance ( $\text{W m}^{-2} \text{K}^{-1}$ )
$\zeta$	ratio between the thickness of a layer and the periodic penetration depth (-)
$\rho$	density ( $\text{kg m}^{-3}$ ) or reflection coefficient (-)
$\sigma$	Stefan-Boltzmann constant ( $5.67 \cdot 10^{-8} \text{ W m}^{-2} \text{K}^{-4}$ )
$\tau$	month with the minimum annual temperature or solar transmission coefficient (-) or building time constant (h)
$\tau_d$	diffuse solar transmission coefficient (-)
$\tau_{e,n}$	beam solar transmission coefficient at normal incidence (-)
$T$	period (s)
$\varphi$	Specific heat flux ( $\text{W m}^{-2}$ ) or phase (rad)
$\phi$	tilt angle (rad)
$\Phi$	cumulative distribution function of weather parameters, months and days (ch. 1) or heat flow (W)
$\Psi$	linear thermal transmittance of a thermal bridge ( $\text{W m}^{-1} \text{K}^{-1}$ ) or ratio between the glazings area and the opaque area of the envelope (-)
$\omega$	angular frequency ( $\text{rad s}^{-1}$ )

### **Subscripts/Superscripts**

<i>0</i>	reference
<i>2dd</i>	referred to two consecutive days
<i>a</i>	referred to the internal air
<i>A</i>	referred to the internal appliances
<i>ad</i>	adiabatic
<i>air</i>	referred to the external air
<i>c</i>	convective
<i>C</i>	cooling
<i>calc</i>	calculated
<i>D</i>	referred to the thermal losses towards the external environment
<i>e</i>	referred to the external side/conditions
<i>eff</i>	effective
<i>EN</i>	according to the European Standards
<i>env</i>	referred to the wall opaque envelope exposed to the external air
<i>f</i>	referred to the floor
<i>FFT</i>	referred to FFT analysis
<i>fr</i>	referred to the window frame
<i>fsky</i>	referred to the reference temperature for external radiative exchanges in TRNSYS
<i>g/gnd</i>	referred to the ground
<i>gl</i>	referred to glazings
<i>gn</i>	referred to thermal gains
<i>H</i>	heating
<i>hor</i>	referred to horizontal surfaces
<i>ht</i>	referred to thermal losses
<i>HVAC</i>	referred to the HVAC system
<i>i</i>	referred to the internal side/conditions
<i>int</i>	referred to the internal gains correction

<i>L</i>	referred to the thermal losses correction or to the lighting
<i>loc</i>	location (e.g., Denver)
<i>lwr</i>	internal longwave radiative gains
<i>m n</i>	monthly or thermal zones
<i>max</i>	maximum
<i>min</i>	minimum
<i>mr</i>	referred to the mean radiant temperature
<i>n</i>	thermal zone or normal incidence
<i>nd</i>	referred to the energy needs
<i>ob</i>	referred to the external obstructions
<i>Oc</i>	referred to the occupants
<i>op</i>	referred to the operative temperature
<i>p</i>	periodic or projected
<i>Proc</i>	referred to the internal processes
<i>r</i>	radiative
<i>range</i>	acceptability range
<i>s</i>	surface
<i>S</i>	referred to Finkelstein-Schafer's statistics
<i>set</i>	setpoint
<i>sh</i>	shading
<i>slab</i>	referred to the slab-on-ground
<i>sol</i>	solar
<i>sol-air</i>	referred to the sol-air temperature
<i>sky</i>	referred to the sky vault
<i>st</i>	in steady state conditions
<i>star</i>	referred to the star network temperature in TRNSYS
<i>swr</i>	internal shortwave radiative gains
<i>sys</i>	referred to the conditioning system
<i>tr</i>	referred to the heat flow by transmission

<i>tot</i>	referred to the total opaque envelope
<i>TRNSYS</i>	referred to TRNSYS code
<i>u</i>	unconditioned
<i>ve</i>	referred to the ventilation
<i>V</i>	virtual
<i>WA</i>	referred to the water mains
<i>win</i>	referred to windows







# **Chapter 1:**

## Introduction and literature review



## 1.1 Introduction

During the last two decades, the goals of building design have changed under a larger and larger awareness of the impact of the building energy consumption on the environment and the attention to the occupants' hygrothermal comfort conditions. In order to pursue high levels of energy efficiency and indoor comfort quality in the design process, detailed instruments of analysis have been developed, such as building energy simulation (BES) tools.

Generally, the more complex a tool, the larger the number of required inputs and providing all of them can represent a relevant issue. This led to use BES codes also to elaborate simpler models or correlations between the results and the envelope characteristics for helping, for instance, in exploring many alternatives in the early stages of the design process and assessing the performance of existing buildings.

This research analyses the possibilities given by an extensive use of the BES for the evaluation of the building envelope energy performance and some of the different issues related to BES. In particular, the focus is on the following topics:

- *Weather data and external conditions in BES*

This part discusses the problem of the weather data file in BES. In particular, the representativeness of the simulation results is investigated by using both single reference years and original multi-year weather data. Moreover, the problem of the definition of the suitable boundary condition when the envelope is not directly exposed to the outside condition, such as for walls and floors in touch with the soil, is analysed.

The aim of this section is to give an answer to the question: *which external boundary conditions can be used in BES and how the heat transfer through the ground can be modelled?*

- *BES validation and comparison*

Like all the modelling software, BES tools need validation. Even if two validated codes are considered, some discrepancies are still present because the different implemented models are characterized by different levels of approximation of real phenomena and this can affect the final results. In order to further investigate the elements of disagreement and the resulting effects on BES outputs, a comparative procedure is described in this part, considering energy needs and peak loads.

The aim of this section is represented by the question: *which is the uncertainty introduced by the choice of the BES tool and in which way can the effect of disagreement elements be detected?*

- Characterization of the envelope components behaviours with BES

BES tools can be used also for characterizing the dynamic behaviours of the building envelope components. Thus, in this part, the subject of the comparison is no more the whole building system but only a single element and the accuracy of some numerical methods implemented in BES tools is investigated under different boundary conditions.

The question of this section is: *how is the behaviour of the building envelope components characterized by BES tools?*

- BES and simplified models

The objectives of this part are the study of the coherence between the results provided by BES tools and the simplified models proposed by the European technical Standards, the assessment of the sources of disagreement and the improvement of the considered simplified models.

The question for this last part is: *which is the level of agreement between the detailed and the simplified methods and how could it be improved?*

The discussed topics can involve an issue of general representativeness or absolute accuracy (such as the description of the weather or the reliability of the simplified methods results) or a problem of confidence or relative accuracy of the provided results, depending on some assumptions and hypothesis in the description of the physical phenomenon. In Table 1.1 the investigated topics are distinguished according to this criterion and reported together with other topics discussed in literature about the problem of relative and absolute accuracy in BES.

In the following paragraphs the different parts of the research work are introduced. For each one, a general description of the motivation for its study and a literature review are provided.

*Table 1.1 - Contents Table. In italic and grey other topics present in literature related to the ones discussed in this research work and to the accuracy.*

	<i>Representativeness of the results (absolute accuracy)</i>	<i>Confidence level of the results (relative accuracy)</i>
<b><i>Boundary conditions: weather data</i></b>	Analysis of the representativeness of the hourly data used in BES (and so the corresponding averages in the simplified methods) with respect to the collected measurements over a multi-year period.	<i>Development of self-correlated weather data. Effects of the choice of the solar radiation models. Models for the external infrared exchanges.</i>
<b><i>Boundary conditions: heat transfer through the soil</i></b>	Analysis of the method proposed by the technical Standard EN ISO 13370:2007 to evaluate the boundary conditions and the heat flows for walls/floors in contact with the soil.	Analysis of particular assumptions in the EN ISO 13370:2007 method which can lead to discrepancies between simplified methods and detailed approaches, such as the modelling of non 1-dimensional heat flows and the determination of its time lag.
<b><i>Description of the thermo-physical, geometrical and operative characteristics</i></b>	<i>Uncertainty on the thermophysical properties. Diagnosis and calibration for existing buildings.</i>	Study of the role of the detail level in the description of the thermo-physical properties of the envelope in the alignment between BES tools. In particular, focus on the constant parameters not under the user's control.
<b><i>Modelling of the behaviour of the envelope</i></b>	<i>Comparison with measurements. Numerical and simplified algorithms.</i>	Study of the relative differences between BES due to the implemented numerical heat transfer methods.
<b><i>Modelling of the internal heat exchanges and the heat balance</i></b>	Evaluation of the quasi-steady state method proposed by the technical Standard EN ISO 13790:2008.	Study of the influence on the final results of different models in the heat balance or thermal fluxes estimation between BES tools. Study of assumptions and hypotheses in the EN ISO 13790:2008 model and comparison with BES.

## 1.2 Weather data and external conditions in BES

The first advantage of BES tools is the possibility to consider dynamic boundary conditions and, so, the opportunity to evaluate the building-system behaviour under a transient regime. The boundary conditions are unsteady both on the internal and on the external side of the building envelope.

Inside the thermal zone, different ventilation rates, setpoint conditions, occupancy levels and, in general, control strategies and occupants' behaviours can be considered. Getting all information required for modelling the internal conditions is not easy: without detailed data and with design aims, many of these parameters are typically held constant in accordance with the average values prescribed by technical Standards. Designers and professionals can also study different scenarios by making hypotheses on the profiles of these variables.

As regards the outdoor, the weather conditions have to be as representative as possible of the real recordings. With this requisite, for instance for the elaboration of the beam and diffuse solar radiation on differently tilted and oriented surfaces, many mathematical and statistical models have been developed and implemented in BES software to try to simulate the weather condition as well as possible in different locations. Four parameters are generally required as hourly-discretized inputs for the description of the weather conditions: the dry bulb temperature, the global solar radiation on the horizontal, the relative humidity and, in some cases, also the wind speed and its direction. Even if some algorithms have been proposed to generate hourly data starting from the monthly averages, the BES preferably requires to have weather data profiles derived from measurements and representative of the locations chosen for the simulation. The use of the same type of weather data is also important for the assessment of the building energy performance by means of dynamic simulations, in the context of the building energy certification.

A different problem is faced when defining the boundary conditions for those buildings with an extensive part of their envelope in touch with the ground, such as partially underground warehouses or shops or new innovative concepts of building. Differently from the weather data used for simulating buildings above the ground, the temperature of the soil adjacent to the envelope is generally unknown and it is a complex function of the external conditions, the properties of the ground, the indoor conditions and the insulation level of these parts of the building envelope.

In chapter 2 the issue of the weather data for a year-long simulation is discussed, focusing, in particular, on the representativeness of the building energy needs and peak loads elaborated

by using a test reference year respect to the distribution of the results of a multi-year weather data series. In the last part of the chapter the prescriptions given by the technical Standard EN ISO 13370:2007 to calculate the boundary temperature for walls and floors in touch with the ground, have been assessed.

### **1.2.1 Literature review: Weather data for BES**

In many design applications, the use of simplified calculation methods, such as the quasi-steady state method proposed by the EN ISO 13790:2008 (CEN, 2008) for the evaluation of the building energy consumption, cannot provide results detailed enough to allow advanced investigations aimed at achieving both a high energy efficiency and an adequate occupants' visual and thermal comfort. This fact is requiring the recourse to the detailed dynamic simulation tools by professionals more and more frequently.

The higher capability in calculating detailed outputs by simulations codes requires more complex and detailed inputs. As regards the weather data, while in simplified methods the user needs only a dataset of monthly mean values of dry bulb temperature, solar radiation and relative humidity, as the ones in the Italian Standard UNI 10349:1994 (UNI, 1994) calculated starting from the data collected during the period 1951-1970, in simulation tools the weather data inputs generally require at least an hourly discretization.

We can distinguish three kinds of data for dynamic simulation (Keeble, 1990):

- the multi-year weather data;
- the typical year;
- the representative days.

The multi-year weather data are the best solution, in case of trend and sensitivity analyses of the building performance to the variability of the weather solicitations, aimed at a design robust to the climatic changes (Struck *et al.*, 2009). Complete multi-year series, with low measurement errors and a good representativeness, are available for a limited number of localities in Italy, since the regional environmental protection agencies (ARPAs) have started to collect weather data in the urban areas only around 20 years ago, in the best cases (Baggio *et al.*, 2010).

Typical weather data years are simply a single year of hourly data representative of the typical trend in a multi-year dataset. The representative days are hourly data for some average days chosen to describe typical climatic conditions (e.g., summer conditions).

The use of a typical year (or representative days) instead of multi-year weather data leads to a loss of information but it is less time-consuming and it is preferred when the effects of missing



or wrong data in the collected series have to be mitigated. The use of typical year is also necessary in order to provide a single standard weather reference condition for assessing the energy performance of a building in a particular location. The typical reference years (TRY) were defined by Lund (1974 and 1991) and Lund and Eidorff (1980) and have to be characterized by:

- *true frequencies* (i.e., the TRY should be a good approximation of the mean values derived from a long period of measurements);
- *true sequences* (i.e., the weather situations must follow each other in a similar manner to the recorded data);
- *true correlations* (i.e., the weather data are cross-correlated variables).

The last feature is probably one of the most important, as remembered also by Guan (2009) in Figure 1.1.

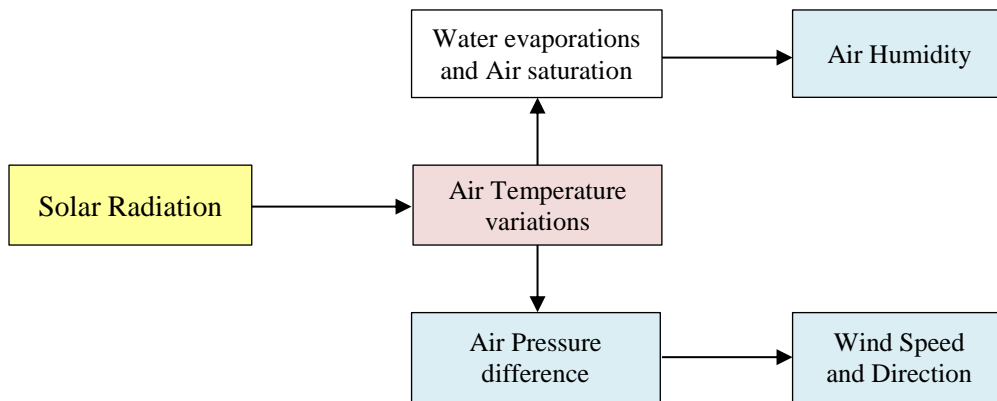


Figure 1.1 - Relations between the different variables according to Guan (2009)

In literature different approaches are available for the construction of a TRY but each one starts from the calculation of some primary parameters (e.g., daily solar radiation) and a secondary variable for the selection of the representative month from the collected data, as suggested by Hall *et al.* (1978). In accordance with Harriman *et al.* (1999), the choice of the primary variables should be done considering the perspective of the final use of the TRY, distinguishing the sizing and the energy assessment. Moreover, Hensen (1999) remarked that a proper statistical weighting for the primary parameters should be used, based on the type building which will be analysed.

Gansler *et al.* (1994) compared different reference year weather files to the multi-year series for the calculation of the performance of a solar system. Similarly, Sorrentino *et al.* (2012) assessed different approaches for the calculation of the TRY, by studying the sensitivity of the

energy production of a PV module and a building energy needs in Palermo to the chosen method. They found that, in particular for the building energy need evaluation, the best solution is to use weights for the selection of the TRY months.

In Italy, for the revision of the technical standard UNI 10349, which is in progress, starting from ARPA's data the procedure described in the European technical Standard EN ISO 15927-4:2005 (CEN, 2005) was selected for developing the new *test reference year* (TRY<sub>EN</sub>). Its selection method is based on the dry bulb temperature, the solar radiation and the relative humidity as primary variables and the wind speed as secondary one and no weighting coefficients are considered for them.

### ***1.2.2 Literature review: Heat transfer by components in touch with the ground***

In the last decades, the pursuit of better building energy performance has led to an average increase of the thickness of the thermal insulation layer of the envelopes. Therefore, the ground heat losses – traditionally considered of minor importance – have become more and more significant for the building energy balance assessment. Walls and floors directly in touch with the ground are complex to model either by dynamic simulations or through analytical solutions. In particular, a difficult step in the analysis is the determination of the boundary conditions to be assigned to the surfaces in contact with soil, whose temperature cannot be considered as undisturbed.

Hagentoft (1988), Claesson and Hagentoft (1991), Hagentoft and Claesson (1991) have developed accurate calculation methods for evenly insulated floors. In these studies the heat transfer through the floor in contact with the ground is modelled using a conformal mapping in the complex plane, assuming a semi-infinite ground layer and a floor with definite width. The solution is derived for steady-state, periodic and single-step boundary conditions in temperature. When the external wall itself is used as thermal protection (e.g., the edge insulation slab case), the same author derived an analytical solutions for the steady-state ground heat loss for buildings with only perimeter insulations (Hagentoft, 2002a and 2002b). Furthermore, the complexity of the underground structures has been analysed by Hagentoft (1996a, 1996b) also considering the presence of aquifers. Other authors (Delsante, 1988 and 1989; Anderson, 1991; Davies, 1993; Mihalakakou *et al.*, 1995) studied models for evaluating the heat flux and the temperature of the interface between the slab-on-ground and the soil. Rantala (2005) proposed a semi-analytical model and compared it with measurements and *FEM* modeling.

The technical standard EN ISO 13370:2007 (CEN, 2007c) provides methods for the calculation of heat transfer coefficients and heat flow rates for building components in thermal

contact with the ground, including slab-on-ground floors, suspended floors and basements. The Standard defines an equivalent thermal transmittance of a floor, which depends on its characteristic dimension (i.e., the ratio between the area of the floor and half its perimeter), on its total equivalent thickness (i.e., sum of the actual floor thickness and the product between the floor thermal resistance and the soil thermal conductivity) and on the thermal conductivity of the soil. This technical Standard gives also some indications about the conditions to be considered in the use of quasi steady-state methods and within the dynamic simulation.

An interesting aim of the research in this field, is the test and implementation of reliable calculation procedures for the thermal dispersion through the building envelope towards the ground, in modelling the building with dynamic simulation software, such as TRNSYS and EnergyPlus, which will be analysed in chapter 3.

### 1.3 BES validation and comparison

Many BES tools have been developed in the last decades and for a user it is not easy to select the one to adopt for his analyses. The user should identify which are the required outputs (e.g., only the estimation of energy needs or also thermal and visual comfort indicators), what he wants to model (e.g., only the envelope or also each component of the HVAC system) and which is the possible level of detail for the modelling activity (e.g., a single zone or a multi-zone model). In this way, a list of explicit user's needs can be prepared for addressing the selection towards a specific tool. Whatever it is, the most important user's expectation is that the results provided by the chosen BES are reliable. Moreover, the possibility to compare different BES tools is relevant, not only for the user but also for the addressee of his work. These last two aspects are generally not investigated by a user looking for the most convenient BES tool and they can be considered implicit needs.

As indicated in Figure 1.2, the explicit user's needs directly affect his selection of the BES tool. The non-explicit needs, instead, have to be already satisfied by the BES tool, as they are a minimum requirement. Thus, they have to be considered in the dynamic simulation tool development process as primary targets. To determine if the boundaries of reliabilities are achieved, the software has to be validated and, then, presented to the interested users for the selection. From one hand, the validation can be an important instrument to identify the errors and to improve the general quality of the BES code. From the other hand, also the users can evaluate the performance of the different software by comparing with reference cases and assessing their reliability and capability.

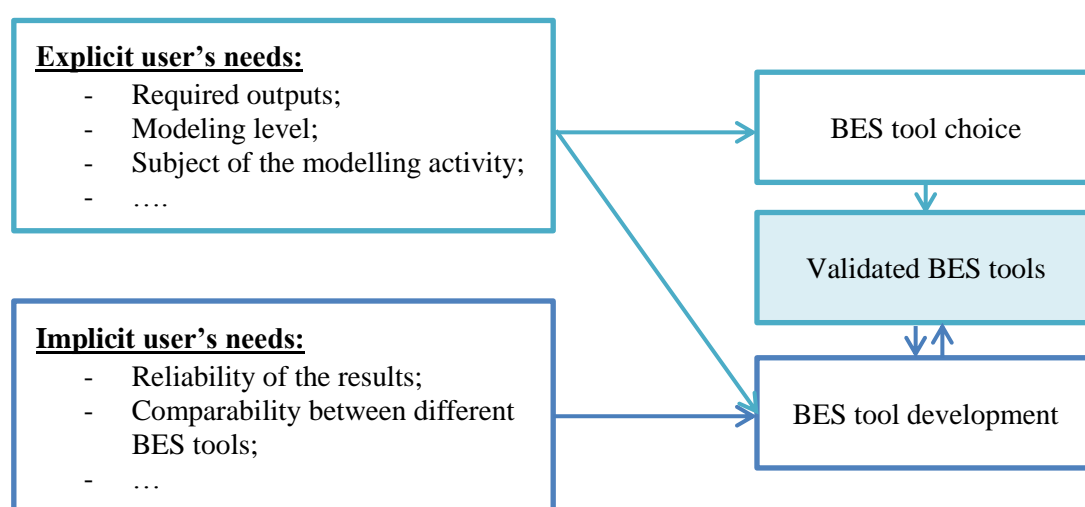


Figure 1.2 - Correlation between user's needs and availability of validate BES tools

From a researcher's point of view, these BES tool characteristics are crucial for his work. The outcome of his research has to be independent of the used simulation software, in order to have a general worthiness and, for example, to find some correlations between the thermophysical properties of the building envelope components and the whole energy performance and to refine simplified methods, as in this thesis.

### ***1.3.1 Literature review***

Building simulation codes are more and more frequently supporting the evaluation of the energy performance of new and existing buildings and used to size and design the building systems by architects and engineers. Moreover their use allows researchers to define, tune and review different simplified methods (van Dijk and Arkesteijn, 1987), such as the quasi-steady state approach of the standard EN ISO 13790:2008 proposed in the calculation of energy performance of buildings for energy labelling and certification.

Although some of the most well known, such as HVACSIM+, TRNSYS, EnergyPlus, BLAST and DOE2, implement quite similar approaches to solve the building thermal balance, in particular for the calculation of the dynamic behaviour of the opaque envelope, the provided results can significantly differ from one to another code within the wide range of configurations that characterizes the real applications. Even if the degrees of freedom and the options allowed to the user's choices are correctly used, small details regarding the implemented components or algorithms or different approaches in the definition of the boundary conditions, of the buildings and plants configuration and in the management of the output can lead to different estimation of the energy needs or of the power peak loads for the same building. The most common causes of discrepancies, as an insufficient detail in the component and system models or even errors in the implementation of the algorithms, have been the main target of the investigation since the early works in the '80s, which indicated the need for validation methodologies.

Many efforts have been done since then in order to improve the agreement and accuracy of software tools through the definition of a validation procedure. Describing the results of validation activities at the Solar Energy Research Institute (now National Renewable Energy Laboratory), Judkoff (1988) introduced a three-step approach based on analytical verification (validation against simple analytical test cases), empirical verification (comparison to the available data of empirical cases) and code-to-code comparison (evaluation of several different codes with different thermal solution approaches in a variety of representative cases). Some indications on the empirical validation tests performed by the Solar Energy Research Institute in cooperation with the International Energy Agency and other partners were also provided.

Jensen (1995) analyzed the validation procedure defined within the PASSYS Project of the European Commission DGXII for Science Research and Development of the European Commission, emphasizing the importance of parametric sensitivity statistical analysis and residual statistical analysis when comparing results from different sources, such as the different statistical sensitivity analysis techniques considered by Lomas and Eppel (1992). The validation methodology described adds to a whole model validation approach (comprising the three steps of sensitivity analysis, empirical validation and comparative validation) a parallel validation of each single process or element of the model.

Lomas *et al.* (1997) illustrated the results of a more recent extensive empirical validation program of the International Energy Agency (IEA) Annex 21 and Task 12, which produced five empirical validation benchmarks. The report by Moinard and Guyon (1999) refers to the IEA Task 22, aimed to test the ability of models to predict temperature and energy consumption of a test cell. Under the same IEA Task 22 Palomo del Barrio and Guyon (2003, 2004) developed mathematical data analysis techniques to identify and explain the differences between simulation and measurements.

Neymark *et al.* (2005) developed a new data set and test specifications appropriate for the inclusion of empirical validation cases in the framework of the comparative test approach defined by the IEA Building Energy Simulation Test (BESTEST) method. As regards analytical approaches, they involve the comparison of the simulation results with analytical solution of particular processes or of specific cases (conduction, convection and long wave radiation models, solar gains, ground coupling, plant components, etc). Some of those solutions have also been included in the framework of the BESTEST method, as reported by Neymark and Judkoff (2009) for the ground coupled heat transfer or by Neymark *et al.* (2002) for HVAC components. As regards the comparative approaches, the U.S. Department of Energy (DOE), through the National Renewable Energy Laboratory (NREL), the IEA and the American Society of Heating, Refrigerating and Air-Conditioning Engineers (ASHRAE) have been cooperating in order to develop standard methods of test (validation and diagnosis) for computer software.

Those procedures, the BESTEST, were developed under IEA Tasks 8, 12, 22 and 34. ASHRAE (ASHRAE, 2011) recently published the updated ANSI/ASHRAE Standard 140-2011 Standard Method of Test for the Evaluation of Building Energy Analysis Computer Programs, which parallels many of the tests in the first IEA BESTEST.

Besides the BESTEST configurations for the building envelope simulation, other ones have been developed to evaluate the ground contact cases and the HVAC plants, as synthesized by Judkoff and Neymark (2008).

A BES tool which successfully passes the BESTEST cases, is able to provide results in agreement with the ones of the reference codes, which are representative of what is commonly accepted as the current state of the art in BES (Judkoff and Neymark, 1995). In this context, further comparative investigations are of interest, not only to detect the elements of disagreement but also to quantify their influence.

## 1.4 Building envelope characterization with BES

The BES tools can be used for advanced design aims, which are beyond the simple estimation of the energy needs over a monthly or an yearly period. For instance, the BES codes can be used to design passive systems which minimize the energy needs and keep the indoor thermal comfort conditions setpoints by controlling the balance between the different thermal flows and, so, using the air-conditioning system as less as possible. Consequently, it is necessary to model accurately not only the dynamic behaviour of the whole building system but the one of the single components of the envelope.

The characterization of the dynamics of the envelope gets a larger importance during the cooling season. From one hand, by studying properly the envelope thermal inertia, it is possible to shift part of the heat gain flows leading to cooling needs during the less critical time of the day (e.g., during the nighttime and applying a night ventilation strategy or, in case of non-residential buildings, during the non-occupancy time). On the other hand, the dynamic properties of the envelope can strongly influence the indoor thermo hygrometric comfort sensation of the occupants: a proper design can limitate the need of future interventions and the use of the air-conditioning system.

The BES tools can help in advanced building design but, again, the problem of the accuracy of the provided results has to be taken into account. In chapter 4, the dynamic properties of the opaque envelope defined in the technical Standard EN ISO 13786:2007 (CEN, 2007d) have been used as index variables to assess the different opaque envelope behaviour simulated with numerical methods. Also the transparent components have been studied, by comparing the internal surface temperature simulated by EnergyPlus and TRNSYS in order to underline possible differences to take into account for an indoor comfort analysis, besides the evaluation of the energy needs.

### 1.4.1 Literature review

In addition to the general purpose of a more efficiency energy use in the buildings, one specific aim of the EPB Directive 2010/31/EU (formerly 2002/91/EC) is referred to the increase of the buildings energy performances in summer conditions. A reliable assessment of the cooling consumptions may be considered as a first useful step to understand how to improve the building thermal behaviour, which depends basically on complex correlations between gains, losses and storage of heat, which are described in the chapter 3 for what concerns the air heat balance models and in chapter 5 for the quasi-steady state model by EN ISO 13790:2008.



Moreover, the prediction of the cooling load allows to assess the impact of passive solar techniques in reducing the energy demand for cooling.

The dynamic behaviour of the opaque components can be described, for instance, by means of the properties defined in the technical Standard EN ISO 13786:2007 (i.e., the periodic thermal transmittance, the decrement factor and the time shift), considering sinusoidal variations of temperature or heat flow. These dynamic thermal characteristics are used also in product specifications of building components, in the calculation of the internal temperature in a room - as proposed by the technical Standard EN ISO 13792:2005 in annex A.3 (CEN, 2005), in the assessment of the daily peak power and energy needs for heating or cooling, or even for estimating the effects of intermittent heating or cooling.

The importance of those properties is widely discussed in the literature. Ulgen (2002) investigated both experimentally and theoretically the time lag and decrement factor for different wall compositions under sinusoidal sol-air temperature solicitation. Asan and Sancaktar (1998) and Asan (2006) numerically investigated time lags and decrement factors under sinusoidal sol-air temperature solicitation for 26 different building materials finding dependences on heat capacity, thermal diffusivity and thickness of the layer. Kontoleon and Bikas (2007) and Kontoleon and Eumorfopoulou (2008) imposed non sinusoidal periodical solicitation, for South-oriented walls or for differently oriented walls respectively, and analyzed the effect of the outdoor absorption coefficient on time lag, decrement factor and temperature variations. Luo *et al.* (2007) compared different definitions for the time lags and decrement factors for different wall compositions already described in literature. Yumrutas *et al.* (2007) developed a theoretical methodology to find total equivalent temperature differences for cooling loads calculation based on sol-air temperature, time lags and decrement factors.

While the EN ISO 13786:2007 approach is based on analytical calculation under sinusoidal boundary conditions, there are several approaches for the assessment of the dynamic properties in transient (non sinusoidal) regime, usually based on numerical methods. Some of them, such as the Transfer Functions Methods (*TFM*) by Mitalas and Arseneault (1971) and the Finite Difference Methods (*FDM*) are also implemented in widely used software as TRNSYS – specifically the Direct Root Finding method, *DRF* (Solar Energy Laboratory, 2005) or EnergyPlus – the State-Space Method, *SS* (U.S. DoE, 2012), introduced in chapter 3.

The implementation of EN ISO 13786:2007 procedure with a non sinusoidal forcing temperature can be a useful way to assess, by means of simple dynamic parameters, the behaviour of the opaque components predicted by numerical methods.

For what concerns the transparent components, the contribution of the windows physical properties to the building energy needs and the simultaneous influence of their characteristics on the thermal sensation of occupants have been studied by many authors from different points of view. Hwang and Shu (2011) investigated the effect of different envelope parameters on thermal comfort and in their analysis compared the cooling energy need of a space controlled by a thermostat with a PMV-based control, implementing the approach of Kang *et al.* (2010). As regards the importance of the glazing system in the optimization of energy need both during the heating and the cooling season, Gasparella *et al.* (2011) underlined the fact that energy optimization does not only depend on the use of insulating glasses, but also on the quantity of solar radiation admitted by the windows. Successively the same authors (Gasparella *et al.*, 2012) analysed the relation between long-term internal thermal comfort, energy performance, kind of glazing and window size, according to the classic definition of the PMV approach. The PMV are function of many parameters and, in particular, of the mean radiant temperature. While for the opaque components, when insulated, their internal surface temperature is generally closer to the setpoint conditions, for the transparent ones there is a larger influence of the external environment conditions because of their lower thermal resistance and the solar radiation absorbed. Moreover, the dynamic response of the glazings is faster than the one of the opaque walls and so, in particular for those configurations with large windows, the indoor thermal comfort is largely conditioned by the window characteristics. In this context, the accurate estimation of the surface temperature of these components assumes a significant importance.

## 1.5 BES and simplified models

The European Union, aware of the fact that the building energy consumption is responsible for more than 1/3 of the finale energy uses of the Member States, proposed by means of the Directive 2002/91/EC and the EPB Directive 2010/31/EU to implement the energy labelling of buildings in order to drive the market towards the development of more sustainable buildings as common standard and to renovate the existing ones by improving their performances and making them interesting to the market itseft. In different contexts, such as for the household appliances, the energy labelling has revealed a good strategy to achieve the energy consumption targets.

After the definition of the strategy, a crucial issue was the choice of the methodology to assess the energy performance. The EU Directives allow to use two approaches: enhanced dynamic simulation analyses or simplified methods defined in the European technical Standards. The two alternatives are characterized by different levels of complexity of the inputs, discretizations of the outputs and, generally speaking, by different possibilities of analysis with the provided outputs. The choice of allowing two approaches – one simplified and easy to use, another more complex and detailed, on one hand is facilitating the spread of the building energy evaluation from the early stages of the design activity and on the other hand it lets the more expert professionals to use detailed tools for advanced designing activities. In this way, the BES tools, which currently are only partially used by the architects and engineerings, could become a future designing standard accepted and encouraged in the EPB Directive framework.

In order to achieve the goals of the EU Directives, whatever the method used for the evaluation, its reliability is crucial to ensure the EPB Directive effectiveness. Incoherent results could affect the confidence given by the market to the building energy certification as valid instrument to express the energy efficiency quality of a given building. Thus, the monthly quasi-steady state method is supposed to give monthly or seasonal results in good agreement with the monthly or seasonal results by BES tools.

In this last chapter of this research work, the problem of the agreement of the results by simplified or detailed simulation approaches is discussed, pointing out the entity of the discrepancies, their causes and proposing some correction factors in order to improve the coherencce between the quasi-steady state methods with respect to the more advanced ones.

### **1.5.1 Literature review**

According to the Energy Performance of Building (EPB) Directive 2010/31/EU and the former 2002/91/EC, in order to implement the energy labelling of buildings, the energy performance can be evaluated either with analytical approaches or with enhanced simulation tools. As observed by Tronchin and Fabbri (2008), the coherence of the methods is of crucial importance in order to give a perception of the reliability of this instrument to the market and to ensure the EPB Directive effectiveness. Moreover, the European Standard EN ISO 13790:2008 suggests to use the dynamic simulation in improving and tuning the proposed quasi-steady state method, by refining the estimation of the utilization factor (i.e., the dynamic parameter that reduces the thermal gains for heating need calculation and the thermal losses for cooling). The utilization factor is a function of the ratio between the thermal losses and the thermal gains. Those are calculated through simplified expressions. Extending the method of studying the dynamic factor by van Dijk and Arkesteijn (1987), the Standard proposes the recourse to dynamic simulation also in determining the thermal losses and gains.

Many authors have already made some efforts in calibrating the EN ISO 13790:2008 approach, such as Jokisalo and Kurnitski (2007), Corrado and Fabrizio (2007), Orosa and Oliveira (2010) and Oliveira Panão *et al.* (2011). They proposed some changes to the correlations in order to adapt the method to the climatic conditions, especially for the cooling season, and the building stock characteristics in their respective countries but the general problem appears to be still unsolved, as large discrepancies have been found. In their study of the utilization factor, other authors, such as Yohanis and Norton (1999), considered the number of zones in a building, in addition to its time constant, focusing on one of the issues related to the simplified methods already identified by van Dijk and Arkesteijn.

As indicated by van Dijk and Arkesteijn and remarked by Corrado and Fabrizio, the utilization factor considers the mismatch between heat losses and gains leading to heating or cooling energy needs. What is of crucial importance, then, is that the heat losses and gains are determined accurately.

#### **1.5.1.1 Thermal losses**

As done by Van der Veken *et al.* (2004), the comparison between the dynamic simulation results and the analytical approaches (detailed or simplified) can be helpful in looking for disagreements sources, which can lead to different evaluations of the building energy needs or mismatches and errors in the refinement of the quasi-steady state method. Referring to the

thermal losses, among the causes of error or discrepancies, the ones depending on the definition of the boundary conditions and on the calculation of the thermal losses appear to play a crucial role (Judkoff *et al.*, 2008). One of them can be the reference temperature considered to describe the internal conditions.

For the transmission losses, which represent the first component of thermal losses, the quasi-steady state model linearizes and considers the internal long wave radiation exchanges in parallel with the convection exchange with the air node, assuming an equivalent operative reference temperature (i.e., a weighted average of the air temperature of the conditioned zone and the mean radiant temperature of the envelope delimiting the zone itself). In contrast, many of the simulation codes perform a detailed analysis of the internal long wave radiation exchange and refer to an air heat balance approach with an air temperature as reference.

As regards the ventilation losses, the actual driving gradient is given by the difference between the internal and external air temperatures. Using an operative reference temperature for the ventilation losses evaluation, as indicated by the quasi-steady state approach of the technical standard, leads to incorrect results, in particular with large ventilation rates (van Dijk and Arkesteijn, 1987).

Previous studies in literature (Pietrzyk, 2010) have stressed the importance of distinguishing the total losses into those by transmission and the ones by ventilation, especially in defining statistical models. The evaluation of the link between the transmission heat losses and ventilation losses has also been investigated in relation to the reduction of the building energy needs (Zhou *et al.*, 2008). Other authors (Soleimani-Mohseni *et al.*, 2006) have studied the ventilation flow rate in order to derive some interactions with the operative temperature.

Whatever the pursuit of these studies and the chosen approaches, the correct estimation of the thermal losses appears to be crucial for a correct energy assessment.

### **1.5.1.2 Thermal gains**

According to the quasi-steady state method, the heat gains consist in all thermal fluxes to the internal air node - in their convective quote when they have become convective, not driven by the temperature difference between indoor and outdoor environment. Those can be distinguished in solar gains, internal gains and infrared extra flow towards the sky vault.

In many applications, the solar heat flow entering through the transparent envelope is the most relevant thermal gain component. The control of the entering solar radiation is becoming more and more important in designing passive systems (Orosa and Oliveira, 2012). For instance, Gasparella *et al.* (2011) simulated a well-insulated building with different kind of

glazing systems, with or without fixed shading overhangs and fins for different windows sizes, orientations and European localities, showing the influence of the choice of the glazing on the heating and cooling energy needs and peak loads and underlining that the solar heat gains coefficient plays a role at least as large as the thermal transmittance. The correct estimation of the entering solar radiation is necessary since the early stages of the design process, in particular, when using the simplified quasi-steady methods. Moreover, as underlined by Oliveti *et al.* (2011), the black body cavity hypothesis, according to which the whole solar radiation entering into the thermal zone is absorbed, adopted by the EN ISO 13790:2008 method, is not representative of the real physical phenomena. In many cases a certain amount of the radiation is reflected by the walls and dispersed through the windows themselves. Some authors (Cucumo *et al.*, 1995) proposed some corrections to the internal solar absorptance of the opaque surfaces. Oliveti *et al.* (2011) instead, preferred a correction to the solar transmittance of the glazings in order to take into account the radiation lost because of the reflections. Moreover, another quote is absorbed by the opaque envelope and partly lost toward the outside.

In addition to the entering radiation, the solar gains by transmission through the opaque envelope have also been studied by many researchers in different contexts. Some of them (Oliveira Pañao *et al.*, 2012; Oliveti *et al.*, 2012a) focused on the sunspaces and analysed the EN ISO 13790:2008 calculation method. Other authors paid particular attention to the roofs, underling the importance of the solar absorption coefficient (Suehrcke *et al.*, 2008), especially for the cooling energy needs.

Among the heat fluxes independent of the temperature difference there are not only actual gains but also some fluxes subtracking heat from the thermal zone. The most important of them is the infrared extra flow towards the sky vault. Oliveti *et al.* (2012b) assessed the methods proposed by the EN ISO 13790:2008 for the calculation of the infrared extra flow towards the sky dome, comparing the Standard with the empirical collected data and finding inaccuracies in the Standard estimations.

As observed for the thermal losses and in literature, the correct estimation of the thermal gains is necessary for a correct energy assessment, in particular for the evaluation of the cooling energy needs.

## 1.6 Statistical approach

Building Energy Simulation tools (BES) gave to designers and professionals the possibility to explore several alternatives in order to find the best or the most convenient one. BES is strictly correlated to the examinations of different boundary, operative or designing conditions and a deep analysis in the early stages of the design activity allows to avoid errors and so expensive correction measures.

The investigation of a large number of cases has to face two main problems: how the different alternatives should be selected and by means of which techniques should be analysed. Statistics can help to get an answer for both the questions. In this research work, the Design of Experiments approach have been followed in order to define the samples to analyse and some inferential techniques, such as the ANOVA, the correlation indexes and the multiple regression models, have been used in order to determine which are the most significant variables and to define some models. In the Annex A, the considered techniques are described and their main advantages and limitations underlined, as well as the context of their application.

### 1.6.1 Design of Experiments

In order to investigate physical phenomena and to analyse the response of a system, both by means of measurements and by means of simulations, experiments can be performed. An experiment consists in a test or in a series of tests, whose aim is to let us learn how a system or a process works. They are used to characterize a behaviour or an answer, to optimize a system or to carry on a design activity. In this research work what has been investigated is not a real system, not an industrial equipment but a model which simulates the building envelope behaviour.

In this study a BES or a simplified calculation are seen as real tools expected to complete specific tasks. Their targets are, for instance, a reliable prediction of the dynamic behaviour of the building envelope and estimation of the energy needs. In this context, the Design of Experiments (DoE) has been applied to assess the capability of these instruments (i.e., to *characterize* their capabilities). Once determined which are the limitations of the instruments, the *DoE* techniques can be also implemented to assess which are the best solution for a specific problem (i.e., to *optimize*). Whatever the target of the experimental activity, the validity of the conclusions mainly depends on how the experiments have been conducted – not only from the practical point of view but in the perspective of which cases have been selected and in which way their different combination have been assessed. For these reasons, a significant role has been given to statistics.





---

# **Chapter 2:**

## **Weather data and external conditions in BES**



## Chapter 2

In this chapter the problem of the description and the use of weather and external boundary conditions in BES tools is discussed. The chapter is divided into two parts: the first one is about the weather data files which can be employed for performing dynamic simulations while in the second one the problem of the heat transfer through the soil according to the European Standard EN ISO 13370:2007 is described.

The first part of the chapter describes the procedure proposed by EN ISO 15927-4:2005 to build a single reference year to use in BES. This approach has been implemented in order to develop reference years weather files for some localities in the North of Italy and in the Netherlands. For this data files, the representativeness respect to the averages of a multi-year analysis has been discussed, considering both the meteorological variables and the annual energy results (i.e., annual heating and cooling energy needs, annual heating and cooling hourly peak loads) over a sample of 48 buildings. Moreover, statistical correlation indexes have been calculated in order to investigate the relationship between the building envelope characteristics and the variability of the results in the multi-year analysis.

In the second part of the chapter, the problem of the boundary conditions to be used in BES for walls and floors in touch with the ground is discussed. The EN ISO 13370:2007 methods for slab-on-ground cases have been assessed by comparison with detailed 3-dimensional finite elements models. Both steady-state and dynamic conditions have been analysed, in order to find out the accuracy of the Standard procedure and the proper discretization of the boundary temperatures in transient conditions.



## Part a: Weather data files for BES

### 2a.1 Method

In this paragraph the procedure given by the technical Standard EN ISO 15927-4:2005 for the calculation of the  $TRY_{EN}$  and the methodology followed for assessing the representativeness of the results, respect to a multi-year analysis, have been presented.

#### 2a.1.1 *TRY calculation in accordance with the EN ISO 15927-4:2005*

The procedure presented by the technical Standard EN ISO 15927-4:2005 to develop a *test reference year* is described in this section.

The construction of a  $TRY_{EN}$  requires both mean values of the meteorological variables and, in particular, the individual frequency distributions and the cross correlations between the parameters. In accordance with the EN ISO 15927-4:2005, at least ten years (not necessarily consecutive) should be used but the longer the period, the better.

A  $TRY_{EN}$  can be built in accordance with the steps described below:

1. calculation of the daily averages  $\bar{p}$  for each primary climatic parameter  $p$ , month  $m$  and year  $y$  of the series;
2. sorting of all the  $\bar{p}$  for a specific month  $m$  of all the available years in increasing order and calculation the cumulative distribution function  $\Phi(p, m, i)$  for each parameter and  $i^{\text{th}}$  day as:

$$\Phi(p, m, i) = \frac{K(i)}{N + 1} \quad (2a.1)$$

where  $K(i)$  is the rank order of the  $i^{\text{th}}$  day and  $N$  is the total number of days for a month over all the available years;

3. sorting of all the  $\bar{p}$  for a specific month  $m$  and year  $y$  in increasing order and calculating the cumulative distribution function  $F(p, y, m, i)$  for each parameter and  $i^{\text{th}}$  day, as

$$F(p, y, m, i) = \frac{J(i)}{n + 1} \quad (2a.2)$$

where  $J(i)$  is the rank order of the  $i^{\text{th}}$  day and  $n$  is the number of days for a specific month;

An example of cumulative probabilities for the dry bulb temperature, the solar irradiance and the relative humidity is represented in Figure 2a.1 for the month of January and the first

three years of the data series of De Bilt in the Netherlands. In this example, the year 1960 seems to be the most representative among the three reported, respect to the cumulative probability over all the period 1958-2011.

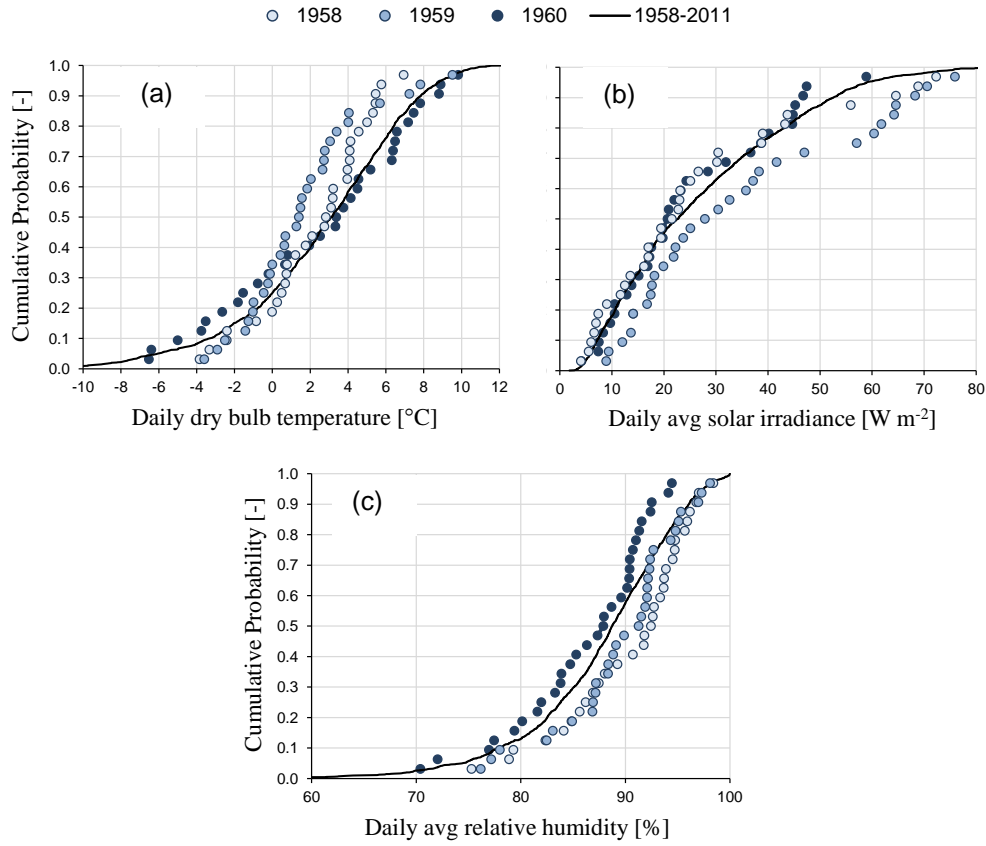


Figure 2a.1 – Cumulative probability for the first 3 years of the series of De Bilt for the dry bulb temperature (a), the solar irradiance (b) and the relative humidity (c)

4. calculation of the statistics by Finkelstein-Schafer for each month  $m$  and year  $y$  as

$$F_S(p, y, m) = \sum_{i=1}^n |F(p, y, m, i) - \Phi(p, m, i)| \quad (2a.3)$$

5. sorting of the months for increasing values of  $F_S$  for each parameter, calculating the ranks for each month and parameter and summing them in order to calculate the total ranking;
6. for each month among the first 3 months with the lowest ranking sum, calculation the deviation between the mean wind speed of the month  $m$  of the year  $y$  and the mean multi-year wind speed: the month with the lowest deviation can be chosen for a  $\text{TRY}_{\text{EN}}$ .

The final 8 hours of a month and the first 8 hours of the next one should be smoothed by means of a cubic spline interpolation in order to avoid discontinuities. Since the adjustment

involves nighttime hours and wind speed is generally not corrected, it applies only to the dry bulb temperature and the relative humidity.

### ***2a.1.2 Selection and analysis of the weather data of the multi-year series***

The collected weather data have generally to be first analysed in order to identify errors and outliers, to find if a certain year can be used or not in the  $TRY_{EN}$  development and, in case, if the wrong data can be fixed by interpolation. In this work, the following criteria have been chosen for the analysis of the raw data:

- *dry bulb temperature:*
  - the values exceeding the 50% of the 99<sup>th</sup> percentile;
  - the data with a derivative larger than  $\pm 4 \text{ K h}^{-1}$ ;
  - periods with constant values for more than 5 h;
- *horizontal global solar radiation:*
  - the values exceeding the solar constant or positive during the nighttime;
- *relative humidity:*
  - the values exceeding 100% or null;
  - periods with constant values for more than 5 h (if lower than the 75<sup>th</sup> percentile);
- *wind velocity:*
  - the values exceeding the 50% of the 99<sup>th</sup> percentile or negative;
  - periods with constant values for more than 5 h (if the registered speed is larger than the anemometer minimum speed).

Known bias errors have been corrected by shifting properly the data involved by this kind of problem.

Since only 2 of the Italian analysed locations comply with the minimum prescription of 10 years given by the EN ISO 15927-4:2005 for the development of a  $TRY_{EN}$ , a slightly less restrictive criterion has been followed: only locations with at least 8 years in the data series and with less the 10% of wrong/missing data for each variable and each year were considered. Wrong and/or missing data have been replaced using the linear interpolation for the temperature, the relative humidity and the wind speed when the consecutive data to correct were less than 6 entries, otherwise a cyclic interpolation has been considered (Prada, 2012).



The monthly values of average dry bulb temperature, daily horizontal solar radiation and relative humidity of the different years and TRY<sub>EN</sub> have been calculated and compared with the distributions of monthly values of the multi-year series, as well as to the monthly values reported in the Italian technical standard UNI 10349:1994, currently used in the quasi-steady state methods by EN ISO 13790:2008 and UNI/TS 11300 parts 1 and 2 (UNI, 2008) for the energy certification of buildings. Moreover, some BES tools as TRNSYS provide some subroutines (as Type 54 in TRNSYS, assessed in the study by Gansler *et al.*) which can develop an hourly profile starting from the average monthly inputs, such as the ones by UNI 10349:1994.

### ***2a.1.3 Analysis of the TRY<sub>EN</sub> weather files representativeness***

The representativeness of the test reference year has been studied by carrying on different dynamic simulations with both TRY<sub>EN</sub> and multi-year data series and analysing the annual energy needs and peak loads (both cooling and heating) of a set of reference buildings characterized by different insulation levels, thermal inertia, sizes and orientations of windows and kind of glazing. The choice of different buildings to assess the representativeness of the weather data allowed also to estimate the sensitivity of the building energy performance to the variability of five North Italy climates by changing the characteristics of the building itself. In this perspective, both buildings more sensitive to the heating energy demand (e.g., the poorly insulated buildings) and ones more sensitive to the cooling energy demand (e.g., buildings with windows with high SHGC) have been considered.

#### **2a.1.3.1 Set of reference buildings**

A sample of 48 different simplified thermal zones has been developed in accordance with a full factorial plan. The base module consists in a single thermal zone with a 100 m<sup>2</sup> squared floor, 3 m high and the façades facing the main cardinal directions. The thermal bridges have been neglected and the floor has been modelled as on a ventilated cave (i.e., without sun exposition and infrared thermal losses towards the sky dome), instead of in touch with the ground, whose sensitivity and response to the variability of the external conditions are very low considering a limited number of years because of its very high thermal inertia, as it will be discussed in the second part of this chapter.

All the opaque components have been modelled with a two-layer structure with insulation on the external side and a massive layer on the internal one, with a thermal resistance around  $0.8 \text{ m}^2 \text{ K W}^{-1}$ . The solar absorptance is 0.3 for both sides of the vertical walls and for the internal side of the roof, 0.6 for the external side of the roof and the internal side of the floor and 0 for the external side of the floor. The thermal properties of the considered materials are reported in Table 2a.1.

*Table 2a.1 - Materials thermal properties*

Property	Timber	Concrete	Insulation
Thermal conductivity $\lambda \text{ [W m}^{-1} \text{ K}^{-1}]$	0.13	0.37	0.04
Specific Heat Capacity $c \text{ [J kg}^{-1} \text{ K}^{-1}]$	1880	840	1470
Density $\rho \text{ [kg m}^{-3}]$	399	1190	40
Thickness $s \text{ [m]}$	0.1	0.3	0.05/0.15
Thermal resistance $R \text{ [m}^2 \text{ K W}^{-1}]$	0.77	0.81	1.25/3.75

The windows are positioned all on the same façade and consist in a double-pane glazing ( $U_{gl} = 1.1 \text{ W m}^{-2} \text{ K}^{-1}$ ) and in a timber frame ( $U_{fr} = 1.2 \text{ W m}^{-2} \text{ K}^{-1}$ ), whose area is the 20% of the whole window area. The internal gains have been assumed equal to  $4 \text{ W m}^{-2}$ , half radiative and half convective, as indicated by the EN ISO 13790:2008 for residential dwellings. The ventilation rate has a constant rate of 0.3 ach/h, as suggested by the Italian technical Standard UNI/TS 11300-1:2008.

The considered variables are the most relevant building envelope parameters and, with the exception of the window orientation, each one presents a high and a low level:

- the insulation level of the envelope components (5 cm or 15 cm of polystyrene) in order to have two levels of thermal transmittance (e.g., for the vertical walls,  $U = 0.45 \text{ W m}^{-2} \text{ K}^{-1}$  and  $U = 0.21 \text{ W m}^{-2} \text{ K}^{-1}$ );
- the thermal inertia of the opaque elements (area specific heat capacity of the internal layer equal to  $75 \text{ kJ m}^{-2} \text{ K}^{-1}$  for the timber structure and equal to  $300 \text{ kJ m}^{-2} \text{ K}^{-1}$  for the concrete);

- the solar heat gain coefficient  $SHGC$  of the glazing (equal to 0.608 or 0.352);
- size of the windows ( $A_{win} = 14.56 \text{ m}^2$  or  $A_{win} = 29.12 \text{ m}^2$ );
- the orientations of the windows (East, South or West).

The different cases have been simulated with TRNSYS, considering the following assumptions:

- the timestep is coherent with the hourly discretization of the weather data, in order to avoid interpolation strategy influencing, in particular, the peak load results;
- constant convection coefficients have been selected, in accordance with the standard EN ISO 6946:2007 (CEN, 2007a);
- the long wave radiation exchange are considered, according to the star network approach by TRNSYS;
- the heating and the cooling set-point have been fixed to 20 °C and 26 °C in accordance with the UNI/TS 11300-1:2008 prescriptions for residential buildings, but they are applied all year long, i.e. no specific heating and cooling seasons have been defined.

#### **2a.1.4 Statistics analysis**

The variability of the energy results has been analysed, in order to find which building envelope parameters are significantly correlated with the dispersion of the results.

In order to study the variability of the energy performance and its correlation with the building envelope characteristics, the results with the TRY<sub>EN</sub> weather files have been considered as a benchmark. The deviations between the energy needs and peak loads simulated in each year and the ones of the TRY<sub>EN</sub> have been calculated and analysed by means of Pearson's correlation index and Spearman's index. Positive and the negative differences have been distinguished because of the monotonic definition of the indexes. For a description of these correlation indexes, see Annex A.

The considered variables have been distinguished into the ones describing the envelope characteristics and the ones describing the external conditions.

For the energy need deviations, the variables considered in this analysis are:

- the variables aimed at describing the dynamic behaviour of the opaque envelope, such as  $Y_{ie,env} [\text{W m}^{-2} \text{ K}^{-1}]$ , the area-weighted average periodic thermal transmittance,  $\Delta t_{ie,env}$

[h], the area-weighted average time shift, and  $k_i \cdot A_{tot}$  [kJ K<sup>-1</sup>], the total internal heat capacity, defined in the EN ISO 13786:2007 and described in chapter 4a;

- $U_{env}$  [W m<sup>-2</sup> K<sup>-1</sup>], the area-weighted average thermal transmittance of the opaque envelope;
- $SHGC$  [-], the solar heat gain coefficient of the glazing;
- $A_{gl}$  [m<sup>2</sup>], the glazing area;

In order to take into account of the variability of the weather conditions, the deviations of the area-weighted *equivalent Heating/Cooling Degree Days* [K d] have been calculated using a particular year and the ones of the TRY<sub>EN</sub> (both for the opaque envelope and for the transparent one).

The  $HDD_{sol-air, env}$ ,  $CDD_{sol-air, env}$ ,  $HDD_{sol-air, gl}$  and  $CDD_{sol-air, gl}$  have been calculated for each orientation considering respectively the sol-air temperature for the opaque components and the equivalent sol-air temperature for the transparent components, according to the Eq. (2a.4) and (2a.5) (Gasparella *et al.*, 2011):

$$\theta_{sol-air, env} = \theta_e + \frac{I\alpha + h_{r,sky}(\theta_{sky} - \theta_e)}{h_{se}} \quad (2a.4)$$

$$\theta_{sol-air, gl} = \theta_e + \frac{SHGC \cdot I}{U_{gl}} + \frac{h_{r,sky}(\theta_{sky} - \theta_e)}{h_{se}} \quad (2a.5)$$

Area-weighted heating/cooling degree days have been then calculated for each year and used for determining the deviations  $\Delta HDD_{sol-air, env}$ ,  $\Delta CDD_{sol-air, env}$ ,  $\Delta HDD_{sol-air, gl}$  and  $\Delta CDD_{sol-air, gl}$ .

For the peak loads deviations, the variables are the same, with the exception of the ones describing the variability of the external solicitation:

- $\Delta \theta_{min}$  [°C], the deviation between the minimal annual external temperature for a considered year and the one for the TRY<sub>EN</sub>, has been used instead of  $\Delta HDD_{sol-air, env}$  and  $\Delta HDD_{sol-air, gl}$ ;
- $\Delta H_{hor}$  [MJ m<sup>-2</sup>], the deviation between the total horizontal solar radiation per square meter and  $\Delta \hat{H}_{2dd}$  [MJ m<sup>-2</sup>], the deviation between the annual peak of the 2-days cumulated solar radiation incident on the windows for a considered year and the one for the TRY<sub>EN</sub>, instead of  $\Delta CDD_{sol-air, env}$  and  $\Delta CDD_{sol-air, gl}$ .

## 2a.2 Results

The raw data were available for the capital cities of each province in 4 North Italy Regions: Emilia-Romagna, Lombardia, Trentino-Alto Adige/Südtirol and Valle d'Aosta. The selection procedure and the chosen criteria led to identify 5 cities: Aosta (with 8 years available), Bergamo (10 years), Monza (9 years), Trento (10 years) and Varese (9 years).

Since it is of interest to assess the effect of a large number of years for the development of a  $TRY_{EN}$ , also the Dutch location of De Bilt (Province of Utrecht) has been considered, with more than 50 available years with all the outliers and wrong data already checked and fixed by the Royal Netherlands Meteorological Institute (KNMI). A series of 54 years (1958-2011) has been used for the development of the  $TRY_{EN}$  and for the evaluation of the energy performance of the same sample of buildings.

### *2a.2.1 Average monthly data*

The monthly values of average dry bulb temperature, daily horizontal solar radiation and relative humidity of the different years and  $TRY_{EN}$  have been calculated and compared, as in Figure 2a.2 for the location of Trento and in Figure 2a.3 for De Bilt. For the other Italian localities, see Annex B.

The years considered for the development of the  $TRY_{EN}$ , the selected months and their daily average values for the dry bulb temperature, the global solar radiation on the horizontal and the relative humidity have been reported in Table 2a.2 and in Table 2a.3, for the Italian localities, and in Table 2a.4 for the Dutch one.

In Table 2a.2 the monthly average values of the  $TRY_{EN}$  for the five Italian cities have been compared also to the data reported into the Italian technical Standard. In Table 2a.4, for De Bilt, the deviations with the median values of the complete weather data series have also been reported.

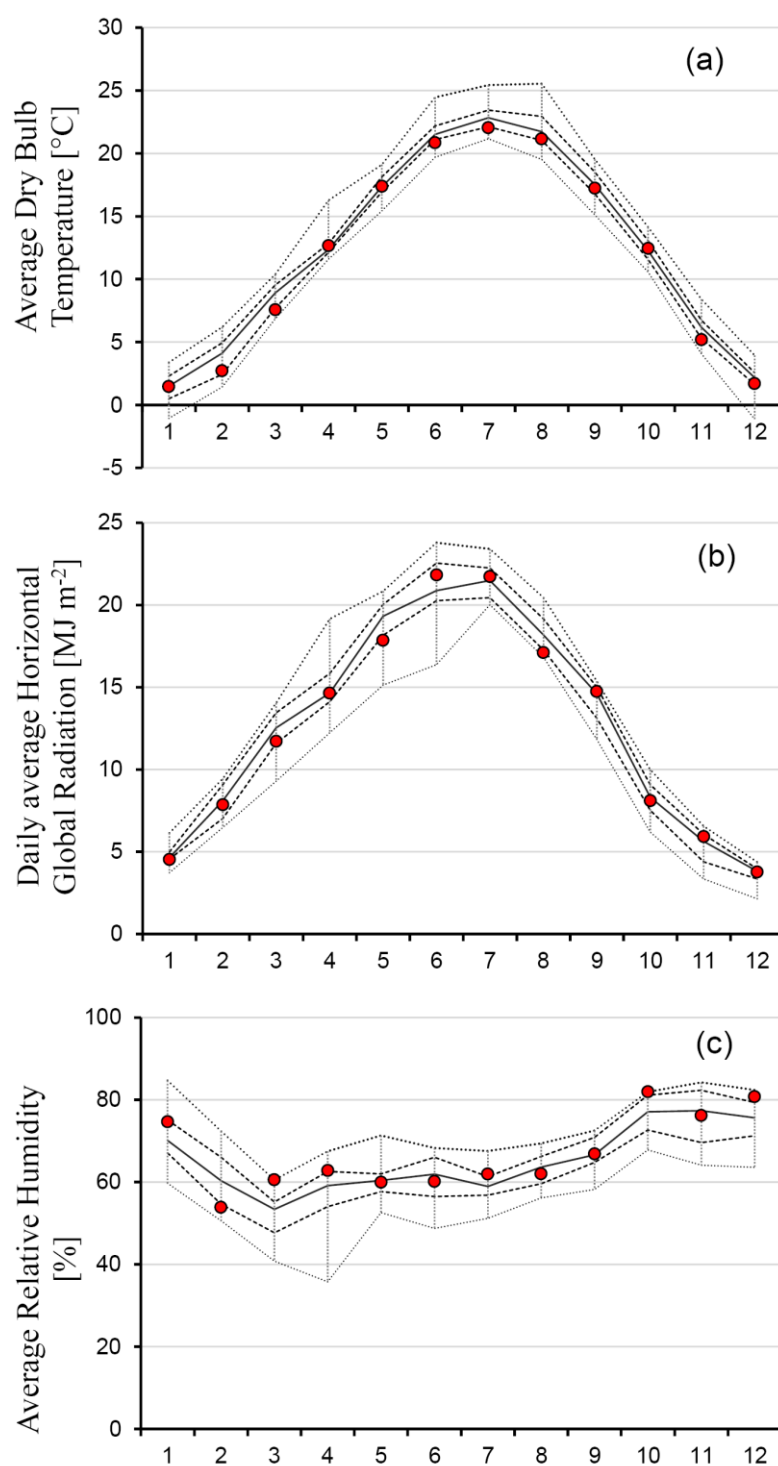


Figure 2a.2 - (a) Average monthly temperature (b) average daily horizontal global radiation and (c) average monthly relative humidity for Trento. The red dots represent the TRY<sub>EN</sub> monthly values, the external dotted lines represent the maximum and the minimum for the multi-year series, the internal dotted lines the first and the third quartile ( $Q_1$  and  $Q_3$ ), while the continuous line is the median

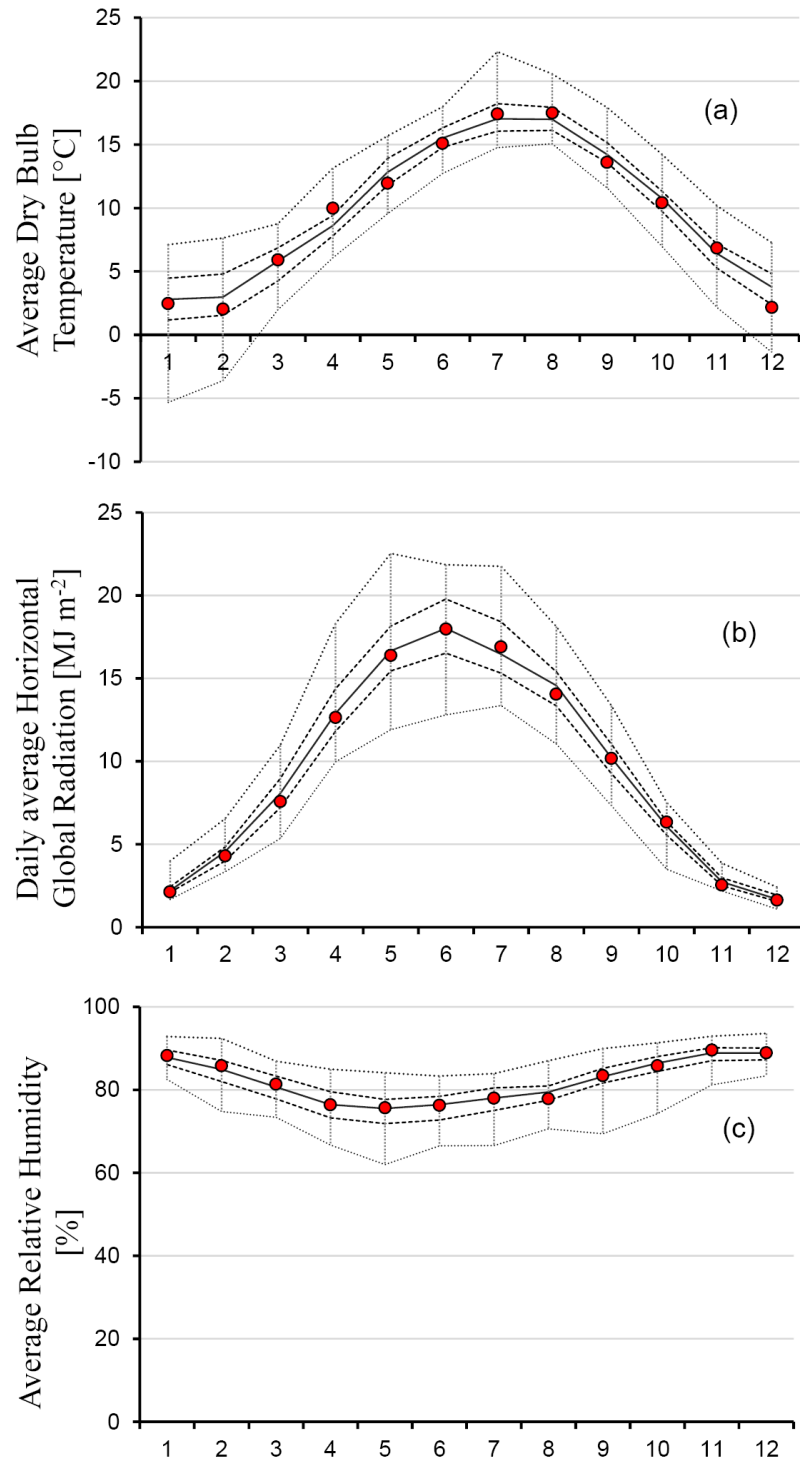


Figure 2a.3 - (a) Average monthly temperature (b) average daily horizontal global radiation and (c) average monthly relative humidity for De Bilt. The red dots represent the TRY<sub>EN</sub> monthly values, the external dotted lines represent the maximum and the minimum for the multi-year series, the internal dotted lines the first and the third quartile ( $Q_1$  and  $Q_3$ ), while the continuous line is the median

Table 2a.2 - Monthly average variables of the  $TRY_{EN}$  (white columns) compared with the UNI 10349:1994 ones (grey columns)

[°C]	Average Dry Bulb Temperature									
	Aosta		Bergamo		Monza*		Trento		Varese	
January	1.80	-0.30	2.18	3.90	2.44	1.70	1.48	1.50	1.96	1.20
February	3.82	2.60	4.82	4.90	5.86	4.20	2.72	4.50	4.81	1.90
March	8.47	6.70	7.53	8.90	9.39	9.20	7.58	9.00	9.31	6.00
April	12.20	11.00	11.41	13.30	11.96	14.00	12.65	13.70	12.46	10.40
May	17.07	14.70	14.52	17.00	15.63	17.90	17.39	17.20	17.85	14.00
June	20.12	18.70	20.55	21.30	23.08	22.50	20.84	21.20	21.07	17.70
July	21.02	20.50	22.02	23.70	23.90	25.10	22.04	23.50	22.07	20.50
August	21.39	19.40	21.97	23.30	23.28	24.10	21.14	22.70	23.55	19.60
September	16.76	15.90	17.74	19.90	19.24	20.40	17.24	19.50	19.60	16.40
October	11.35	10.30	10.84	14.20	13.84	14.00	12.45	13.60	12.96	11.20
November	4.80	4.80	7.64	8.60	7.77	7.90	5.19	7.40	6.62	5.30
December	2.26	0.80	2.21	4.50	4.14	3.10	1.70	2.90	1.77	1.90
[MJ m <sup>-2</sup> ]	Daily Average Global Radiation on the Horizontal									
	Aosta		Bergamo		Monza*		Trento		Varese	
January	3.65	5.30	4.18	4.20	3.74	3.80	4.54	4.90	4.10	5.00
February	6.95	8.00	9.09	6.90	5.61	6.70	7.87	8.40	6.67	7.34
March	12.76	12.10	12.08	11.30	11.12	11.60	11.71	13.70	10.95	11.40
April	16.16	15.70	14.66	15.60	12.70	16.50	14.64	17.70	14.22	15.40
May	17.64	18.20	19.04	19.10	15.88	20.00	17.85	20.90	17.25	19.10
June	18.85	19.90	21.04	20.60	18.57	22.20	21.83	23.20	17.37	20.50
July	18.75	21.00	20.73	22.40	17.98	24.00	21.72	24.60	16.73	22.00
August	16.13	17.50	18.82	18.80	15.43	19.40	17.12	20.20	15.21	18.20
September	12.49	13.20	14.75	14.00	12.02	14.00	14.75	15.50	12.28	13.70
October	7.25	8.70	7.73	9.10	5.28	8.40	8.10	9.40	6.69	9.00
November	3.63	6.10	5.32	4.70	3.60	4.40	5.91	5.50	3.28	5.60
December	1.89	5.80	3.72	3.90	2.49	3.30	3.77	4.10	3.02	4.70
[%]	Average Relative Humidity									
	Aosta		Bergamo		Monza*		Trento		Varese	
January	57.47	83.45	84.07	83.13	89.79	85.47	74.65	83.47	65.98	73.28
February	59.52	79.33	73.25	73.11	53.84	78.24	53.86	79.46	76.92	71.12
March	54.17	72.79	71.84	66.77	69.69	81.08	60.57	72.07	67.78	73.61
April	50.68	70.96	78.97	59.61	71.38	72.79	62.81	71.80	81.79	70.60
May	60.71	73.34	76.12	68.88	64.45	64.69	59.95	67.76	73.15	71.48
June	57.94	70.52	71.29	62.68	51.42	67.55	60.15	69.31	80.07	83.49
July	56.57	69.00	71.34	62.99	54.25	54.51	61.93	63.13	75.77	73.98
August	61.41	73.59	73.51	63.38	56.58	67.06	62.02	64.45	78.41	71.46
September	59.10	75.32	72.91	65.23	59.88	80.19	66.83	72.87	82.88	77.30
October	64.37	81.30	85.36	71.79	73.72	88.38	81.91	76.44	85.44	79.80
November	66.11	87.12	81.51	79.87	76.19	89.96	76.16	83.76	90.00	96.49
December	70.96	85.01	83.81	79.94	81.56	87.97	80.72	84.31	86.99	89.11

\*Before 2004 the Monza was part of the Province of Milan and in UNI 10349:1994 the average values are reported only for the capital cities, so the data of Monza (now Province) are compared with those of Milan (around 15 km SW from Monza and in the same climatic zone).



Table 2a.3 – Selected months for the  $TRY_{EN}$ 

	<b>Aosta</b>	<b>Bergamo</b>	<b>Monza</b>	<b>Trento</b>	<b>Varese</b>
<b>Number of years</b>	8	10	9	10	9
<b>Years</b>	2000-2005; 2007-2008	1998-2005; 2007-2008	1999-2007	1996-1998; 2002-2008	1997-2000; 2003; 2005-2008
January	2001	2004	2003	1998	2003
February	2005	2008	2002	1996	2000
March	2000	2005	2003	2004	2007
April	2000	2004	2003	2004	2006
May	2001	2004	2004	2006	2007
June	2001	2004	2005	2004	1998
July	2002	2004	2005	2004	1997
August	2002	2004	2004	2005	1998
September	2004	2003	2004	2008	2006
October	2003	2003	2000	2005	1999
November	2000	2004	2004	2005	1997
December	2004	1999	2004	2008	2008

Table 2a.4 - Monthly average variables, monthly deviations (in grey column) with the monthly median values of the weather data series and selected year of the  $TRY_{EN}$ 

	<b>Average Dry Bulb Temperature [°C]</b>		<b>Daily Average Global Horizontal Radiation [MJ m<sup>-2</sup>]</b>		<b>Relative Humidity [%]</b>		<b>Selected Year</b>
	$TRY_{EN}$	$\Delta$	$TRY_{EN}$	$\Delta$	$TRY_{EN}$	$\Delta$	
January	2.48	-0.32	2.14	-0.07	88.22	0.39	1965
February	2.04	-0.93	4.30	-0.26	85.79	0.94	1984
March	5.90	0.09	7.57	-0.50	81.37	0.72	2008
April	9.98	1.39	12.64	-0.25	76.40	-0.01	2000
May	11.95	-0.89	16.39	-0.26	75.63	0.11	1973
June	15.10	-0.41	17.98	-0.03	76.26	-0.18	1964
July	17.41	0.39	16.89	0.43	77.95	-0.07	1985
August	17.50	0.52	14.06	-0.51	77.86	-1.62	1999
September	13.60	-0.62	10.17	-0.04	83.38	0.21	2008
October	10.41	-0.34	6.33	0.24	85.76	-0.66	2010
November	6.84	0.43	2.55	-0.19	89.58	0.73	2008
December	2.16	-1.61	1.63	-0.06	88.91	0.05	1964

### 2a.2.2 Annual energy needs and peak loads

In the next page, in Figures 2a.4 and 2a.5 the results for the energy needs and peak loads of the 48 thermal zones of the sample have been represented for the Italian localities.

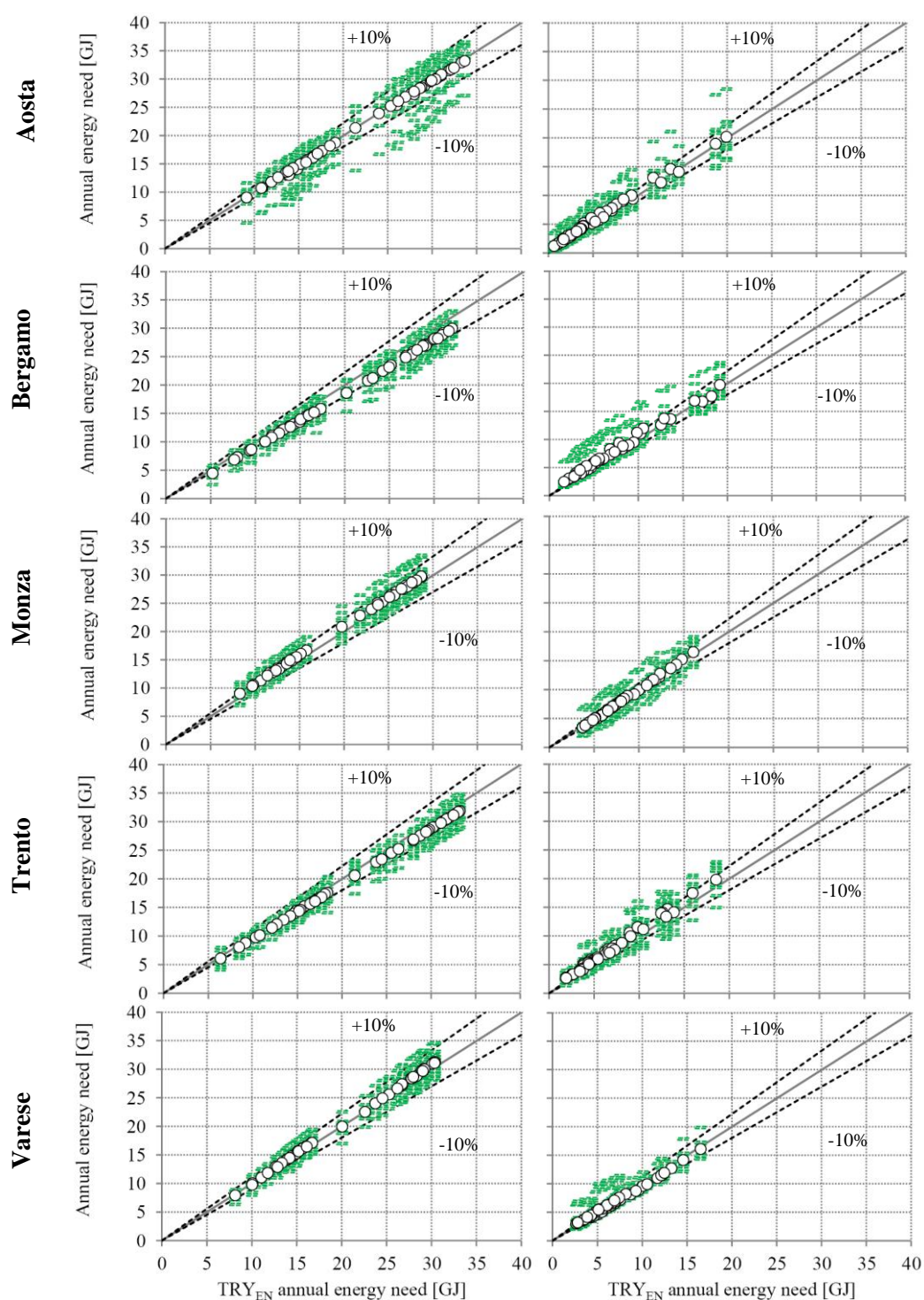


Figure 2a.4 - Heating (left) and cooling (right) energy needs: average energy needs (dots) and annual results in the multi-year series respect to the TRY<sub>EN</sub> values

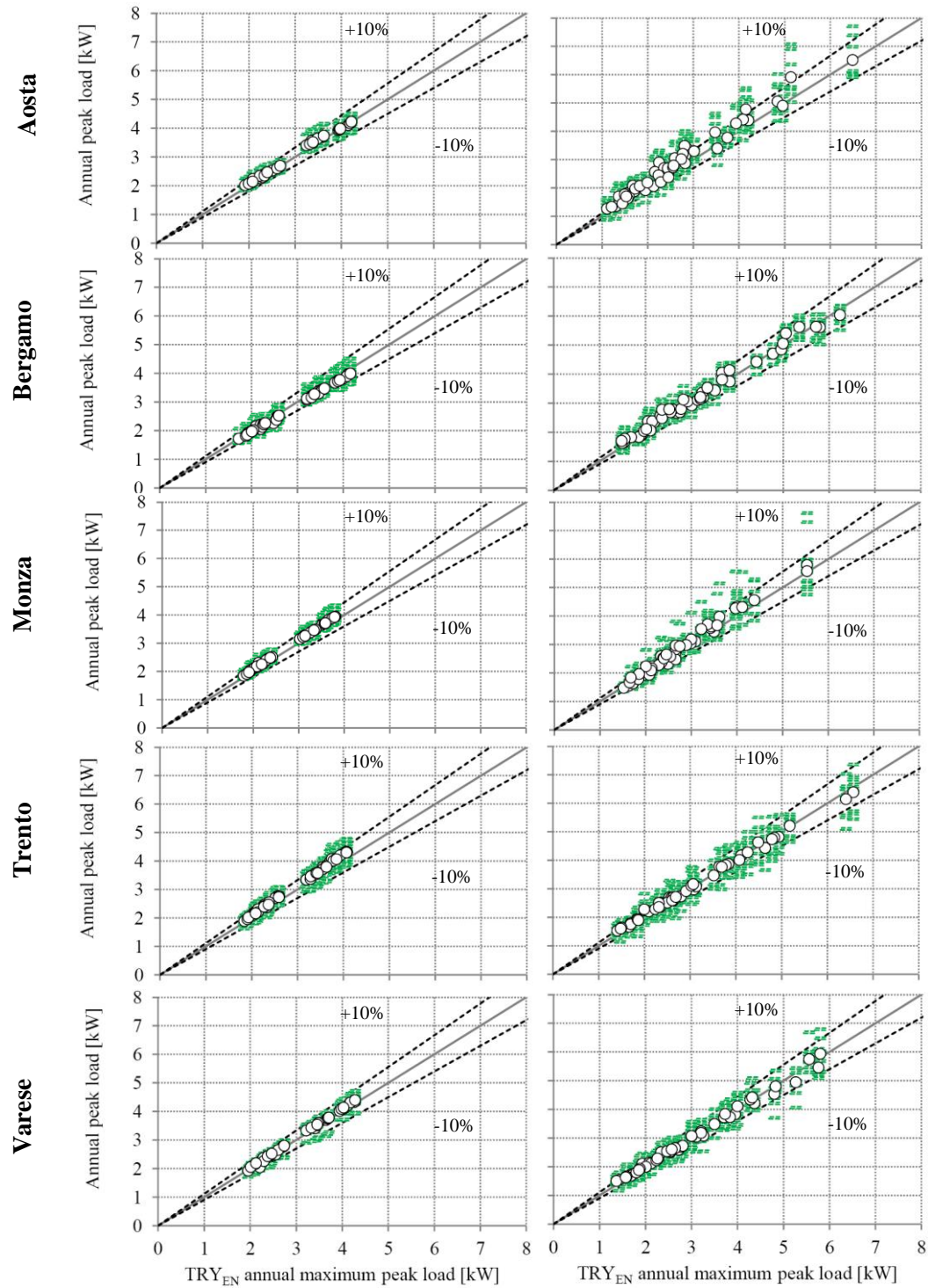


Figure 2a.5 - Heating (left) and cooling (right) peak loads: average peak loads (dots) and annual results in the multi-year series respect to the TRY<sub>EN</sub> values

In Figure 2a.6 the results for the energy needs of 48 thermal zones of the sample have been represented for the De Bilt.

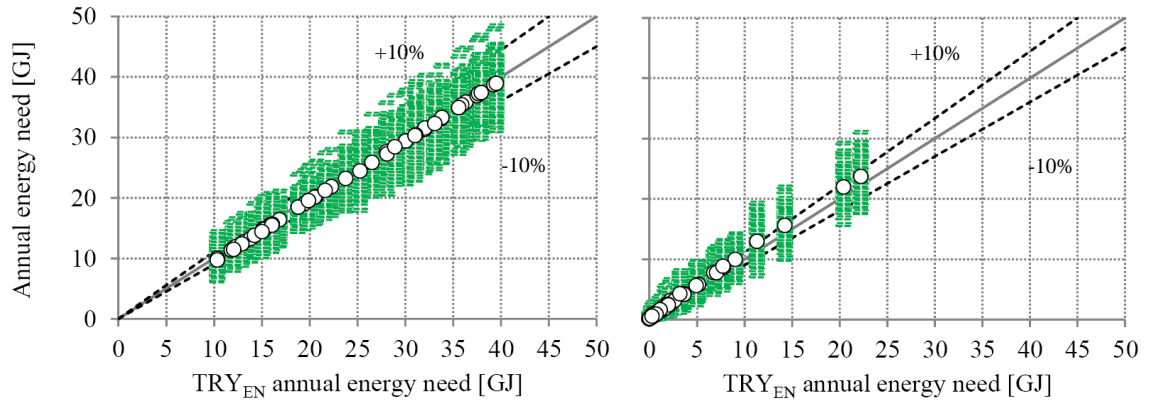


Figure 2a.6 - Heating (left) and cooling (right) energy needs: average energy needs (dots) and annual results in the multi-year series respect to the TRY<sub>EN</sub> values for De Bilt

And in Figure 2a.7 the heating and cooling peak loads are represented.

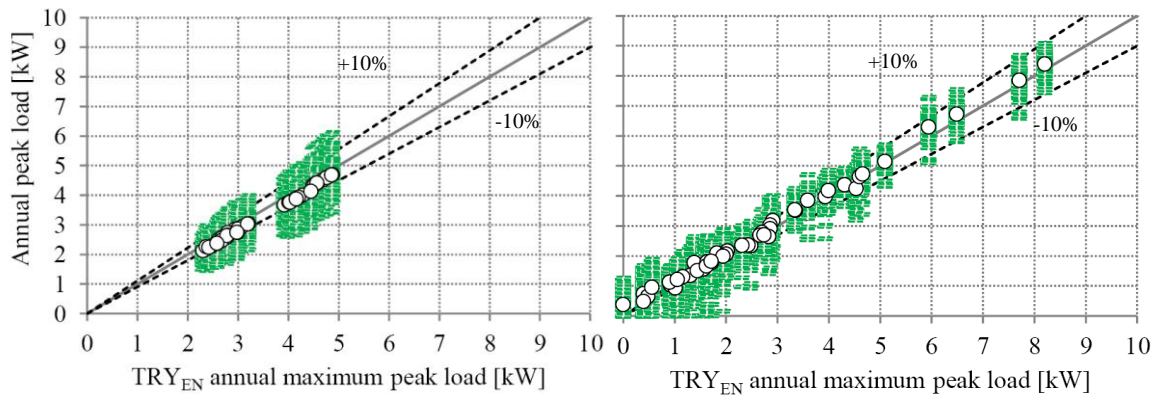


Figure 2a.7 - Heating (left) and cooling (right) peak loads: average peak loads (dots) and annual results in the multi-year series respect to the TRY<sub>EN</sub> values for De Bilt

### 2a.2.3 Statistics analysis

The indexes for the energy needs deviation have been represented in Figure 2a.8 and the ones for the peak loads in Figure 2a.9. Only the Italian locations have been considered, since De Bilt, characterized by completely different climatic conditions but, in particular, by a very larger number of years respect to the other localities, could lead to misleading results.

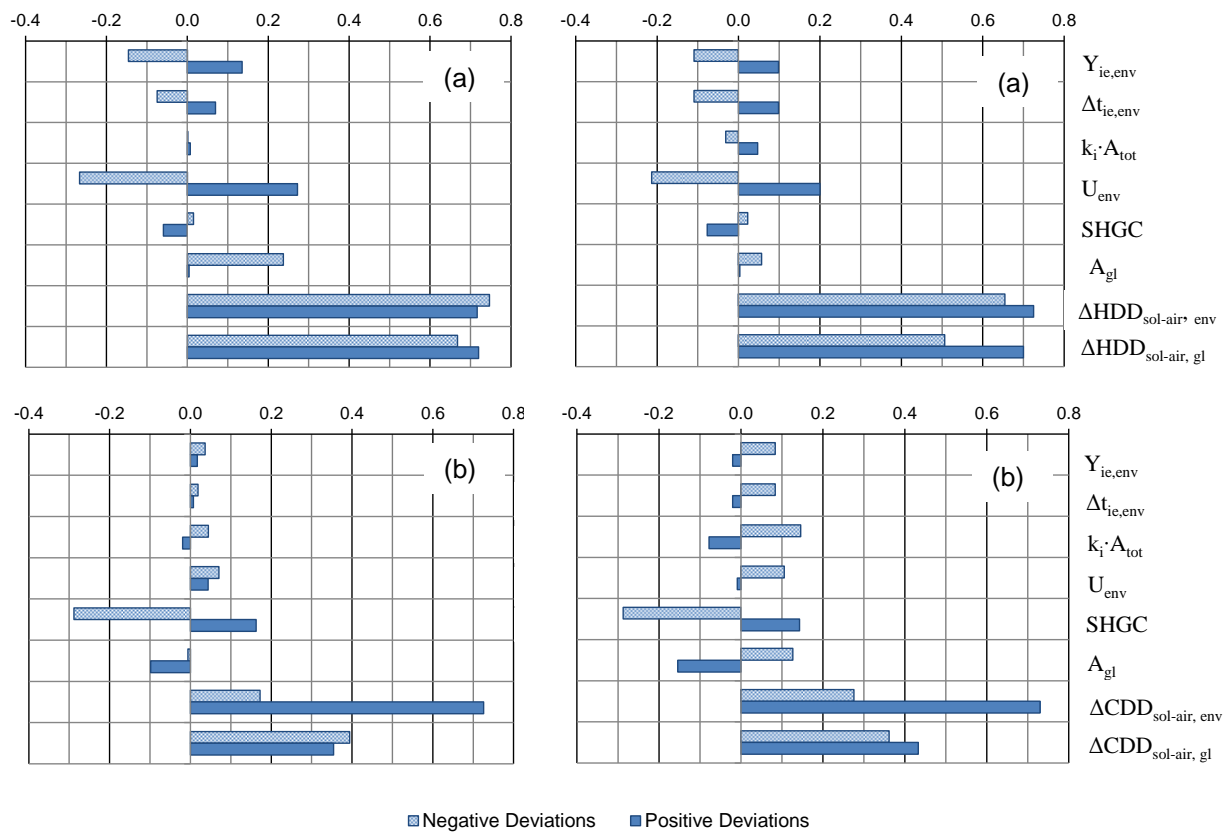


Figure 2a.8 - Correlations of the building envelope characteristics and the deviations of the annual heating energy needs (a) and annual cooling energy needs (b), evaluated by means of Pearson's index (left) and Spearman's index (right)

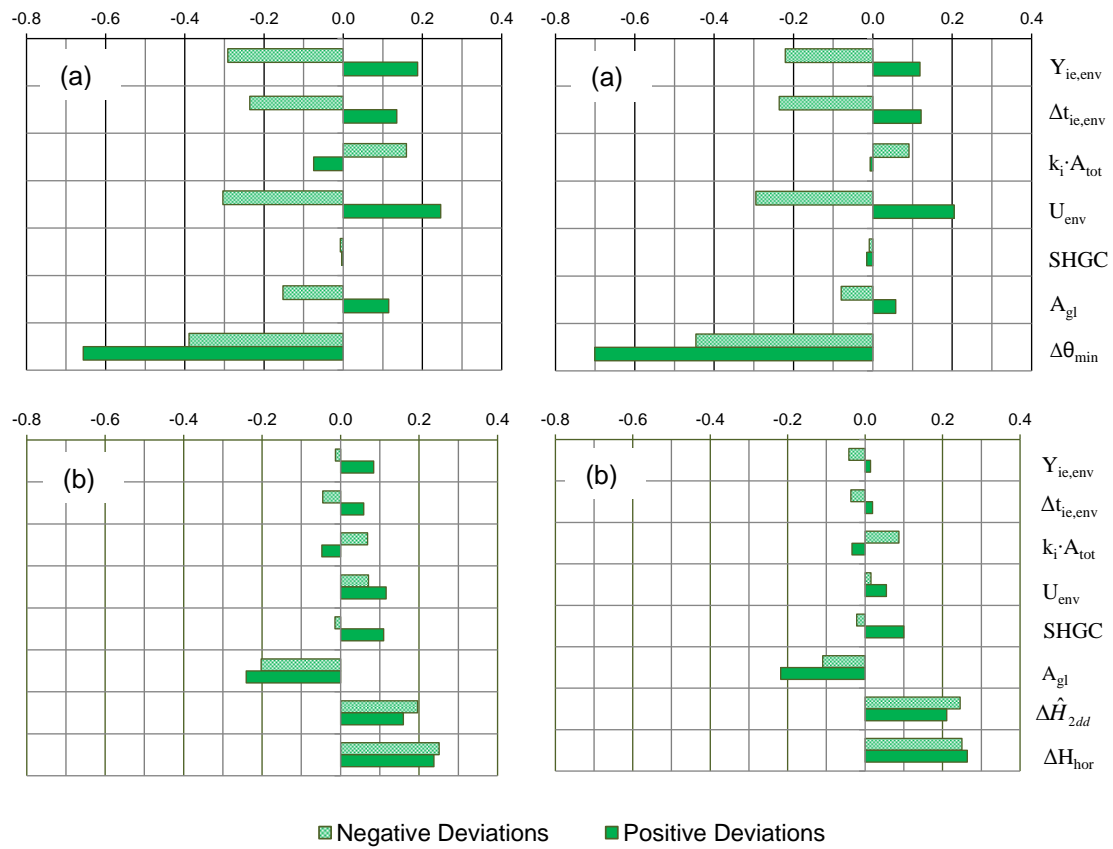


Figure 2a.9 - Correlations of the building envelope characteristics and the deviations of the annual heating peak loads (a) and annual cooling peak loads (b), evaluated by means of Pearson's index (left) and Spearman's index (right)



## 2a.3 Discussion

### 2a.3.1 Average monthly data

Looking at the Figures 2a.2, 2a.3 and those in Annex B, it can be noticed that the  $TRY_{EN}$  monthly value is generally within the range between the first quartile  $Q_1$  and the third quartile  $Q_3$ . Nevertheless, it is rarely close to the median for the three climatic parameters at the same time, especially for the Italian locations with a limited number of years in the starting collected data. Generally speaking, this is a consequence of the statistical method proposed by EN ISO 15927-4:2005 for the selection of each month, which minimizes the sum of the differences of the three parameters together.

In the perspective of the issue of the coherence between the BES tools and quasi-steady state method, analysed in depth in chapter 5, the average values have been evaluated. As regards the dry bulb temperature, in Aosta and in Varese the new  $TRY_{EN}$  are higher than the UNI 10349:1994 data (about +1.3 °C and +2.3 °C on an annual basis, respectively) while in Bergamo and Trento tend to be lower (about -1.7 °C and -1.2 °C, respectively). In Monza there are some months with lower values than the Standard and other higher but it has to be remarked that Monza is compared to the data of nearby city of Milan, since its mean values are not reported in UNI 10349:1994.

For what concerns the global horizontal solar radiation there is a reduction of the annual values of -10.1%, -19.4%, -10.9% and -15.9%, respectively for Aosta, Monza, Trento and Varese. For Bergamo there is a good agreement (+ 0.4%) but some discrepancies are present for the months of February, July and October.

The calculated relative humidity is lower in Aosta, Monza and Trento (-16.9%, -9.6% and -7.3% the mean annual deviations) and higher in Bergamo (+7.2% the mean annual deviation). In Varese the agreement is good, considering the mean annual values (+1.1%) but there is a significant variability in the different months (e.g., the standard deviation is around +6.1%).

Considering the location of De Bilt, the alignment between the  $TRY_{EN}$  and the medians is better than in the analysed Italian climates but some deviations are still present. As regards the dry bulb temperature, for example, for the month of April and December the  $TRY_{EN}$  values are outside the interquartile range (+1.39 °C and -1.69 °C, respect to the median). Referring to the solar radiation and to the humidity, both  $TRY_{EN}$  values are well aligned to the medians. The average daily solar radiation is in the interquartile range (i.e., between the internal discontinuous

lines in the graphs) and it is within the 5% of the median value (with the exception of the months of February, March and November, where it is slightly exceeded). The relative humidity presents a good alignment and the maximum deviation respect to the median is -1.6% in August.

Looking at Figure 2a.3, it is possible to notice the larger variability of the weather conditions in the 50 years of the series respect to the ones in the 5 North Italy locations, in particular considering the spread between the maximum and the minimum values of the weather variables.

### ***2a.3.2 Annual energy needs and peak loads***

In the discussion of the annual energy needs and peak loads results, the Italian locations are analysed together, since the number of years is more or less the same for each locality, and, after this part, De Bilt is considered.

#### **2a.3.2.1 Annual energy needs and peak loads: North Italy locations**

For the heating energy needs, the average values are generally within the  $\pm 10\%$  range, which means that the error provided by the TRY<sub>EN</sub> weather data respect of the average of multi-year real data is under the 10%.

In the five Italian locations, the general trend of the deviation is not the same:

- in Bergamo and in Trento the TRY<sub>EN</sub> weather files lead to overestimations of the heating energy needs with respect of the average over the multi-year series;
- in Monza the TRY<sub>EN</sub> weather file shows an underestimation;
- in Aosta and in Varese there is a good agreement between the results simulated with the TRY<sub>EN</sub> file and the average values on the multi-year series.

Also for the cooling energy needs, the differences between the TRY<sub>EN</sub> results and the averages on the multi-year series are generally within  $\pm 10\%$ :

- by using the TRY<sub>EN</sub> weather data, in Trento there is an underestimation of the cooling needs while in Bergamo there is a light overestimation;
- for the other localities a good agreement is registered.



For the heating peak loads represented in Figure 2a.5, the deviations between the  $TRY_{EN}$  results and the averages over the multi-year series are within a range of 10%:

- for all the locations except Bergamo the  $TRY_{EN}$  weather file causes a light underestimation, which is more marked for Trento;
- in Bergamo there is an overestimation by the  $TRY_{EN}$  weather file.

Also for the cooling peak loads, the results are generally within the  $\pm 10\%$  range but the deviations present a larger variability. The  $TRY_{EN}$  weather file causes an underestimation for Aosta while for the other locations there is a good agreement.

Both for the energy needs and the peak loads, for the heating analysis the results are well aligned while for the cooling one a certain variability can be observed, demonstrating that the considered buildings present different responses to the use of a  $TRY_{EN}$  weather file instead of the multi-years data.

#### **2a.3.2.2 Annual energy needs and peak loads: De Bilt**

In the previous paragraph some considerations about the representativeness of the  $TRY_{EN}$  weather data have been done. Even if the deviations respect to the average energy needs and peak loads are within a range of 10%, in some case the  $TRY_{EN}$  were not well representative, clearly overestimating or underestimating the average energy performance of the sample of considered buildings.

The main limitation of the weather data developed according to the EN ISO 15927-4:2005 for the Italian localities is related to a low number of years which makes not easy to find the properly representative month. Moreover, by using the same weights for each main primary parameter and giving the same importance to the three weather variables at the same time, the task becomes more difficult with this limited number of data. In this second part of the annual energy results analysis, a location with a large number of collected data is considered in order to see if the representativeness problem can be mitigated with more data.

Respect to the results for the North Italy locations, a larger spread is encountered and it is due to the larger variability of climatic conditions during the considered period. The annual heating needs simulated by using the  $TRY_{EN}$  are well representative of the long-term averages over the whole data series. For the annual cooling energy needs there is a light underestimation by the  $TRY_{EN}$  respect to the long-term averages.

The heating peak loads are clearly overestimated by using the  $TRY_{EN}$  but within the  $\pm 10\%$  range. Similarly to what observed in the Italian localities, for the cooling peak loads there is a larger variability but the  $TRY_{EN}$  is in good agreement with the long-term averages.

As a whole, it can be stated that a large number of years allows to get better results in term of representativeness of the developed  $TRY_{EN}$ , even if the problem doesn't seem to be completely solved, since some discrepancies are still present.

In order to optimize the representativeness of the weather data, in accordance with what found by some authors in literature and coherently with what prescribed by the EN ISO 15927-4:2005, the  $TRY_{EN}$  calculation procedure can be modified introducing weighting factors for the different primary variables to develop TRY for specific purposes (e.g., heating or cooling energy needs evaluation). This is partially already done for the design days according to the EN ISO 15927-2:2009 (CEN, 2009) and could be extended to the TRY calculations.

### **2a.3.3 Statistics analysis**

Looking at Figure 2a.8, the parameter whose correlation with the variability of the heating energy needs is more easily found, is, as expected, the deviation of the equivalent heating degree days. In the reduction of the variability, an important role belongs to the characteristics of the opaque components (limiting  $U_{env}$ ,  $Y_{ie,env}$  and  $\Delta t_{ie,env}$  the variability of the energy needs is reduced) but it has be remarked that the correlation level is small, particularly if compared to the one of the equivalent heating degree days. For the cooling deviations, the most correlated parameter, besides the deviation of the cooling degree days, is the solar heat gain coefficient. Also the glazing area appears to have a light correlation for the positive deviations.

Looking at Figure 2a.9, for the heating peak loads the most influencing parameter on the variability is the deviation of the minimum external temperature. The opaque components are the most correlated with the variability of the peak deviations, both on the steady and dynamic points of view. For the cooling peak loads, the variables chosen for describing the external forcing solicitation are not able to fully justify the variability by themselves. With the exception of the glazing area, the correlations appear very weak, suggesting that interactions between the different characteristics (dynamics of the opaque components and entering solar radiation through the glazings) could be pursued to reduce the variability of the cooling peak loads.

Generally, Pearson's and Spearman's indexes assume similar values, especially when the correlation is relevant, suggesting that the most relevant correlations can be approximated by linear trends in the monotonic domains.

## 2a.4 Main findings

In this part of chapter 2, a comparison between the  $TRY_{EN}$  weather files calculated in accordance with the EN ISO 15927-4:2005 procedure and the original multi-year series of the data has been carried on for different locations, analysing the annual energy needs and the peak loads of a set of reference buildings.

Analysing the monthly average temperatures, solar radiation and humidity it has been noticed that the correspondence with the  $TRY_{EN}$  values and the averages is not good for the 3 parameters at the same time. About the building energy performance considered as representativeness index (i.e., annual heating and cooling energy needs and peak loads), the deviations of  $TRY_{EN}$  results from the mean of the results of the multi-year series are within 10% but in some cases (as for Trento and Bergamo) the  $TRY_{EN}$  overestimates/underestimates respect to the average values. In order to verify if the problem can be solved by using a larger number of years for the development of the test reference year, the location of De Bilt, with more than 50 years available, has been analysed. The representativeness, respect to the North Italy localities with only 10 years, is improved but some discrepancies are still present. This suggests a possible change of the standard procedure by introducing weighting coefficients, in order to develop different  $TRY_{EN}$  to use for specific purposes, as already underlined in literature and by the EN ISO 15927-4:2005 itself or done specifically for the design days (as in EN ISO 15927-2:2009).

In order to show how the multi-year series could be used for a design robust to the climatic variability, the correlations between the building envelope characteristics and the variability of the energy performances in a multi-year analysis have also been considered for the Italian locations. When a building characterized by low values of thermal transmittance and dynamic parameters of the opaque components is simulated, the variability of the heating energy needs and peak loads is more limited. The solar heat gain coefficients and the window size are correlated with the cooling energy needs and peak loads (and, so, generally speaking, the reduction of the entering solar radiation can limit the variability of the cooling energy performance).



## Part b: Boundary conditions for walls and floors in touch with the ground in BES

### 2b.1 Method

In this paragraph, the cases and the methods considered for the analysis, those presented in EN ISO 13370:2007 and the finite element modelling (*FEM*), have been described.

#### 2b.1.1 Tested slab on ground cases and boundary conditions

There are many configurations of walls and floors in touch with the ground. In this study, the simplest one (i.e., the slab-on-ground) has been selected for carrying on the analysis.

As reference cases, slabs-on-ground with a 20 cm thick clay block floor slab and variable thickness of the insulation layer (0-5-10 cm) have been chosen. The clay block has a thermal conductivity of  $0.25 \text{ W m}^{-1} \text{ K}^{-1}$ , a density of  $850 \text{ kg m}^{-3}$  and a specific heat capacity of  $840 \text{ J kg}^{-1} \text{ K}^{-1}$  while the insulation layer has a thermal conductivity of  $0.04 \text{ W m}^{-1} \text{ K}^{-1}$ , a density of  $40 \text{ kg m}^{-3}$  and a specific heat capacity of  $1470 \text{ J kg}^{-1} \text{ K}^{-1}$ . Two positions of the insulation layer (internal or external side) and three different kinds of soil (clay, sand or rock) have been considered. The part of the building above the ground has a 3 m of internal height and it is entirely composed by the same opaque structure considered for the slab.

The internal area of the floor is  $100 \text{ m}^2$  and its shape has been varied considering a square floor (i.e., 1:1 aspect ratio, defined as the ratio between the floor sides) and three different rectangular shapes (with 1:4, 2:4, 3:4 aspect ratios). In Table 2b.1 the thermal properties of the soil and the floor slab are reported and in Table 2b.2 the external dimensions of the sides for the different aspect ratios.

Table 2b.1 - Thermal properties of the soil and thermal conductance of the considered floors

	Soil			Floor slab
	$\lambda [\text{W m}^{-1} \text{ K}^{-1}]$	$\rho c [\text{J m}^{-3} \text{ K}^{-1}]$		$A [\text{W m}^{-2} \text{ K}^{-1}]$
clay	1.5	$3.0 \cdot 10^6$	no insulation	1.25
sand	2	$2.0 \cdot 10^6$	5cm insulation	0.49
rock	3.5	$2.0 \cdot 10^6$	10cm insulation	0.30

*Table 2b.2 - Size and external dimensions of the floor*

<b>Dimensions</b> Insulation (m)		<b>0.00</b>	<b>0.05</b>	<b>0.10</b>
<b>4:4</b>	<b>Side1</b>	10.40	10.50	10.60
	<b>Side2</b>	10.40	10.50	10.60
<b>3:4</b>	<b>Side1</b>	9.06	9.16	9.26
	<b>Side2</b>	11.94	12.04	12.14
<b>2:4</b>	<b>Side1</b>	14.54	14.64	14.74
	<b>Side2</b>	7.47	7.57	7.67
<b>1:4</b>	<b>Side1</b>	5.40	5.50	5.60
	<b>Side2</b>	20.40	20.50	20.60

The surface convective coefficients have been calculated in accordance with the technical Standard EN ISO 6946:2007 and they are  $25 \text{ W m}^{-2} \text{ K}^{-1}$  for the external wall and ground surfaces, while for the internal ones,  $7.69 \text{ W m}^{-2} \text{ K}^{-1}$ ,  $10 \text{ W m}^{-2} \text{ K}^{-1}$  and  $5.88 \text{ W m}^{-2} \text{ K}^{-1}$ , for the vertical wall, the ceiling and the floor, respectively. Both steady state and transient analyses have been performed.

In the steady state analysis, the boundary temperatures are a fixed at  $-5 \text{ }^{\circ}\text{C}$  for the external air, as prescribed in the design calculation for many locations in the Northern Italy by the UNI EN 12831:2006 (UNI, 2006), and at  $20 \text{ }^{\circ}\text{C}$  for the internal air, while an equivalent convective thermal condition is imposed for all the internal and external walls surfaces.

For the steady state conditions, the specific heat flux has been calculated in order to compare the different cases. It has been computed dividing up the heat flow through the ground - obtained by means of the finite elements model and evaluated at the internal floor surface - by the floor area and by the difference of temperature (i.e.,  $|\theta_i - \theta_e| = 25^{\circ}\text{C}$ ) used for the simulations in steady state regime.

$$\varphi_g = \frac{\Phi}{A \cdot |\theta_i - \theta_e|} \quad (2b.1)$$

$$\Delta_g = \frac{\Phi}{\Phi_{tot}} \cdot 100 \quad (2b.2)$$

The transient analysis is divided into a first part, in which a daily outdoor temperature variation is considered, and a second part where a yearly period is investigated. For both cases a fictive external forcing temperature with a mean value of  $-5 \text{ }^{\circ}\text{C}$  and an amplitude of  $15 \text{ }^{\circ}\text{C}$  is considered but in the first case the period is 24 h while in the second one it is 1 year-long with a

daily discretization. The daily variation has been considered to evaluate the potential effects on the building dynamic response while the yearly one for the assessment of the time lag between the annual forcing signal and the heat flux through the ground.

The first transient analysis has been performed for the cases with a square floor (4:4 aspect ratio) and the profiles of temperatures and flows of the 10<sup>th</sup> day have been studied in order to have stabilized profiles. The case without insulation, with a 4:4 aspect ratio building and a clay soil, has been selected in order to perform a yearly simulation and it has been run till a stabilized regime is reached.

### ***2b.1.2 EN ISO 13370:2007 method***

The slab-on-ground floors are defined by the technical Standard as any kind of floor consisting of a slab in contact with the ground over its whole area, whether or not supported by the ground over the whole area, and situated at the level (or near the level) of the external ground surface.

The floor slab may be without insulation layer, or evenly insulated (above, below or within the slab) over its whole area. A correction on the thermal transmittance is also foreseen by the technical Standard if the floor has horizontal or vertical edge insulation. The thermal transmittance depends on the characteristic dimension of the floor,  $B'$  (i.e., area of the floor divided by half of the perimeter) given by Eq. (2b.3), and on the total equivalent thickness,  $d_t$ , given by Eq. (2b.4).

$$B' = \frac{A}{0.5P} \quad (2b.3)$$

$$d_t = w + \lambda(R_{si} + R_f + R_{se}) \quad (2b.4)$$

The characteristic dimension  $B'$  assumes the following values for the tested cases: 5 m (4:4 aspect ratio), 4.95 m (3:4 aspect ratio), 4.71 m (2:4 aspect ratio) and 4 m (1:4 aspect ratio).

The thermal resistance of dense concrete slabs and thin floor coverings may be neglected. Hardcore filling below the slab is assumed to have the same thermal conductivity as the ground, and its thermal resistance should not be included. The thermal transmittance  $U$  is computed using Eq. (2b.5) for the case with  $d_t < B'$  (i.e., not insulated and moderately insulated floors), or Eq. (2b.6) for the case with  $d_t > B'$  (i.e., well-insulated floors).



$$U = \frac{2\lambda}{\pi B' + d_t} \ln \left( \frac{\pi B'}{d_t} + 1 \right) \quad (2b.5)$$

$$U = \frac{\lambda}{0.457 \cdot B' + d_t} \quad (2b.6)$$

The steady state ground heat transfer coefficient  $H_g$  between internal and external environments is then obtained using Eq. (2b.7).

$$H_g = AU + P\Psi_g \quad (2b.7)$$

In this analysis, the linear transmittance relevant to the thermal bridges (i.e.,  $\Psi_g$  relevant to the wall-floor junction) has been evaluated applying the finite element modelling procedure in agreement with EN ISO 10211:2007 (CEN, 2007b).

In accordance with the technical Standard, the monthly heat flow rate can be evaluated using an external yearly sinusoidal forcing temperature or monthly average temperatures. In the first case the Standard proposes a sinusoidal function which can be used for determining both the internal and the external temperatures  $\theta_{k,m}$  for each month  $m$  of the year:

$$\theta_{k,m} = \bar{\theta}_k - \hat{\theta}_k \cos \left( 2\pi \frac{m - \tau}{12} \right) \quad (2b.8)$$

where  $k$  stands for  $i,e$  (internal or external),  $\bar{\theta}_k$  is the yearly average temperature,  $\hat{\theta}_k$  is the yearly amplitude and  $\tau$  indicates the month characterised by the minimal temperature.

Considering a fixed internal temperature, as in this study, the heat flow for the month  $m$  is:

$$\Phi_m = H_g (\bar{\theta}_i - \bar{\theta}_e) + H_{pe} \hat{\theta}_e \cos \left( 2\pi \frac{m - \tau - \beta}{12} \right) \quad (2b.9)$$

where  $H_{pe}$  is the external periodic heat transfer coefficient which is defined differently for the various slabs. For the uninsulated slab-on-ground:

$$H_{pe} = 0.37P\lambda \ln \left( \frac{\delta}{d_t} + 1 \right) \quad (2b.10)$$

with  $\delta$  is the periodic penetration depth. Its value is 2.2 m for the clay, 3.2 m for the sand and 4.3 m for the rock soil.

The  $\beta$  parameter is the time lag of the heat flow with the respect of the external temperature:

$$\beta = 1.5 - 0.42 \ln \left( \frac{\delta}{d_t + 1} \right) \quad (2b.11)$$

A typical value of the time lag for the slab-on-ground without edge insulation is 1 month.

Considering the monthly average external temperatures, the time shift is neglected and the heat flow for the month  $m$  becomes:

$$\Phi_m = H_g (\bar{\theta}_i - \bar{\theta}_e) + H_{pe} (\bar{\theta}_e - \theta_{e,m}) \quad (2b.12)$$

The EN ISO 13370:2007 provides instructions to identify the boundary conditions for the dynamic simulation codes. A ground layer thick 0.5 m and a virtual layer have to be added to the floor. The virtual layer thermal resistance can be calculated as:

$$R_V = \frac{I}{U} - R_{si} - R_f - R_g \quad (2b.13)$$

And  $R_g$  is the thermal resistance of the 0.5 m of soil. At the bottom of the virtual layer is applied a virtual temperature  $\theta_v$ :

$$\theta_{v,m} = \theta_{i,m} - \frac{\Phi_m}{AU} \quad (2b.14)$$

The accuracy in determining the virtual boundary temperature is so dependent on the heat flow calculation accuracy.

### **2b.1.3 Finite elements modelling**

The slab on ground test case has been discretised using a 3-dimensional geometry. Taking advantage of the geometry symmetries, only a quarter of the building has been modelled in agreement with the standard procedure. The Partial Differential Equations (PDE's) discretization and solution procedure has been carried out by means of finite elements approach (*FEM*). The temperature values of the external and internal air have been assumed as boundary conditions. Both steady state and time-variable conditions on the external air have been considered for the simulations.

The total number of cells ranges between  $6.5 \cdot 10^5$  and  $1.4 \cdot 10^6$ , depending on the building aspect ratio. The calculations have been performed in double precision (convergence parameter equal to  $10^{-10}$ ), so that ensuring an accurate energy balance, independently from the materials and the boundary conditions. The 3-dimensional heat flux at the ground has been computed at the internal surface of the floor slab.

The procedure proposed in the Standard EN ISO 10211:2007 has been followed and the scheme in Figure 2b.1 has been assumed to carry out a detailed simulation of the whole building-ground system. 2D *FEM* simulations have been carried out in order to estimate the linear thermal transmittance associated with the wall-floor junction  $\Psi_g$ .

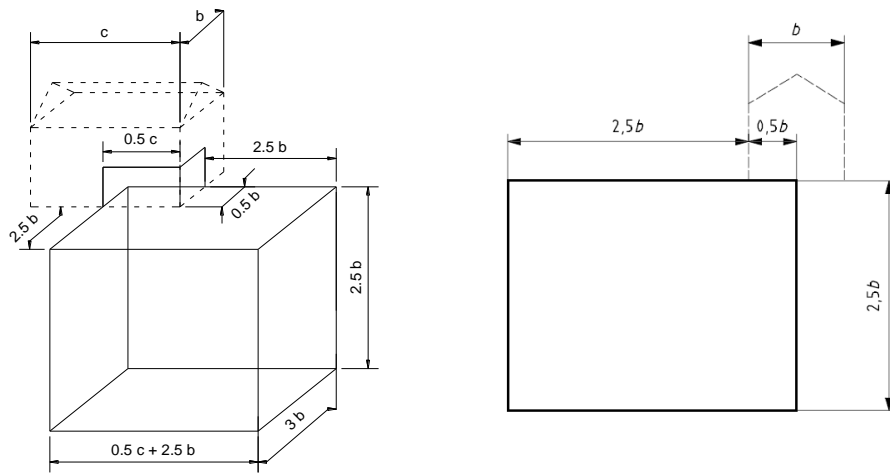


Figure 2b.1 - 3-dimensional model (left) and 2-dimensional model (right) according to EN ISO 10211:2007

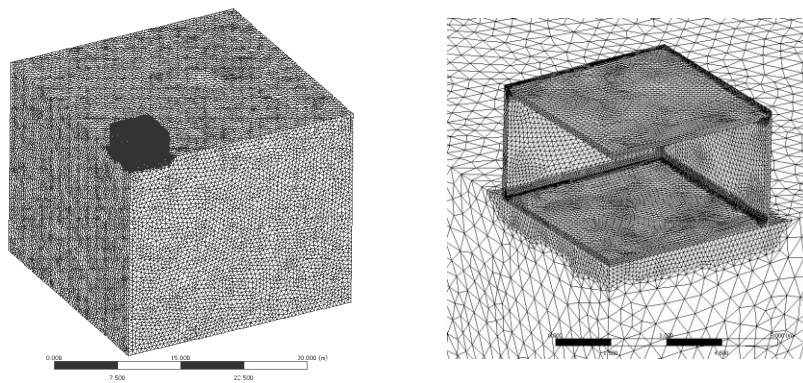


Figure 2b.2 – Example of FEM model geometry and mesh

## 2b.2 Results

### 2b.2.1 Steady-state conditions: FEM and EN 13370:2007 models

Figure 2b.3 shows the ground specific heat flux  $\phi_g$  and the ground heat flow share  $\Delta_g$  as functions of ground and floor slab thermal properties.

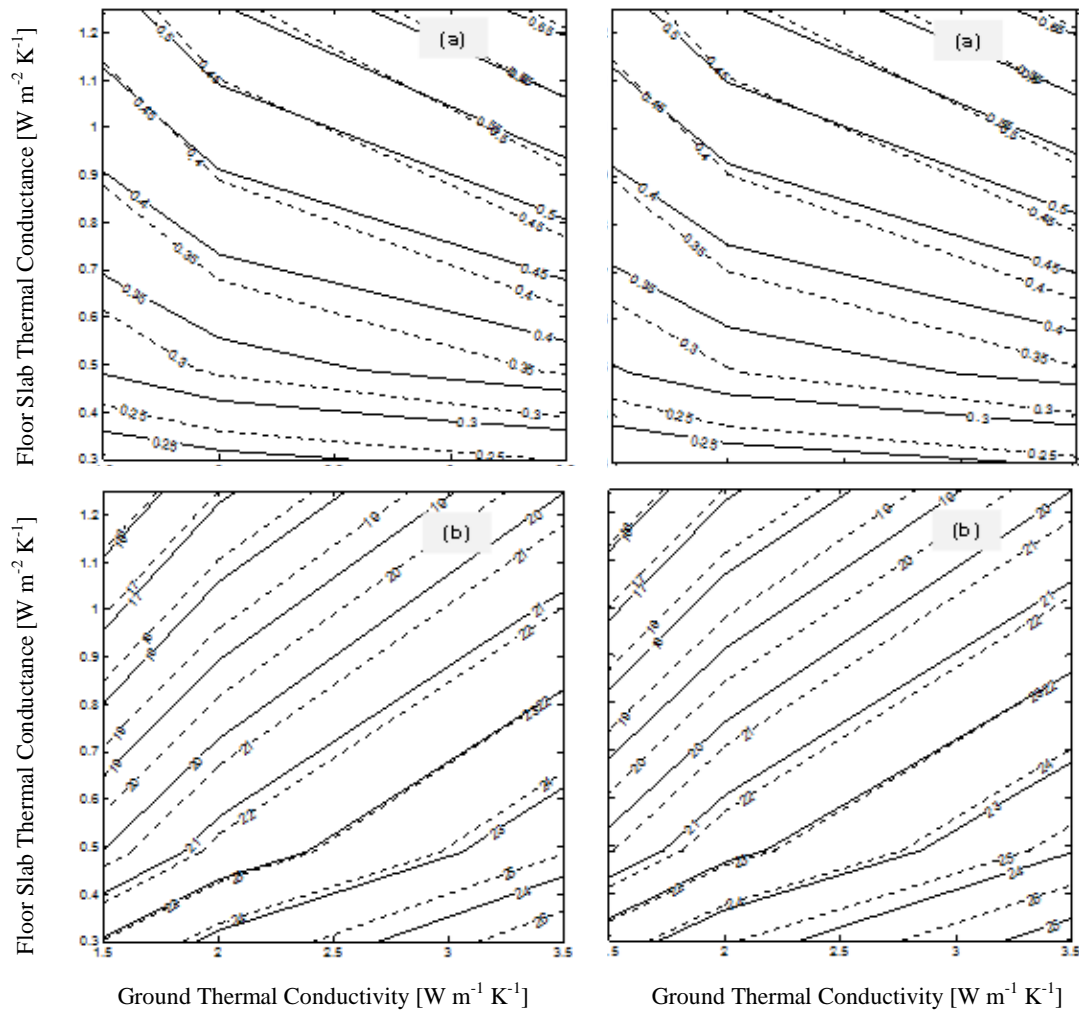


Figure 2b.3 – Specific equal heat flux curves  $[\text{W m}^{-2}]$  (a, on the top) and ground heat flow share curves [%] (b, on the bottom) computed by the FEM model as a function of ground and floor slab thermal properties: thermal insulation layer either on the external (left) or on internal (right) side (continuous lines refer to 1:4 aspect ratio and dashed line to 4:4 aspect ratio)

The absolute and percentage deviations between the specific heat fluxes elaborated by means of the *FEM* approach and the ones by means of the EN ISO 13370:2007 procedure have been calculated and represented in Figure 2b.4 as functions of floor slab thermal conductance, aspect ratios and ground type.

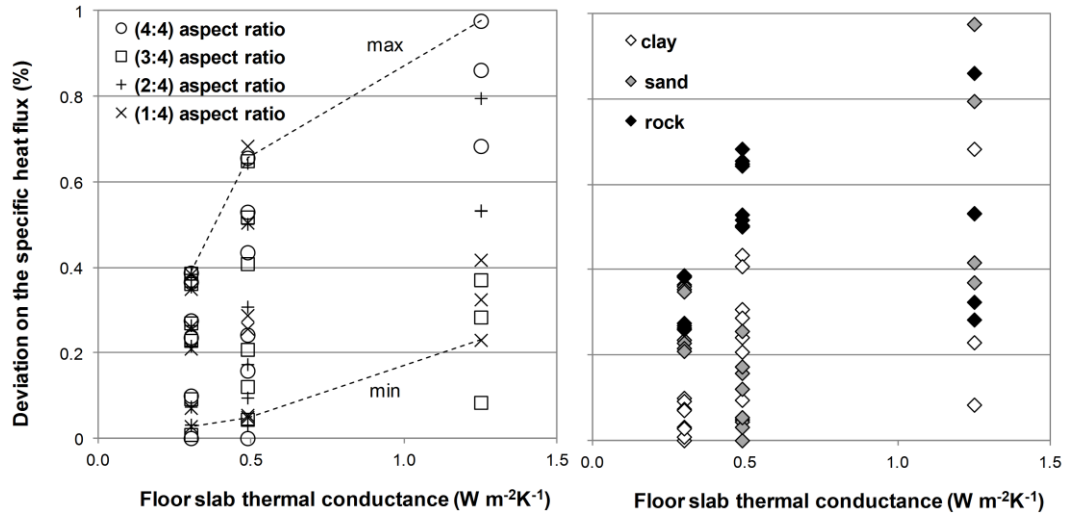


Figure 2b.4 - Absolute percentage deviations between the specific heat flux at the ground computed by means of the finite elements model (steady state regime) and by means of the EN ISO 13370:2007 procedure as a function of floor slab thermal conductance, aspect ratios (on the left) or ground type (on the right). Dashed lines represent the envelope curves relevant either to the maximum or the minimum values for the limit aspect ratios (4:4 and 1:4)

### 2b.2.2 Periodic sinusoidal regime

In the previous paragraph, the accuracy of the EN ISO 13370:2007 method has been assessed by means of a comparison with the *FEM* methods to pay attention, in particular, to the effects of the aspect ratio and of the kind of soil. In this section, the results of the *FEM* models, run in a periodic sinusoidal regime, have been reported.

For the daily sinusoidal regime, the results, expressed in terms of the temperature on the bottom of the slab  $\theta_{slab}$  and heat flow  $\Phi$  at the floor internal surface - obtained through the *FEM* simulations in dynamic regime - have been compared with a steady state case  $\theta_{slab,st}$  and  $\Phi_{st}$  seen in the previous paragraph. An example of the results, for an uninsulated case, with rock soil, has been reported in Figure 2b.5.

As stated in the Paragraph 2b.1, also for the yearly regime the stabilization has been pursued and it has been achieved after a three periods run. The internal heat flow  $\Phi$  and the temperature on the bottom of the slab-on-ground floor  $\theta_{slab}$  have been represented in Figure 2b.6.

The heat flow values have been used for the estimation of the monthly virtual temperatures in agreement with the technical Standard procedure, as in Figure 2b.7.

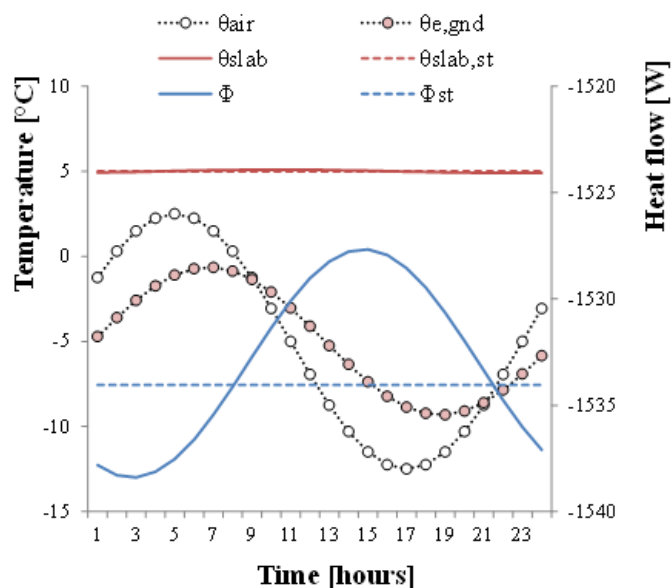


Figure 2b.5 - Daily variation of the temperatures and heat flows: comparison of the FEM model in dynamic regime with the steady state approach (rock soil, uninsulated floor slab and 4:4 aspect ratio)

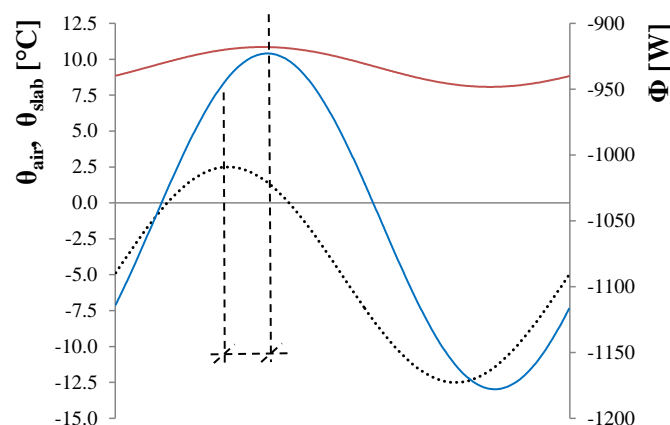


Figure 2b.6 - Yearly variation of the external temperature  $\theta_{air}$  (black dotted lines) for an uninsulated floor slab, 4:4 aspect ratio and clay soil: the temperature on the bottom of the slab-on-ground floor  $\theta_{slab}$  (red solid line) and internal heat flow  $\Phi$  (blue solid line) calculated by the FEM simulation

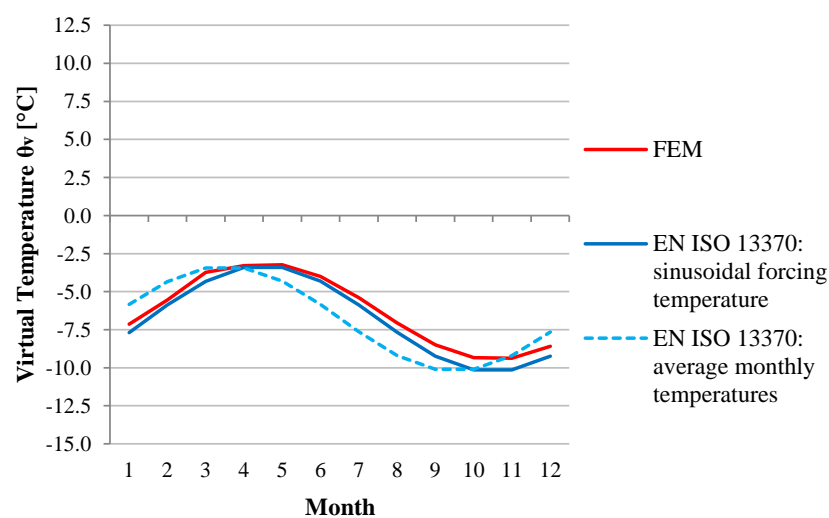


Figure 2b.7 - Virtual temperatures calculated starting from different monthly heat flow rate (rock soil, uninsulated floor slab and 4:4 aspect ratio)

## 2b.3 Discussion

The results presented in the previous section are here presented, distinguishing the steady state and the dynamic problems.

### *2b.3.1 Steady-state conditions: FEM and EN 13370:2007 models*

The effect of the shape can be analysed looking at Figure 2b.3, where the continuous lines refer to 1:4 aspect ratio and dashed line to 4:4 aspect ratio. Also the position of the insulation layer - either considered on the external or on internal side - has been here taken into account, in Figure 2b.3 (left) and (right), respectively.

In particular, in the bottom of the Figure, the ground heat flow share, expressed as percentage, is indicated. It represents the ground heat flow on the total heat flow exchanged by the building through envelope as if it was homogeneously opaque. As expected, the contribution of the heat losses towards the ground becomes more significant as the thermal conductance of the envelope decreases (the thermal conductance of the whole envelope is equal to the floor slab one). Considering the same conditions, the share of the ground heat flow is lower for 4:4 aspect ratio than the ones relevant to the 1:4 ratio, confirming the higher performance of compact structures regarding the heat exchange through the ground. Moreover, assuming the same envelope thermal conductance, the use of an insulation layer on the internal side gives a slightly higher ground heat flow share than the one obtained using the same layer on the external side.

The specific heat flux computed by means of the *FEM* model has been considered as a benchmark and an assessment of the deviations between the one computed by means of the finite elements model and the one calculated by means of the EN ISO 13370:2007 procedure has been carried out. Figure 2b.4 shows the computed deviations (as absolute values) as a function of floor slab thermal conductance and either aspect ratios (on the left) or ground type (on the right). Dashed lines represent the envelope curves relevant to the maximum and the minimum values for the limit aspect ratios (4:4 and 1:4 respectively). As a whole, the computed deviations are characterised by small values, always lower than 1%, with a decreasing trend as the floor slab thermal conductance decreases. Regarding the shape of the building, the higher the slab thermal conductance values, the higher the differences between buildings with low and high aspect ratios. Buildings structures with 4:4 ratio are subjected to higher errors when using the Standard procedure, resulting in values up to 0.98%. This residual discrepancy is due to the



modelling of the thermal bridges, whose linear coefficient has been derived in a 2-dimensional analysis.

The variation in the thermal properties of the ground (i.e., varying the kind of soil) also affects the performance of the Standard computation if compared with the *FEM* modelling. In particular, the maximum deviations have been detected for the rocky and sandy grounds, which are characterised by the higher thermal conductivities. On the contrary, the values of the deviations relevant to the clay soil - which is characterised by the lowest thermal conductivity - are generally lower.

### ***2b.3.2 Periodic sinusoidal regime***

Considering the daily regime, the maximum deviations in terms of heat flow (5.36 W) have been computed in the uninsulated floor slab in case of rock having the highest thermal diffusivity ( $1.75 \times 10^{-6} \text{ m}^2 \text{ s}^{-1}$ ), followed by sand (5.04 W, thermal diffusivity  $1.00 \times 10^{-6} \text{ m}^2 \text{ s}^{-1}$ ) and clay (4.92 W), whose thermal diffusivity value ( $5.00 \times 10^{-7} \text{ m}^2 \text{ s}^{-1}$ ) is the lowest. When the floor is insulated the deviations are approximately 1 W. Considering the percentage deviation of the peak respect to the steady state value, for the uninsulated cases the deviation is less than 0.5% and for the insulated ones less than 0.2%. Consequently, steady state boundary conditions could be assumed in hourly dynamic simulation, especially when interested in evaluating short periods of few or just one design day.

As concerns the yearly regime, the temperature on the bottom of the slab and the internal heat flow of the slab have a displacement with respect to the external air temperature. The time shift is equal to 32 days (approximately 1 month, coherently with the Standard suggestion).

Analysing the results arising from the yearly analysis, the *FEM* daily-discretised results have been used for the computation of the monthly average heat flow rates which have been compared to the ones calculated in accordance with EN ISO 13370:2007. The heat flow evaluated considering the technical Standard sinusoidal forcing temperature and a time lag equal to a month presents deviations lower than the 3% with respect to the *FEM* analysis, for the studied case. Nevertheless, the deviations are within a larger range (-5% to 10%) if the *FEM* approach is compared to the EN ISO 13370:2007 monthly average values method. This suggests that the time shift has to be considered for an accurate estimation of the thermal losses through the slab-on-ground floor.

In Figure 2b.7, the virtual temperature, to use as boundary condition in dynamic simulations, has been calculated with the three approaches (i.e., by means of the FEM monthly averages thermal fluxes, the EN ISO 13370:2007 method with the sinusoidal forcing temperature and the EN ISO 13370:2007 monthly method). The accuracy is again affected by the correct estimation of the time shift. Thus, the sinusoidal forcing temperature approach presents deviations lower than 1 °C on the temperatures while for the average monthly method the deviations are within a larger range of 2 °C.

## 2b.4 Main findings

The calculation method provided by the technical Standard EN ISO 13370:2007 to define the boundary temperature to use for walls and floors in touch with the ground, both for quasi-steady state and BES approaches, has been discussed.

The Standard method has been compared to *FEM* simulations in steady state conditions in order to assess its accuracy and discrepancies less than 1% have been found for the tested cases. They can be ascribed to the 2-dimensional method used by the technical Standard to evaluate the thermal bridges: if the 3-dimensional approach described in the EN ISO 10211:2007 is followed, the residual difference between the two methods is expected to be negligible.

In order to find the proper time-discretization for the BES ground boundary conditions, both few days-long *FEM* simulations with an hourly discretization and a year-long *FEM* simulation with a daily discretization have been performed and compared to the Standard procedures. The effects of the daily-period forcing temperature result negligible for the study of the heat transfer through the soil. Moreover, the comparison underlined the importance of the correct estimation of the time lag of the flux through the soil by the Standard in order to get an accurate evaluation both of the flux and the boundary temperature by the EN ISO 13370:2007 method.

Further developments involve:

1. the assessment of more realistic forcing solicitations, non-sinusoidal;
2. the evaluation of the other configurations proposed by the technical Standard EN ISO 13370:2007, as well as different aspect ratios in order to investigate the influence of the non 1-dimensional heat flows;
3. the investigation of the external periodic heat transfer coefficient  $H_{pe}$  proposed by the technical Standard, in particular of the formulations taking into account of the cases with edge insulations (and so of their thermal bridges).

According to the EN ISO 10211:2007, also this coefficient can be calculated considering the thermal fluxes elaborated by means of *FEM* analysis and in this way, the different formula proposed by the EN ISO 13370:2007 assessed.

# **Chapter 3:**

## BES validation and comparison



## Chapter 3

The problem of the influence of the BES tool choice on the final results is discussed in this chapter. The state of the art of the validation of BES tools by means of the BESTEST approach is firstly presented. Then, the extensive comparative approach developed to extend the indications of the comparative validation procedure of the BESTEST approach, is described. Two well-known BES tools, TRNSYS 16.1 and EnergyPlus 7, have been considered for the application of both methodologies.

The annual energy needs and hourly peak loads, both heating and cooling, have been determined for both simulation codes and compared with the limits of the acceptability ranges for the BESTEST qualification cases (i.e., the cases used for the comparative validations). Moreover, also the results of the BESTEST sensitivity cases (i.e., the deviations between two qualification cases) have been analysed.

In the extensive comparison, monthly instead of annual energy needs and peak loads have been considered, analysing as well the time of occurrence of the peaks, for a large number of configurations developed in accordance with a factorial plan and aimed at assessing several combinations of alternatives for the building envelope characteristics and to evaluate the main sources of disagreement. Moreover, while in the BESTEST cases the so called most accurate models have been considered, for the extensive approach all inputs and assumptions under the user's control have been aligned, in order to point out the impact of the different models and algorithm of these two BES codes.

The resulting deviations between TRNSYS and EnergyPlus have been analysed with statistical techniques.



## 3.1 Methods

In this first section of this chapter the methodologies followed to assess the deviations between BES tools have been presented. In the first part the ANSI/ASHRAE 140:2011 BESTEST procedure is described and in the second one the developed extensive comparative approach.

### 3.1.1 ANSI/ASHRAE 140:2011 - BESTEST

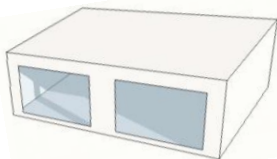
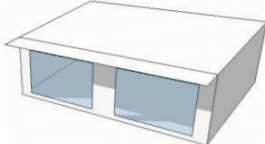
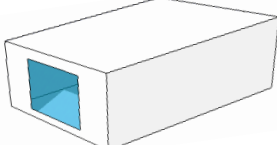
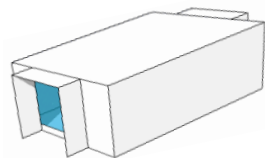
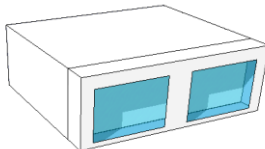
The BESTEST is a whole model comparison validation method with a marked diagnostic profile. The BESTEST procedure requires to evaluate the simulation code on some building configurations of different and increasing detail and complexity by using the best algorithms among the ones available in the code, according to a stage-gate approach: before testing the  $(n+1)$  case, the BES tool should pass the  $n$  case. “Passing” a test means that the results provided by the BES tool are in agreement with the ones of the reference codes, which are not expected to be necessarily representative of the “truth” but of what is commonly accepted as the current state of the art in BES (Judkoff and Neymark, 1995). When clearly failing a test (e.g., substantial disagreement with the acceptability ranges), additional diagnostic cases are available to identify the source of the disagreement problem.

In Table 3.1 the characteristics of the qualification cases have been reported. In particular, the envelope BESTEST considers a specific reference climate (Denver) and is based on the evaluation of the annual energy requirement and peak loads, time of occurrence of the peak and hourly temperature profile for the free floating cases.

In this section, two well known simulation codes, TRNSYS 16.1 and EnergyPlus 7, both already evaluated according to the BESTEST approach, although not in those versions, in particular as regards the envelope (Bradley *et al.*, 2004; Henninger and Wittel, 2010), have been assessed. An older version of TRNSYS, as well as BLAST and DOE2, the codes used for developing EnergyPlus, belong to the group of reference BES tools. Version 16.1 and version 7 have been considered respectively for TRNSYS and EnergyPlus as they do not differ significantly from those tested in the references and in the meantime are quite consolidated; the most significant difference between the considered version of TRNSYS and the last release (version 17) is that in the latter a 3D internal radiation model is also available as an option for the user.



Table 3.1 - BESTEST qualification cases

Geometry characteristics	Opaque envelope heat capacity	HVAC control strategies
<p><b>Cases 600/900:</b> South-faced windows</p> 	<p><b>Cases 6x0/960</b> Lightweight cases: Walls: <math>k_i = 9.2 \text{ kJ m}^{-2} \text{ K}^{-1}</math> Floor: <math>k_i = 18.7 \text{ kJ m}^{-2} \text{ K}^{-1}</math> Roof: <math>k_i = 8.4 \text{ kJ m}^{-2} \text{ K}^{-1}</math></p>	<p><b>Base cases</b> Heating setpoint of 20 °C Cooling setpoint of 27 °C</p>
<p><b>Cases 610/910:</b> South-faced windows with overhangs</p> 	<p><b>Cases 9x0</b> Massive cases: Walls: <math>k_i = 64.0 \text{ kJ m}^{-2} \text{ K}^{-1}</math> Floor: <math>k_i = 72.1 \text{ kJ m}^{-2} \text{ K}^{-1}</math> Roof: <math>k_i = 8.4 \text{ kJ m}^{-2} \text{ K}^{-1}</math></p>	<p><b>Cases 640/940</b> Nighttime setback: Heating setpoint of 10 °C (from 23:00 to 7:00) Heating setpoint of 20 °C (from 7:00 to 23:00) Cooling setpoint of 27 °C</p>
<p><b>Cases 620/920:</b> East and West oriented windows</p> 		<p><b>Cases 650/950</b> Night ventilation: Mechanical ventilation on and cooling system off (from 18:00 to 7:00) Mechanical ventilation off and cooling system on (from 7:00 to 18:00) Heating system always off</p>
<p><b>Cases 630/930:</b> East and West oriented windows with overhangs and fins</p> 		
<p><b>Case 960:</b> Multizone with a South-faced sunspace</p> 		

The qualification case 990, aimed at assessing the heat transfer via the ground, has not been considered, as a specific group of other BESTEST cases has been developed for studying this problem.

To better evaluate the behaviour of the analysed simulation codes with respect to the acceptability ranges of the BESTEST cases, percentage deviations have been calculated as in Eq. (3.1) and compared.

$$\Delta_{range} = \frac{x - \min}{\max - \min} \quad (3.1)$$

If  $\Delta_{range}$  is negative, the result of a considered case is under the minimum limit and if it is larger than 1, over the upper limit. Both the results of the qualification cases and the ones of the sensitivity cases have been studied.

### **3.1.2 Extensive comparison**

In order to generalize the BESTEST results, TRNSYS and EnergyPlus have been compared over a wide range of configurations of a building module composed by a single-storey thermal zone with 100 m<sup>2</sup> floor area. The outputs analysed in the extensive comparison are the same of the BESTEST approach but with a different time-discretization: instead of annual values, monthly heating and cooling energy needs and hourly peak loads were compared, together with the hour of occurrence of the peaks.

With the purpose to extend the range of configurations for the comparison, a parametric approach has been assumed. On one hand this complements the BESTEST validation process with a parametrical analysis over a larger number of conditions. On the other hand it gives very important information about the relative uncertainty (inaccuracy) and reliability of the results obtained with any of the considered simulation codes. This is particularly important when the simulation codes are directly used for energy certification of buildings or for tuning the simplified or quasi-steady state approaches such as the quasi-steady state method proposed by the technical Standards EN ISO 13790:2008.

The way of selection of the set of building configurations allowed to investigate the effects of 7 variables (amount of surface exposed to the external conditions, opaque envelope base material, level of insulation, windows orientation, windows area, kind of glazing, presence of internal gains) in determining the differences between the two simulation codes. Other possible causes of difference, such as the thermal exchange of envelope elements in touch with the ground, were neglected as they are conceptually related more to the modelling approach of

some specific boundary conditions, as seen in chapter 2. Some alternative or optional control parameters under the user's choice, as the one considered by the different models for managing the external long wave radiation exchange towards the sky vault, have been assumed in a coherent way. All the possible causes of disagreement have been investigated among those algorithms and models implemented by the two software for the solution of the building thermal balance, as well as those parameters not under the user's control, such as the surface emissivity in TRNSYS.

From the combination of the values of the above variables, 1620 different configurations have been obtained, each of which providing 12 monthly values for heating and cooling needs and for heating and cooling peaks for each of the two considered climatic conditions (Milan and Messina). Thanks to this large number, the results have been analysed with inferential statistical approaches, which allowed to evaluate the agreement between the outputs and to characterize the weight of the different variables on the found deviations. As a benchmark, the monthly results of BESTEST configurations 600, 610, 620, 630, 640 and 650, and 900, 910, 920, 930, 940, 950 and 960 in the two considered climatic conditions and after the alignment were added in the comparison.

### **3.1.2.1 Reference building module and set of configurations**

The set of configurations required in the comparative analysis is obtained as variations of a reference building, a single-storey module with 100 m<sup>2</sup> of floor area, whose concept is represented in Figure 3.1. The whole opaque envelope is composed by a two layers structure. The internal layer is made of one of the 3 considered base materials (timber, clay block or concrete) with a thickness chosen to give a thermal resistance of about 0.8 m<sup>2</sup> K W<sup>-1</sup>, as 0.2 m of clay block.

An insulation layer, whose thickness has been varied to give different configurations as described below, is applied on the external side. The thermophysical characteristics of the materials used are reported in Table 3.2.

The external solar absorption coefficients of the walls and for the roof (when not adiabatic) are respectively 0.3 and 0.6 while the internal one is 0.3 for both. The floor external absorptance is 0 when exposed to the external ambient (i.e., the solar radiation component on this surface is equal to zero) and the internal one is 0.6.

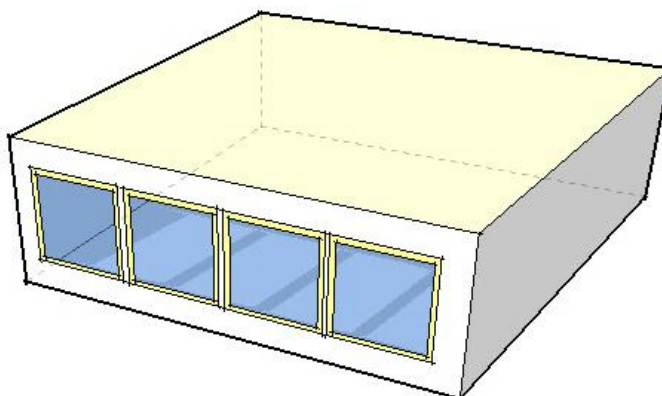


Figure 3.1 – Conceptual view of the base module

Table 3.2 - Opaque Envelope thermal properties

	<b>Timber</b>	<b>Clay block</b>	<b>Concrete</b>	<b>Insulation</b>
Thermal Conductivity [W m <sup>-1</sup> K <sup>-1</sup> ]	0.13	0.25	0.37	0.04
Density [kg m <sup>-3</sup> ]	399	893	1190	1470
Specific heat [J kg <sup>-1</sup> K <sup>-1</sup> ]	1880	840	840	40

The windows are considered as positioned on a unique vertical wall and orientation, in order to emphasize the consequences of different entering solar radiation distributions during the day. They have been modelled with Window6 LBNL tool and used as input for both EnrgyPlus and TRNSYS. The wall opposed to the windows is assumed to be adiabatic. The window frame is a low performing timber frame ( $U_{fr} = 3.2 \text{ W m}^{-2} \text{ K}^{-1}$ ) with the single glass or an improved performance frame in the other cases ( $U_{fr} = 1.2 \text{ W m}^{-2} \text{ K}^{-1}$ ), always with a frame area covering about the 20 % of the whole window area.

For the ventilation, a constant rate of 0.3 ach/h of outside air has been imposed, in accordance to the average value prescribed by the Italian standard UNI/TS 11300-1:2008 for residential buildings.

To define the different cases, the following variables of interest (also called factors in the following) have been selected:

1. the amount of envelope surface exposed to the external environment (expressed by the ratio between the surface itself and the volume);
2. the base material of the opaque envelope (the material of the internal layer);
3. the level of insulation added to the internal layer;
4. the percentage ratio of glazings  $A_{gl}$  to floor area  $A_f$ ;
5. the orientation of the windowed wall;
6. the kind of glazings;
7. the presence of internal gains;
8. the climatic conditions.

For each of the above factors, a certain number of alternatives (levels) were considered as reported in Table 3.3. The amount of exposed surface (factor 1) permits to consider buildings with different exposed surface but equal volumes and the presence of adiabatic envelope components (3 combinations). The base material and insulation level (variables 2 and 3) allow to consider the different thermal dynamic behaviour of the opaque envelope (9 combinations). The window percentage area, window orientation and kind of glazings (factors 4, 5 and 6) allow to examine the effect of window insulation and solar control properties under different solar radiation profiles (30 combinations). The internal gains (variable 7) permits to analyze the presence of internal partially radiant loads (2 combinations). Finally, the climate (variable 8) allows to evaluate the effect of different temperature and radiation conditions over two very different Italian climates (2 combinations).

Table 3.3 - Variables (factors) and alternatives (levels) in the simulation plan

(1) Exposed surface ratio $S/V$ [ $\text{m}^2 \text{m}^{-3}$ ]	a	one wall, the floor and the ceiling adiabatic; $S/V=0.30 \text{ m}^{-1}$
	b	one wall and the floor adiabatic; $S/V=0.63 \text{ m}^{-1}$
	c	one wall adiabatic; $S/V=0.97 \text{ m}^{-1}$
(2) Base material for the internal layer $R$ [ $\text{m}^2 \text{K W}^{-1}$ ] Area specific heat capacity $k_i$ [ $\text{kJ m}^{-2} \text{K}^{-1}$ ]	a	Timber 0.10 m; area specific heat capacity $75 \text{ kJ m}^{-2} \text{K}^{-1}$
	b	Clay block 0.20 m; area specific heat capacity $150 \text{ kJ m}^{-2} \text{K}^{-1}$
	c	Concrete 0.30 m; area specific heat capacity $300 \text{ kJ m}^{-2} \text{K}^{-1}$
(3) Insulation thickness $s$ [cm] (Thermal Transmittance $U_{env}$ [ $\text{W m}^{-2} \text{K}^{-1}$ ])	a	0 cm – $U_{env} = 1.03 \text{ W m}^{-2} \text{K}^{-1}$
	b	5 cm – $U_{env} = 0.45 \text{ W m}^{-2} \text{K}^{-1}$
	c	10 cm – $U_{env} = 0.29 \text{ W m}^{-2} \text{K}^{-1}$
(4) Ratio $A_{gl}/A_f$	a	11.7%
	b	23.4%
(5) Orientation of $A_{gl}$	a	East
	b	South
	c	West
(6) Kind of glazing $U_{gl}$ [ $\text{W m}^{-2} \text{K}^{-1}$ ]	a	(S) single glass; $U_{gl} = 5.68 \text{ W m}^{-2} \text{K}^{-1}$ , $SHGC = 0.855$
	b	(DH) double glazing high solar transmittance; $U_{gl} = 1.140 \text{ W m}^{-2} \text{K}^{-1}$ , $SHGC = 0.608$
	c	(DL) double glazing low solar transmittance; $U_{gl} = 1.099 \text{ W m}^{-2} \text{K}^{-1}$ , $SHGC = 0.352$
	d	(TH) triple glazing high solar transmittance; $U_{gl} = 0.613 \text{ W m}^{-2} \text{K}^{-1}$ , $SHGC = 0.575$
	e	(TL) triple glazing low solar transmittance; $U_{gl} = 0.602 \text{ W m}^{-2} \text{K}^{-1}$ , $SHGC = 0.343$
(7) Internal gains $q_i$ [ $\text{W m}^{-2}$ ]	a	$q_i = 0 \text{ W m}^{-2}$ of floor surface
	b	$q_i = 4 \text{ W m}^{-2}$ of floor surface (50% by convection and 50% by radiation)
(8) Climatic conditions $HDD_{20}$ [ $\text{K d}$ ]	a	Messina – $HDD_{20}$ : 707 K d
	b	Milan – $HDD_{20}$ : 2 404 K d

### 3.1.2.2 Assumptions for the simulation

Differently from validation approach of the BESTEST procedure, which requires for diagnostic purpose to use the best and more detailed algorithms offered by each simulation code, for the aims of the present work the input data have been pre-processed and the calculation hypotheses aligned. This has been pursued with regard to the outside and inside surface exchanges and selecting the appropriate models for the conduction heat exchanges within the envelope components, as described below.

The air heat balance approach implemented by both codes is expressed as:

$$\Phi_{c,i} + \Phi_{ve} + \Phi_{i,c} + \Phi_{sys} = C_a \frac{d\theta_a}{dt} \quad (3.2)$$

The convection term  $\Phi_{c,i}$  exchange with the internal surfaces of the envelope is determined by imposing the surface heat balance equations on the external and on the internal surfaces, which per unit of area are expressed as:

$$q_{sole} + q_{r,e} + q_{c,e} + q_{tr,e} = 0 \quad (3.3)$$

$$q_{sol,i} + q_{i,swr} + q_{r,i} + q_{i,lwr} + q_{c,i} + q_{tr,i} = 0 \quad (3.4)$$

Some of the terms in the balances can be estimated in different ways. The main points are summarized in the following paragraphs.

#### ***External surface exchanges***

##### Climatic conditions and solar radiation on the horizontal and on tilted surfaces

In coherence with the aims of the last part of this study (the comparison with the simplified methods), it was decided to rebuild hourly profiles compatible with the mean monthly data reported in the Italian standard UNI 10349:1994 using the TRNSYS subroutine Type 54.

The Type 54 allows to generate hourly weather data for a whole year in a chosen location from the monthly average values of global horizontal solar radiation, temperature, humidity and, in case, wind speed (neglected in this work since constant convective coefficients and ventilation rate have been considered). The subroutine allows also to split the horizontal radiation into the direct and diffuse components in accordance with Erbs' algorithm (Erbs *et al.*, 1982).

The Perez algorithm (Perez *et al.*, 1990) implemented in EnergyPlus has been selected in this study to evaluate the radiation on tilted surfaces. An albedo coefficient of 0.2 has been

considered. The elaborated profiles of dry bulb and dew point temperature, relative humidity, global, direct and diffuse radiation on a horizontal surface and on the principal orientations for vertical surfaces have been used as input to EnergyPlus and TRNSYS.

### Long wave radiation exchanges

The infrared exchange depends firstly on the characteristic emissivity of the considered surface. As TRNSYS imposes fixed values of 0.9 for all external opaque surfaces while EnergyPlus allows the user to select this parameter in the range between 0 and 1 either for the internal or the external ones, also in this second code the external surface emissivity has been set to 0.9.

The different models used by the two software for calculating the long wave exchanges with the external environment should be commented. The external infrared exchange is calculated in EnergyPlus (Walton, 1983; McClellan and Pederson, 1997) dividing the flux into 3 components: to the sky vault, to the ground and of air absorption (when the view factor of the sky is not 1):

$$q_{r,e} = q_{r,gnd} + q_{r,sky} + q_{r,air} = \varepsilon\sigma F_{gnd} \cdot (\theta_{s,e}^4 - \theta_{gnd}^4) + \varepsilon\sigma F_{sky} \beta \cdot (\theta_{s,e}^4 - \theta_{sky}^4) + \varepsilon\sigma F_{air} \cdot (\theta_{s,e}^4 - \theta_{air}^4) \quad (3.5)$$

with

$$F_{gnd} = 0.5 \cdot (1 + \cos\phi) \quad (3.6)$$

$$F_{sky} = 0.5 \cdot (1 - \cos\phi) \quad (3.7)$$

$$\beta = \sqrt{0.5 \cdot (1 + \cos\phi)} \quad (3.8)$$

To determine  $F_{air}$  for the different air absorption for non-horizontal tilt, the view factor of the sky is multiplied by  $1 - \beta$ .

The equation is then linearized:

$$q_{r,e} = h_{r,gnd} \cdot (\theta_{s,e} - \theta_{gnd}) + h_{r,sky} \cdot (\theta_{s,e} - \theta_{sky}) + h_{r,air} \cdot (\theta_{s,e} - \theta_{air}) \quad (3.9)$$

with the three coefficients  $h_{r,n}$  ( $n = gnd, sky, air$ ):

$$h_{r,n} = \varepsilon\sigma F_n \cdot \frac{\theta_{s,e}^4 - \theta_n^4}{\theta_{s,e} - \theta_n} \quad (3.10)$$

Moreover the temperature  $\theta_{gnd}$  is approximatively considered as equal to  $\theta_{air}$ .



The model adopted in TRNSYS is based on the exchange between the surface temperature and a reference temperature  $\theta_{fsky}$ , which is calculated as a mean of the air and of the sky vault temperatures, weighted by the respective view factors in compliance with the following equations:

$$q_{r,e} = \varepsilon \sigma F_{sky} \cdot (\theta_{s,e}^4 - \theta_{fsky}^4) \quad (3.11)$$

$$\theta_{fsky} = (1 - F_{sky}) \cdot \theta_{air} + F_{sky} \cdot \theta_{sky} \quad (3.12)$$

In order to take into account of the air absorption effect also in TRNSYS, a value of 0.35, which corresponds to the product  $F_{sky} \beta$ , has been chosen instead of the usual 0.5 for vertical surfaces.

The EnergyPlus value of the sky fictive temperature, obtained from the hourly profile for horizontal orientation long wave flux, was used also in TRNSYS in place of the output of the subroutine Type 69, calculated from external temperature and humidity and from the amount of horizontal diffuse radiation on the horizontal global one.

### Convective exchanges

In EnergyPlus, different models of various levels of complexity and approximation are available to evaluate the convective flow: the convective coefficients can be fixed as a user's input or can be determined dynamically from the roughness of the walls and the boundary conditions. In the considered release of TRNSYS, on the contrary, the convective coefficient needs to be provided by the user.

A constant value of  $20.0 \text{ W m}^{-2} \text{ K}^{-1}$  has been adopted, in accordance with the prescriptions of the technical standard EN ISO 6946:2007, annex A, for both the simulation codes.

### ***Internal surface exchanges***

#### Entering solar radiation

Both codes distribute the diffuse component of the entering solar radiation equally on all the surfaces delimiting the zone. With respect to the direct component, in TRNSYS, it is distributed over the different surfaces by a proper fraction called *geosurf* which is defined by the user for each surface. In EnergyPlus, more detailed algorithms consider also the reflections of the direct radiation entering into the zone.

The compromise between these two approaches was to adopt in EnergyPlus the *FullExterior* choice, which establishes that all the direct radiation transmitted falls on the floor and possible reflections are added to the diffuse components, and, in TRNSYS to set the *geosurf* to 1 for the floor and to 0 for the remaining walls.

Chatziangelidis and Bouris (2009) assessed the influence of using a detailed view factor algorithm for the distribution of the entering solar radiation on the different surfaces or the *geosurf* method in TRNSYS and observed that the variation in the surface temperature and thermal loads are negligible.

### Long wave radiation

In TRNSYS 16.1 the calculation is based on Seem's star-network algorithm (Seem, 1987), which puts in parallel the radiative and convective exchanges from each internal surface in a single heat flux towards a fictive temperature node  $\theta_{star}$ . In turn, through a suitable thermal resistance, the fictive node exchanges with the air of the zone a thermal power equivalent to the sum of the convective exchanges at the internal surfaces. As regards the long wave radiation, TRNSYS assumes the internal surfaces, both of the opaque and transparent envelope, as black.

In contrast, EnergyPlus implements a detailed algorithm based on the view factor calculations between the surfaces, considered as grey (Hottel and Sarofim, 2007). An internal long wave radiation emissivity of 0.999 has been chosen for the opaque envelope to approximate TRNSYS. A value of 0.84 is the fixed choice for the transparent envelope surfaces.

### Convective exchanges

Constant values were assumed also for the internal convection heat transfer coefficient. In accordance with the prescriptions of the EN ISO 6946:2007, appendix A, the selected values are  $5.0 \text{ W m}^{-2} \text{ K}^{-1}$  for vertical ascending flux,  $0.7 \text{ W m}^{-2} \text{ K}^{-1}$  for vertical descending and  $2.5 \text{ W m}^{-2} \text{ K}^{-1}$  for horizontal flux.

### ***Conduction thermal flow in the opaque envelope components***

Among the 4 possible models offered by EnergyPlus to calculate the thermal flux transmitted through the opaque envelope, the transfer functions model *TFM* was selected to compare with the equivalent method used by TRNSYS. It should be said that the two *TFM* models implemented are different: TRNSYS refers to the Direct Root Finding (*DRF*) model while EnergyPlus applies the State-Space Method (*SS*).

As known, the *TFM* method is based on the evaluation of a time series of terms which depend on the boundary conditions and on the solution calculated for the previous period of time. The coefficients of the series are calculated on a reference period of time that is called wall timebase. Following the ASHRAE suggestions, for stability reasons, in TRNSYS a wall timebase of 1 hour has been selected for the kind of walls considered in this study.

In EnergyPlus, instead, a wall timebase equal to the simulation timestep is always assumed (10 minutes is suggested).

The simulation timestep proposed by EnergyPlus has been used for both simulation codes, except for the 640 and 940 BESTEST cases, for which a shorter timestep was required in order to evaluate the heating peak loads due to the startup after the temperature night setback, as described below. For a detailed comparison between the Space State Method, the Direct Root Finding and other numerical approaches, see chapter 4a.

### 3.1.2.3 Statistical analysis

A statistical analysis of the deviations between the two software has been performed. This technique allowed to confirm the findings of the descriptive statistics and to evaluate the weight of each variable in introducing the differences. The inferential statistical technique applied is the multivariate linear regression with a confidence level of 95% described in Annex A and the variables considered in the regression model have been selected through the stepwise algorithm.

For the deviations of heating and cooling energy needs, the examined variables are the following:

- *The opaque envelope thermal properties:*
  - the area weighted mean thermal transmittance of the opaque walls  $U_{env}$  [ $\text{W m}^{-2} \text{K}^{-1}$ ];
  - the area weighted mean periodic thermal transmittance  $Y_{ie,env}$  [ $\text{W m}^{-2} \text{K}^{-1}$ ] and timeshift  $\Delta t_{ie,env}$  [h], determined in accordance with the EN ISO 13786:2007 detailed approach;
  - the product of the total opaque envelope area multiplied by its internal heat capacity  $\kappa_i \cdot A_{tot}$  [ $\text{kJ K}^{-1}$ ], determined in accordance with the EN ISO 13786:2007 detailed approach;
- *The transparent envelope thermal properties:*
  - the thermal transmittance of the windows  $U_{win}$  [ $\text{W m}^{-2} \text{K}^{-1}$ ];
  - the solar heat gain coefficient SHGC [-];

- *The envelope areas:*
  - the externally exposed opaque walls area  $A_{env}$  [ $\text{m}^2$ ];
  - the windows area  $A_{win}$  [ $\text{m}^2$ ];
- *The boundary conditions:*
  - the total monthly solar radiation received by the opaque envelope  $H_{env}$  [MJ];
  - the monthly radiation received by the windows  $H_{win}$  [MJ];
  - the mean monthly external temperature  $\theta_{air}$  [ $^{\circ}\text{C}$ ];
  - the internal gains  $q_i$  [ $\text{W m}^{-2}$ ].

For the deviations of heating and cooling hourly peaks, the considered variables are the same with the exception of the boundary conditions:

- *for the heating peaks deviations:*
  - instead of the mean value, the outdoor temperature monthly minimum has been considered,  $\theta_{air, min}$  [ $^{\circ}\text{C}$ ];
  - the solar gains have been completely neglected;
- *for the cooling peaks deviations*, in place of the total radiation received, two variables have been selected:
  - the monthly horizontal solar radiation for the location examined  $H_{hor}$  [MJ  $\text{m}^{-2}$ ];
  - the monthly peak of the 2-days rolling cumulated solar radiation incident on the windows  $\hat{H}_{2dd}$  [MJ  $\text{m}^{-2}$ ].

In this analysis, only the listed main factors have been considered, neglecting the interactions between them.

## 3.2 Results

The results are presented in this part, distinguishing the original BESTEST results, the BESTEST after the alignment described in the extensive comparative approach and the simulation plan results.

### 3.2.1 BESTEST cases

The results have been reported in Figure 3.2 (for the energy needs) and in Figure 3.3 (for the peak loads). As stated before, both the results of the qualification cases (blue) and the ones of the sensitivity cases (green) have been represented.

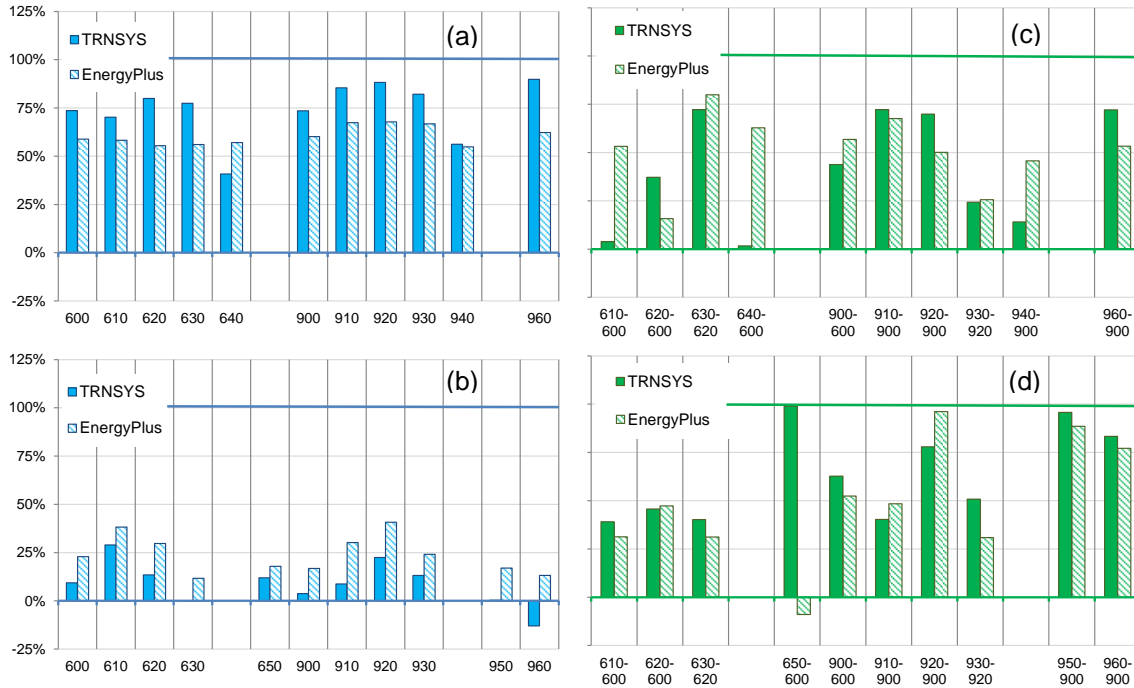
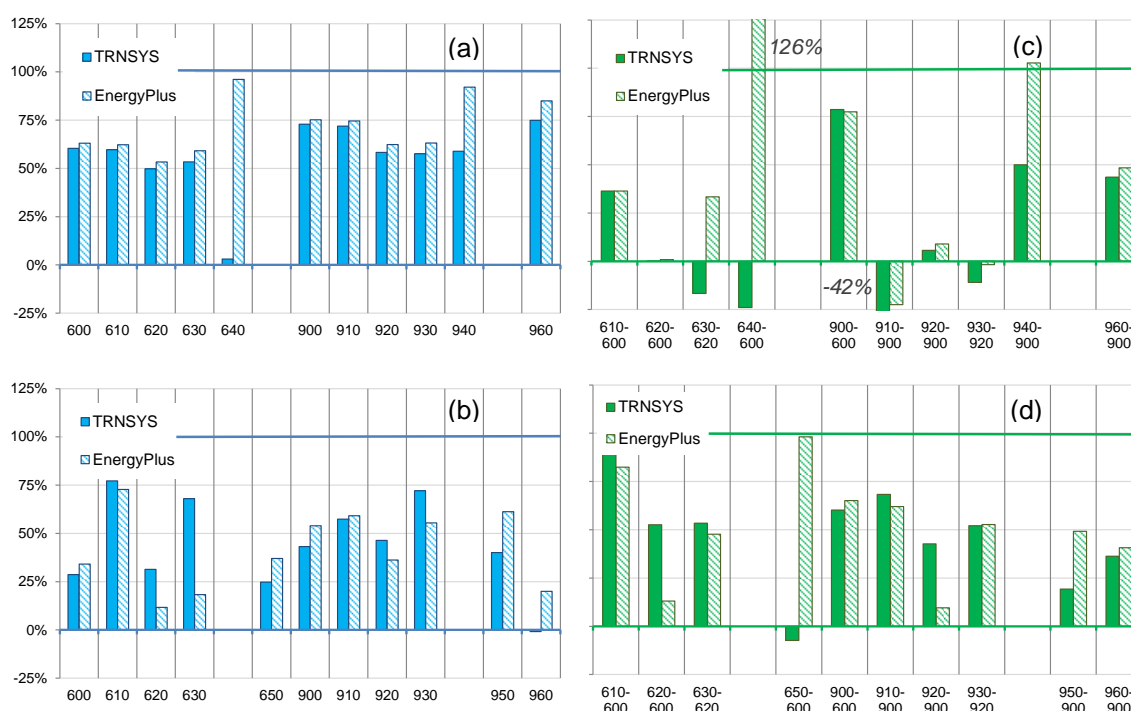


Figure 3.2 - Percentage deviations in the annual heating (a) and cooling (b) energy needs calculations with respect to the normalized BESTEST ranges and percentage deviations in the heating (c) and cooling (d) energy needs sensitivity with respect to the normalized sensitivity BESTEST ranges for TRNSYS and EnergyPlus



*Figure 3.3 - Percentage deviations in the annual heating (a) and cooling (b) peak loads calculations with respect to the normalized BESTEST ranges and percentage deviations in the heating (c) and cooling (d) energy needs sensitivity with respect to the normalized sensitivity BESTEST ranges for TRNSYS and EnergyPlus*

### 3.2.2 Alignment in the BESTEST cases

The effects of the assumptions adopted to align the input data and the simulation hypotheses have been evaluated by comparing the BESTEST configurations 600, 610, 620, 630, 640 and 650, and 900, 910, 920, 930, 940, 950 and 960 in the BESTEST climatic reference conditions of Denver. The differences between the monthly energy needs or monthly hourly peak loads obtained with EnergyPlus and with TRNSYS have been plotted against the energy needs or peak loads calculated with TRNSYS, respectively in the left and in the right part of Figure 3.4.

The positions of the new results respect to the BESTEST acceptability ranges have been reported in Figure 3.5 for the heating and cooling annual energy needs and in Figure 3.6 for the heating and cooling peak loads.

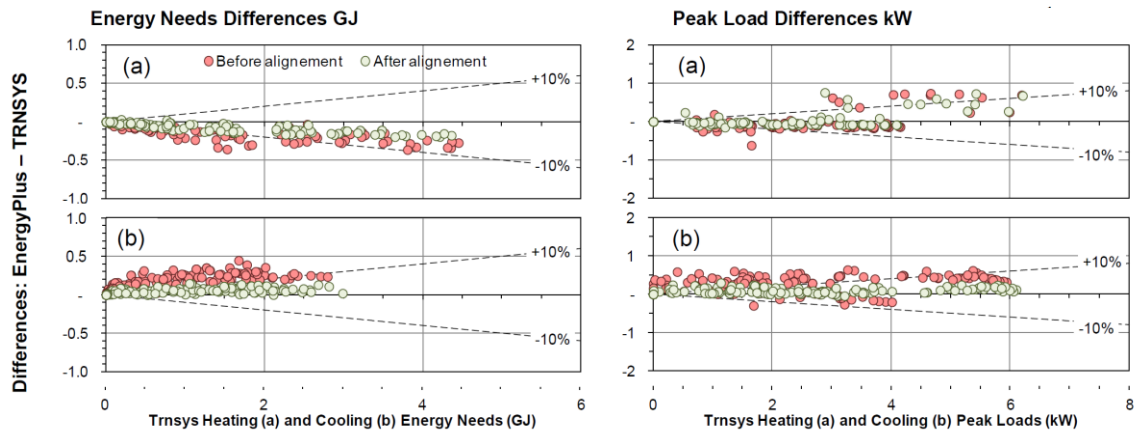


Figure 3.4 - Monthly differences for the heating (a) and cooling (b) energy needs (on the left) and monthly hourly peak loads (on the right) between EnergyPlus and TRNSYS with respect to TRNSYS energy needs and peak loads results for the BESTEST cases in the reference climatic conditions of Denver

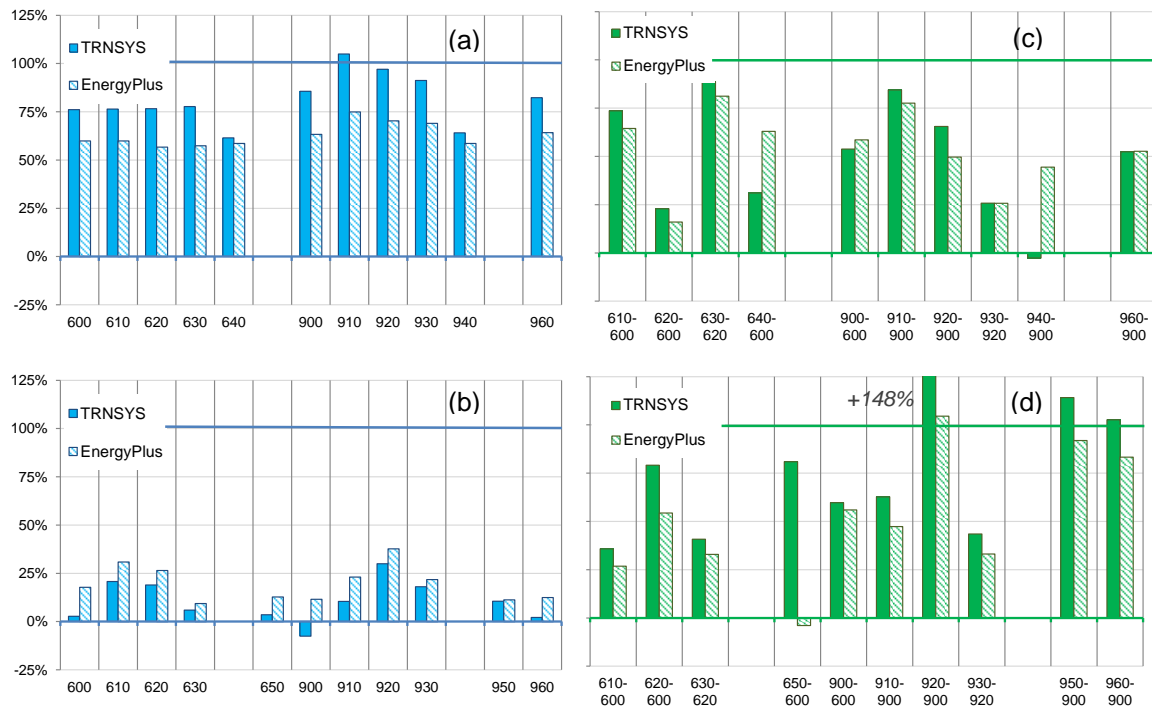


Figure 3.5 - Percentage deviations in the annual heating (a) and cooling (b) energy needs calculations with respect to the normalized BESTEST ranges and percentage deviations in the heating (c) and cooling (d) energy needs sensitivity with respect to the normalized sensitivity BESTEST ranges for TRNSYS and EnergyPlus after the alignment

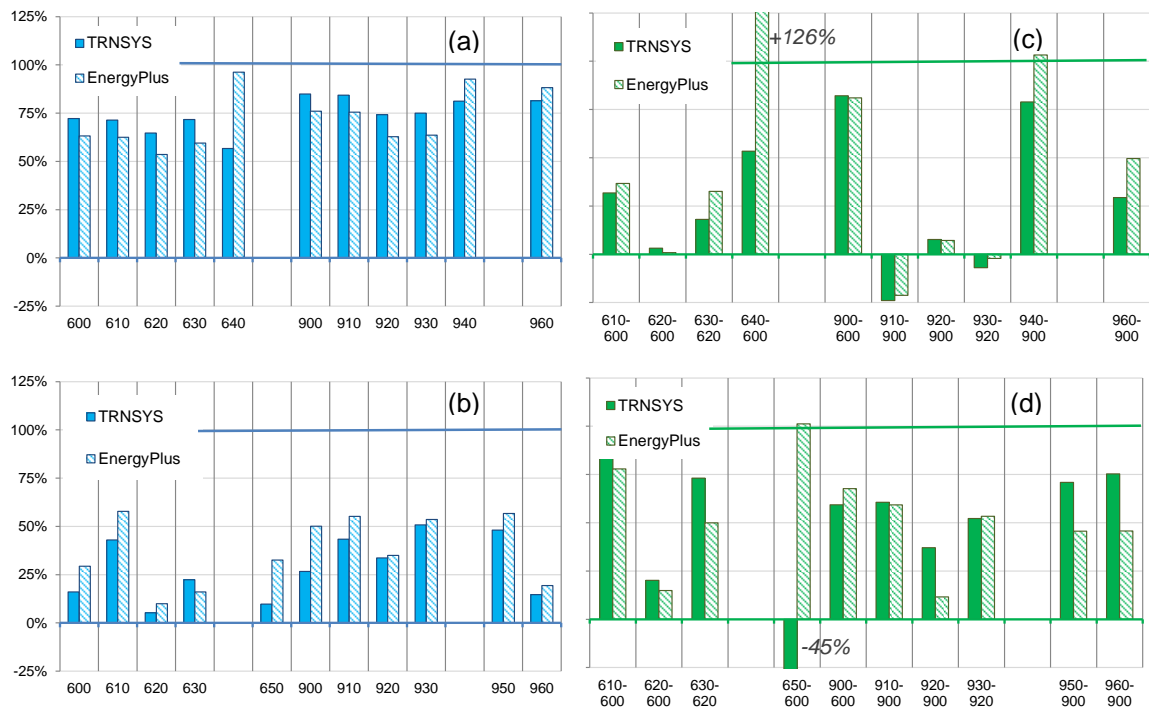


Figure 3.6 - Percentage deviations in the annual heating (a) and cooling (b) peak loads calculations with respect to the normalized BESTEST ranges and percentage deviations in the heating (c) and cooling (d) energy needs sensitivity with respect to the normalized sensitivity BESTEST ranges for TRNSYS and EnergyPlus after the alignment



### 3.2.3 Simulation plan results

The differences between the monthly energy needs obtained with EnergyPlus and with TRNSYS have been plotted against the energy needs calculated with TRNSYS (Figure 3.7 for Milan and Figure 3.8 for Messina).

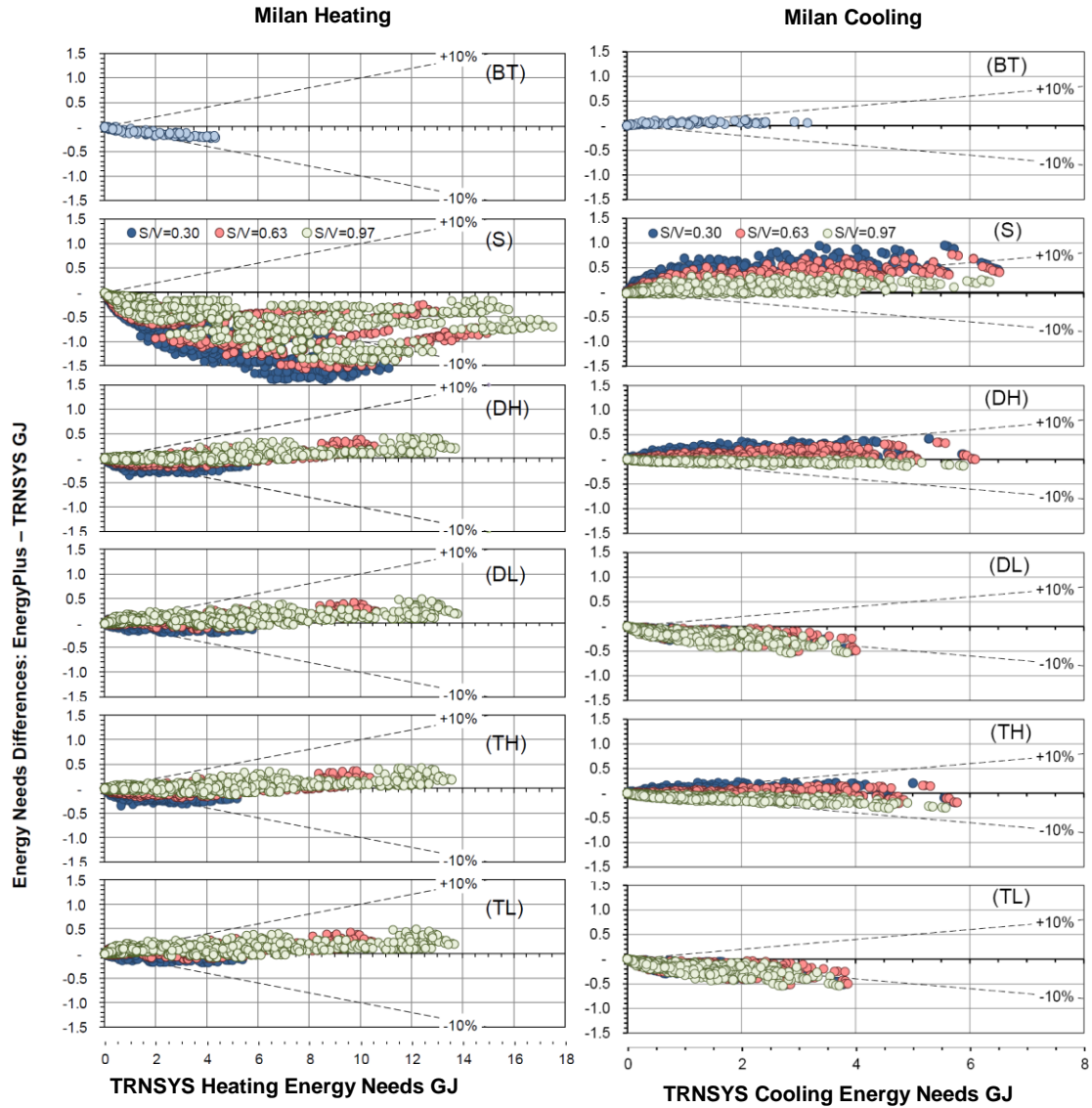


Figure 3.7 - Monthly differences for the heating and cooling energy needs for Milan between the two simulation codes with respect to TRNSYS results for BESTEST cases (BT) and for different glazing type (S = single; DH = Double with high SHGC; DL = Double with low SHGC; TH = Triple with high SHGC; TL = Triple with low SHGC) and for different ratios S/V

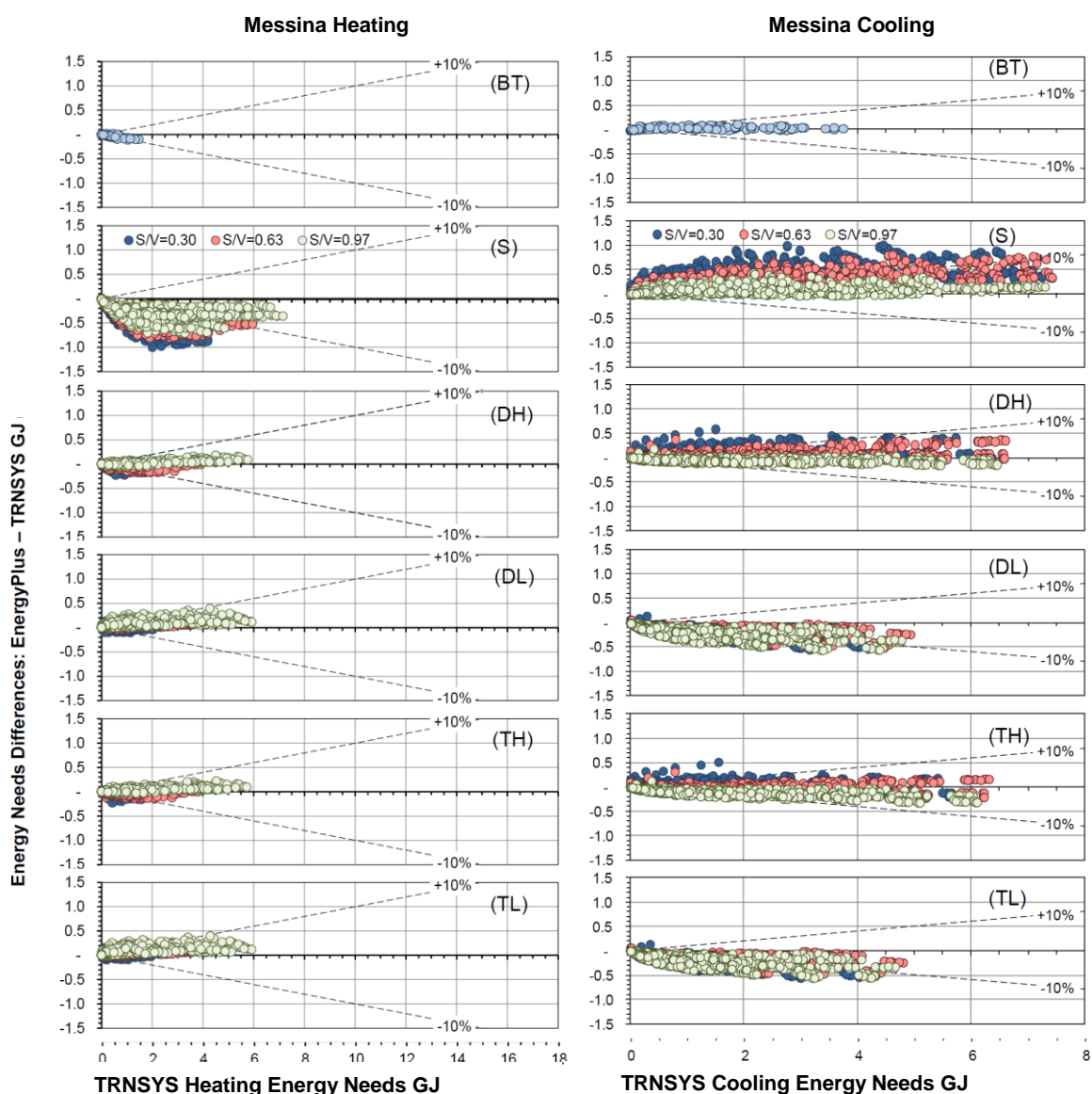


Figure 3.8 - Monthly differences for the heating and cooling energy needs for Messina between the two simulation codes with respect to TRNSYS results for BESTEST cases (BT) and for different glazing type (S = single; DH = Double with high SHGC; DL = Double with low SHGC; TH = Triple with high SHGC; TL = Triple with low SHGC) and for different ratios  $S/V$

The mean differences and standard deviation between EnergyPlus and TRNSYS results for both locations have been reported in percentage and absolute terms in Table 3.4 and 3.5 respectively.

*Table 3.4 - Mean percentage differences and corresponding standard deviations between Energy Plus and TRNSYS with respect to TRNSYS results for different kind of glazing. Results with energy needs under 3.6 MJ or peak loads under 50 W are not considered*

Kind of glazing	Heating Needs [%]		Cooling Needs [%]		Heating Peaks [%]		Cooling Peaks [%]	
	Mean	Standard Deviation	Mean	Standard Deviation	Mean	Standard Deviation	Mean	Standard Deviation
S	-29.63	±6.82	21.69	±7.57	-22.10	±5.04	2.81	±0.33
DH	-9.11	±1.56	0.73	±0.12	-7.40	±1.41	-0.83	±0.33
DL	6.24	±1.55	-25.49	±6.76	-1.20	±0.73	-22.94	±5.65
TH	-6.91	±1.21	-6.85	±1.26	-7.48	±1.41	-6.85	±1.88
TL	9.20	±2.91	-26.08	±7.12	-0.48	±0.10	-21.81	±5.80
Total	-6.63	±1.83	-6.00	±1.86	-8.13	±2.76	-9.25	±2.75
BESTEST	-11.18	±1.32	8.85	±1.10	-4.23	±0.49	7.24	±1.70

*Table 3.5 - Mean differences and corresponding standard deviations between Energy Plus and TRNSYS with respect to TRNSYS results for different kind of glazing. Results with energy needs under 3.6 MJ or peak loads under 50 W are not considered*

Kind of glazing	Heating Needs [MJ]		Cooling Needs [MJ]		Heating Peaks [W]		Cooling Peaks [W]	
	Mean	Standard Deviation	Mean	Standard Deviation	Mean	Standard Deviation	Mean	Standard Deviation
S	-461.56	±106.21	178.41	±62.26	-489.52	±111.69	53.55	±6.28
DH	-15.71	±2.70	25.69	±4.37	-46.93	±8.96	-26.31	±10.56
DL	49.25	±12.26	-162.50	±43.13	-6.26	±3.82	-358.18	±88.22
TH	-9.25	±1.62	-40.93	±7.51	-54.57	±10.32	-143.87	±39.45
TL	58.60	±18.50	-161.60	±44.11	-8.15	±1.67	-321.89	±85.57
Total	5.29	±1.46	-6.61	±2.05	-133.26	±45.22	-149.81	±44.60
BESTEST	-18.47	±2.18	13.54	±1.68	-12.12	±1.39	100.76	±23.64

In the next Figure, the behaviour of the deviations between the heating and cooling peak loads by TRNSYS and EnergyPlus for the location of Milan is reported, distinguished by kind of glazings and S/V ratio.

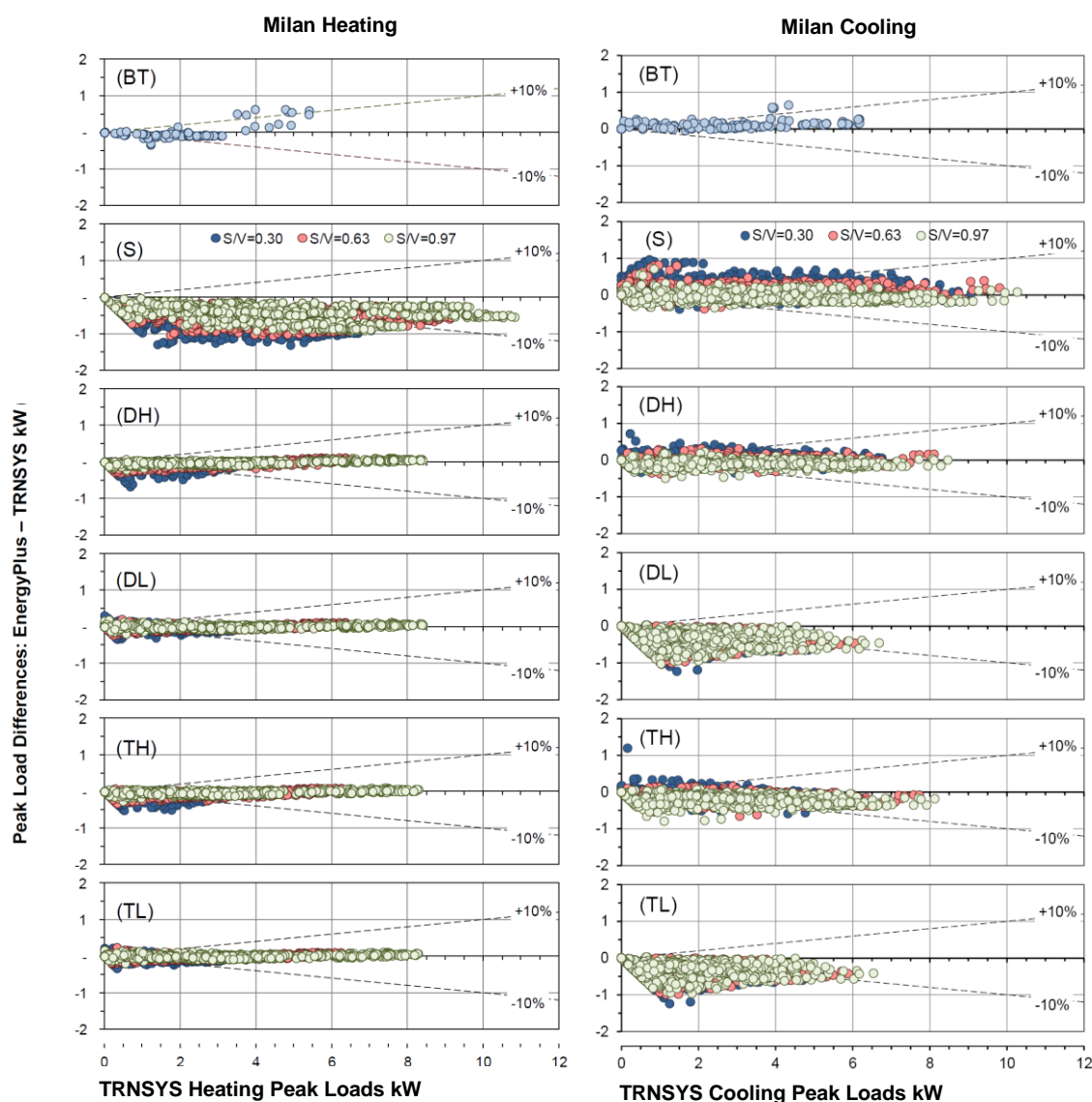


Figure 3.9 - Monthly differences for the heating and cooling peak loads for Milan between the two simulation codes with respect to TRNSYS results for BESTEST cases (BT) and for different glazing type (S = single; DH = Double with high SHGC; DL = Double with low SHGC; TH = Triple with high SHGC; TL = Triple with low SHGC) and for different ratios S/V

In Figure 3.10, the behaviour of the deviations between the heating and cooling peak loads by TRNSYS and EnergyPlus for the location of Milan is reported, distinguished by kind of glazings and S/V ratio.

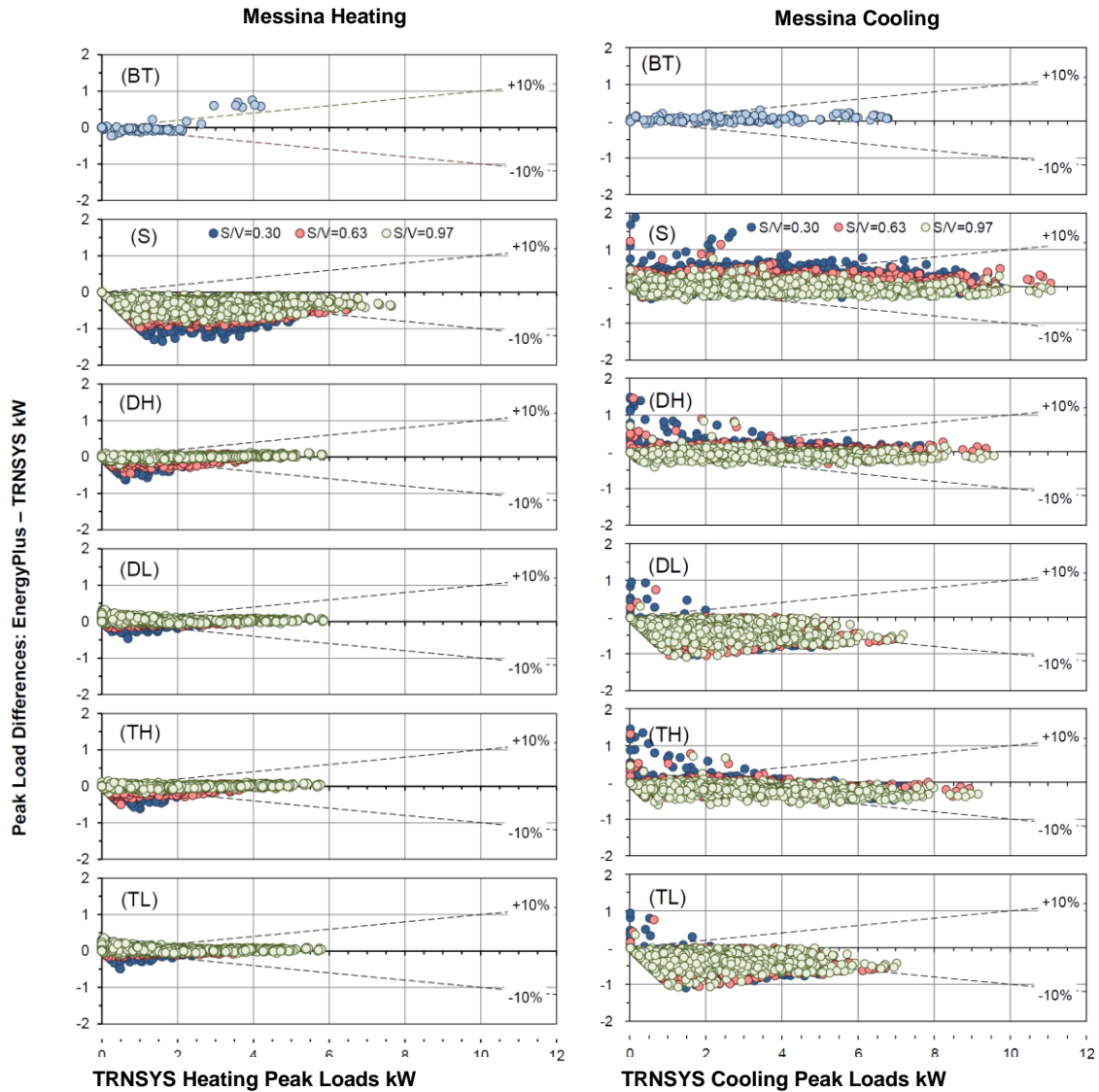


Figure 3.10 - Monthly differences for the heating and cooling peak loads for Messina between the two simulation codes with respect to TRNSYS results for BESTEST cases (BT) and for different glazing type (S = single; DH = Double with high SHGC; DL = Double with low SHGC; TH = Triple with high SHGC; TL = Triple with low SHGC) and for different ratios S/V

Finally, the difference of the time of occurrence of the monthly hourly peak load has been considered. The frequency distribution of those differences has been reported in Figure 3.11.

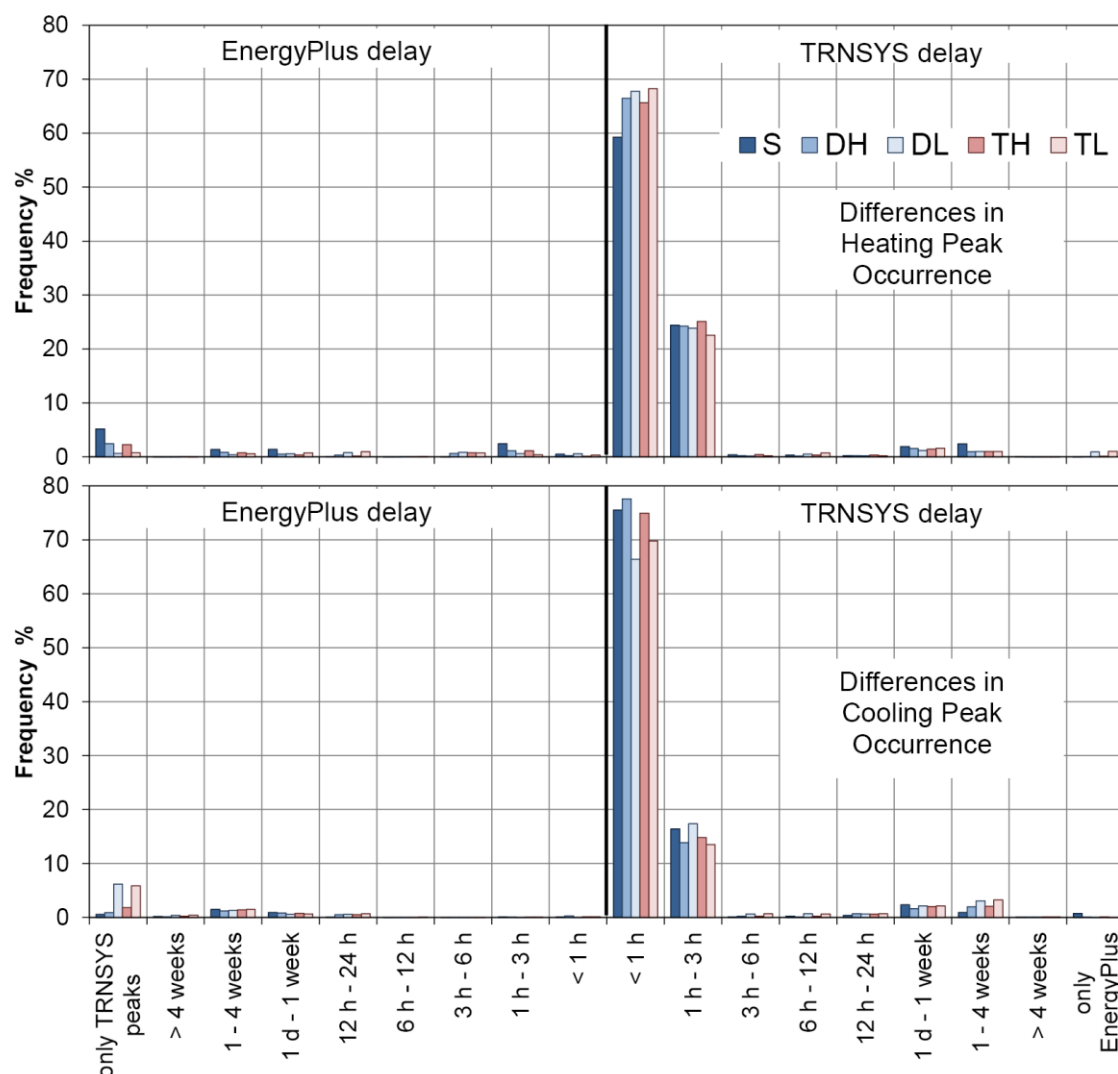


Figure 3.11 - Frequency distribution of the differences for the occurrence time of heating (on the top) and cooling (on the bottom) monthly peak loads between the two simulation codes for different glazing type (S = single; DH = Double with high SHGC; DL = Double with low SHGC; TH = Triple with high SHGC; TL = Triple with low SHGC)

### 3.2.3.1 Statistical analysis results

The standardized coefficients of the regression models found after the statistical analysis have been reported in Figure 3.12 and Table 3.6 and, both for the heating and the cooling deviations. All the coefficients calculated in the regressions are characterized by a significant p-value (lower than 1%).

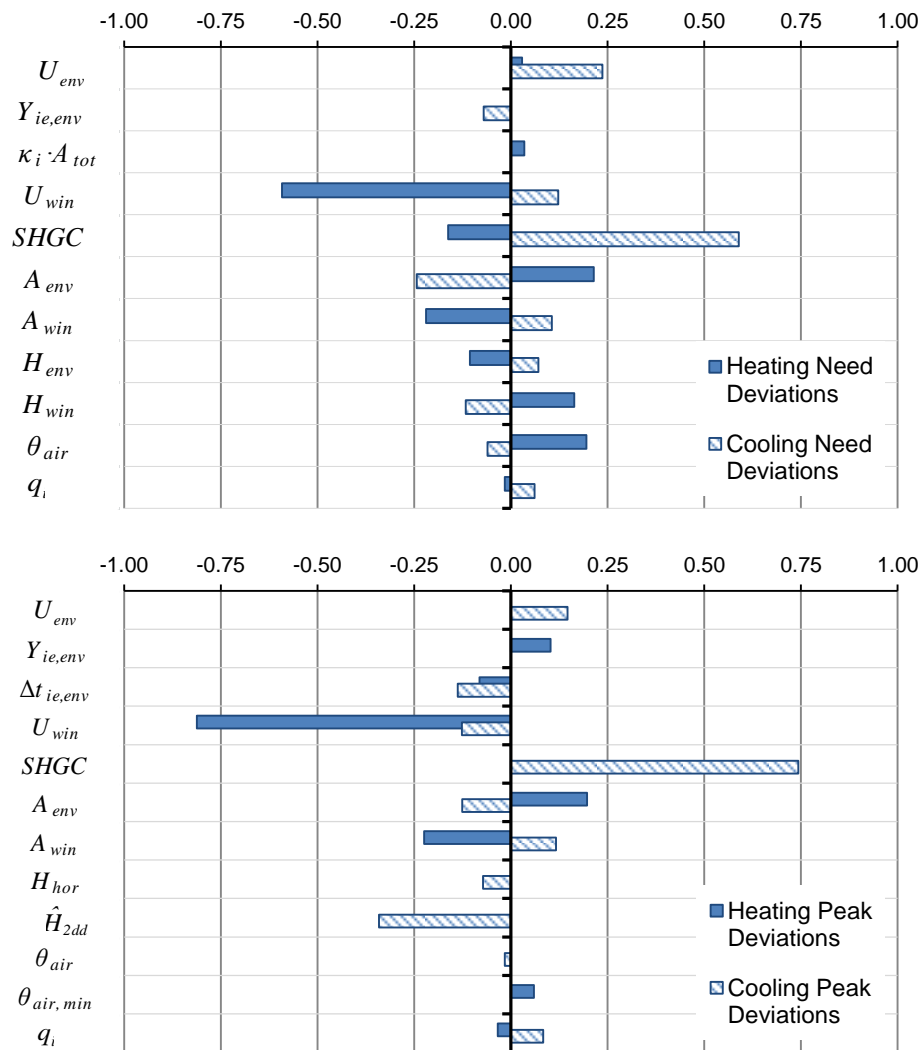


Figure 3.12 - Standardized coefficients of the regression models for the energy need deviations (a) and the peak load deviations (b)

Table 3.6 - Regression models for the deviation of the heating and cooling monthly energy needs expressed and for heating and cooling monthly hourly peak loads

Heating needs deviations		Cooling needs deviations		Heating peaks deviations		Cooling peaks deviations	
$R^2_{adj}=0.632$		$R^2_{adj}=0.568$		$R^2_{adj}=0.767$		$R^2_{adj}=0.555$	
$U_{win}$	-0.592	$SHGC$	0.589	$U_{win}$	-0.812	$SHGC$	0.743
$\theta_{air}$	0.195	$A_{env}$	-0.244	$A_{win}$	-0.224	$\hat{H}_{2dd}$	-0.341
$A_{env}$	0.214	$U_{env}$	0.236	$A_{env}$	0.197	$A_{env}$	-0.126
$A_{win}$	-0.219	$\theta_{air}$	-0.061	$\theta_{air, min}$	0.060	$H_{hor}$	-0.072
$SHGC$	-0.162	$U_{win}$	0.122	$q_i$	-0.034	$U_{env}$	0.146
$H_{win}$	0.164	$q_i$	0.061	$\Delta t_{ie,env}$	-0.081	$q_i$	0.083
$H_{env}$	-0.106	$Y_{ie,env}$	-0.071	$Y_{ie,env}$	0.103	$A_{win}$	0.116
$\kappa_i \cdot A_{tot}$	0.035	$H_{env}$	0.071			$U_{win}$	-0.127
$U_{env}$	0.029	$H_{win}$	-0.117			$\Delta t_{ie,env}$	-0.138
$q_i$	-0.016	$A_{win}$	0.106			$\theta_{air}$	-0.016



### 3.3 Discussion

#### 3.3.1 *BESTEST cases*

As regards the heating energy needs, both simulation codes are within the ranges, with TRNSYS generally closer to the upper boundary than EnergyPlus. Considering the sensitivity, both TRNSYS and EnergyPlus are within the boundaries but they are characterized by different behaviours. For what concerns the cooling energy needs, both simulation codes are very close to the lower boundary and for the case 960 (multizone with a sunspace) TRNSYS 16.1 underestimates of the 12% (-183 MJ respect to the limit of 1481 MJ). For the sensitivity, in EnergyPlus the case 650-600 (night ventilation for lightweight structures) underestimates and  $\Delta_{range}$  is -9% (but the predicted sensitivity is only -43 MJ under the lower limit of -5108 MJ).

As regards the heating peak loads, the two simulation codes are always within the acceptability range and in good agreement with the exception of the case 640 (nighttime heating setback with lightweight structures). For the sensitivity evaluation, EnergyPlus is generally within the boundaries, with the exception of case 640-600 (nighttime heating setback respect to the base case, for lightweight structures), where there is an overestimation, with  $\Delta_{range}$  around 126% (+270 W respect to the upper boundary of 2600 W) and case 910-900 (presence of overhangs on the South-oriented windows for massive cases), where there is an underestimation, with  $\Delta_{range}$  around -22% (but only -3.6 W respect to the lower boundary of 3 W). TRNSYS is under the lower boundary in the cases 630-620 and 930-920 (presence of overhangs and fins for East/West oriented windows, both with lightweight and massive structures), 910-900 and 640-600 (sensitivity to the nighttime heating setback for lightweight structures) of, respectively, -17% (-4 W respect to the lower boundary of -21 W), -11% (-11 W respect to the lower boundary of 27 W), -42% (-6.7 W respect to the lower boundary of 3 W) and -24% (-252 W respect to the lower boundary of 1546 W). Since the heating peaks occur during the nighttime, the problems with the sensitivity to the presence of overhangs and fins suggest a correlation with the modelling of the thermal losses towards the sky vault. Referring to the cooling peak loads, both TRNSYS and EnergyPlus are in the acceptability ranges. For what concerns the sensitivity, only for the case 650-600 TRNSYS is under the lower limit of -7.3% (-4 W respect to the lower boundary of -163 W).

Generally, both TRNSYS and EnergyPlus are in a good agreement with the limits of the BESTEST qualification cases, even if TRNSYS underestimates the cooling energy needs in the case with the sunspace. As regards the sensitivity cases, both codes are within the boundaries in

most of the cases, with some problems encountered in presence of discontinuous setpoint or with overhangs and fins for the heating peak loads.

### **3.3.2 Alignment in the *BESTEST* cases**

Analysing Figure 3.4 it is possible to see that in all cases the deviations between EnergyPlus and TRNSYS are strongly reduced by adopting the alignment procedure described in the previous paragraphs. The average percentage differences (neglecting the points with less than 3.6 MJ of energy needs and 50 W of peak loads) pass from -14.5% to -6.1% for heating needs, from 54.4% to 14.7% for cooling needs, from -4.2% to -1.1% for heating peak loads and from 8.8% to 7.1% for cooling peak loads. Some points keep a high difference for the heating peak loads in the cases with night temperature setback (cases 640 and 940). Considering that heating peak loads always occur at the first hour of daytime setpoint, this is explained by the different approach of EnergyPlus that assumes the setpoint temperature as the average value to maintain during the calculation timestep and not the value to get at the end of the timestep, as in TRNSYS. As the cases examined in the extensive comparison do not consider night attenuation, this aspect is of marginal impact for the present work.

For what concerns the annual results and the boundaries of the *BESTEST* represented in Figures 3.5 and 3.6, the results are within the acceptability ranges both for the energy needs and peak loads. Some problems are still present for the cases with overhangs and fins in the evaluation of the heating peak loads and for the cases with setback or discontinuous setpoints, both for the heating and cooling peak evaluation, in particular for the lightweight structures. With the exception of the cases with intermittent setpoints, the results for the sensitivity cases of the two simulation codes are closer than the ones in Figures 3.2 and 3.3.

### 3.3.3 *Simulation plan results*

As it can be observed in Figures 3.7 and 3.8, the general trends are the same for both localities, even if for different values. In particular the maximum heating monthly energy need in Messina is only 7.2 GJ while in Milan it is 17.6 GJ, and the maximum cooling energy need in Milan is 6.6 GJ while in Messina it is 7.5 GJ. The aligned results for the BESTEST configurations are also presented in Figures 3.7 and 3.8, showing a reduced range of values and smaller differences when compared to the set of configurations proposed in the present work. The average percentage difference is around -11% for heating and 9% for cooling needs.

As regards the heating energy needs, relevant differences are found between the cases with single glazing (S) and the others. As evidenced by the average percentages, the differences and the respective standard deviations reported in Tables 3.4 and 3.5 and by the trends reproduced in Figures 3.7 and 3.8, EnergyPlus tends to undervalue the needs (or TRNSYS tends to overestimate) for the single glazing, in many cases by more than 10%. The average percentage difference is around -30%. Increasing deviations are given for reducing ratio  $S/V$ . All double and triple glazings tend to behave almost the same way, even if the average percentage differences are negative (-9.1 % for double and -6.9% for triple) for high  $SHGC$  and positive for low  $SHGC$  (6.2% for double and 9.2% for triple).

For all those glazings the deviations tend to stay well under  $\pm 10\%$  for the larger heating needs. Low  $S/V$  ratios in those cases tend to lead to negative deviations for heating needs under 6 GJ. Considering all the cases, EnergyPlus underestimates the heating energy needs of the 6.6% with respect to TRNSYS.

As regards the cooling energy needs, important differences (but closer to the  $\pm 10\%$  range) are for the single glazing cases again, with EnergyPlus overestimating with respect to TRNSYS, especially for low  $S/V$  ratios. The average percentage difference (Table 3.4) is around 22%. As concerns the remaining kind of glazings, there is a good correspondence between the double and triple with high  $SHGC$  (in particular for DH, with an average percentage difference of 0.7%, while the TH has a relative deviation of -6.9%). Larger percentage differences are encountered for the double and triple glazings with low  $SHGC$  (DL and TL, with around -26%). With the higher  $SHGC$ , results are still sensitive to the ratio  $S/V$ , with EnergyPlus showing a slight underestimation for the highest  $S/V$ . With low  $SHGC$  glazings there is a uniform undervaluation by EnergyPlus with respect to TRNSYS, with deviations even under -10% for larger values of cooling needs.

The differences between the monthly hourly peak loads obtained with EnergyPlus and with TRNSYS have been plotted against the peak loads calculated with TRNSYS (Figure 3.9 for Milan and Figure 3.10 for Messina). Again, the general considerations are the same. In particular the maximum hourly heating peak load in Messina is only 7.6 kW while in Milan it is 11 kW, and the maximum cooling peak load in Milan is 10.5 kW while in Messina it is 11.1 kW

The aligned results for the BESTEST configurations are presented in Figures 3.9 and 3.10, as well. Both the range of values and the differences between the two codes are smaller than the ones for the set of configurations considered in the present work. The average percentage difference is around -4.2% for heating and 7.2% for cooling peak loads (Tables 3.4 and 3.5). Again, some more dispersed values are shown in heating for the BESTEST cases with night temperature setback.

As regards the heating peak loads, the difference between the cases with single glazing (S) and the others persists. With single glazings EnergyPlus tends to estimate peak loads lower than the TRNSYS ones by more than 20%: in a large part of the cases, the average percentage difference is -22.1%. A modest increase of the deviation is visible for low  $S/V$  ratio. All double and triple glazings tend to behave almost the same way, with deviations generally well under  $\pm 10\%$ , especially for the larger heating peak loads and in average around -7.4% for high  $SHGC$  and -0.8% for low  $SHGC$ . No sensitivity to the  $S/V$  ratio is clearly visible.

As regards the cooling peak loads, the single glazing cases again show larger differences, even if the average is very small (the average percentage deviation is 2.8%), with EnergyPlus overestimating with respect to TRNSYS for low  $S/V$  ratios. As concerns the remaining kind of glazings, there is a substantial correspondence between TRNSYS and EnergyPlus with the double and triple glazings with high  $SHGC$  (DH and TH, with average percentage differences of -0.8% and -6.8%). Double and triple with low  $SHGC$  (DL and TL) present the same behaviour and there is a diffuse undervaluation by EnergyPlus with respect to the results of TRNSYS, with deviations well under -10%, and in average around -22%. With the higher  $SHGC$ , a slight sensitivity to the  $S/V$  ratio persists. EnergyPlus shows a slight overestimation for the lower  $S/V$  but the deviations are generally small and balanced around zero.

The peculiar behaviour, shown in particular for single glazings, can be explained by the different emissivity factor assumed for long wave radiation by the two codes for transparent surfaces.

In winter, when considering high transmittance glazings, the effect of the temperature differences between the internal window surface and the other internal surfaces is influenced by

the lower emissivity assumed by EnergyPlus, which provides lower internal long wave radiation exchanges. This leads to lower heat losses and energy needs than TRNSYS, in particular for the smallest  $S/V$  ratio.

In summer, the higher thermal transmittance glazings present lower internal temperatures than the other surfaces for a large part of time. Again, reduced long wave radiation reduces losses, giving higher energy needs. On the opposite, the surface temperature of lower thermal transmittance glazings often rises above that of the other opaque components. In that case the behaviour is controlled by a counterbalancing effect of lower long wave radiation exchange with the remaining part of the envelope and high or low solar gains entering into the building, depending on the  $SHGC$ . For a detailed analysis of the prediction of the surface temperature for the glazings and the adiabatic envelope, by EnergyPlus and TRNSYS, see chapter 4b.

Finally, for what regards the time of occurrence of the peak loads, analysed in Figure 3.11, TRNSYS is generally late in both heating and cooling cases, but the delay is under one hour in 70% of cases (almost 80% for cooling peak loads) and under three hours in other 20 %. The single glazing shows a modest number of cases with the heating peak loads calculated by EnergyPlus delaying by more than 1 hour and in some cases by more than 1 week.

### 3.3.3.1 Statistical Analysis

The developed statistical models have been described in Figure 3.12 and in Table 3.6. Since there is not a predictive aim, getting the largest value of the determination coefficient  $R^2_{adj}$  was not the main goal. The weight of each variable can be related to the respective standardized coefficient, defined in Annex A as the product of the non standardized coefficient and the ratio between the standard deviations of the independent variable and that of the dependent one: the larger the standardized coefficient, the larger is the relative impact of both the variability and the correlation of the independent variable on the dependent one.

As regards the heating needs deviations, the most influent factors are the windows thermal transmittance, whose standardized coefficient is negative (probably explaining the behaviour of the single glazing shown in Figures 3.7 and 3.8), the opaque envelope area (which is directly related to the  $S/V$  ratio) and the transparent envelope one. Other significant parameters are related to the environmental conditions (the incident radiation and the external temperature) and the  $SHGC$ .

In the cooling needs deviations model the main variables are the  $SHGC$ , the opaque envelope area, its thermal transmittance and that of the windows. In general, the windows

properties and secondly the opaque areas (and so the  $S/V$  ratio) are significant for describing the deviations variability while the environmental conditions appear to be not so relevant. This confirms what was already seen in Figures 3.7 and 3.8.

Referring to the peak loads analysis, in the heating context the main factor is again the windows thermal transmittance - the higher, the lower are the deviations (probably explaining the single glazings behaviour in Figures 3.9 and 3.10), followed by the windows and the opaque envelope area. The windows area has a negative correlation, similarly to the windows thermal transmittance while the opaque envelope area have a positive correlation (in agreement with the effect of the  $S/V$  in Figures 3.9 and 3.10).

For the cooling peak loads, the main factor is the  $SHGC$ , with a strong positive correlation, followed by the 2-days rolling cumulated solar radiation incident on the windows, the opaque envelope thermal transmittance and area, the windows thermal transmittance and area. The peak loads regressions confirm what observed in Figures 3.9 and 3.10: the main variables affecting the deviations are those related to the windows behaviour, followed by the  $S/V$  ratio.

In summary the statistical analysis confirms the relations observed in the description of the results, adding further details, and in particular the role of some specific quantities such as:

- the window thermal transmittance and the window and opaque envelope area, for heating and cooling energy needs and peak loads differences
- the  $SHGC$  and thermal transmittance of the opaque envelope and of the windows, for cooling needs and peak loads differences.

This strengthens the hypothesis that the differences are mainly depending both on the internal radiation model and on the unsteady state conduction model through the opaque envelope.

### 3.4 Main findings

In this chapter the problem of the validation by comparison between BES tools has been investigated. Two well known simulation codes, TRNSYS 16.1 and EnergyPlus 7, have been tested with the BESTEST cases and compared on a wider sample of building configurations.

The monthly heating and cooling energy needs and hourly peak loads were considered, together with the hour of occurrence of the peaks over a wide range of configurations of a building module composed by a single-storey thermal zone with 100 m<sup>2</sup> floor area with different opaque and transparent envelope composition, exposition and windows orientation. The alignment done for the boundary conditions and the simulation hypotheses, which is not required by the BESTEST approach, permitted considering the relative performance of the two codes only related to the specific approaches adopted for the solution of the building thermal balance.

The most important findings emerging from the comparison are:

- the distribution of the difference related to both energy needs and peak load is larger than that presented by the BESTEST configurations. Considering that the results are obtained after the alignment phase, this allowed to investigate the influencing factors pertaining only or mainly to the building thermal balance solution approaches.
- the kind of glazing and the  $S/V$  ratio are among the most important variables impacting both on energy needs and peak loads, and in particular:
  - with the single glazing the heating and the cooling needs and peak loads differences are emphasized, while with low  $SHGC$  particularly the cooling needs and peak loads differences are increased
  - with the double and triple glazings the same behaviour is observed both for heating energy needs and peak loads
  - the differences increases in almost all the situations as  $S/V$  decreases.
- the inferential statistical analysis confirms the descriptive analysis results and strengthen the hypothesis that the deviations are mainly related to the internal radiation model and to the unsteady state conduction model through the opaque envelope.

In general, the suggested approach permitted to improve the awareness on the relative uncertainty and inaccuracy arising from the assumptions and from the solution approaches adopted by each simulation program. This can be useful in particular when tuning simplified methods, or when using simulation codes for particular purposes such as energy diagnosis of new and existing buildings and when performing calibration of the simulation.

This method can be applied to other codes and also to different releases and improvement of a specific simulation code. The use or the comparison of different simulation codes to each other or with experimental data is confirmed to require a deep knowlegde of the physics of involved phenomena and a careful work of selection and treatment of the input data in order to enhance the accuracy of the results.



---

# **Chapter 4:**

## Building envelope characterization with BES



## Chapter 4

This chapter discusses the performance of BES tools to describe the thermal behaviour of the building envelope components under dynamic conditions. It is divided into two parts: the first one is related to the opaque dispersing envelope while the second one to the glazings components.

In the first part of the chapter the dynamic behaviour of the opaque components is discussed. In particular, the focus is on the numerical methods which are generally implemented in BES tools, such as the Transfer Function Methods (*TFM*), like the Direct Root-Finding method of TRNSYS and the State-Space method of EnergyPlus, and Finite Differences Methods which are used to evaluate the dynamic heat transfer through the opaque envelope. These numerical approaches have been assessed considering the dynamic parameters defined in the technical Standard EN ISO 13786:2007, the periodic thermal transmittance, the decrement factor and the time shift, as index variables for the comparison. Since these dynamic parameters are obtained from the analytical solution under sinusoidal solicitations, the Fast Fourier Technique analysis and the superimposition of effects have been used in order to perform the assessment under more realistic conditions. Different locations, orientations and walls have been studied.

Moreover, in the second part of chapter 4, the internal surface temperature profiles for glazings, elaborated by EnergyPlus and TRNSYS, have been compared, considering also the effect of adiabatic surfaces. The deviations have been calculated and distinguished in different frequency classes.



## Part a: Characterization of the building envelope behaviour by BES

### 4a.1 Methods

In order to assess different numerical approaches, the dynamic parameters described in the EN ISO 13786:2007 have been used as synthetic indexes to characterize the behaviours of a sample of walls, subjected to different periodic external solicitations.

The EN ISO 13786:2007 analytical procedure has been implemented by considering simple sinusoidal solicitations. Therefore, the external periodic forcing equivalent temperatures have been decomposed by means of Fast Fourier Transform (*FFT*) analysis and then the responses have been superimposed, as suggested by other authors (Giaconia and Orioli, 2000; Ciulla *et al.*, 2010), who applied this technique to the analysis and validation of the *TFM*. The *FFT* analysis results have been taken as reference for the study of the numerical methods. The Transfer Function Method (*TFM*) – specifically the *DRF* (TRNSYS) and the *SS* (EnergyPlus) approaches, and the Finite Difference Method (*FDM*) have been assessed.

#### 4a.1.1 EN ISO 13786:2007 method

The EN ISO 13786:2007 characterizes the transient response of a building component by means of three parameters: the periodic transmittance, the decrement factor and the phase displacement of the heat flux. The forcing term on the building component is a sinusoidal function of the temperature, applied either on the internal or on the external side of the component, and, consequently, the originated heat fluxes are also sinusoidal. The heat flux is 1-dimensional and so thermal bridges and non-homogeneous layers are not considered in the calculations.

The Standard defines the periodic thermal admittance  $Y_{mm}$  and the periodic transmittance  $Y_{mi}$  as the ratio between the complex amplitude of the heat flux density through the wall surface adjacent to the  $m$ -zone and the complex amplitude of the temperature of the same zone  $m$  or the one of the zone  $n$  respectively, when the other side temperature is constant.

$$Y_{mm} = \frac{\hat{q}_m}{\hat{\theta}_m} \quad (4a.1)$$

$$Y_{mn} = \frac{\hat{q}_m}{\hat{\theta}_n} \quad (4a.2)$$

Thanks to Eq. (4a.1) and (4a.2) it is possible to compute the decrement factor  $f$  as:

$$f = \frac{|Y_{mn}|}{U} \quad (4a.3)$$

where  $U$  is the thermal transmittance of the wall.

The Standard defines also a heat transfer matrix  $Z$  of each layer, that correlates the complex amplitudes of the temperature and heat flux on one side of the component, for example the external side  $e$ , with the same physical quantities on the other side, for example the internal side  $i$ :

$$Z = \begin{pmatrix} \hat{\theta}_e \\ \hat{q}_e \end{pmatrix} = \begin{pmatrix} Z_{11} & Z_{12} \\ Z_{21} & Z_{22} \end{pmatrix} \cdot \begin{pmatrix} \hat{\theta}_i \\ \hat{q}_i \end{pmatrix} \quad (4a.4)$$

where:

$$Z_{11} = Z_{22} = \cosh(\xi) \cdot \cos(\xi) + j \cdot \sinh(\xi) \cdot \sin(\xi) \quad (4a.5)$$

$$Z_{12} = -\frac{\delta}{2\lambda} \cdot [(\sinh(\xi) \cdot \cos(\xi) + \cosh(\xi) \cdot \sin(\xi)) + j \cdot (\cosh(\xi) \cdot \sin(\xi) - \sinh(\xi) \cdot \cos(\xi))] \quad (4a.6)$$

$$Z_{21} = -\frac{\lambda}{\delta} \cdot [(\sinh(\xi) \cdot \cos(\xi) - \cosh(\xi) \cdot \sin(\xi)) + j \cdot (\cosh(\xi) \cdot \sin(\xi) + \sinh(\xi) \cdot \cos(\xi))] \quad (4a.7)$$

and  $\delta$  is the periodic penetration depth and  $\xi$  the ratio between the thickness of the layer and the penetration depth:

$$\delta = \sqrt{\frac{\lambda \cdot T}{\pi \cdot \rho \cdot c}} \quad (4a.8)$$

$$\xi = \frac{s}{\delta} \quad (4a.9)$$

where  $T$  is the period of the variations.

Since a building component usually consists of several layers, the whole transfer matrix is computed as the product of the single matrixes of each layer. By means of this matrix it is possible to calculate the periodic thermal transmittance  $Y_{ie}$ , the internal and external periodic admittances  $Y_{ii}$  and  $Y_{ee}$ , the time shift  $\Delta t_{ie}$  and the internal and external areal heat capacities  $\kappa_i$  and  $\kappa_e$  as:

$$Y_{ie} = -\frac{1}{Z_{12}} \quad (4a.10)$$

$$Y_{ii} = -\frac{Z_{11}}{Z_{12}} \text{ and } Y_{ee} = -\frac{Z_{22}}{Z_{12}} \quad (4a.11)$$

$$\Delta t_{ie} = \frac{T}{2\pi} \cdot \varphi_{ie} = \frac{T}{2\pi} \cdot \arg(Z_{12}) \quad (4a.12)$$

$$\kappa_i = \frac{T}{2\pi} \cdot \left| \frac{Z_{11}-1}{Z_{12}} \right| \text{ and } \kappa_e = \frac{T}{2\pi} \cdot \left| \frac{Z_{22}-1}{Z_{12}} \right| \quad (4a.13)$$

#### 4a.1.2 The Fourier series analysis and the EN ISO 13786:2007 method

In order to simulate the response of a component subjected to an external real forcing condition, the temperature variation along a characteristic day has been calculated as sol-air temperature  $\theta_{sol-air}$  and decomposed in different harmonics. The EN ISO 13786:2007 procedure has been applied to each harmonic to evaluate the respective periodic thermal transmittance and the system global response has been estimated according to the superimposition principle.

To determine the forcing input, for each considered location and orientation, the sol-air temperature has been estimated from the external periodic conditions (i.e., the solar irradiance, the dry bulb temperature and the fictive sky temperature) elaborated by EnergyPlus for a single component.

As seen in chapter 3, this BES software provides three linearized coefficients for the external infrared exchanges:  $h_{r, gnd}$ ,  $h_{r, air}$  and  $h_{r, sky}$ , respectively for ground, air and sky. Considering the ground temperature equal to the outdoor air temperature (as both in EnergyPlus and in TRNSYS approaches), the whole thermal exchange from the external surface can be expressed as:

$$q_{c+r,e} = (h_{r, gnd} + h_{r, air} + h_{c,e} + h_{r, sky}) \cdot (\theta_{se} - \theta_{air}) + h_{r, sky} \cdot (\theta_{air} - \theta_{sky}) \quad (4a.14)$$

defining:

$$h_{se} = (h_{r, gnd} + h_{r, air} + h_{c,e} + h_{r, sky}) \quad (4a.15)$$

and adding the solar radiation absorbed, the total exchange from the external surface is:

$$q_{c+r+sol,e} = h_{se} \cdot (\theta_{se} - \theta_{air}) + h_{r, sky} \cdot (\theta_{air} - \theta_{sky}) - I\alpha \quad (4a.16)$$

In accordance with the definition of the sol-air temperature  $\theta_{sol-air}$ :



$$q_{c+r+sol,e} = h_{se} \cdot (\theta_{se} - \theta_{sol-air}) \quad (4a.17)$$

therefore:

$$\theta_{sol-air} = \theta_{air} + \frac{I\alpha - h_{r,sky} \cdot (\theta_{air} - \theta_{sky})}{h_{se}} \quad (4a.18)$$

The  $h_{r,sky}$  values are functions of the surface temperatures and, generally, of the surface balances and of the wall properties. Considering periodic regimes and holding constant the solar absorption coefficient and the convective coefficient, they show small deviations according to the different wall typologies considered in this research. Nevertheless, they can be considered negligible: the maximum deviation on the  $\theta_{sol-air}$  is less than 0.07 °C (i.e., the 0.175% of the computed value) while the mean deviation is less than 0.02 °C. Thus, it is possible to assume a unique  $\theta_{sol-air}$  profile for each orientation.

To decompose the forcing signal, the Fast Fourier Transform (*FFT*) algorithm (Press *et al.*, 2007) has been integrated in the developed model, computing the harmonics of the original solicitation. Truncating the series to the ninth harmonic the sol-air temperature approximation is given by:

$$\theta_{sol-air} = \bar{\theta}_{sol-air} + \tilde{\theta}_{sol-air} \approx \bar{\theta}_{sol-air} + \sum_{k=1}^9 \tilde{\theta}_{sol-air,k} = \bar{\theta}_{sol-air} + \sum_{k=1}^9 \hat{\theta}_{sol-air,k} \cdot \sin(\omega_k t + \varphi_k) \quad (4a.19)$$

The approximation given by the *FFT* procedure by means of nine harmonics allows to obtain mean deviations that are less than 1% with respect to the original solicitation of the sol-air temperature.

An example of the results obtained by performing the *FFT* analysis - and summing the results for the first nine harmonics - is shown in Figure 4a.1 for a West oriented vertical wall located in Rome.

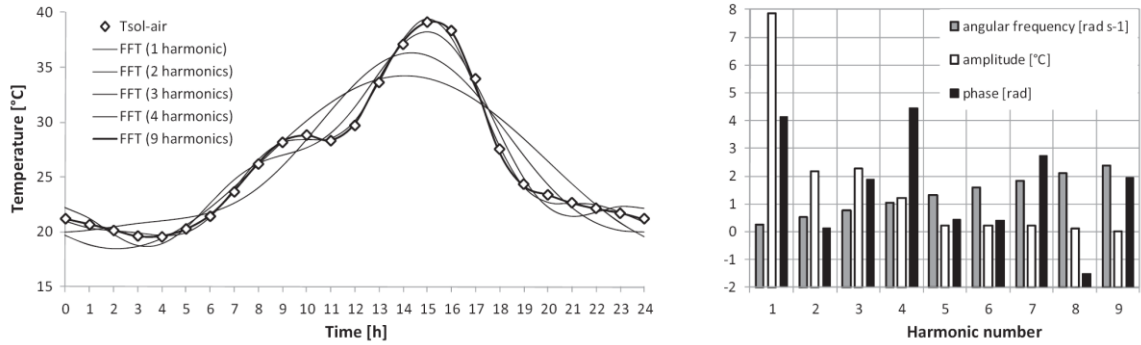


Figure 4a.1 - Fast Fourier Transform (FFT) carried out on the sol-air temperature derived from the measured data of Rome (West oriented vertical wall)

The internal flux was then calculated as:

$$q_{i,calc}(t) = q_{i,FFT}(t) \approx \bar{q}_i + \tilde{q}_{i,FFT}(t) \quad (4a.20)$$

with:

$$\bar{q}_i = U \cdot (\theta_i - \bar{\theta}_{sol-air}) \quad (4a.21)$$

$$\tilde{q}_{i,FFT}(t) = \sum_{k=1}^9 \tilde{q}_{i,FFT,k}(t) = \sum_{k=1}^9 \hat{q}_{i,k} \cdot \sin(\omega_k t + \varphi_k) = \sum_{k=1}^9 |Y_{ie,k}| \cdot \hat{\theta}_{sol-air,k} \cdot \sin(\omega_k t + \varphi_k) \quad (4a.22)$$

where  $\theta_i$  is the internal air temperature and  $Y_{ie,k}$  is the periodic thermal transmittance calculated according to the EN ISO 13786:2007 for the  $k^{th}$  harmonic. For  $k=1$ ,  $Y_{ie,1}$  is the Standard periodic thermal transmittance  $Y_{ie}$ .

The flux amplitude is then given by:

$$\hat{q}_{i,FFT} \approx \frac{1}{2} [\tilde{q}_{i,FFT}]_{\max} - \frac{1}{2} [\tilde{q}_{i,FFT}]_{\min} \quad (4a.23)$$

The response computed by means of the *FFT* procedure has been assumed as the reference result (Giaconia and Orioli, 2000; Ciulla *et al.*, 2010) for the comparison of the detailed simulation (*FDM* and *TFM* approaches).

Following the approach by Corrado and Paduos (2009), the modulus of the calculated periodic thermal transmittance  $Y_{ie,calc}$  has been determined as in Eq. (4a.24) as the ratio between the amplitude of the calculated inlet thermal flux and the amplitude of the forcing sol-air temperature.

$$|Y_{ie,calc}| = \frac{\hat{q}_{i,calc}}{\hat{\theta}_{sol-air}} \quad (4a.24)$$

Eq. (4a.24) has been used also for the calculation of the periodic thermal transmittance for the numerical methods described in the next paragraphs.

#### ***4a.1.3 Transfer functions approach***

The *TF* Methods are based on a time series of temperature and heat flux terms, weighted with different coefficients and used to calculate the temperature and the heat flux on the internal and external surfaces or at the interfaces of two adjacent layers.

There are different ways to define the solution series, such as a time-domain based or a Z transform-domain based. In particular, the methods implemented in the examined simulation codes belong to the second kind. The Direct Root Finding method (*DRF*) in TRNSYS has been developed by Mitalas and Arseneault (1971) while the State-Space method (*SS*) in EnergyPlus by Ceylan and Myers (1980), Seem (1987) and Ouyang and Haghighat (1991). The main differences between the *DRF* and the *SS* methods are related to the number of terms used and the methodology to elaborate their coefficients.

The same external forcing conditions have been used in both software. In particular for calculating the infrared extra flow, as observed in chapter 3, TRNSYS and EnergyPlus have two different methods and so, in order to align the boundary conditions, when a surface has a vertical tilt, the TRNSYS view factor of the sky has been changed and set equal to 0.35, instead of 0.5 and EnergyPlus fictive sky temperature has been used.

The selected timestep for the simulations was 15 minutes.

#### ***4a.1.4 The Finite Difference Method***

A specific simulation tool has been developed for the purposes of the present work, implementing a fully implicit finite difference scheme, in order to solve the heat equation in transient regime for homogeneous media, without heat source and using constant thermo physical properties. The advantage of using such implicit method relies in the fact that it is always stable, independently of the values of the timestep and of the Fourier number.

The wall geometry (i.e., multi-layer wall) has been discretized in a 1-dimensional domain using an integration step of 1 cm, while the timestep has been assumed as 15 minutes, coherently with the one of the *TFM*. Discretization refinement and time step shortening were found to have a negligible effect on the solution. In order to obtain a reliable comparison between different approaches, the same sol-air temperature boundary conditions used for the *FFT* simulations have been applied here.

#### 4a.1.5 Tested walls and boundary conditions

The thermal dynamic transfer properties have been calculated for 15 types of wall, whose layers thicknesses and materials have been reported in Table 4a.1. The cases *A* and *B* are composed by two layers and, respectively, externally and internally insulated. The cases *C* and *D* have 3 layers with the insulating one between two massive layers: the thicker layer is inside in the group *C* and outside in the group *D*. The cases *M*, finally, consist in single-layer walls. The considered materials are a clay block with thermal conductivity  $0.25 \text{ W m}^{-1} \text{ K}^{-1}$ , density  $850 \text{ kg m}^{-3}$  and specific heat  $840 \text{ J kg}^{-1} \text{ K}^{-1}$  and an insulating layer with thermal conductivity  $0.04 \text{ W m}^{-1} \text{ K}^{-1}$ , density  $40 \text{ kg m}^{-3}$  and specific heat  $1470 \text{ J kg}^{-1} \text{ K}^{-1}$ .

The thermal convection coefficient is  $17.78 \text{ W m}^{-2} \text{ K}^{-1}$  for the external side and  $3.07 \text{ W m}^{-2} \text{ K}^{-1}$  for the internal one. The wall absorption coefficient is 0.6 and the emissivity is 0.9. In order to evaluate the behaviour of the wall independently of the rest of the building envelope, the internal radiative exchange has been imposed equal to zero. Thus, a single constant convective surface heat transfer coefficient has been considered in agreement with the Standard EN ISO 13786:2007, assuming internal interactions modeled by means of an equivalent convective node at a fixed temperature of  $26 \text{ }^{\circ}\text{C}$ .

Table 4a.1 – Analysed walls

	Component composition (internal to external side)	Thermal transmittance [ $\text{W m}^{-2} \text{ K}^{-1}$ ]
<i>A5</i>	20 cm clay block; 5 cm insulation	0.413
<i>A10</i>	20 cm clay block; 10 cm insulation	0.273
<i>A15</i>	20 cm clay block; 15 cm insulation	0.203
<i>B5</i>	5 cm insulation; 20 cm clay block	0.413
<i>B10</i>	10 cm insulation; 20 cm clay block	0.273
<i>B15</i>	15 cm insulation; 20 cm clay block	0.203
<i>C5</i>	20 cm clay block; 5 cm insulation; 10 cm clay block	0.355
<i>C10</i>	20 cm clay block; 10 cm insulation; 10 cm clay block	0.246
<i>C15</i>	20 cm clay block; 15 cm insulation; 10 cm clay block	0.188
<i>D5</i>	10 cm clay block; 5 cm insulation; 20 cm clay block	0.355
<i>D10</i>	10 cm clay block; 10 cm insulation; 20 cm clay block	0.246
<i>D15</i>	10 cm clay block; 15 cm insulation; 20 cm clay block	0.188
<i>M10</i>	10 cm clay block	1.299
<i>M20</i>	20 cm clay block	0.855
<i>M30</i>	30 cm clay block	0.637

Three different summer climatic conditions relative to the month of July have been considered, in particular relevant to the North (Milan), to the centre (Rome) and to the South (Palermo) of Italy. Five orientations (North, East, South, West and horizontal) have been assumed in order to assess different solar radiation expositions.

A wall side has been exposed to the typical internal summer condition, with the air temperature fixed to 26 °C, and the other one to a daily profile averaging the external conditions of the month of July. The external solicitation has been elaborated calculating the average profiles for the dry bulb temperature, the solar direct normal radiation, the solar diffuse horizontal radiation and the global horizontal infrared radiation. Any reflected solar component has been neglected, setting the ground reflection coefficient to zero. The mean hourly profiles of dry bulb temperature and global horizontal irradiance in the month of July for the three localities have been reported in Figure 4a.2.

A weather file for EnergyPlus has been created with these profiles and this BES tool has been used for elaborating the fictitious sky temperature, the radiation and the incidence solar beam angle on the different orientations with an hourly discretization. The elaborated data have been read as input directly by TRNSYS, while coherent sol-air profiles were calculated to be used with the other approaches.

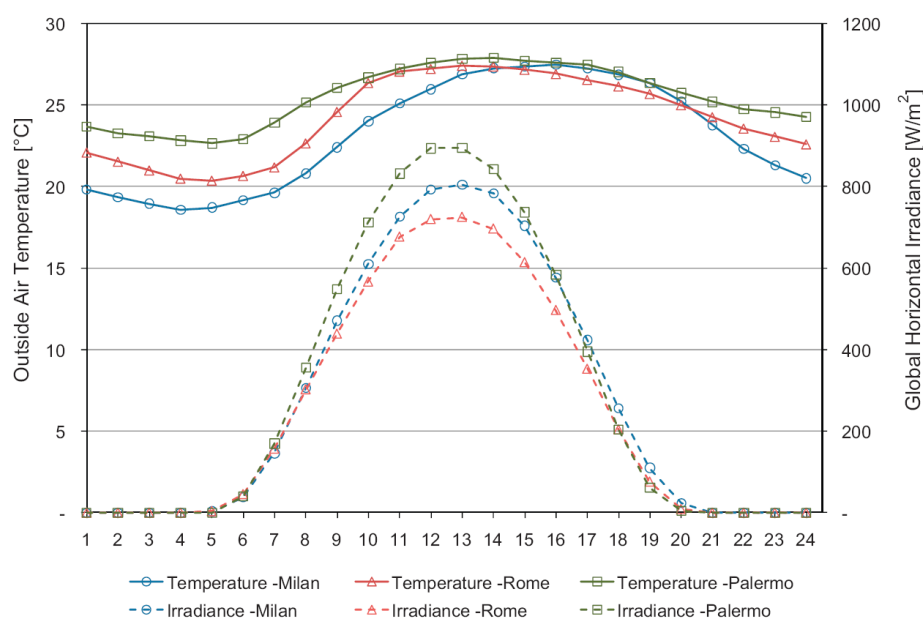


*Figure 4a.2 – Average hourly profiles of the dry bulb temperature and the global horizontal solar irradiance of the chosen climates for the month of July*

To determine the input solicitation for *FFT* and the *FDM* analysis, for each location and all the orientations considered, sol-air temperature with a discretization of 15 minutes has been estimated from the external solicitations elaborated by EnergyPlus for a single component.

## 4a.2 Results

The dynamic parameters calculated according to the numerical approaches have been compared to the results of the *FFT* and EN ISO 13786:2007 method. For the complex amplitude of the calculated thermal flux on the internal surface, the ones determined by means of the numerical methods have been employed to calculate the modulus of the periodic thermal transmittance in accordance with Eq. (4a.24). The time shift has been calculated simply subtracting the occurrence time of the forcing sol-air peak to the occurrence time of the internal flux peak. Time shifts have been reduced to the range of  $-24$  to  $0$  h, in order to simplify the comparison between retarding (less than 12 h of absolute shift) and anticipating (more than 12 h of absolute shift) outputs.

In Tables 4a.2, 4a.3, 4a.4, 4a.5, 4a.6 and 4a.7, the reference dynamic parameters calculated with the *FFT* approach have been reported for the considered walls in the location of Rome, as well as those elaborated with the numerical methods (respectively the *DRF* ones in Tables 4a.2 and 4a.3, the *SS* ones in Tables 4a.4 and 4a.5 and finally the *FDM* ones in Tables 4a.6 and 4a.7).

In Figures 4a.3 and 4a.4, the periodic thermal transmittances and the time shifts for the differently oriented walls in Rome have been represented for the considered approaches.

Only the results obtained for Rome have been reported here: the results for the three locations are very similar but Rome presents slightly larger deviations and for this reason it has been considered in this Paragraph. For Palermo and Milan, see Annex C.



Table 4a.2 - Periodic thermal transmittance according to the conventional EN ISO 13786:2007 one, the FFT and the DRF approaches, with percentage differences between DRF and FFT values for the different orientations in the case of Rome. All values in  $[W m^{-2} K^{-1}]$

	EN 13786	NORTH			EAST			WEST			SOUTH			HORIZONTAL		
		FFT	DRF	$\Delta\%$	FFT	DRF	$\Delta\%$	FFT	DRF	$\Delta\%$	FFT	DRF	$\Delta\%$	FFT	DRF	$\Delta\%$
A5	<b>0.084</b>	0.085	0.083	-1.77%	0.060	0.058	-3.73%	0.066	0.065	-1.81%	0.076	0.075	-2.17%	0.085	0.082	-2.81%
A10	<b>0.045</b>	0.045	0.045	-1.07%	0.032	0.030	-4.93%	0.035	0.035	-0.96%	0.041	0.040	-1.19%	0.045	0.044	-2.29%
A15	<b>0.030</b>	0.030	0.031	4.59%	0.021	0.020	-5.53%	0.023	0.024	3.56%	0.027	0.027	0.71%	0.030	0.030	0.24%
B5	<b>0.129</b>	0.131	0.132	0.15%	0.091	0.088	-2.89%	0.104	0.104	-0.52%	0.118	0.117	-0.25%	0.130	0.130	-0.73%
B10	<b>0.074</b>	0.075	0.076	1.72%	0.052	0.050	-3.47%	0.059	0.060	1.46%	0.067	0.068	0.62%	0.075	0.075	0.59%
B15	<b>0.050</b>	0.050	0.053	5.00%	0.035	0.033	-4.41%	0.039	0.041	4.85%	0.045	0.047	4.61%	0.050	0.052	3.53%
C5	<b>0.049</b>	0.049	0.050	3.66%	0.034	0.034	-0.52%	0.039	0.040	3.20%	0.044	0.045	3.18%	0.048	0.050	3.82%
C10	<b>0.028</b>	0.027	0.029	7.07%	0.019	0.019	0.15%	0.022	0.023	6.05%	0.025	0.026	6.11%	0.027	0.029	7.81%
C15	<b>0.019</b>	0.018	0.020	11.06%	0.013	0.013	0.26%	0.015	0.016	10.25%	0.016	0.018	10.29%	0.018	0.020	12.41%
D5	<b>0.050</b>	0.049	0.051	3.53%	0.034	0.034	-1.28%	0.039	0.040	3.24%	0.045	0.046	2.69%	0.049	0.051	4.03%
D10	<b>0.028</b>	0.027	0.029	6.57%	0.019	0.019	-0.75%	0.022	0.023	6.29%	0.025	0.026	5.79%	0.027	0.029	7.31%
D15	<b>0.018</b>	0.018	0.020	11.45%	0.013	0.012	-1.12%	0.015	0.016	10.15%	0.016	0.018	10.18%	0.018	0.020	12.59%
M10	<b>1.126</b>	1.140	1.130	-0.83%	0.965	0.947	-1.81%	1.038	1.007	-2.99%	1.080	1.058	-2.06%	1.126	1.107	-1.68%
M20	<b>0.419</b>	0.429	0.421	-1.98%	0.296	0.279	-5.47%	0.351	0.338	-3.59%	0.384	0.375	-2.32%	0.425	0.412	-2.91%
M30	<b>0.150</b>	0.150	0.149	-0.77%	0.104	0.119	13.90%	0.117	0.117	-0.51%	0.135	0.132	-2.48%	0.149	0.145	-2.96%

Table 4a.3 - Time shift (in the range -24 to 0 hours) according to the conventional EN ISO 13786:2007 one, the FFT and the DRF approaches, with absolute differences between DRF and FFT values for the different orientations in the case of Rome. All values in [h]

	EN 13786	NORTH			EAST			WEST			SOUTH			HORIZONTAL		
		FFT	DRF	$\Delta$	FFT	DRF	$\Delta$	FFT	DRF	$\Delta$	FFT	DRF	$\Delta$	FFT	DRF	$\Delta$
A5	<b>-9.1</b>	-6.0	-5.0	1.0	-11.0	-10.0	1.0	-7.0	-7.0	-	-9.0	-8.0	1.0	-9.0	-8.0	1.0
A10	<b>-9.9</b>	-6.0	-5.0	1.0	-12.0	-11.0	1.0	-8.0	-7.0	1.0	-10.0	-9.0	1.0	-9.0	-8.0	1.0
A15	<b>-10.9</b>	-8.0	-7.0	1.0	-13.0	-11.0	2.0	-9.0	-9.0	-	-11.0	-10.0	1.0	-10.0	-9.0	1.0
B5	<b>-8.1</b>	-5.0	-4.0	1.0	-9.0	-8.0	1.0	-6.0	-5.0	1.0	-8.0	-7.0	1.0	-8.0	-7.0	1.0
B10	<b>-8.9</b>	-5.0	-4.0	1.0	-10.0	-9.0	1.0	-7.0	-6.0	1.0	-9.0	-8.0	1.0	-8.0	-7.0	1.0
B15	<b>-9.9</b>	-6.0	-5.0	1.0	-12.0	-10.0	2.0	-8.0	-7.0	1.0	-10.0	-8.0	2.0	-9.0	-8.0	1.0
C5	<b>-12.9</b>	-10.0	-8.0	2.0	-15.0	-15.0	-	-12.0	-11.0	1.0	-13.0	-12.0	1.0	-13.0	-12.0	1.0
C10	<b>-13.9</b>	-11.0	-9.0	2.0	-16.0	-15.0	1.0	-13.0	-11.0	2.0	-14.0	-13.0	1.0	-14.0	-12.0	2.0
C15	<b>-14.9</b>	-12.0	-10.0	2.0	-17.0	-15.0	2.0	-14.0	-12.0	2.0	-16.0	-14.0	2.0	-15.0	-13.0	2.0
D5	<b>-13.3</b>	-10.0	-9.0	1.0	-15.0	-15.0	-	-12.0	-11.0	1.0	-14.0	-13.0	1.0	-13.0	-12.0	1.0
D10	<b>-14.3</b>	-11.0	-9.0	2.0	-17.0	-15.0	2.0	-13.0	-12.0	1.0	-15.0	-13.0	2.0	-14.0	-13.0	1.0
D15	<b>-15.3</b>	-12.0	-10.0	2.0	-18.0	-16.0	2.0	-14.0	-12.0	2.0	-16.0	-14.0	2.0	-15.0	-13.0	2.0
M10	<b>-2.8</b>	-1.0	0.0	1.0	-2.0	-1.0	1.0	-2.0	-1.0	1.0	-2.0	-2.0	-	-3.0	-2.0	1.0
M20	<b>-6.8</b>	-4.0	-3.0	1.0	-6.0	-6.0	-	-5.0	-4.0	1.0	-6.0	-6.0	-	-6.0	-6.0	-
M30	<b>-10.7</b>	-7.0	-7.0	-	-12.0	-12.0	-	-9.0	-9.0	-	-11.0	-10.0	1.0	-10.0	-9.0	1.0

*Table 4a.4 - Periodic thermal transmittance according to the conventional EN ISO 13786:2007 one, the FFT and the SS approaches, with percentage differences between SS and FFT values for the different orientations in the case of Rome. All values in [ $W m^{-2} K^{-1}$ ]*

	EN 13786	NORTH			EAST			WEST			SOUTH			HORIZONTAL		
		FFT	SS	$\Delta\%$	FFT	SS	$\Delta\%$	FFT	SS	$\Delta\%$	FFT	SS	$\Delta\%$	FFT	SS	$\Delta\%$
A5	<b>0.084</b>	0.085	0.081	-4.32%	0.060	0.058	-2.52%	0.066	0.064	-4.00%	0.076	0.076	-1.01%	0.085	0.080	-5.93%
A10	<b>0.045</b>	0.045	0.045	-1.48%	0.032	0.031	-1.80%	0.035	0.035	-1.36%	0.041	0.040	-2.11%	0.045	0.042	-6.61%
A15	<b>0.030</b>	0.030	0.029	-1.79%	0.021	0.021	1.29%	0.023	0.023	-0.62%	0.027	0.027	1.05%	0.030	0.028	-3.94%
B5	<b>0.129</b>	0.131	0.127	-3.61%	0.091	0.090	-0.78%	0.104	0.100	-3.93%	0.118	0.117	-0.26%	0.130	0.125	-4.51%
B10	<b>0.074</b>	0.075	0.072	-4.64%	0.052	0.052	0.44%	0.059	0.057	-4.65%	0.067	0.067	-0.71%	0.075	0.071	-5.07%
B15	<b>0.050</b>	0.050	0.049	-3.35%	0.035	0.036	3.74%	0.039	0.038	-3.03%	0.045	0.044	-1.76%	0.050	0.047	-6.21%
C5	<b>0.049</b>	0.049	0.048	-1.11%	0.034	0.034	0.86%	0.039	0.038	-0.51%	0.044	0.045	2.43%	0.048	0.048	-0.36%
C10	<b>0.028</b>	0.027	0.027	-0.69%	0.019	0.020	5.02%	0.022	0.022	0.12%	0.025	0.026	3.18%	0.027	0.028	0.52%
C15	<b>0.019</b>	0.018	0.018	-0.29%	0.013	0.014	10.12%	0.015	0.015	0.27%	0.016	0.017	3.27%	0.018	0.018	1.37%
D5	<b>0.050</b>	0.049	0.048	-1.50%	0.034	0.035	1.96%	0.039	0.039	-1.28%	0.045	0.045	1.26%	0.049	0.049	-0.86%
D10	<b>0.028</b>	0.027	0.027	-1.27%	0.019	0.020	5.93%	0.022	0.022	-0.56%	0.025	0.025	1.79%	0.027	0.027	0.53%
D15	<b>0.018</b>	0.018	0.018	-0.77%	0.013	0.014	9.75%	0.015	0.014	-0.38%	0.016	0.017	2.09%	0.018	0.018	1.67%
M10	<b>1.126</b>	1.140	1.120	-1.75%	0.965	0.921	-4.56%	1.038	1.022	-1.54%	1.080	1.093	1.17%	1.126	1.104	-1.96%
M20	<b>0.419</b>	0.429	0.401	-6.58%	0.296	0.288	-2.63%	0.351	0.327	-6.83%	0.384	0.372	-3.02%	0.425	0.395	-6.98%
M30	<b>0.150</b>	0.150	0.143	-4.61%	0.104	0.101	-2.85%	0.117	0.113	-3.86%	0.135	0.131	-2.83%	0.149	0.140	-6.31%

*Table 4a.5 - Time shift (in the range -24 to 0 hours) according to the conventional EN ISO 13786:2007 one, the FFT and the SS approaches, with absolute differences between SS and FFT values for the different orientations in the case of Rome. All values in [h]*

	EN 13786	NORTH			EAST			WEST			SOUTH			HORIZONTAL		
		FFT	SS	$\Delta$	FFT	SS	$\Delta$	FFT	SS	$\Delta$	FFT	SS	$\Delta$	FFT	SS	$\Delta$
A5	<b>-9.1</b>	-6.0	-7.0	-1.0	-11.0	-11.0	-	-7.0	-7.0	-	-9.0	-9.0	-	-9.0	-9.0	-
A10	<b>-9.9</b>	-6.0	-7.0	-1.0	-12.0	-12.0	-	-8.0	-9.0	-1.0	-10.0	-10.0	-	-9.0	-9.0	-
A15	<b>-10.9</b>	-8.0	-7.0	1.0	-13.0	-15.0	-2.0	-9.0	-9.0	-	-11.0	-12.0	-1.0	-10.0	-12.0	-2.0
B5	<b>-8.1</b>	-5.0	-5.0	-	-9.0	-10.0	-1.0	-6.0	-7.0	-1.0	-8.0	-8.0	-	-8.0	-8.0	-
B10	<b>-8.9</b>	-5.0	-6.0	-1.0	-10.0	-11.0	-1.0	-7.0	-8.0	-1.0	-9.0	-9.0	-	-8.0	-9.0	-1.0
B15	<b>-9.9</b>	-6.0	-7.0	-1.0	-12.0	-12.0	-	-8.0	-9.0	-1.0	-10.0	-10.0	-	-9.0	-10.0	-1.0
C5	<b>-12.9</b>	-10.0	-9.0	1.0	-15.0	-15.0	-	-12.0	-12.0	-	-13.0	-13.0	-	-13.0	-12.0	1.0
C10	<b>-13.9</b>	-11.0	-10.0	1.0	-16.0	-16.0	-	-13.0	-13.0	-	-14.0	-14.0	-	-14.0	-13.0	1.0
C15	<b>-14.9</b>	-12.0	-11.0	1.0	-17.0	-17.0	-	-14.0	-14.0	-	-16.0	-15.0	1.0	-15.0	-15.0	-
D5	<b>-13.3</b>	-10.0	-10.0	-	-15.0	-15.0	-	-12.0	-12.0	-	-14.0	-14.0	-	-13.0	-13.0	-
D10	<b>-14.3</b>	-11.0	-11.0	-	-17.0	-16.0	1.0	-13.0	-13.0	-	-15.0	-15.0	-	-14.0	-14.0	-
D15	<b>-15.3</b>	-12.0	-12.0	-	-18.0	-17.0	1.0	-14.0	-14.0	-	-16.0	-16.0	-	-15.0	-15.0	-
M10	<b>-2.8</b>	-1.0	-1.0	-	-2.0	-2.0	-	-2.0	-2.0	-	-2.0	-3.0	-1.0	-3.0	-3.0	-
M20	<b>-6.8</b>	-4.0	-3.0	1.0	-6.0	-7.0	-1.0	-5.0	-5.0	-	-6.0	-6.0	-	-6.0	-6.0	-
M30	<b>-10.7</b>	-7.0	-7.0	-	-12.0	-14.0	-2.0	-9.0	-9.0	-	-11.0	-12.0	-1.0	-10.0	-12.0	-2.0

Table 4a.6 - Periodic thermal transmittance according to the conventional EN ISO 13786:2007 one, the FFT and the FDM approaches, with percentage differences between FDM and FFT values for the different orientations in the case of Rome. All values in  $[W m^{-2} K^{-1}]$

	EN 13786	NORTH			EAST			WEST			SOUTH			HORIZONTAL		
		FFT	FDM	$\Delta\%$	FFT	FDM	$\Delta\%$	FFT	FDM	$\Delta\%$	FFT	FDM	$\Delta\%$	FFT	FDM	$\Delta\%$
A5	<b>0.084</b>	0.085	0.082	-3.55%	0.060	0.058	-3.54%	0.066	0.064	-3.26%	0.076	0.076	-0.55%	0.085	0.081	-4.87%
A10	<b>0.045</b>	0.045	0.044	-3.66%	0.032	0.031	-3.27%	0.035	0.034	-3.49%	0.041	0.041	-0.22%	0.045	0.043	-5.25%
A15	<b>0.030</b>	0.030	0.028	-4.21%	0.021	0.020	-3.69%	0.023	0.022	-3.78%	0.027	0.026	-1.06%	0.030	0.028	-5.98%
B5	<b>0.129</b>	0.131	0.126	-3.81%	0.091	0.088	-2.53%	0.104	0.100	-3.91%	0.118	0.117	-0.41%	0.130	0.125	-4.53%
B10	<b>0.074</b>	0.075	0.072	-3.86%	0.052	0.050	-3.83%	0.059	0.057	-4.07%	0.067	0.067	-0.82%	0.075	0.071	-5.18%
B15	<b>0.050</b>	0.050	0.048	-4.45%	0.035	0.033	-4.68%	0.039	0.038	-4.55%	0.045	0.044	-1.07%	0.050	0.047	-5.93%
C5	<b>0.049</b>	0.049	0.046	-5.03%	0.034	0.032	-5.61%	0.039	0.037	-5.18%	0.044	0.043	-2.37%	0.048	0.045	-6.34%
C10	<b>0.028</b>	0.027	0.026	-5.35%	0.019	0.018	-5.94%	0.022	0.021	-5.61%	0.025	0.024	-2.88%	0.027	0.025	-6.86%
C15	<b>0.019</b>	0.018	0.017	-5.95%	0.013	0.012	-6.27%	0.015	0.014	-6.30%	0.016	0.016	-3.56%	0.018	0.017	-7.45%
D5	<b>0.050</b>	0.049	0.047	-4.92%	0.034	0.033	-4.68%	0.039	0.037	-4.62%	0.045	0.044	-2.24%	0.049	0.046	-6.52%
D10	<b>0.028</b>	0.027	0.026	-5.15%	0.019	0.018	-5.14%	0.022	0.021	-4.91%	0.025	0.024	-2.53%	0.027	0.026	-6.49%
D15	<b>0.018</b>	0.018	0.017	-5.80%	0.013	0.012	-5.75%	0.015	0.014	-5.43%	0.016	0.016	-2.95%	0.018	0.017	-6.90%
M10	<b>1.126</b>	1.140	1.115	-2.18%	0.965	0.938	-2.78%	1.038	1.013	-2.37%	1.080	1.086	0.52%	1.126	1.094	-2.87%
M20	<b>0.419</b>	0.429	0.414	-3.57%	0.296	0.287	-2.75%	0.351	0.336	-4.07%	0.384	0.382	-0.37%	0.425	0.406	-4.37%
M30	<b>0.150</b>	0.150	0.143	-4.87%	0.104	0.100	-4.03%	0.117	0.112	-4.31%	0.135	0.133	-1.84%	0.149	0.140	-5.92%

Table 4a.7 - Time shift (in the range -24 to 0 hours) according to the conventional EN ISO 13786:2007 one, the FFT and the FDM approaches, with absolute differences between FDM and FFT values for the different orientations in the case of Rome. All values in [h]

	EN 13786	NORTH			EAST			WEST			SOUTH			HORIZONTAL		
		FFT	FDM	$\Delta$	FFT	FDM	$\Delta$	FFT	FDM	$\Delta$	FFT	FDM	$\Delta$	FFT	FDM	$\Delta$
A5	<b>-9.1</b>	-6.0	-5.0	1.0	-11.0	-11.0	-	-7.0	-7.0	-	-9.0	-9.0	-	-9.0	-9.0	-
A10	<b>-9.9</b>	-6.0	-6.0	-	-12.0	-12.0	-	-8.0	-8.0	-	-10.0	-10.0	-	-9.0	-9.0	-
A15	<b>-10.9</b>	-8.0	-7.0	1.0	-13.0	-13.0	-	-9.0	-9.0	-	-11.0	-11.0	-	-10.0	-10.0	-
B5	<b>-8.1</b>	-5.0	-4.0	1.0	-9.0	-9.0	-	-6.0	-6.0	-	-8.0	-8.0	-	-8.0	-7.0	1.0
B10	<b>-8.9</b>	-5.0	-5.0	-	-10.0	-10.0	-	-7.0	-7.0	-	-9.0	-9.0	-	-8.0	-8.0	-
B15	<b>-9.9</b>	-6.0	-6.0	-	-12.0	-11.0	1.0	-8.0	-8.0	-	-10.0	-10.0	-	-9.0	-9.0	-
C5	<b>-12.9</b>	-10.0	-9.0	1.0	-15.0	-15.0	-	-12.0	-11.0	1.0	-13.0	-13.0	-	-13.0	-12.0	1.0
C10	<b>-13.9</b>	-11.0	-10.0	1.0	-16.0	-16.0	-	-13.0	-12.0	1.0	-14.0	-14.0	-	-14.0	-13.0	1.0
C15	<b>-14.9</b>	-12.0	-11.0	1.0	-17.0	-17.0	-	-14.0	-14.0	-	-16.0	-15.0	1.0	-15.0	-15.0	-
D5	<b>-13.3</b>	-10.0	-10.0	-	-15.0	-15.0	-	-12.0	-12.0	-	-14.0	-14.0	-	-13.0	-13.0	-
D10	<b>-14.3</b>	-11.0	-11.0	-	-17.0	-16.0	1.0	-13.0	-13.0	-	-15.0	-15.0	-	-14.0	-14.0	-
D15	<b>-15.3</b>	-12.0	-12.0	-	-18.0	-17.0	1.0	-14.0	-14.0	-	-16.0	-16.0	-	-15.0	-15.0	-
M10	<b>-2.8</b>	-1.0	-1.0	-	-2.0	-2.0	-	-2.0	-2.0	-	-2.0	-2.0	-	-3.0	-3.0	-
M20	<b>-6.8</b>	-4.0	-3.0	1.0	-6.0	-7.0	-1.0	-5.0	-5.0	-	-6.0	-6.0	-	-6.0	-6.0	-
M30	<b>-10.7</b>	-7.0	-7.0	-	-12.0	-12.0	-	-9.0	-9.0	-	-11.0	-11.0	-	-10.0	-10.0	-

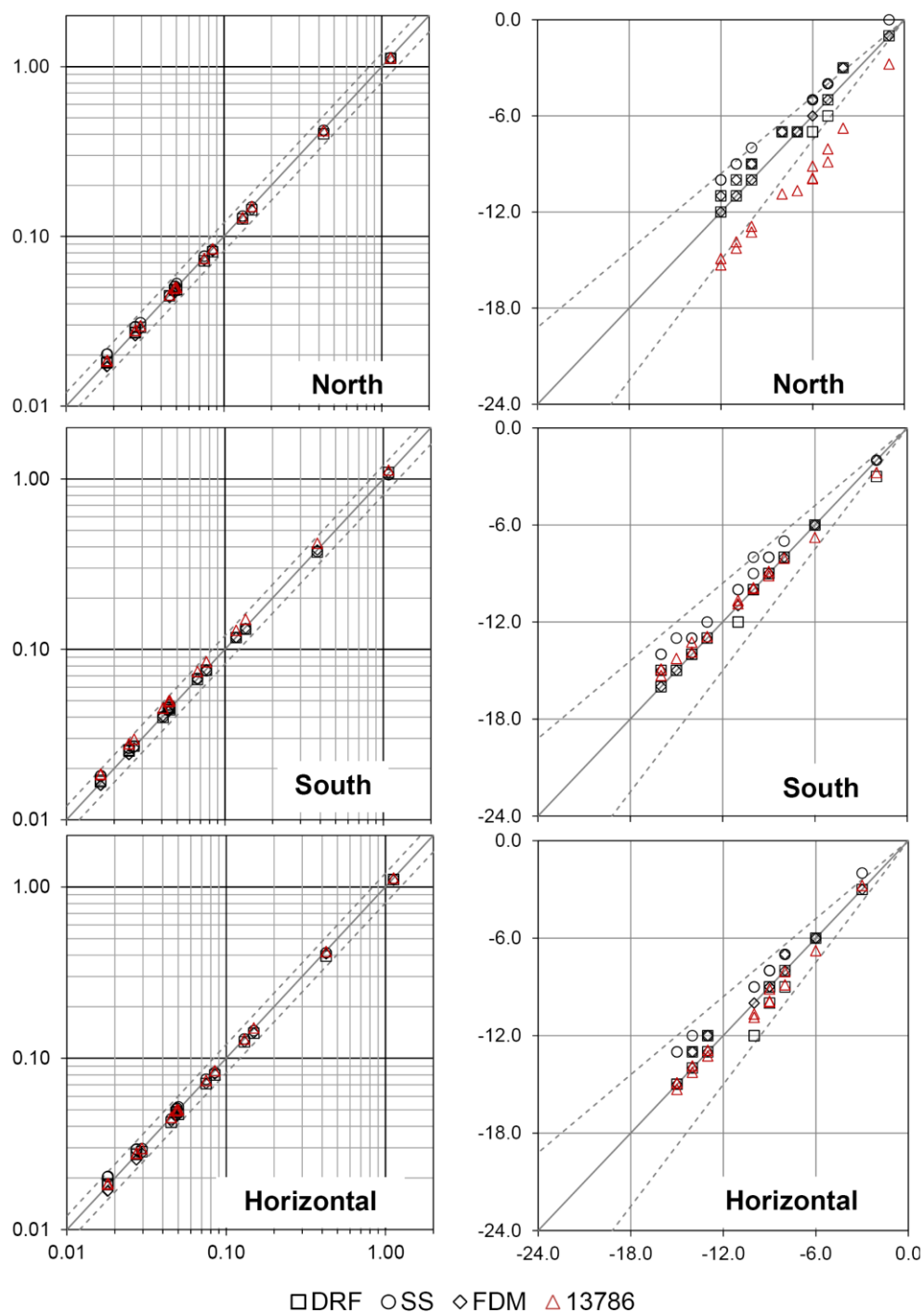


Figure 4a.3 - Periodic thermal transmittances in  $[W m^{-2} K^{-1}]$  (left) and time shifts in [h] (right) for the conditions of Rome for the South, North and Horizontal walls respect to the reference FFT parameters. Dotted lines represent the  $\pm 20\%$  range

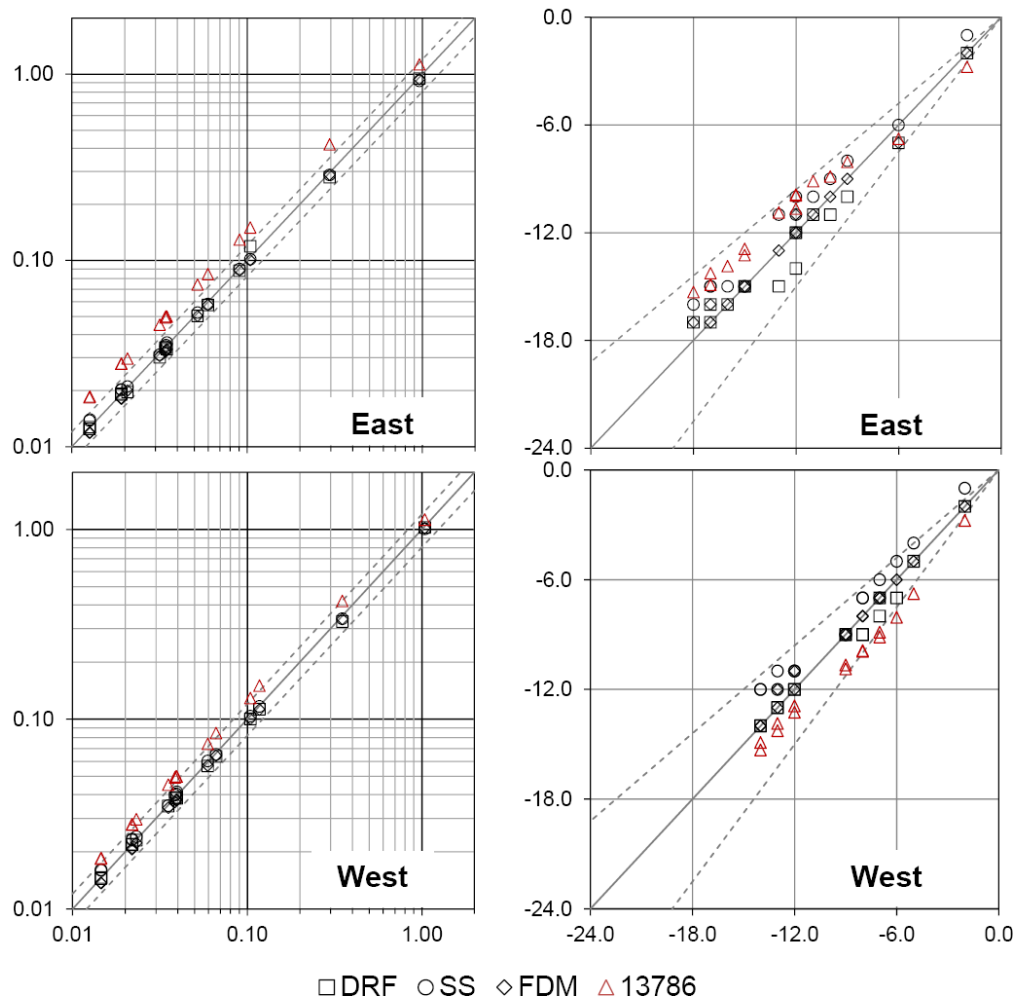


Figure 4a.4 - Periodic thermal transmittances in  $[W m^{-2} K^{-1}]$  (left) and time shifts in  $[h]$  (right) for the conditions of Rome for the East and West-oriented walls respect to the reference FFT parameters. Dotted lines represent the  $\pm 20\%$  range

### 4a.3 Discussion

The Standard results significantly differ from the *FFT* results for many cases, both for the periodic thermal transmittance and for the time shift, as it can be seen in the Tables of the previous paragraph. This means that the Standard dynamic parameters are not representative of the real dynamic response under non-sinusoidal conditions, as observed by Gasparella *et al.* (2011b).

As regards the wall components, as well as for the three climatic zones chosen in the present work, the deviations between the *FDM*, *DRF* and *SS* approaches can be considered negligible both for the periodic thermal transmittance and for the time shift, as it can be seen by comparing Figures 4a.3 and 4a.4 for Rome to the ones for Milan and Palermo in Annex C. Anyway, some differences are present and various levels of agreement can be distinguished.

For what concerns the periodic thermal transmittance, about the *DRF* method, in Rome there is an average percentage overestimation for all the orientations except the East (respectively +3.23% for the North, +2.58% for the West, +2.25% for the South and +2.6% for the horizontal); for the East-faced walls there is an average percentage underestimation of -1.44%. The *DRF* method generally underestimates for the walls of the groups *A* and *M*, while overestimates in the other cases. The largest overestimations (around +10%) are encountered for the cases *C15* and *M15*. For Milan all the average percentages are positive but with lower absolute values respect to Rome: +0.64% for the North, +0.51% for the East, +0.96% for the West, +1.02% for the South and +0.81% for the horizontal orientation. The cases *C15* and *M15* are still the most critical but with lower deviations respect to Rome (around 5%). For Palermo, the mean percentage deviations are +1.80%, -0.43%, +0.60%, -3.51% and +1.46% for the North, East, West, South and horizontal orientations, respectively. The deviations are generally negative for the South orientation. Also in this location, with the exception of the South oriented walls, cases *C15* and *M15* are those with the largest differences.

As a whole, in Rome the *SS* method underestimates the periodic thermal transmittance, in particular for the North, West and horizontal orientations, whose average percentage deviations are, respectively, -2.52%, -2.14% and -2.98%. For the East and the South orientations there are slightly average overestimations (+1.60% and +0.30%, respectively). In Milan and Palermo the percentage averages underline a general underestimation respect to the *FFT* reference, which is

more marked in the second locality, where they are around -5%, independently of the orientation.

The *FDM* always underestimates respect to the *FFT* results (-4.42% for the North, -4.30% for the East, -4.39% for the West, -1.49% for the South and 5.70% for the horizontal cases). Similar values are present for Milan and Palermo, with the exception of the South-faced walls in Palermo, whose percentage deviation is around -5%.

About the time shift, the maximum differences are generally of 1 h respect to the *FFT* method. The *DRF* method is generally late while the *SS* presents a good agreement with the *FFT* results for many cases. The results obtained through the *FDM* are almost equal to the *FFT* reference. As a whole, the agreement between the numerical methods and the *FFT* reference is better in Milan and Palermo respect to Rome.

As regards the different orientations, the computed periodic thermal transmittance values are lower for East and West-faced walls, with the minimum value reached for the East orientation, in agreement with the findings by Kontoleon and Eumorfopoulou (2008) for walls with a composition similar to the analysed ones. The maximum time shift value has been observed for the East orientation.

#### 4a.4 Main findings

In this first part of chapter 4 the problem of the characterization of the behaviour of some building envelope components has been discussed. In particular, the focus was on the dynamic behaviour of the opaque walls.

About the analysis of the dynamic behaviour of opaque components exposed to the external conditions, the Transfer Function Methods implemented in TRNSYS and EnergyPlus, as well as an implicit finite difference scheme solution (*FDM*), have been assessed. As index variables for the assessment of the numerical methods, the dynamic parameters proposed by the technical Standard EN ISO 13786:2007 (i.e., the periodic thermal transmittance, the time shift and the decrement factor) have been used. Since these dynamic parameters are defined considering a sinusoidal forcing temperature, by means of the Fast Fourier Transform (*FFT*) analysis and the principle of superposition of the effects, some “real” forcing sol-air temperatures have been considered and the dynamic response of a sample of walls under those conditions evaluated.

The numerical methods are in agreement with the *FFT* results, with some small deviations for what concerns the time shift. The Direct Root Finding method implemented in TRNSYS, for instance, is generally late respect to the State Space in EnergyPlus and the *FDM*.

For the considered walls, especially the lightweight and uninsulated ones, the analysis allowed also to observe that under “real” forcing conditions, the dynamic parameters elaborated considering a fundamental harmonic as forcing signal – as those proposed by the EN ISO 13786:2007 and generally used as index variables to characterize the walls dynamic behaviour, are not representative.





## **Part b: Glazings and adiabatic surface temperatures**

### **4b.1 Methods**

In chapter 3, different possible sources of discrepancy between EnergyPlus and TRNSYS have been analysed and, finally, the modelling of the internal infrared heat exchanges, in particular for the windows, appeared to be the main cause of difference between the monthly heating and cooling energy needs and peak loads elaborated by these two codes.

The reason of the discrepancy has been attributed mainly to the different implemented models: while in EnergyPlus a detailed method based on the view factor calculation is implemented, in TRNSYS these heat exchanges are modelled with Seem's star network and all surfaces are characterized by an emissivity equal to 1 (i.e., they are black surfaces). Especially this last hypothesis, which appears not particularly relevant for the opaque components, has been significant for the alignment of the results between the two codes because of its effect on the glazing surfaces. Indeed, since the internal emissivity of glazings is 0.84 but in TRNSYS it is unitary, a relative deviation of 16% is introduced between these two simulation codes in the calculation of infrared exchanges and it is enhanced by the large difference between the glazings surface temperature and the one of the rest of the envelope. Moreover, in this perspective the presence of adiabatic surfaces can slightly influence the deviations.

In this part, in order to complete the comparative analysis, the hourly internal surface temperature profiles elaborated by TRNSYS and EnergyPlus have been analysed, both for the glazings and the adiabatic surfaces. The considered cases are extracted from the dataset simulated for the comparison between TRNSYS and EnergyPlus (see the previous chapter for more details).

In particular, both for Messina and Milan, the represented cases have the following characteristics:

- the windows are East-oriented and with the smaller size ( $A_g/A_f = 11.67\%$ );
- the internal gains are null;
- the insulation of the opaque components is null;
- the massive layer is clay block.

The East orientation has been chosen because it leads to a more interesting external solicitation: while, for instance, a South oriented surface is exposed to the solar radiation all daytime and so its surface temperature gradually reaches a maximum and then decreases, an East oriented window presents a peak of surface temperature in the morning and then quickly it

decreases. Thus, it is of interest to compare TRNSYS and EnergyPlus in the estimation of the surface peak temperature: indeed a relative error in the estimation of the peak temperature can affect the estimation of the mean radiant temperature and so the operative temperature of the thermal zone. Some preliminary analyses showed that the size of the windows is not so relevant in influencing the deviations between the glazing surface temperatures elaborated by the two simulation codes: the deviations changes between the cases with larger windows and those with smaller ones are within a range of  $\pm 0.2$  °C for most of the hours. For this reason, the smaller windows have been chosen. Since the profile analysis is more focused on the dynamics of the surface heat balance and the internal gains are constant, they have been set to zero. The uninsulated walls have been considered, as more influenced by the external solicitations and so characterized by larger differences in their internal surface temperatures, which means larger variability in heat radiative exchanges. All the 5 different considered glazings have been tested, as well as the cases  $S/V = 0.3$  and  $S/V = 0.97$ . In addition to the previous ratios, also a case without adiabatic surfaces (i.e.,  $S/V = 1.07$ ) has been simulated.

In order to assess the possible improvement of the alignment between the glazings surface temperature considering the same internal unitary emissivity, the simulations have been repeated with specific windows with  $\varepsilon_{gl}=1$  modelled in EnergyPlus IDF Editor. The characteristics of these windows are the same of the ones built with Window6 tool by LBNL and used in chapter 3 and in the first part of the present analysis, with the exception of the internal emissivity.

A sample of weeks representative of the winter conditions and another representative of the summer ones, have been analysed. Moreover, the annual distributions of the deviations between the surface temperatures elaborated by EnergyPlus and TRNSYS for the chosen sample of cases have been studied. The deviations between the hourly surface temperatures have been calculated by subtracting the values by TRNSYS to each one by EnergyPlus. The deviations have been distinguished in 10 groups: from 0 to +0.5 °C, from +0.5 °C to +1 °C, from +1 °C to +2 °C, from +2 °C to +4 °C and more than +4 °C for the cases where EnergyPlus overestimates respect to TRNSYS and, similarly when it is TRNSYS to overestimates respect to EnergyPlus.

## **4b.2 Results**

### ***4b.2.1 Sample of cases with the original glazings***

The hourly surface temperatures of the glazings and of the adiabatic vertical walls have been reported in Figures 4b.1 and 4b.2 for a sample of hours in winter conditions (from the 14<sup>th</sup> till the 21<sup>st</sup> of January) of Milan and Messina and in Figures 4b.3 and 4b.4 for a sample of hours in summer conditions (from the 14<sup>th</sup> till the 21<sup>st</sup> of July), respectively of Milan and Messina. In Figures 4b.5 and 4b.6 the winter and the summer surface temperatures for the glazings in case of absence of adiabatic surfaces have been represented.

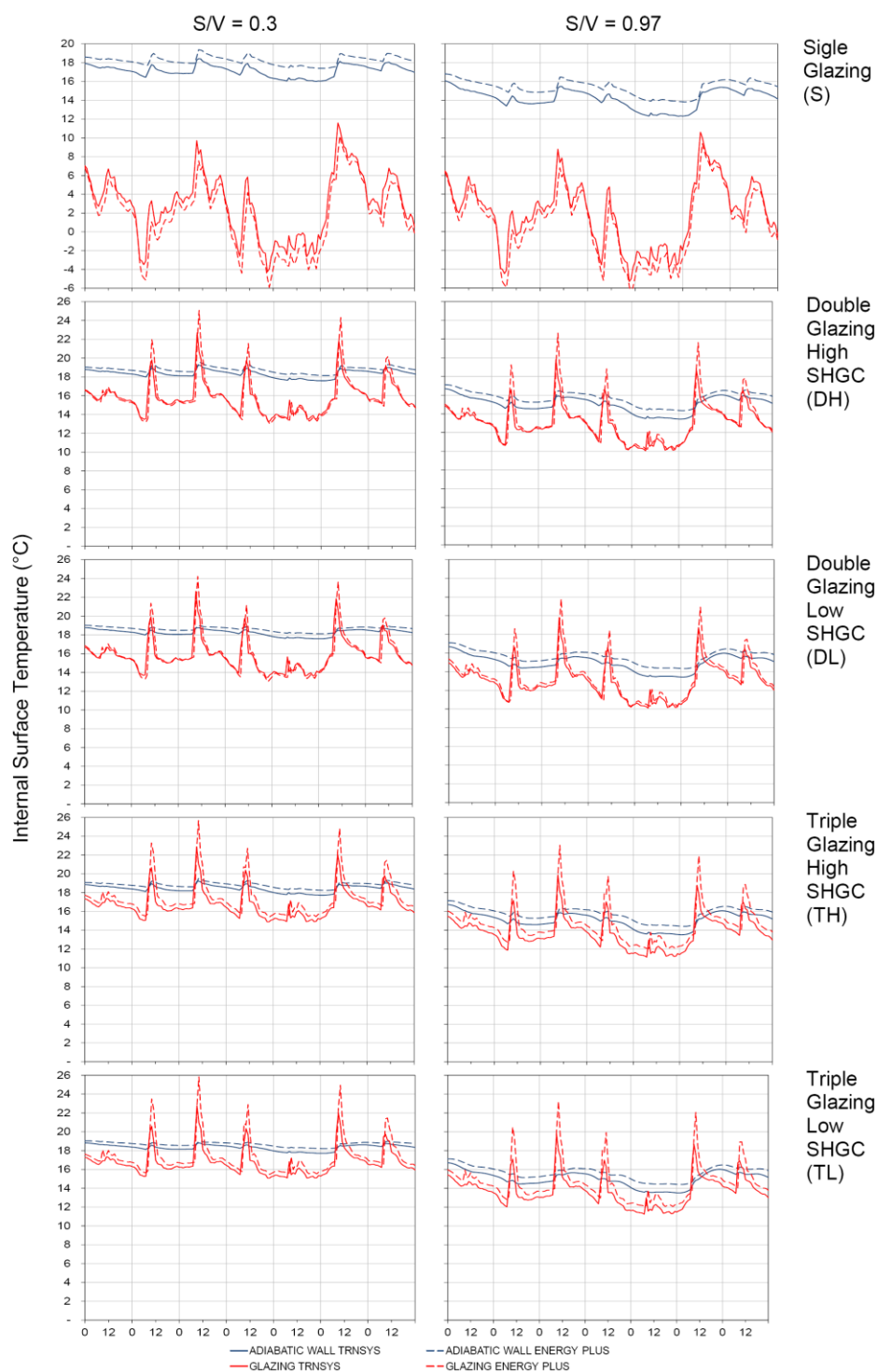


Figure 4b.1 – Winter (from 14/01 till 21/01) surface temperatures in Milan for the different glazings with  $S/V=0.3$  and  $S/V=0.97$

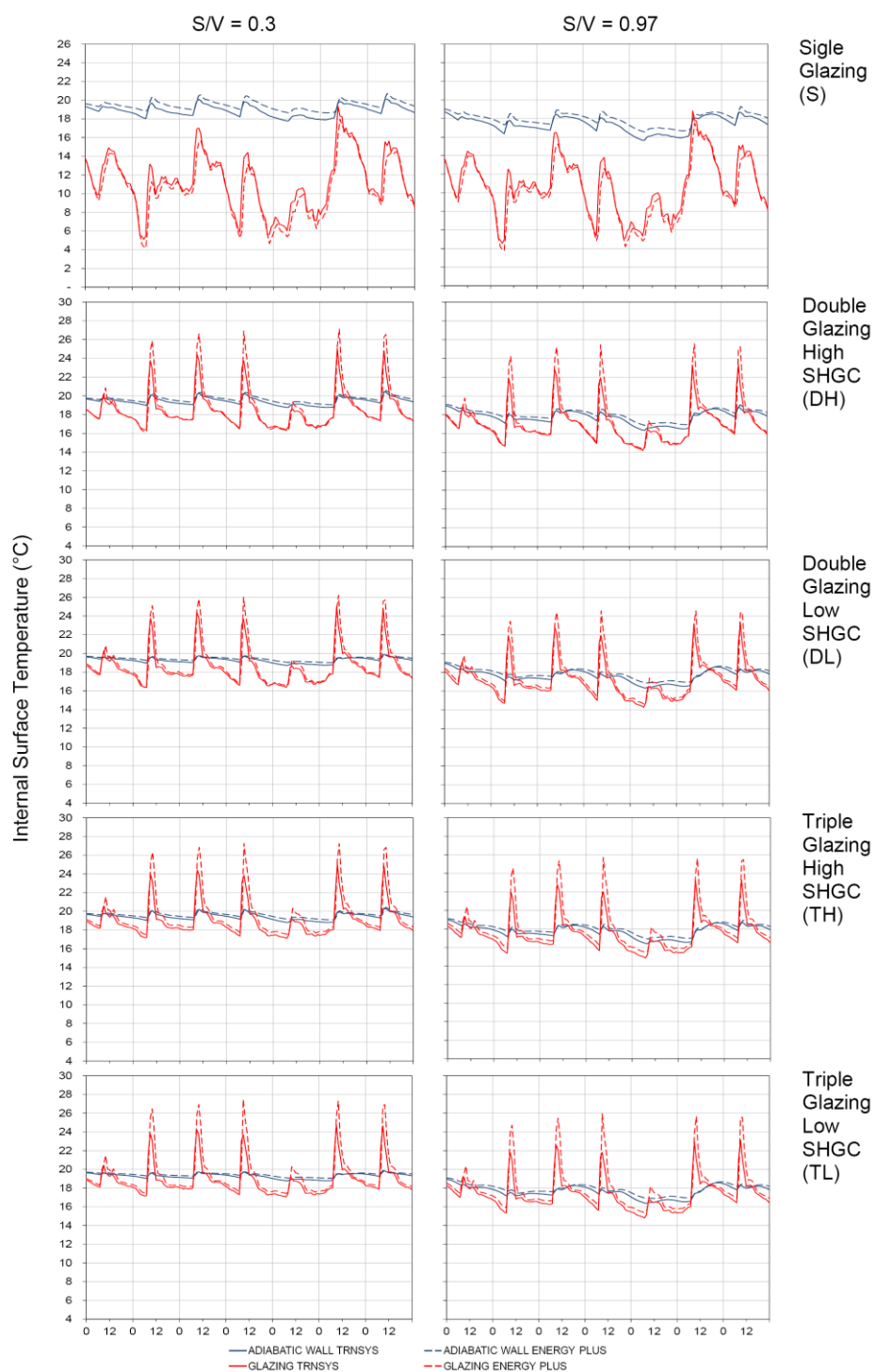


Figure 4b.2 – Winter (from 14/01 till 21/01) surface temperatures in Messina for the different glazings with  $S/V=0.3$  and  $S/V=0.97$

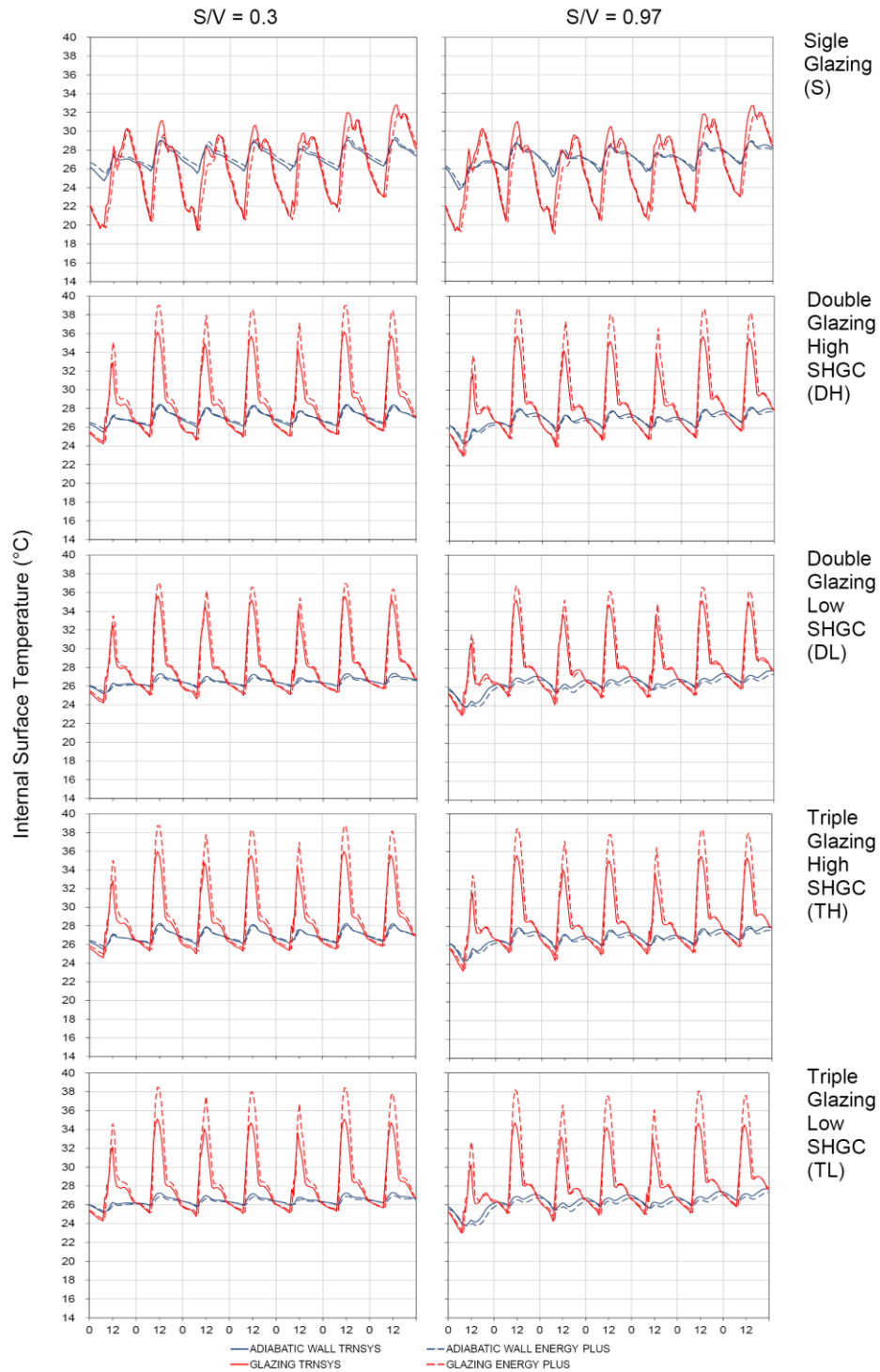


Figure 4b.3 – Summer (from 14/07 till 21/07) surface temperatures in Milan for the different glazings with  $S/N=0.3$  and  $S/N = 0.97$

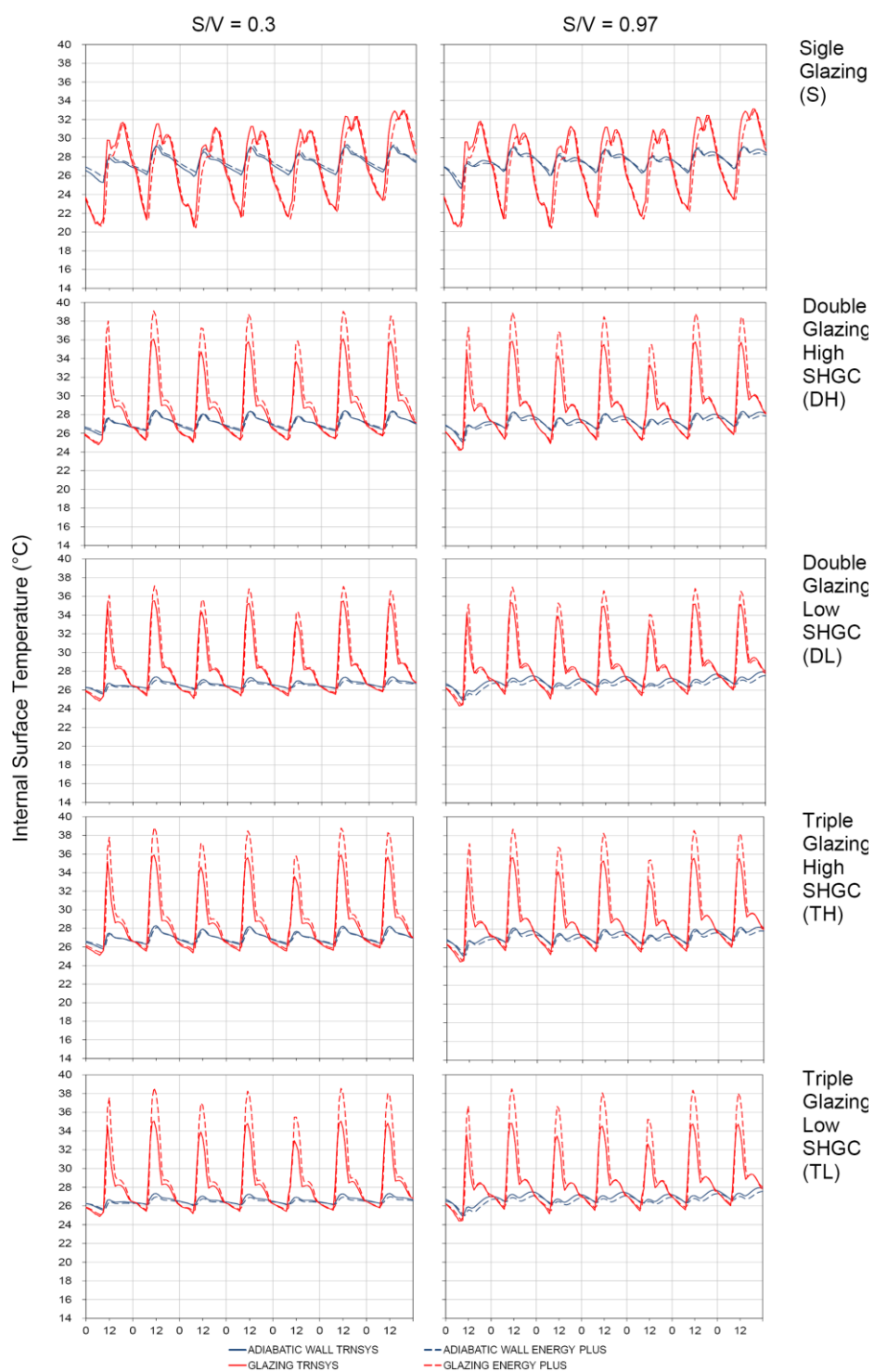


Figure 4b.4 – Summer (from 14/07 till 21/07) surface temperatures in Messina for the different glazings with  $S/V=0.3$  and  $S/V=0.97$



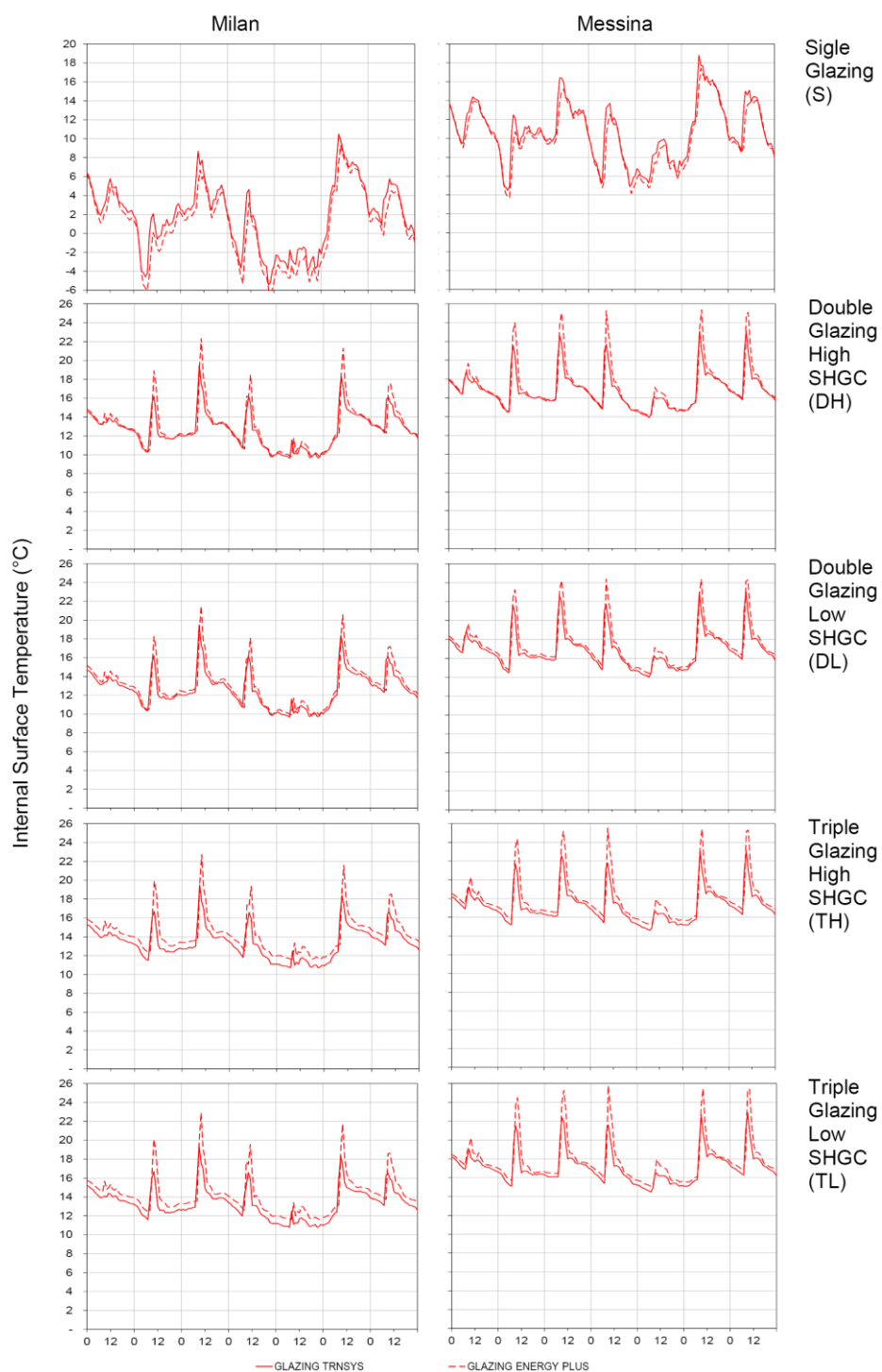


Figure 4b.5 – Winter (from 14/01 till 21/01) surface temperatures in Milan and Messina for the different glazings with  $S/V=1.07$

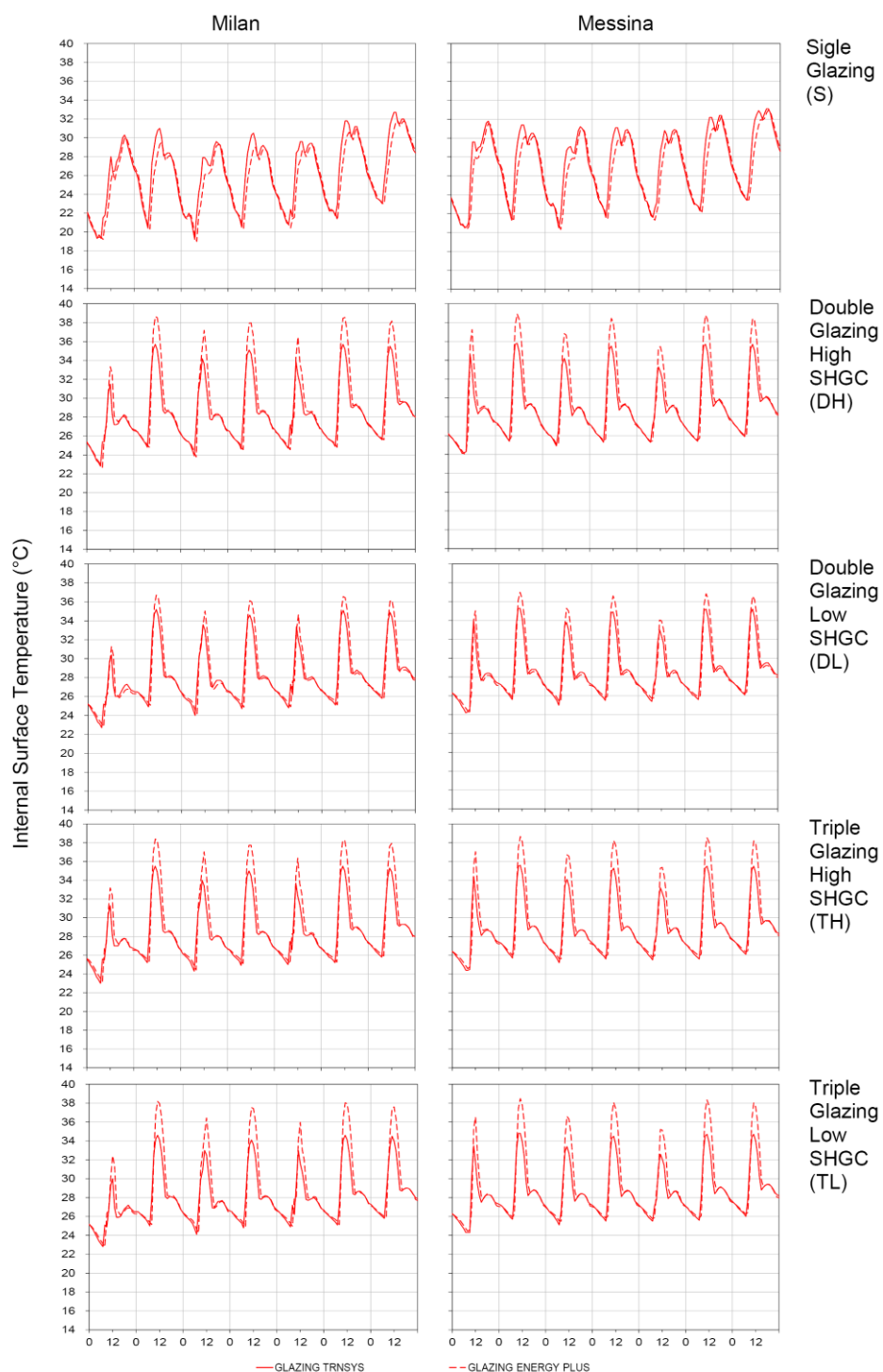


Figure 4b.6 – Summer (from 14/07 till 21/07) surface temperatures in Milan and Messina for the different glazings with  $S/N=1.07$

For what concerns the adiabatic surfaces, the distributions have been reported in Figures 4b.7 and 4b.8, respectively for Milan and Messina.

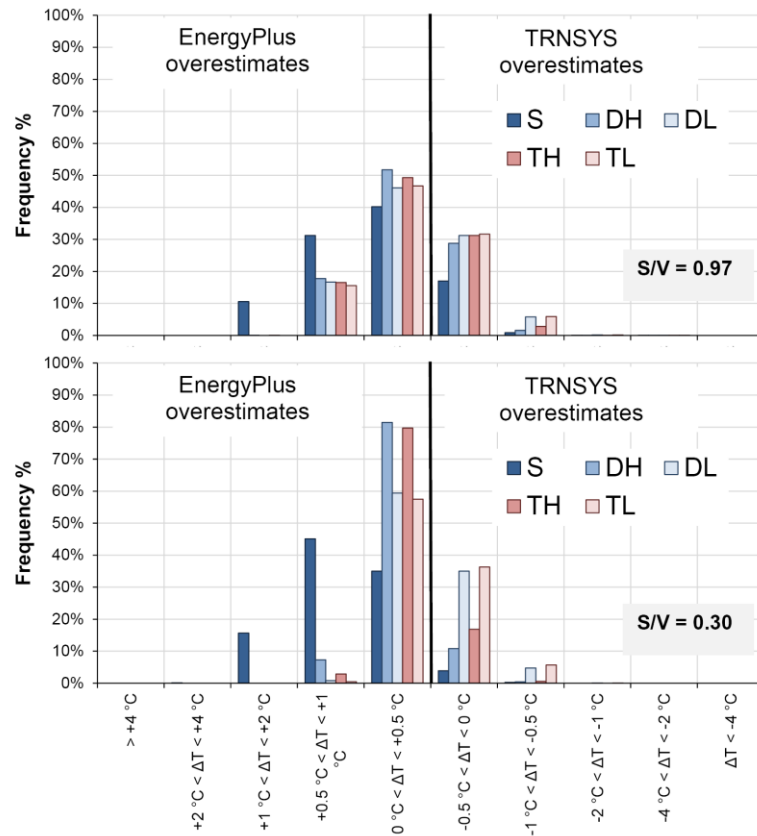


Figure 4b.7 - Distribution of the deviations between the surface temperatures of the adiabatic walls in EnergyPlus and TRNSYS in Milan

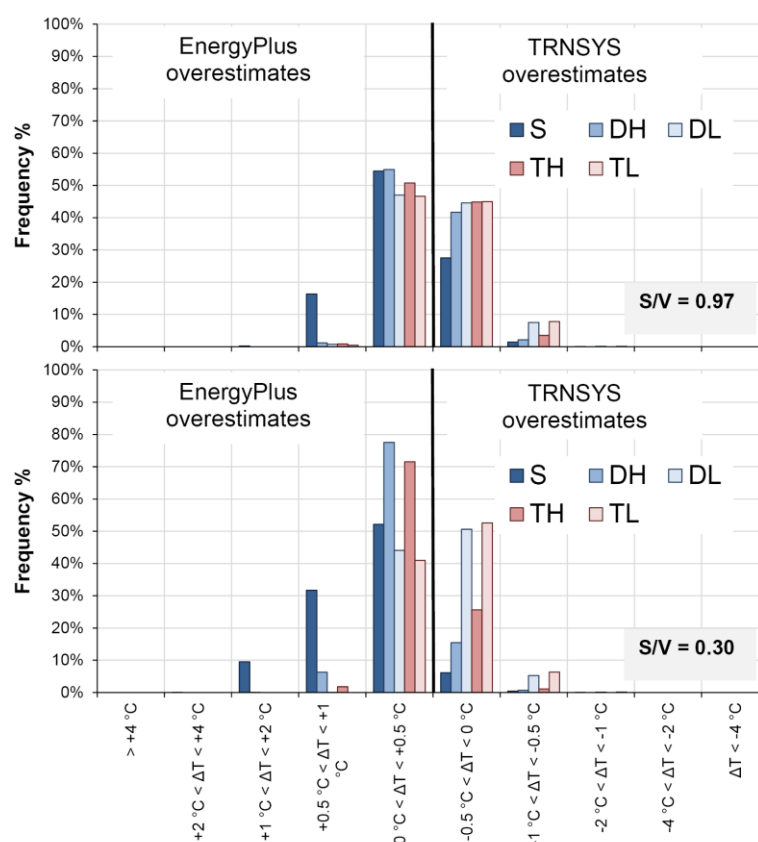


Figure 4b.8 - Distribution of the deviations between the surface temperatures of the adiabatic walls in EnergyPlus and TRNSYS in Messina

For the glazing surfaces, the distributions have been reported in Figures 4b.9 and 4b.10, respectively for Milan and Messina.

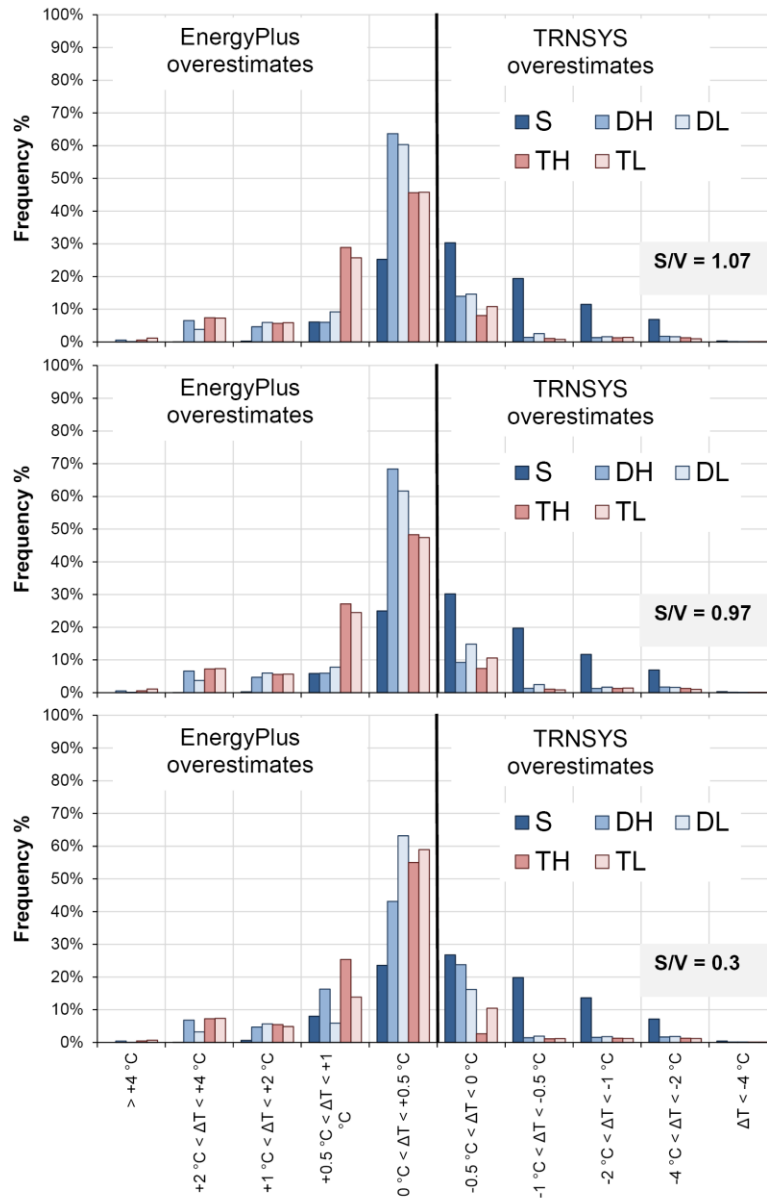


Figure 4b.9 - Distribution of the deviations between the surface temperatures of the glazings in EnergyPlus and TRNSYS in Milan

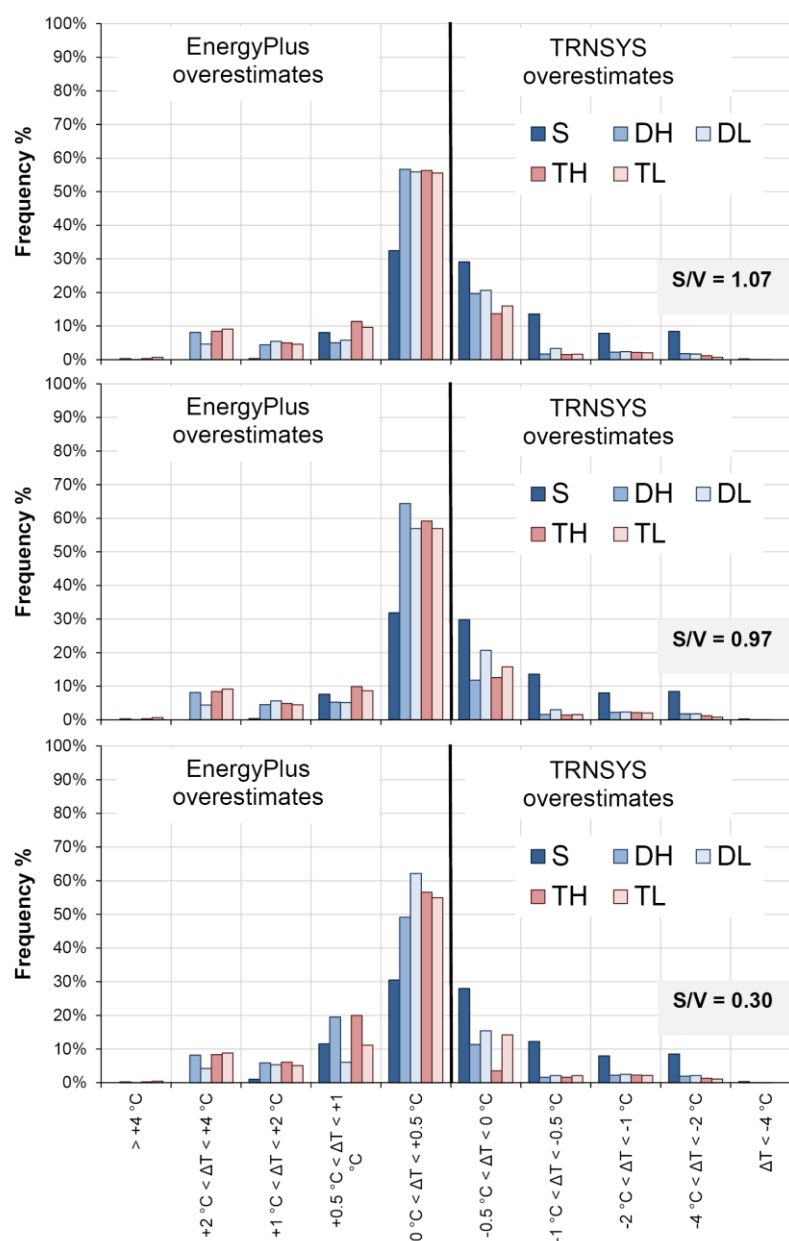


Figure 4b.10 - Distribution of the deviations between the surface temperatures of the glazings in EnergyPlus and TRNSYS in Messina

#### 4b.2.2 Sample of cases with glazings with unitary emissivity

In Figures 4b.11 and 4b.12 the frequency analysis results for the second sample of cases have been reported

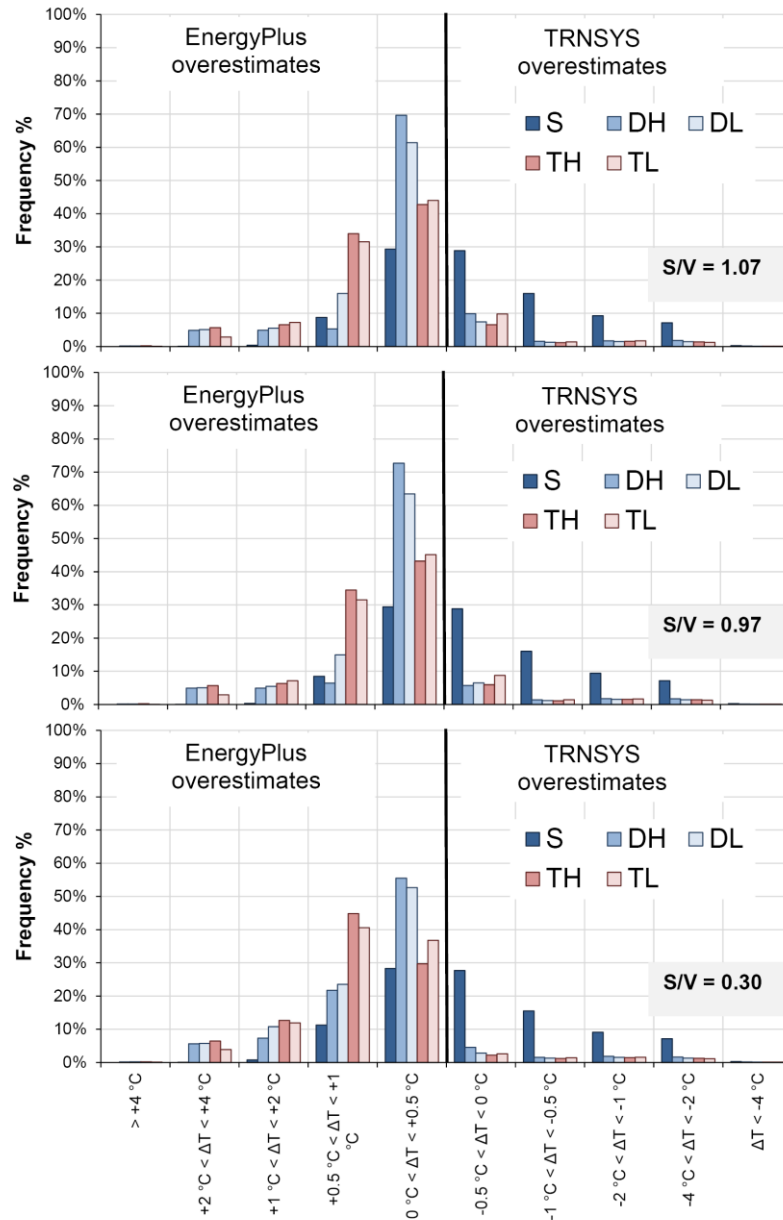


Figure 4b.11 - Distribution of the deviations between the surface temperatures of the glazings in EnergyPlus ( $\epsilon_{gl}=1$ ) and TRNSYS in Milan

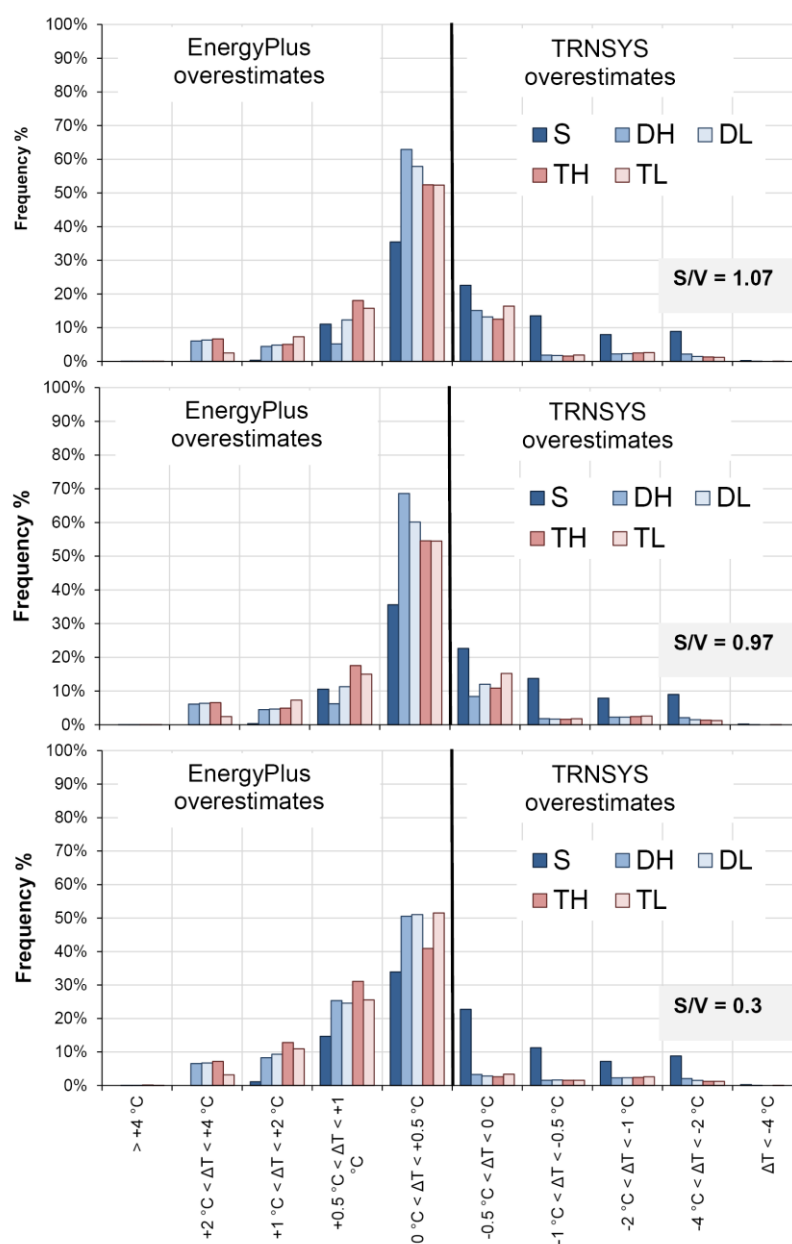


Figure 4b.12 - Distribution of the deviations between the surface temperatures of the glazings in EnergyPlus ( $\epsilon_{gl}=1$ ) and TRNSYS in Messina



## 4b.3 Discussion

### 4b.3.1 Sample of cases with the original glazings

In Figures 4b.1-4b.6, several surface temperature profiles have been represented.

About the adiabatic surfaces, for what concerns the two climates, the main difference is related to the elaborated temperature: the difference between the one by TRNSYS and the one by EnergyPlus is smaller in the climate of Messina. The general behaviour is the same for both locations. During the winter period, EnergyPlus always overestimates the temperature of the adiabatic surfaces (generally less than +1 °C respect to TRNSYS) and this is particularly evident for the case with single glazing. During the summer period, in the case with single glazing EnergyPlus tends slightly to overestimate the temperature of the adiabatic surfaces, while with the other glazings it underestimates.

Increasing the S/V ratio, the discrepancy between the two simulation tools little increases. As regards the glazings, both in summer and in winter conditions, EnergyPlus underestimates the internal surface temperatures of the single pane glass respect to TRNSYS. For the other glazings, EnergyPlus generally overestimates, in particular when the windows are hit by the solar radiation and the difference between the simulated temperatures can become also between +2 °C and +4 °C. Generally, the peaks of surface temperature in TRNSYS seem more smoothed than in EnergyPlus. As confirmed in Figure 4b.5 and 4b.6, where the cases with  $S/V = 1.07$  are reported, the deviations between the glazing surface temperatures elaborated by the two BES codes seem not particularly influenced by the presence of adiabatic surface (i.e., the discrepancies are not strongly correlated with the interaction between adiabatic and transparent surfaces).

Most of the deviations have an absolute value lesser than 0.5 °C but different behaviours can be observed. In Messina the percentage of the deviations falling in the ranges  $\pm 0.5$  °C is higher than in Milan, where the overestimation by EnergyPlus respect to TRNSYS is more marked. For the cases with  $S/V = 0.97$ , the deviations for insulating glazings have the same behaviours with balanced positive and negative deviations while for the single pane glass most of the temperatures elaborated by EnergyPlus are larger than the ones by TRNSYS. Passing to the lower S/V ratio, the behaviour of the insulating glazings changes: they seem almost independent on the SHGC only with a high S/V ratio.

#### ***4b.3.2 Sample of cases with glazings with unitary emissivity***

The main effect of the unitary emissivity for the glazings in EnergyPlus is to decrease the larger deviations, independently of which simulation code overestimate the glazings surface temperature respect to the other one. The decrement of the number of cases in the largest deviation categories led to an increase of the frequency in the central classes (e.g., the ones with deviations less than 0.5 °C and from 0.5 to 1 °C, considering the absolute values). The central positive and negative categories are not affected by the same variation and generally the first ones present an increase while the second ones a reduction. This leads to larger asymmetry between those cases characterized by an overestimation of the glazing surface temperatures in EnergyPlus respect to TRNSYS: basically the surface temperatures estimated by the latter are larger than the ones of the last one but the discrepancies are limited. EnergyPlus overestimations are particularly evident for the triple glazings in the simulations with emissivity equal to 1 and are more frequent when the S/V ratio is lower. For instance, in the climate of Milan, the number of hours whose deviation is between +0.5 °C and +1 °C is larger than the one between 0 and 0.5 °C for the triple glazings when the S/V is 0.3.

As a whole, even if for these last cases the emissivity is aligned, residual discrepancies are still present and are related to the different model of internal heat exchanges and other different models and algorithms directly or indirectly affecting the internal surface heat balance, such the TFM approaches discussed in the first part of this chapter.

#### **4b.4 Main findings**

In order to complete the comparison between EnergyPlus and TRNSYS of chapter 3, the surface temperature profiles of glazings and adiabatic surfaces have been analysed. The discrepancies and the different behaviours for the studied kind of glazings have been discussed and it has been found that, for the peak surface temperatures, deviations of 2-4 °C between the two simulation codes are present, even if most of the cases the differences are lower than 1 °C and with a general overestimation of the surface temperatures calculated by EnergyPlus respect to TRNSYS values.

In both the climates there is a clear overestimation of the surface temperature by EnergyPlus respect to TRNSYS for the insulating glazings while there is a general underestimation for the single pane glass. It can be noticed that most of the time the differences are within +0.5 and -0.5 °C, especially for the most efficiency glazings. The agreement between the different insulating glazings is better in Messina than in Milan and the reduction of the S/V ratio by introduction of adiabatic in place of dispersing walls lead to a light increase of the variability of the responses.

# **Chapter 5:**

## BES and simplified models



## Chapter 5

In chapter 5 the issue of the coherence between the energy needs elaborated by means of BES tools and those by simplified models is discussed. In particular, as BES tool TRNYS has been chosen and as simplified method the one proposed by the technical Standard EN ISO 13790:2008 (i.e., the quasi-steady state method).

The annual energy needs calculated according to the EN ISO 13790:2008 monthly method have been firstly assessed by means of some BESTEST cases. Then, the analysis has been focused on the evaluation of the thermal flows rather than the final energy need results. Both heat losses and gains, calculated with the EN ISO 13790:2008 and simulated with TRNSYS according to the same Standard prescriptions, have been analysed.

The main sources of disagreement have been investigated both for the thermal losses and the thermal gains. In particular, for the first ones the effect of the setpoint temperature (air temperature or operative temperature) and the ventilation rates have been studied. For the gains, instead, some assumptions of the EN ISO 13790:2008, such as the black body cavity hypothesis for the solar radiation transmitted through the transparent surfaces or the neglected fractions of gains dispersed by conduction through the envelope, have been discussed. Correction factors have been estimated by means of statistical techniques in order to provide a better agreement between the thermal flows estimated according to the quasi-steady state approach and by BES.

Finally, the effect of the proposed corrections on the final energy needs has been assessed.



## Part a: Assessment of the quasi-steady state method with the BESTEST cases

### 5a.1 Method

In order to carry on a preliminary analysis of the performances of the EN ISO 13790:2008 method, the BESTEST approach has been implemented. Only 4 qualification cases have been studied (i.e., cases 600, 620, 900 and 920), because for those the base model proposed by the Standard can be assessed without being influenced by additional models or correction factors, such as the shading reduction factors for overhangs and fins (cases 610, 630, 910 and 930), the intermittent heating or cooling (cases 640, 650, 940 and 950) of the presence of a sunspace (case 960).

Since in literature some problems have been experienced in particular by using the quasi-steady state method in cooling-dominated climate, as the Mediterranean ones, instead of using the climate of Denver, the assessment has been done for the climates of Messina and Milan. In order to define specific reference limits for these two climates, the method by Melo *et al.* (2012) has been followed. The BESTEST simulations carried on with TRNSYS for Denver climate in chapter 3 have been employed as reference to calculate the confidence intervals from the acceptability boundaries.

$$CI_{\max} = \frac{Q_{\max, \text{Denver}} - Q_{\text{TRNSYS}, \text{Denver}}}{Q_{\text{TRNSYS}, \text{Denver}}} \quad (5a.1)$$

$$CI_{\min} = \frac{Q_{\min, \text{Denver}} - Q_{\text{TRNSYS}, \text{Denver}}}{Q_{\text{TRNSYS}, \text{Denver}}} \quad (5a.2)$$

The new limits have been calculated for each location *loc* by means of Eq. (5a.3) and (5a.4):

$$Q_{\max, \text{loc}} = (1 + CI_{\max}) \cdot Q_{\text{TRNSYS}, \text{loc}} \quad (5a.3)$$

$$Q_{\min, \text{loc}} = (1 + CI_{\min}) \cdot Q_{\text{TRNSYS}, \text{loc}} \quad (5a.4)$$



## 5a.2 Results and Discussion

The results have been reported in Figure 5a.1 and 5a.2, for Milan and Messina, respectively. In Figure 5a.1 the results for Milan can be analysed. The heating energy needs are within the confidence intervals for all considered cases with the exception of case 600, where the heating need is slightly underestimated (around -7.5%). For the annual cooling energy needs, they are generally overestimated respect to the boundaries, with the exception of the case 600.

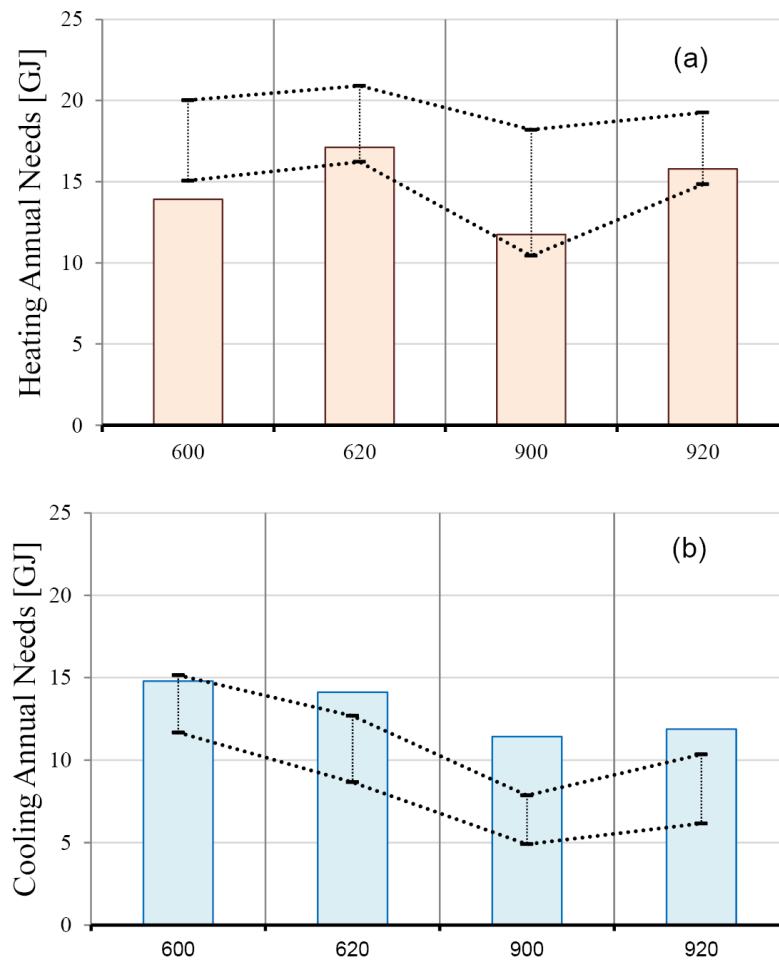


Figure 5a.1 - Quasi-steady state method assessed with the BESTEST cases 600, 620, 900, 920 for the location of Milan: annual heating (a) and cooling (b) energy needs. The dotted lines delimitate the confidence interval

For the location of Messina, the annual heating energy needs are within the acceptance range only for the massive cases (900 and 920), characterized by a time constant of 20 h. For the lightweight cases (time constant around 5 h) the heating needs are largely underestimated. As

regards the annual cooling energy needs, they are always overestimated by the Standard model, in particular for the massive cases.

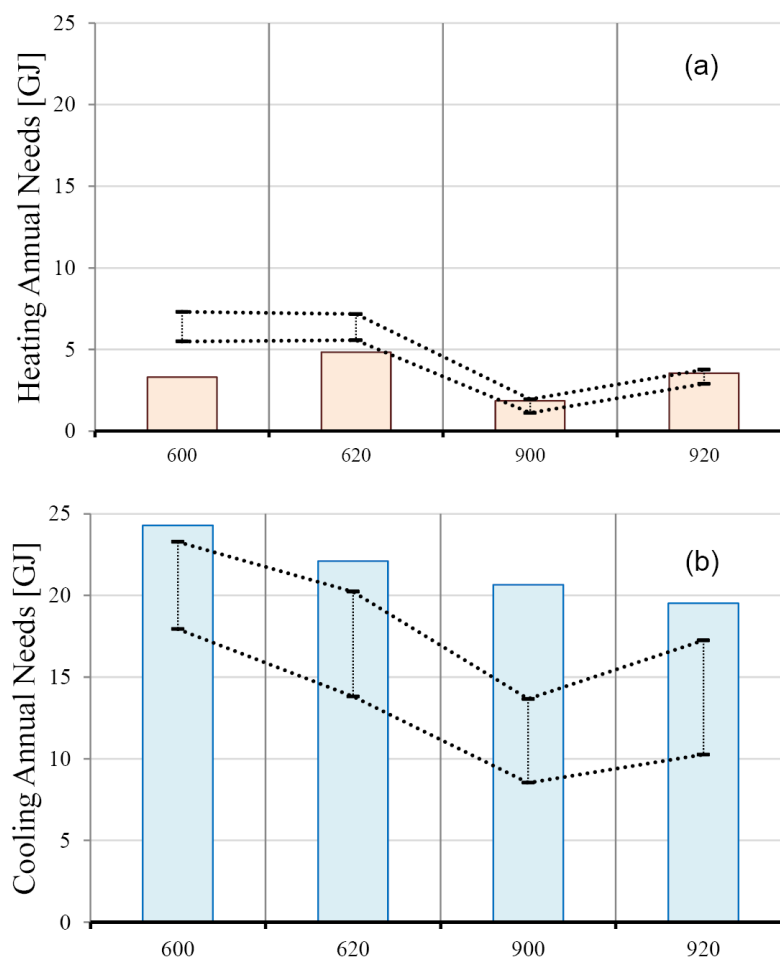


Figure 5a.2 – Quasi-steady state method assessed with the BESTEST cases 600, 620, 900, 920 for the location of Messina: annual heating (a) and cooling (b) energy needs. The dotted lines delimitate the confidence interval

Considering these four qualification cases, it can be noticed that the quasi-steady state method is generally not in agreement with the BESTEST confidence intervals for the annual cooling energy needs, which are generally overestimated. About the annual heating energy needs, there is more coherence with the BESTEST, especially for Milan, where the heating needs are more relevant. Larger discrepancies are encountered for the lightweight structures.

### 5a.3 Main findings

A preliminary analysis has been carried on by considering some of the BESTEST qualification cases. In particular, those cases considering intermittent heating, cooling or ventilation setpoints have been neglected, since different approaches are presented by the EN ISO 13790:2008 to model these configurations in quasi-steady state conditions. Moreover, also the cases presenting overhangs and fins have not been considered, since the Standard proposes only shading factors to correct the window area exposed to the solar radiation and in this chapter the aim is to assess the base methodology. Thus, only the cases 600, 620, 900 and 920 have been studied here. As it is of interest to evaluate the performance of the quasi-steady state method in the South Europe climates, specific acceptance ranges have been considered for these locations.

The annual energy needs estimated are not within the boundaries for most of the considered configurations. It can be observed that for the annual heating energy needs are in the acceptance ranges for the massive structures while they are under the lower boundary for the lightweight ones. For the annual cooling energy needs, the EN ISO 13790:2008 monthly method is almost always over the higher boundary, providing an overestimation of the energy demand.

## Part b: Comparison between the thermal losses by BES and by EN ISO 13790:2008 quasi-steady state method

### 5b.1 Methods

As seen in the discussion of the literature in chapter 1, the main difference between the air heat balance in BES and the quasi-steady state method, consists in the chosen reference temperature (i.e., air or operative temperature). In this part of the analysis, the main sources of discrepancies besides the air and the operative temperature, which are the presence of envelope insulation, the ventilation rate and the presence of different amount of adiabatic surfaces, have been discussed.

A statistically derived correction factor has been introduced in order to improve the estimation of an operative equivalent temperature starting from the air temperature setpoint. This allows to improve the agreement of the quasi-steady state method with the results of simulation by BES tools – TRNSYS in this case, when considering an air temperature setpoint. For the multiple regression method used, see Annex A.

In the following three sections, the method proposed by the technical Standard EN ISO 13790:2008 is described, as well as the approach by TRNSYS and the simulation assumptions. A description of the followed simulation plan is also provided.

#### 5b.1.1 EN ISO 13790:2008 model

In accordance with the standard EN ISO 13790:2008, the thermal losses  $Q_{ht}$  through the envelope and by ventilation can be calculated with the Eq. (5b.1).

$$Q_{ht} = Q_{tr} + Q_{ve} \quad (5b.1)$$

The thermal transmission losses through the envelope directly exposed to the outdoors are:

$$Q_{tr} = H_{tr} \cdot (\theta_{i,set} - \theta_e) \cdot t \quad (5b.2)$$

Considering only dispersions of the heated zone towards the outside environment and neglecting the thermal bridges, the overall transmission heat transfer coefficient is:

$$H_{tr} = H_D = \sum_{k=1}^n A_k U_k \quad (5b.3)$$

The surface longwave radiation exchanges are linearized and superimposed to the convective ones and, because of these simplifications and in coherence with the definition of  $H_D$  and of the thermal transmittance  $U$ , an operative temperature is considered as reference temperature. It can be assumed as a weighted average of the air and mean radiant temperatures, considering equal weights if complying with the EN ISO 13790:2008:

$$\theta_{op} = 0.5 \cdot \theta_a + 0.5 \cdot \theta_{mr} \quad (5b.4)$$

The ventilation thermal losses are defined as:

$$Q_{ve} = H_{ve} \cdot (\theta_{i,set} - \theta_e) \cdot t \quad (5b.5)$$

where:

$$H_{ve} = \rho_a c_a \left( \sum_{k=1}^n b_{ve,k} \dot{V}_k \right) \quad (5b.6)$$

In the considered cases the temperature adjustment factor  $b_{ve,k}$  is 1 because the supply air temperature is equal to the external air temperature.

The use of an operative temperature reference also for the calculation of ventilation losses is not strictly correct. For that reason it is expected that some discrepancies arise between simulation and simplified calculation results even if the same operative temperature setpoint is used, and that those differences increase for increasing ventilation rates. The second issue is that generally the operative temperature is not known when using the method, in particular when air temperature setpoints are considered.

### ***5b.1.2 Thermal losses calculation procedure with the dynamic simulation approach***

In order to evaluate the thermal losses by means of dynamic simulation, the EN ISO 13790:2008 prescribes to calculate the energy needs setting to zero the internal gains, the solar gains and the infrared extra flow to the sky vault. The simulation heating and cooling setpoints have to be the same (null regulation band). The thermal losses can be calculated from the heating energy need and the cooling energy need:

$$Q_{ht} = Q_{H,nd} - Q_{C,nd} \quad (5b.7)$$

To compare the simulated losses to the quasi steady state results, boundary conditions and calculation parameters for the simulation have to be coherent with the ones assumed in the

quasi-steady state approach. The simulations have been performed twice: the first time considering an air temperature setpoint, as commonly done in BES tools, and the second time imposing an operative temperature setpoint, coherently with the EN ISO 13790:2008.

As regards the external conditions, the hourly weather data have been calculated by means of the subroutine Type 54 in TRNSYS starting from the monthly average values reported by the Italian technical standard UNI 10349:1994.

As concerns the internal conditions, an iterative approach was adopted to perform the simulation with an operative temperature control, because in the subroutine Type 56 only an air temperature setpoint is allowed:

- imposing the weighting factors to the internal air temperature and the mean radiative temperature calculated at each timestep, the resulting operative temperature was calculated;
- the air temperature setpoint in Type 56 was then corrected given the target operative temperature setpoint, repeating the calculations again, till convergence.

The balanced weights indicated in Eq. (5b.4) have been considered. For a detailed explanation of the air heat balance model implemented in Type 56 in TRNSYS, see chapter 3.

According to the EN ISO 6946:2007 for quasi steady state methods, the global surface heat transfer coefficients are distinguished in convective and radiative coefficients. Due to the detailed long wave radiation models adopted by TRNSYS, only the convective coefficients could be set to the values prescribed by the standard also in the simulation:  $20 \text{ W m}^{-2} \text{ K}^{-1}$  for the external side, and 5.0, 0.7 or  $2.5 \text{ W m}^{-2} \text{ K}^{-1}$  respectively for upward, downward and horizontal flow on the internal side.

As concerns the radiation exchanges, as observed in chapter 3, both internal ( $\varepsilon=1$ ) and external emissivity values ( $\varepsilon=0.9$ ) are non-modifiable in TRNSYS. In principle, attempting to improve the coherence between detailed simulation and quasi steady state calculation, the internal long wave radiation heat transfer coefficient used in the quasi steady state approach could be calculated according to:

$$h_r = 4 \cdot \sigma \cdot \varepsilon \cdot T_{mr}^3 \quad (5b.8)$$

The same unitary internal emissivity used in TRNSYS can be assumed, but the surfaces temperature is not known in advance and can only be approximated with the same value used in the BES as temperature setpoint, as suggested by the standard itself. Thus, different surface radiative heat transfer coefficients have been considered coherently with the chosen setpoints.

### ***5b.1.3 Reference building model and set of configurations***

The difference between the air and the operative temperature, which impacts on the correspondence between the transmission losses calculated with quasi-steady state approach or detailed simulation, when using an air temperature setpoint, is largely affected by the insulation level of the envelope. Moreover, as is also pointed out by the standard EN ISO 13790:2008 itself and van Dijk and Arkesteijn (1987), it is also expected that also large ventilation rates lead to relevant discrepancies with the quasi steady state methods, and not only when using air temperature setpoint for the simulation. Therefore, in this first part of the comparison between BES tools and simplified method the focus is on different ventilation rates and insulation levels of the envelope, as well as on the kind of temperature setpoint. The simulations were performed considering air temperature and operative temperature setpoints and then compared with the ones calculated with quasi steady-state method. As concerns the values of setpoint, a typical heating season setpoint temperature for residential applications (20 °C) and the second one with a typical cooling setpoint temperature (26 °C) have been assumed, in accordance with the prescriptions by the EN ISO 13790:2008.

The simulation plan considered in chapter 3 has been properly adapted in order to study the thermal losses, even if some variables, such as the thermal capacity of the walls or the SHGC of the glazings, not related to the thermal losses but affecting the selection the components themselves, have been taken into account with the perspective of the thermal gains and the energy needs analysis. The same single base building module with 100 m<sup>2</sup> of floor area and a horizontal roof has been considered and a selected group of parameters has been varied within a predefined set of values, obtaining a variety of configurations.

The opaque envelope is composed by a two layers structure, whose thermo-physical characteristics are reported in Table 3.2 in chapter 3. An insulation layer, with a thickness depending on the simulation plan, is positioned on the external side. Three possible materials have been considered for the internal layer (timber, clay block or concrete) with a thickness chosen to have a thermal resistance around 0.8 m<sup>2</sup> K W<sup>-1</sup>, as 0.2 m of clay block. The window frame is a timber frame with a low performance ( $U_{fr} = 3.2 \text{ W m}^{-2} \text{ K}^{-1}$ ) if coupled with the single glass and high performance ( $U_{fr} = 1.2 \text{ W m}^{-2} \text{ K}^{-1}$ ) in the other cases. The frame area covers about the 20 % of the whole window area.

The following geometrical and thermo-physical characteristics have been determined in accordance with the factorial plan:

1. the amount of envelope surface exposed to the external conditions;
2. the ventilation rate;
3. the level of insulation added to the internal layer;
4. the base material of the opaque envelope (taken into account in this part of the analysis because of the small differences of the three layers thermal resistances);
5. the percentage ratio of glazings  $A_{gl}$  to floor area  $A_f$ ;
6. the kind of glazing;
7. the climatic conditions.

For each of the above factors, the considered levels are reported in Table 5b.1.

Also in this part the presence of thermal bridges has been neglected but the motivation is slightly different:

- to be coherent with the simplified method, they have to be implemented in TRNSYS as massless elements without area with a lineic thermal transmittance and so they are uneffective in the evaluation of the operative temperature, making their contribution null;
- in case of air temperature setpoint, it can be considered to play a neutral role comparing the simulation and the quasi steady state approaches.

As the aim was to evaluate the losses by thermal transmission through opaque and transparent elements directly exposed to the outdoor air (i.e. with external air convection boundary conditions), when the floor is not adiabatic, it has been assumed as directly in contact with the external air without any solar contribution, as if it was on a well-ventilated cavity. For the comparison between the approach followed by the quasi-steady state method and enhanced numerical methods for the heat transfer through the soil, see chapter 2b.

The first factor allows to consider different ratios between the dispersing surface and the effect of different percentages of adiabatic surface in the total envelope. The second one analyses the ventilation rates, taking into account both its absence (e.g., thermal losses only by transmission) and other rates, in addition to the typical value for residential dwellings of 0.3 ach/h in accordance with the Italian technical Standard UNI/TS 11300-1:2008. The variation of the thickness of the insulation layer from 0 to 10 cm (factor 3) and the kind of glazings (factor 6), allow to evaluate configurations ranging from non-insulated buildings to well insulated ones. The factors 1, 5 and 6 allow to analyse the internal infrared exchanges between the glazings and



the adiabatic surface and their effects on the mean radiant temperature of the thermal zone. Two climates have been considered to calculate the thermal losses for different profiles of external temperatures.

*Table 5b.1 - Factors and levels in the simulation plan for thermal losses*

<b>1</b>	<b>a</b>	one wall, floor and ceiling adiabatic; $S/V=0.30 \text{ m}^{-1}$
	<b>b</b>	one wall and floor adiabatic; $S/V=0.63 \text{ m}^{-1}$
	<b>c</b>	one wall adiabatic; $S/V=0.97 \text{ m}^{-1}$
<b>2</b>	<b>a</b>	0 ach/h (no ventilation rate)
	<b>b</b>	0.3 ach/h (typical for residential dwellings)
	<b>c</b>	0.6 ach/h
	<b>d</b>	0.9 ach/h
<b>3</b>	<b>a</b>	0 cm – $U_{env} = 1.03 \text{ W m}^{-2} \text{ K}^{-1}$
	<b>b</b>	5 cm – $U_{env} = 0.45 \text{ W m}^{-2} \text{ K}^{-1}$
	<b>c</b>	10 cm – $U_{env} = 0.29 \text{ W m}^{-2} \text{ K}^{-1}$
<b>4</b>	<b>a</b>	Timber
	<b>b</b>	Clay-block
	<b>c</b>	Concrete
<b>5</b>	<b>a</b>	11.7%
	<b>b</b>	23.4%
<b>6</b>	<b>a</b>	(S) single glass - $U_{gl} = 5.68 \text{ W m}^{-2} \text{ K}^{-1}$ , $SHGC = 0.855$
	<b>b</b>	(DH) double glazing high solar transmittance - $U_{gl} = 1.140 \text{ W m}^{-2} \text{ K}^{-1}$ , $SHGC = 0.608$
	<b>c</b>	(DL) double glazing low solar transmittance - $U_{gl} = 1.099 \text{ W m}^{-2} \text{ K}^{-1}$ , $SHGC = 0.352$
	<b>d</b>	(TH) triple glazing high solar transmittance - $U_{gl} = 0.613 \text{ W m}^{-2} \text{ K}^{-1}$ , $SHGC = 0.575$
	<b>e</b>	(TL) triple glazing low solar transmittance - $U_{gl} = 0.602 \text{ W m}^{-2} \text{ K}^{-1}$ , $SHGC = 0.343$
<b>7</b>	<b>a</b>	Messina – $HDD_{20}$ : 707 K d
	<b>b</b>	Milan – $HDD_{20}$ : 2 404 K d

Considering 3 shape ratios, 4 ventilation rates, 3 possible insulation thicknesses, 3 base materials, 2 different ratios between the window surface and the floor and 5 types of glazings, 1080 different configurations have been evaluated for each month of each climate. 25920 monthly values have been elaborated for each of the each of the 4 setpoint conditions (air temperatures 20 °C and 26 °C, operative temperatures 20 °C and 26 °C).

## 5b.2 Results

The different setpoint temperature strategies in TRNSYS have been considered, assuming the EN ISO 13790:2008 results as benchmark. Firstly the different setpoint strategies have been compared for a null ventilation rate, in order to investigate the deviation induced by choosing air temperature setpoint or operative setpoint in dynamic simulation. Then the effects of different the ventilation rates have been analysed. The comparative graphs have been reported only for the cases without ventilation: for the other cases, see Annex D.

### *5b.2.1 Transmission heat losses and effects of the ventilation rate*

In Figure 5b.1, the transmission thermal losses simulated with the air temperature setpoints and with the operative temperature setpoints have been plotted against the quasi steady state results for the case of 20 °C. The cases with a 26 °C setpoint present similar trends and behaviours.

For both setpoint strategies, the results have first distinguished by S/V ratio. The cases without insulation have been highlighted in darker colour and regression lines have been added to distinguish trends and deviations.

The histograms in Figure 5b.2 and in Figure 5b.3 represent the percentage deviation of the linear trend line slopes from the unitary value for a setpoint of 20 °C and 26 °C, respectively.

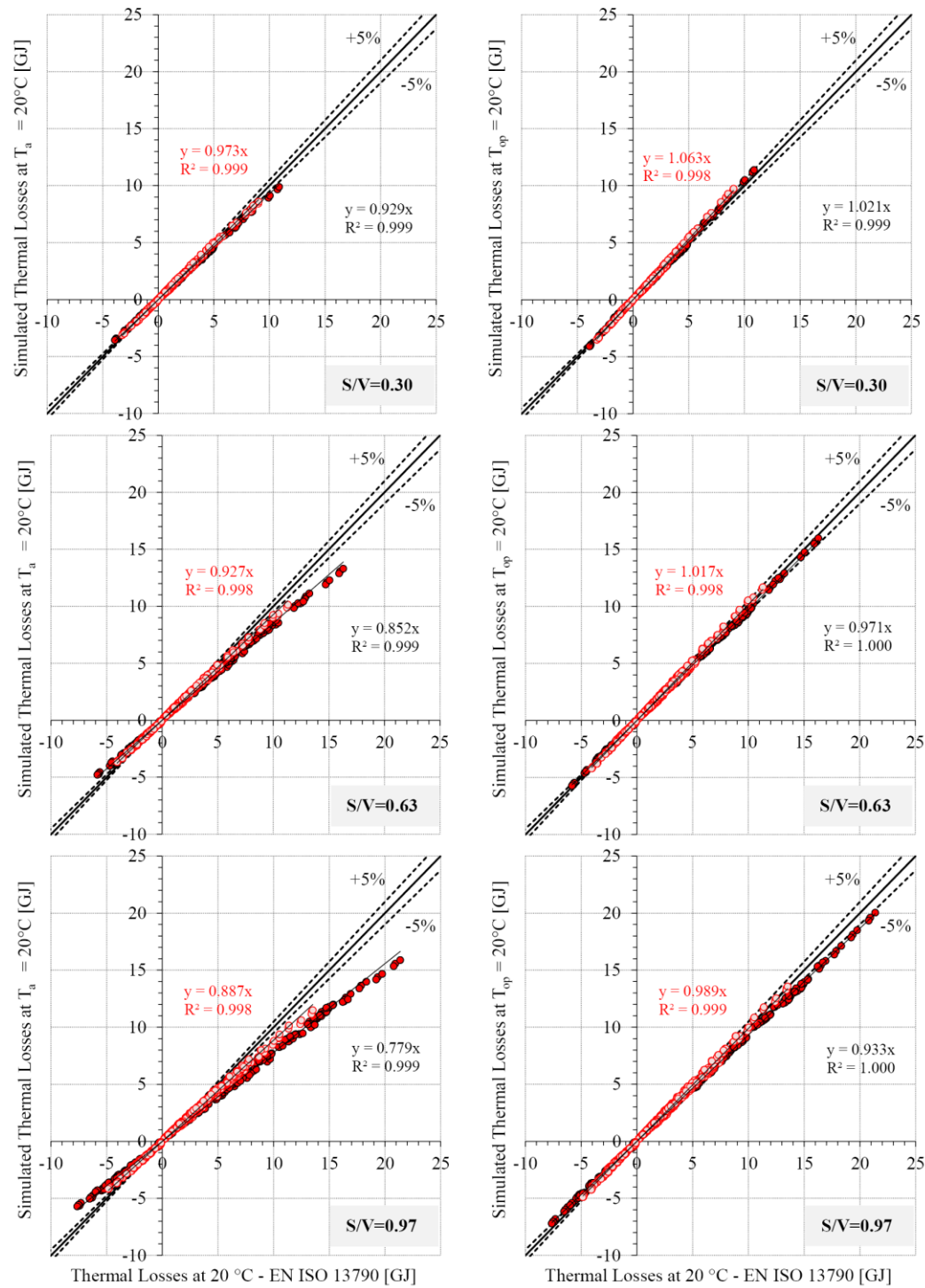


Figure 5b.1 - Simulated thermal losses with air temperature setpoint (on the left) and operative setpoint (on the right), without ventilation for the different S/V. Insulated cases in lighter colours

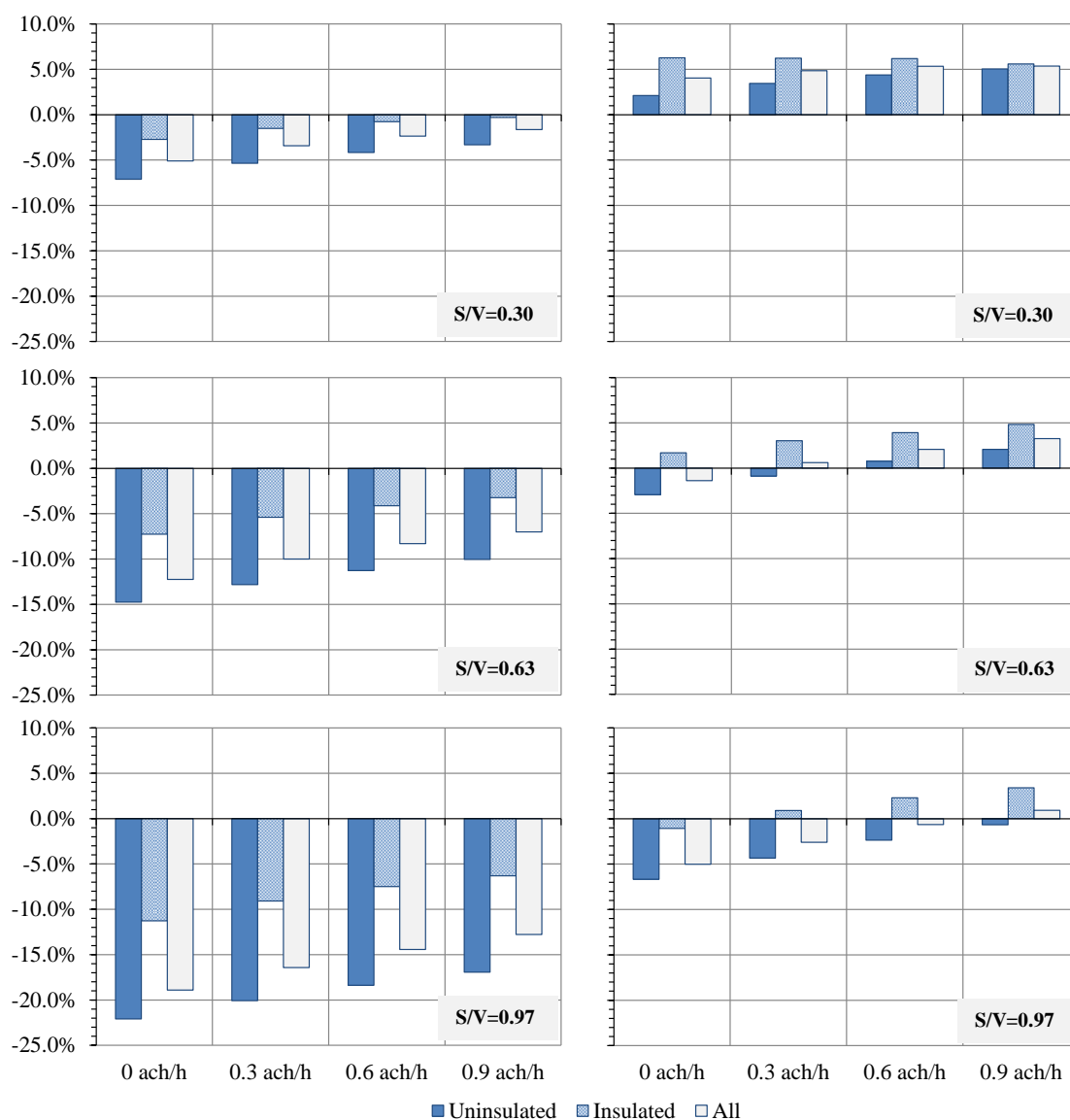


Figure 5b.2 - Percentage deviation of the simulated thermal losses with air temperature setpoint (on the left) and operative setpoint (on the right) of 20 °C respect to the losses calculated with the quasi steady state approach for different air change rates and S/V ratios



Figure 5b.3 - Percentage deviation of the simulated thermal losses with air temperature setpoint (on the left) and operative setpoint (on the right) of 26 °C respect to the losses calculated with the quasi steady state approach for different air change rates and S/V ratios

### 5b.2.2 Setpoint correction factor for the calculation of thermal losses by transmission

As it can be observed in literature and in the results of the previous paragraph, the main source of discrepancy is the kind of temperature considered as reference. Assuming as a setpoint the operative temperature is not realistic in most of the applications and so a correction factor has been calculated for all cases and a regression analysis has been performed in order to find a

general equation for determining the correction starting from the envelope characteristics. The developed model is reported in Eq. (5b.9) and it is characterized by an adjusted determination index  $R^2_{adj}$  equal to 0.85. The 11 coefficients have been reported in Table 5b.2.

$$f_L = k_0 + \theta_e \cdot (k_1 + k_2 \cdot x_{env} + k_3 \cdot x_{win}) + U_{env} (k_4 + k_5 \cdot x_{env} + k_6 \cdot x_{env} \cdot \theta_e) + U_{win} (k_7 \cdot x_{win} + k_8 \cdot x_{win} \cdot \theta_e) + k_9 \cdot x_{ad} + k_{10} \cdot \theta_{i,set} \quad (5b.9)$$

The correction factor is a function of the monthly average external temperature, the mean thermal transmittance of the dispersing opaque components, the mean thermal transmittance of the windows, the setpoint value and the composition of the envelope. In particular, the last is described distinguishing the fraction of dispersing opaque components, the fraction of windows and the one of adiabatic surfaces:

$$x_{env} + x_{win} + x_{ad} = 1 \quad (5b.10)$$

The determined correction factor is coherent with the PASSYS project (1989), that suggests a correction function of the outdoor temperature and the overall thermal losses coefficient to correlate the air and the mean radiant temperatures.

*Table 5b.2 - Regression coefficients for the correction factor for the thermal losses*

<b>k<sub>0</sub></b>	<b>k<sub>1</sub></b>	<b>k<sub>2</sub></b>	<b>k<sub>3</sub></b>	<b>k<sub>4</sub></b>	<b>k<sub>5</sub></b>	<b>k<sub>6</sub></b>	<b>k<sub>7</sub></b>	<b>k<sub>8</sub></b>	<b>k<sub>9</sub></b>	<b>k<sub>10</sub></b>
1.031	-1.456E-3	2.091E-3	2.451E-3	- 0.01465	-0.2093	0.01022	-0.1044	4.518E-3	0.05882	-2.084E-3

The sample used for the regression consists mainly in positive thermal losses (e.g., when the average external temperature is lower than the air temperature setpoint of 20 or 26 °C: negative values are, actually, thermal gains). In consequence of that, Eq. (5b.11) should be used only for setpoints close to the range 20 – 26 °C and when the average external temperature is lower than the setpoint.

## 5b.3 Discussion

### 5b.3.1 Transmission heat losses

Analysing the graphs in Figure 5b.1, it can be noticed that the linear regressions always show a very high index of determination R-squared in all the considered conditions, given that the results have been distinguished by shape ratio and presence of insulation. All other factors, such as windows size, kind of glazings, climate and also the thickness of insulation for the insulated cases, seem rather ineffective in spreading the results away from the trendlines.

Apart from the coefficient of determination, the equations of the trendlines reported in the charts enable to quantify the deviation of the results of the simulation carried on with difference reference temperatures as setpoints from the ones of the quasi-steady state method: the more the slope coefficient is different from 1, the more will be the deviation of the simulation results respect to the Standard method. The largest deviations are shown when using an air temperature setpoint for the simulations, whose results underestimate the absolute value of thermal losses. As one could expect, the differences are particularly large for the non-insulated cases with a high S/V ratio, with an undervaluation around 22%, but also in the insulated cases, the use of air temperature setpoint leads to absolute simulated losses larger than 10% with respect of the ones of the quasi-steady state method. Reducing the S/V ratio (i.e., increasing the percentage of adiabatic surface), the mean radiant temperature becomes higher, together with the operative temperature, and so the deviations between the simulations and the EN ISO 13790:2008 method get lower. With a S/V equal to 0.3, the underestimation is around 7% for the uninsulated cases and less than 3% for the insulated ones.

The operative temperature setpoint enlarges the difference between internal and external air temperature, giving higher absolute transmission and ventilation losses. For the high S/V, the underestimation is less than 7% for the uninsulated cases and around 1% for the insulated ones. For more compact structures (e.g.,  $S/V=0.3$ ), instead, there is a slight overestimation in the simulated results, around 2% for the uninsulated cases and more than 6% for the insulated ones.

### ***5b.3.2 Effects of the ventilation rate***

Looking at the Figures 5b.2 and 5b.3, it is easy to see that, when considering an air temperature setpoint, increasing the ventilation rate reduces the difference with the estimation of the thermal losses by the simulation approach, whatever the amount of adiabatic surfaces. This is due to the fact that larger absolute ventilation losses tend to compensate more the difference between transmission losses. For  $S/V$  larger than 0.3, the air temperature setpoint still keeps critical for all the considered ventilation rates, in particular in the non-insulated cases whose deviations are always larger than 10%.

When using an operative temperature setpoint, the trend is generally the same but in that case the effect does not compensate the already positive deviation of transmission losses. The ventilation losses are underestimated in absolute value by the quasi-steady state approach: larger ventilation rate increases less the absolute ventilation losses in the quasi-steady state method than in the simulations. The only exception to this behaviour is for the insulated cases with aspect ratio equal to 0.3 and 20 °C setpoint and the insulated ones with the same aspect ratio but a 26 °C setpoint and ventilation rate larger than 0.6 ach/h, for which increasing let the ventilation rate the deviations slightly decrease. Since the mean radiant temperature is independent from the ventilation rate and it is larger than the operative temperature setpoint in many of these last cases, the air temperature setpoint used by TRNSYS in the air-heat balance is lower than the setpoint of 20 or 26 °C (indeed, the thermal losses estimated by TRNSYS are lower than the ones calculated with the EN ISO 13790:2008 method). That also affects the ventilation thermal losses which are overestimated by the quasi-steady state approach and make the global percentage deviation decrease in absolute terms.

With the operative temperature setpoint, the deviations are generally within a range of 5%, except for the uninsulated cases without ventilation and  $S/V=0.97$  and for the insulated ones with  $S/V=0.3$ .



### 5b.3.3 Setpoint correction factor for the calculation of thermal losses by transmission

In order to discuss the improvements given by the correction factor for the operative temperature setpoint in EN ISO 13790:2008 method, in Figure 5b.4 an example of its application for the calculation of the thermal losses by transmission on the same cases presented in paragraph 5b. 1.3 is represented, considering both the 20 °C and the 26 °C setpoints. The correspondence between the new thermal losses and the simulated ones is good (+0.3%), with larger errors for low values of the thermal losses.

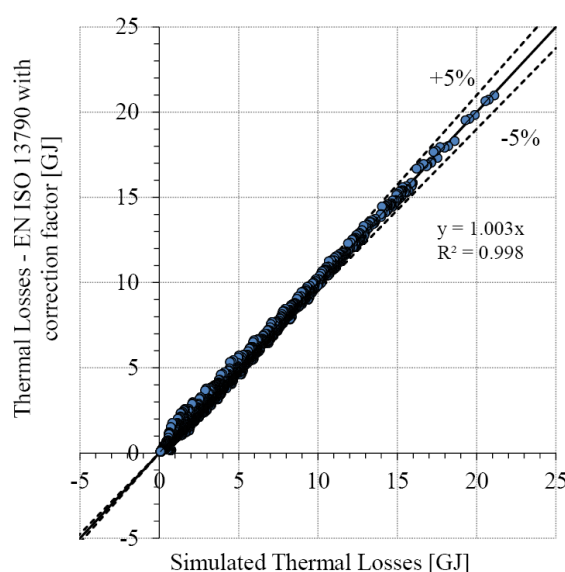


Figure 5b.4 - Comparison between the corrected EN ISO 13790 method and the air temperature setpoint simulations

The correction factor and the agreement between simulated and modified EN ISO 13790:2008 approach have been assessed also considering the BESTEST cases 600, 620, 900 and 920. Differently from the original cases described in chapter 3 and considered in the part *a* of the present chapter, this time the floor in touch with the ground (with a thermal transmittance of  $0.039 \text{ W m}^{-2} \text{ K}^{-1}$ ) has modeled directly as adiabatic. The thermal losses have been calculated and simulated both for the heating setpoint of 20 °C and the cooling setpoint of 27 °C considered in the BESTEST cases.

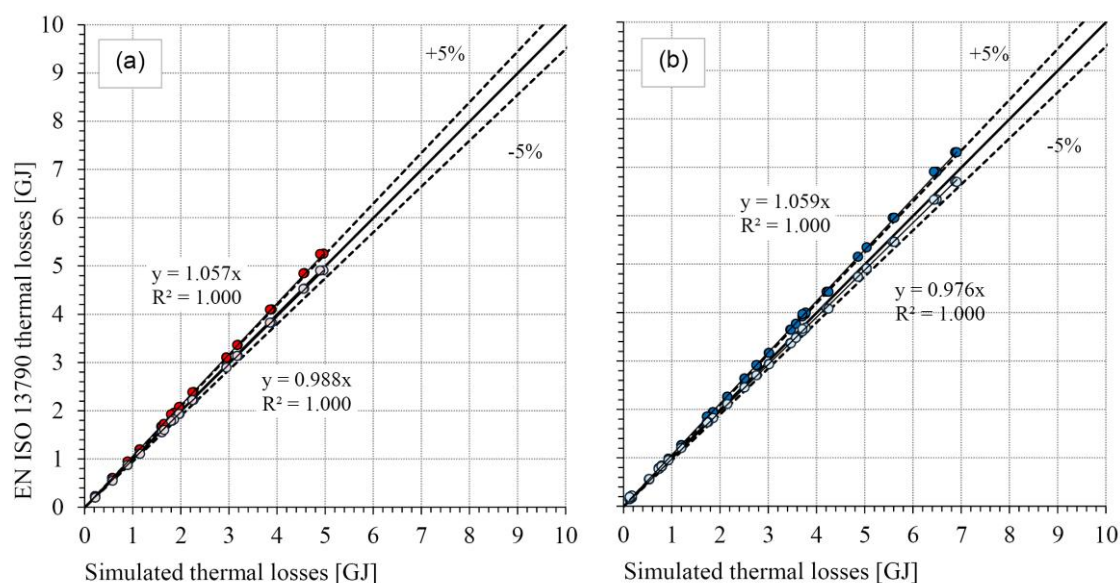


Figure 5b.5 – Thermal losses with a setpoint of 20 °C (a) and 27 °C (b), calculated by means of the EN ISO 13790:2008 method (dark colour) and with the correction factor (light colour)

Since the dispersing opaque envelope is partially insulated for the vertical walls ( $U \sim 0.5 \text{ W m}^{-2} \text{ K}^{-1}$ ) and insulated for the roof ( $U = 0.318 \text{ W m}^{-2} \text{ K}^{-1}$ ), the agreement between BES and quasi-steady state method is good with an overestimation around 6% by this last approach. By using the correction factor for the operative temperature setpoint of the EN ISO 13790:2008 method, the coherence is improved: considering the 20 °C setpoint there is an underestimation of -1.2% and considering the 27 °C setpoint an underestimation of -2.4%.

## **5b.4 Main findings**

The present part of chapter 5 is focused on the analysis of the thermal losses, paying attention to the effect of the main known sources of disagreement when comparing the thermal losses calculated by means of the EN ISO 13790:2008 quasi-steady state approach to the simulated ones. The role of the setpoint chosen for the simulation has been discussed, as well as the inaccuracy in the evaluation of the thermal losses by ventilation when an operative temperature setpoint is considered.

The main source of discrepancy is given by the linearization of the radiative and convective heat exchanges in the quasi-steady state method and, consequently, the use of an operative temperature setpoint. It is particularly relevant when uninsulated opaque envelopes are considered and the simplified model results compared to the ones simulated considering an air temperature setpoint.

In order to improve the alignment between the EN ISO 13790:2008 monthly method and the BES results with an air temperature setpoint, a correction factor has been proposed. The correction factor is a statistically derived function of the building envelope characteristics. It has been assessed both on the same sample of cases used for its development and on the BESTEST cases, revealing a significant improvement of the agreement between the thermal losses estimated according to the considered approaches.

## Part c: Comparison between the thermal gains by BES and by EN ISO 13790:2008 quasi-steady state method

### 5c.1 Methods

In this third part of the chapter about the extensive comparison between the quasi-steady state method and the BES, a large number of configurations has been simulated with TRNSYS in order to calculate the different components of the heat gains and to compare them with the EN ISO 13790:2008 monthly procedure. By means of different statistical analyses, some correction factors have been determined to identify the elements responsible of disagreement and to improve the accuracy of the technical Standard, estimating the actual amount of heat gains.

In the following three sections, the calculation methods proposed by the technical Standard EN ISO 13790:2008, as well as the approach by TRNSYS and the simulation assumptions, are described.

#### 5c.1.1 EN ISO 13790:2008 model

The technical standard EN ISO 13790:2008 considers as heat gains  $Q_{gn}$  the term of the heat balance that is independent of the gradient of temperature between the indoor and the outdoor environments. Positive sign is assumed for heat added to the air node, while negative for subtracted. The thermal gains are defined as:

$$Q_{gn} = Q_i + Q_{sol} \quad (5c.1)$$

The internal heat gains are:

$$Q_i = t \cdot \sum_k \Phi_{i,mn,k} + t \cdot \sum_l (1 - b_{tr,l}) \Phi_{i,mn,u,l} \quad (5c.2)$$

where the effect of the heat sources from adjacent unconditioned thermal zones is considered with a contribution weighed by the reduction factor  $b_{tr,l}$  defined in the standard ISO 13789:2007 (CEN, 2007). Different heat sources (occupants, appliances, lighting, hot and mains water, HVAC system, processes and goods) can be identified:

$$\Phi_i = \Phi_{i,Oc} + \Phi_{i,A} + \Phi_{i,L} + \Phi_{i,WA} + \Phi_{i,HVAC} + \Phi_{i,Proc} \quad (5c.3)$$

Case by case, it is possible to estimate the heat gain due to each single sources, even if national typical values are generally proposed by national annexes or technical Standards. Whatever the entity of the internal gains, the EN ISO 13790:2008 states that they should be considered as half radiative and half convective gains in more detailed calculation methods such as BES.

Similarly to the internal gains, the solar gains are estimated considering also the solar gains of the adjacent unconditioned thermal zones, properly weighed by the reduction factor  $b_{tr,l}$ :

$$Q_{sol} = t \cdot \sum_k \Phi_{sol,mm,k} + t \cdot \sum_l (1 - b_{tr,l}) \Phi_{sol,mm,u,l} \quad (5c.4)$$

In particular, the heat flow by solar gains consists in the heat flow by solar gains through a general element  $k$  of the building envelope, deducted the infrared extra flow towards the sky-dome:

$$\Phi_{sol,k} = F_{sh,ob,k} A_{sol,k} I_{sol,k} - F_{sky,k} \Phi_{sky,k} \quad (5c.5)$$

where  $F_{sh,ob,k}$  is the shading reduction factor for the external obstacles on  $A_{sol,k}$ , the effective solar collecting area of the element  $k$ , with a view factor of the sky  $F_{sky,k}$ .  $I_{sol,k}$  is the solar irradiance on the element  $k$  and  $\Phi_{sky,k}$  its infrared extra flow.

The effective solar collecting area is defined differently depending on the type of element.

For the glazings, it is calculated as:

$$A_{sol} = F_{sh,gl} g_{gl} (1 - F_{fr}) A_{win,p} \quad (5c.6)$$

The overall projected window area  $A_{win,p}$  is reduced in order to take into account of the frame factor  $F_{fr}$ , the total solar transmittance of the glazing  $g_{gl}$  and the shading reduction factor for movable shadings  $F_{sh,gl}$ , neglected in this work. The term  $g_{gl}$  is calculated in accordance with Eq. (5c.7):

$$g_{gl} = F_w g_{gl,n} \quad (5c.7)$$

where  $g_{gl,n}$  is the solar energy transmittance for radiation perpendicular to the glazing and  $F_w$  is the correction factor for non-scattering glazings which takes into account for the different incidence angles. The scattered glazings are not considered in this work and are treated

separately also by the Standard. An approximated value of  $F_w$  is 0.9 but, if available, the values indicated by the technical Standard of the EU Member States should be used. The values reported by the draft of the revUNI/TS 11300-1:2012 (UNI, 2012) have been considered.

For the opaque surfaces:

$$A_{sol} = \alpha_{S,env,k} \cdot R_{se} \cdot U_{env,k} \cdot A_{env,k} \quad (5c.8)$$

where  $A_{env,k}$  and  $U_{env,k}$  are, respectively, the projected area and the thermal transmittance of the opaque component  $k$ ,  $R_{se}$  its external surface resistance and  $\alpha_{S,env,k}$  its absorption coefficient.

The infrared extra flow can be calculated by means of Eq. (5c.9):

$$\Phi_{sky} = R_{se} \cdot U_{env,k} \cdot A_{env,k} \cdot h_{re} \cdot (\theta_e - \theta_{sky}) \quad (5c.9)$$

The average difference between the air temperature  $\theta_e$  and the sky fictive temperature  $\theta_{sky}$  can be approximated as 11 K at the latitudes of interest (e.g., around 45 °N). Assuming an external surface temperature equal to the air temperature, the surface radiative heat exchange coefficient  $h_{re}$  can be calculated as:

$$h_{re} = 4 \cdot \sigma \cdot \varepsilon \cdot \left( 273.15 + \frac{\theta_e + \theta_{sky}}{2} \right)^3 \quad (5c.10)$$

### 5c.1.2 Effective solar transmittance by Oliveti et al.

Oliveti *et al.* (2011) proposed a change to the solar transmittance calculation, in order to take into account of the amount dispersed through the glazings because of the reflections by the internal surfaces (i.e., assuming a more realistic hypothesis than the black body cavity). In Eq. (5c.7), instead of  $g_{gl,n}$ , the solar transmittance at normal incidence angle, they propose to calculate an effective solar heat gain coefficient at normal incidence, as:

$$g_{gl,n,eff} = \tau_{e,n} \cdot \alpha_{cav} + q_i + \tau_{e,n} \cdot (1 - \alpha_{cav}) \cdot q_e \quad (5c.11)$$

Where  $\tau_{e,n}$  is the beam solar transmission coefficient at normal incidence,  $\alpha_{cav}$  is the cavity absorption coefficient and  $q_i$  and  $q_e$  are secondary internal and external radiative-convective heat transfer factors, in accordance with EN 410:1998 (CEN, 1998):

$$\begin{aligned}
 g_{gl,n} &= \tau_{e,n} + q_i \\
 \tau_e + \rho_e + \alpha_e &= 1 \\
 \alpha_e &= q_i + q_e
 \end{aligned} \tag{5c.12}$$

$q_i$  can be calculated in accordance with EN 410:1998 coherently with the kind of glazing: Eq. (5c.13) for single pane glass, Eq. (5c.14) for double glazings and Eq. (5c.15) for triple glazings.

$$q_i = \alpha_e \cdot \frac{h_{si}}{h_{se} + h_{si}} \tag{5c.13}$$

$$q_i = \frac{\left( \frac{\alpha_{e1} + \alpha_{e2}}{h_{se}} + \frac{\alpha_{e2}}{\Lambda} \right)}{\left( \frac{1}{h_{si}} + \frac{1}{h_{se}} + \frac{1}{\Lambda} \right)} \tag{5c.14}$$

$$q_i = \frac{\left( \frac{\alpha_{e3}}{\Lambda_{23}} + \frac{\alpha_{e3} + \alpha_{e2}}{\Lambda_{12}} + \frac{\alpha_{e3} + \alpha_{e2} + \alpha_{e1}}{h_{se}} \right)}{\left( \frac{1}{h_{si}} + \frac{1}{h_{se}} + \frac{1}{\Lambda_{12}} + \frac{1}{\Lambda_{23}} \right)} \tag{5c.15}$$

where  $\alpha_e$  is the absorption factor of the glass ( $\alpha_{e1}$  the external glass and  $\alpha_{e2}$  the internal glass in the double glazings and  $\alpha_{e1}$  the external glass and  $\alpha_{e3}$  the internal glass in the triple glazings),  $h_{se}$  and  $h_{si}$  the external and internal heat transfer coefficients,  $\Lambda$  the conductance of the layers between two glasses surfaces ( $\Lambda_{12}$  the conductance between the external surface and half of the intermediate glass pane and  $\Lambda_{23}$  the conductance between the internal surface and half of the intermediate glass pane, for the triple glazings).

$\alpha_{cav}$  is defined by Oliveti *et al.* (2011) as:

$$\alpha_{cav} = 1 - a \cdot \exp \left( -b \cdot \left( \frac{\alpha_m}{\Psi} \right)^c \right) \tag{5c.16}$$

where the coefficients a, b, c are calculated in accordance with Eq. (5c.17) as functions of the transmission coefficient of the diffusion radiation of the glazings  $\tau_d$ ,  $\alpha_m$  is area-weighted

mean absorption coefficient for the cavity and  $\Psi$  is the ratio between the glazing area and the opaque area of the cavity.

$$\begin{aligned} a &= 3.500 - 5.453 \cdot \tau_d + 4.516 \cdot \tau_d^2 \\ b &= 3.700 - 5.388 \cdot \tau_d + 3.462 \cdot \tau_d^2 \\ c &= 0.124 + 0.545 \cdot \tau_d - 0.355 \cdot \tau_d^2 \end{aligned} \quad (5c.17)$$

### 5c.1.3 Thermal gains calculation procedure with the dynamic simulation approach

As observed several times in this work, TRNSYS implements and solves an air heat balance model as function of the convective thermal exchanges:

$$\Phi_{c,i} + \Phi_{ve} + \Phi_{i,c} + \Phi_{sys} = C_a \frac{d\theta_a}{dt} \quad (5c.18)$$

The convective part  $\Phi_{i,c}$  of the internal gains is the only one directly involved in the balance of Eq. (5c.18). The other gains (i.e., the radiative part of the internal gains and the solar gains) indirectly affect the air heat balance through the radiation exchanges with the internal surface of the envelope.

Per unit of surface:

$$q_{c,i} + q_{sol,i} + q_{i,swr} + q_{r,i} + q_{i,glwr} + q_{tr,i} = 0 \quad (5c.19)$$

The radiative part of the internal gains (both shortwave  $q_{i,swr}$ , for instance from internal lighting, and longwave  $q_{i,glwr}$ ) and  $q_{sol,i}$ , the solar irradiance entering through the glazings are here considered. In particular, as seen in chapter 3, in TRNSYS the diffuse entering solar radiation is distributed homogenously on the various surfaces of the envelope while the beam entering component is controlled by a distribution parameter called *geosurf*. Following the suggestions of the BESTEST procedure (Judkoff and Neymark, 1995), the *geosurf* is imposed equal to 1 for the floor and 0 for the other surfaces, so that the entering beam solar radiation first falls entirely on this surface. A further development can involve the study of the correlation between the distribution of the beam solar radiation and the predicted energy needs.

The solar radiation is then partially absorbed by each surface in accordance with its absorption coefficient and partially reflected as diffuse solar radiation. Due to the reflections, a



certain amount of the total entering solar radiation is lost through the transparent surfaces, as observed by Oliveti *et al.* (2011). It is also clear that not the whole heat gains involved in the internal surface heat balance are affecting the air heat balance because a fraction of the absorbed terms is lost by transmission. All these effects have been recognized by the EN ISO 13790:2008 as sources of disagreement between the quasi-steady state approach and detailed simulations.

Among the gains, also the thermal fluxes subtracting heat from the thermal zone but independent of the temperature difference are considered, such as the extra flow infrared radiation towards the sky vault. The temperatures of the external surfaces are defined by the following balance equation:

$$q_{c,e} + q_{sol,e} + q_{r,e} + q_{tr,e} = 0 \quad (5c.20)$$

The extra flow infrared radiation towards the sky vault is considered in the total external long wave radiation  $q_{r,e}$  and the part involving radiative exchanges with the external elements assumed at the air temperature has been already taken into account in the thermal losses calculation. Also in this case, the estimation of the effect on the indoor air heat balance of the solar heat gains for the opaque components and the infrared extra flow are affected by the heat transfer between the internal and the external surfaces of the envelope.

In order to evaluate the thermal gains by means of dynamic simulation, the EN ISO 13790:2008 prescribes first to calculate the thermal losses, as in the first part of the present chapter. This time the internal gains, the solar gains and the infrared extra flow to the sky vault are set as in a standard simulation but the heating and cooling setpoints have to assume the same value (as for the calculation of the thermal losses). The thermal gains can be calculated from the previously determined thermal losses and from the heating and cooling energy needs of this second set of simulations:

$$Q_{gn} = Q_{ht} - (Q_{H,nd} - Q_{C,nd}) \quad (5c.21)$$

Since the heat gains are independent from the chosen simulation setpoint, using either air or operative temperatures is irrelevant, as well as considering a value of 20 °C or 26 °C. In this analysis an air temperature setpoint of 20 °C has been assumed and the results have been used in Eq. (5c.21), together with the correspondent set of thermal losses.

As in the part *b*, in order to compare simulated and quasi-steady state results, boundary conditions and calculation parameters for the simulation have been selected coherently with the ones assumed in the quasi steady state approach. As regards the external conditions, the hourly

weather data have been calculated by means of the subroutine Type 54 starting from the monthly average values reported by the Italian technical standard UNI 10349:1994 and used in the simplified method. The horizontal global solar radiation is split into the beam and the diffuse components in accordance with the Erbs' algorithm implemented in the Type 54. The diffuse components of the solar radiation on the vertical façades have been calculated in accordance with the algorithm by Perez *et al.* (1990). The mean daily solar radiation on a monthly base has been calculated for each orientation and used in the quasi-steady state method instead of the ones reported in the UNI 10349:1994. Starting from the horizontal infrared flux reported in the EPW weather files, the fictive sky temperature has been calculated for each timestep and used in TRNSYS simulations. As for the solar radiation, monthly averages have been calculated for the quasi-steady state method, in place of the gradient of 11 K suggested by the EN ISO 13790:2008. Constant internal heat gains equal to  $4 \text{ W m}^{-2}$  has set in TRNSYS, half convective and half radiative as the Standard prescribes.

The same surface convective coefficients have been considered both in TRNSYS and in the quasi-steady state method and the long wave radiation heat transfer coefficients have been recalculated, as in the part *b*.

#### **5c.1.4 Reference building model and set of configurations**

The simulation plan has been modified in order to study the heat gain problem. For the general characteristics of the simulation plan, see part *b*. The following geometrical and thermo-physical characteristics have been studied in accordance with the factorial plan:

1. the amount of envelope surface exposed to the external conditions;
2. the level of insulation added to the internal layer;
3. the base material of the opaque envelope;
4. the percentage ratio of glazings  $A_{gl}$  to floor area  $A_f$ ;
5. the orientation of the windows, all positioned in the same façade;
6. the kind of glazings;
7. the climatic conditions.

For each of the above factors, a certain number of levels were considered, as reported in Table 5b.1 in the previous part. Since not pertinent with the topic of the third part, the ventilation rate has been neglected as variable and the simulations have been performed considering 0 ach/h. The orientation of the windows has been introduced in particular to assess more profiles of entering radiation and the possible levels for this variable are 3: East, South or

West-oriented windows, all in the same façade in order to simplify the statistical analysis of the results.

As concerns the opaque components, the absorption coefficients of the sun-exposed walls are 0.3 for the vertical walls (both sides) and for the ceiling (internal side), 0.6 for the roof (external side) and for the internal floor. When a surface is exposed to the external environment but not to the sun, its coefficient is 0. It is the case of the non-adiabatic floors directly in contact with the external air, modelled as if they are on a well-ventilated cavity. The absorption coefficient of the window frame is 0.6.

The first factor allows to consider different ratios between the dispersing surface and so can influence the amount of solar gains received by the opaque components and the infrared extra flow (from the external side) and the dispersion of the entering solar radiation absorbed (on the internal side). Similarly, the variation of the thickness of the insulation layer between 0 and 10 cm (factor 2) affects the heat exchanges from the internal and external surfaces. The kind of glazings (factor 6), is probably the most important in this analysis because it strongly influences the entering solar radiation, which is generally the major heat gain source, together with the factors 4 and 5. Factor 5 is also important in affecting the profile of the entering solar radiation during the day. Two climates (Milan and Messina) have been considered. Since the comparison is on a thermal flow and on a monthly basis, as stated in the thermal losses part, the heat capacity of the opaque envelope (factor 3) is not supposed to be relevant for the monthly heat gain flow calculation and it has been considered as variable because of the small deviations in the thermal resistance of the 3 alternatives and with the perspective of further development on the calculation of the utilization factor and the energy needs in the last part of the chapter. Considering 3 shape ratios, 3 possible insulation thicknesses, 3 base materials, 2 different ratios between the window surface and the floor, 5 types of glazings and 3 orientations, 810 different configurations have been evaluated for each month of each climate. 19440 monthly values have been elaborated.

In order to implement the procedure by Oliveti *et al.*, some additional information are required. For the glazings considered in this analysis, the different properties and the effective global solar heat gain coefficients are reported in Tables 5c.1 and 5c.2.

Table 5c.1 - Properties of the considered glazing systems

	(S)	(DH)	(DL)	(TH)	(TL)
$\tau_{e,n}$	0.771	0.513	0.256	0.477	0.256
$\tau_d$	0.689	0.439	0.205	0.391	0.191
$\alpha_e$	0.173	0.294	0.448	0.276	0.425
$\alpha_{e1}$	0.173	0.200	0.356	0.143	0.302
$\alpha_{e2}$	-	0.094	0.092	0.082	0.067
$\alpha_{e3}$	-	-	-	0.051	0.056
$A$ [W m <sup>-2</sup> K <sup>-1</sup> ]	-	1.416	1.353	-	-
$A_{12}$ [W m <sup>-2</sup> K <sup>-1</sup> ]	-	-	-	0.342	0.336
$A_{23}$ [W m <sup>-2</sup> K <sup>-1</sup> ]	-	-	-	0.342	0.336
$q_i$	0.0436	0.0903	0.0958	0.0914	0.0900
$q_e$	0.1294	0.2037	0.3522	0.1846	0.3350

Table 5c.2 - Effective solar heat gain coefficients

	(S)		(DH)		(DL)		(TH)		(TL)	
	Size1	Size2	Size1	Size2	Size1	Size2	Size1	Size2	Size1	Size2
$\Psi$	3.8%	7.9%	3.8%	7.9%	3.8%	7.9%	3.8%	7.9%	3.8%	7.9%
$\alpha_m$	0.400	0.407	0.400	0.407	0.400	0.407	0.400	0.407	0.400	0.407
$\alpha_{cav}$	0.946	0.886	0.964	0.923	0.974	0.950	0.967	0.930	0.975	0.951
$g_{gl,n,eff}$	0.778	0.738	0.589	0.572	0.347	0.343	0.556	0.541	0.342	0.338
$g_{gl,n}$	0.855		0.608		0.352		0.575		0.343	
$\Delta g_{gl,n}$	-9.0%	-13.7%	-3.1%	-5.9%	-1.4%	-2.6%	-3.3%	-5.9%	-0.3%	-1.5%

As it can be observed in Table 5c.2, the higher the solar heat gain coefficient and the larger the glazings area, the lower the effective solar heat gain coefficient.

## 5c.2 Results

The thermal gains have been analysed considering separately their 4 main components (entering solar gains through the glazings, solar gains transmitted through the opaque elements, internal gains and infrared extra flow towards the sky vault) and some correction factors based on the envelope properties have been developed, with two main purposes: to find the source of discrepancy and to provide a statistically derived correction based on them. In Figures 5c.1, 5c.2 and 5c.3 the thermal gains evaluated in accordance with the EN ISO 13790:2008 method and the simulated ones have been compared, as well as the corrected results and the simulated ones. The coefficients of the regressions to correlate the correction factors with the envelope characteristics are reported in Table 5c.3. For the entering solar radiation, also the model by Oliveti *et al.* (2011) has been implemented in alternative to the EN ISO 13790:2008 method to calculate the effective global solar transmittance of glazings.

### 5c.2.1 Entering solar heat gains

The solar gains entering through the transparent envelope have been represented in Figure 5c.1 - a, on the top. For the analysed cases, a correction factor  $f_{sol,gl}$  has been determined and a regression has been performed in order to correlate  $f_{sol,gl}$  with the characteristics of the envelope:

$$f_{sol,gl} = k_0 + U_{env} \cdot (k_1 + k_2 \cdot x_{env}) + x_{win} \cdot (k_3 + k_4 \cdot U_{win}) + k_5 \cdot x_{ad} \quad (5c.22)$$

The regression, with an adjusted index of determination  $R^2_{adj}$  of 0.957, underlines also the importance of the interactions between the windowed fraction (calculated with respect of the whole envelope, including the adiabatic surfaces, as in part *b*) with the window thermal transmittance and the opaque dispersing fraction with the mean opaque thermal transmittance (with a standardized coefficient of -0.527 and -0.448, respectively).

The results provided by using the  $g_{gl,n,eff}$  according to the method by Oliveti *et al.* instead of  $g_{gl,n}$  in the quasi-steady state approach are represented in Figure 5c.2.

The correction factor has been recalculated starting from the effective solar transmittance: the model is similar to the previous one and it is presented in Eq. (5c.23) but with different regression coefficients, reported in table. The  $R^2_{adj}$  of the model is a little lower than the previous one (0.941 instead of 0.957).

$$f_{sol,gl}' = k_0 + U_{env} \cdot (k_1 + k_2 \cdot x_{env}) + U_{win} \cdot (k_3 + k_4 \cdot x_{win}) + k_5 \cdot x_{ad} \quad (5c.23)$$

### 5c.2.2 Solar heat gains by transmission

The solar heat gains by transmission through the opaque envelope have been represented in the graphs of the second line of Figure 5c.1.

The correction factor  $f_{sol,env}$  has been determined as in Eq. (5c.24):

$$f_{sol,env} = k_0 + k_1 \cdot A_{env} + x_{env} \cdot (k_2 \cdot x_{ad} + k_3 \cdot U_{env} + k_4 \cdot \theta_e) + k_5 \cdot U_{env} + k_6 \cdot U_{win} \quad (5c.24)$$

The regression has an adjusted  $R^2_{adj}$  of 0.948 and the most influencing parameters are the opaque dispersing surface (with a standardized coefficient of 1.165) and the interaction between the opaque and the adiabatic fractions (0.609).

### 5c.2.3 Internal gains

The internal gains have been represented in the graphs on the bottom of Figure 5c.1.

The correction factor  $f_{int}$  has been determined as in Eq. (5c.25):

$$f_{int} = k_0 + U_{env} \cdot (k_1 + k_2 \cdot x_{env}) + k_3 \cdot U_{win} \cdot x_{win} \quad (5c.25)$$

The regression adjusted  $R^2_{adj}$  is 0.99 and the interaction between the fraction of opaque surface and its mean thermal transmittance and the one between the fraction of window surface and its thermal transmittance have the same standardized coefficients (around -0.5).

### 5c.2.4 Infrared extra flow towards the sky vault

Finally, the infrared extra flows towards the sky vault have been represented in Figure 5c.2 and the correction factor  $f_{r,sky}$  in Eq. (5c.26).

$$\begin{aligned} f_{r,sky} = & k_0 + x_{env} \cdot (k_1 \cdot x_{ad} + k_2 \cdot U_{env} + k_3 \cdot \theta_e) + U_{win} \cdot (k_4 + k_5 \cdot x_{win}) \\ & + k_6 \cdot x_{ad} + k_7 \cdot \theta_e + k_8 \cdot U_{env} \end{aligned} \quad (5c.26)$$

The adjusted determination index is 0.878 and the most influencing parameters are the interaction between the thermal transmittance of the opaque envelope and its fraction (standardized coefficient equal to -0.418) and the fraction of adiabatic surface (0.665).

In the following Table the regression coefficients for the regressive models determined for the estimation of the correction factors are reported.

*Table 5c.3 - Regression coefficients for the determination of the correction factors for thermal gains*

<i>Entering solar gains</i>								
<b>k<sub>0</sub></b>	<b>k<sub>1</sub></b>	<b>k<sub>2</sub></b>	<b>k<sub>3</sub></b>	<b>k<sub>4</sub></b>	<b>k<sub>5</sub></b>			
0.9346	-0.1014	0.1531	-0.2889	-0.3248	2.487E-2			
<i>Entering solar gains (with the model by Oliveti et al.)</i>								
<b>k<sub>0</sub></b>	<b>k<sub>1</sub></b>	<b>k<sub>2</sub></b>	<b>k<sub>3</sub></b>	<b>k<sub>4</sub></b>	<b>k<sub>5</sub></b>			
0.9314	-0.1086	-0.1566	6.949E-3	-0.2266	2.821E-2			
<i>Transmitted solar gains</i>								
<b>k<sub>0</sub></b>	<b>k<sub>1</sub></b>	<b>k<sub>2</sub></b>	<b>k<sub>3</sub></b>	<b>k<sub>4</sub></b>	<b>k<sub>5</sub></b>	<b>k<sub>6</sub></b>		
-0.3265	4.964E-3	3.780	-0.4017	6.765E-3	0.3228	-5.766E-2		
<i>Internal gains</i>								
<b>k<sub>0</sub></b>	<b>k<sub>1</sub></b>	<b>k<sub>2</sub></b>	<b>k<sub>3</sub></b>					
0.9885	-4.610E-2	-9.773E-2	-0.1709					
<i>Infrared extra flow towards the sky vault</i>								
<b>k<sub>0</sub></b>	<b>k<sub>1</sub></b>	<b>k<sub>2</sub></b>	<b>k<sub>3</sub></b>	<b>k<sub>4</sub></b>	<b>k<sub>5</sub></b>	<b>k<sub>6</sub></b>	<b>k<sub>7</sub></b>	<b>k<sub>8</sub></b>
1.044	-0.3144	-0.1433	2.217E-3	7.914E-3	-0.1562	0.2187	-3.738E-3	-5.795E-2

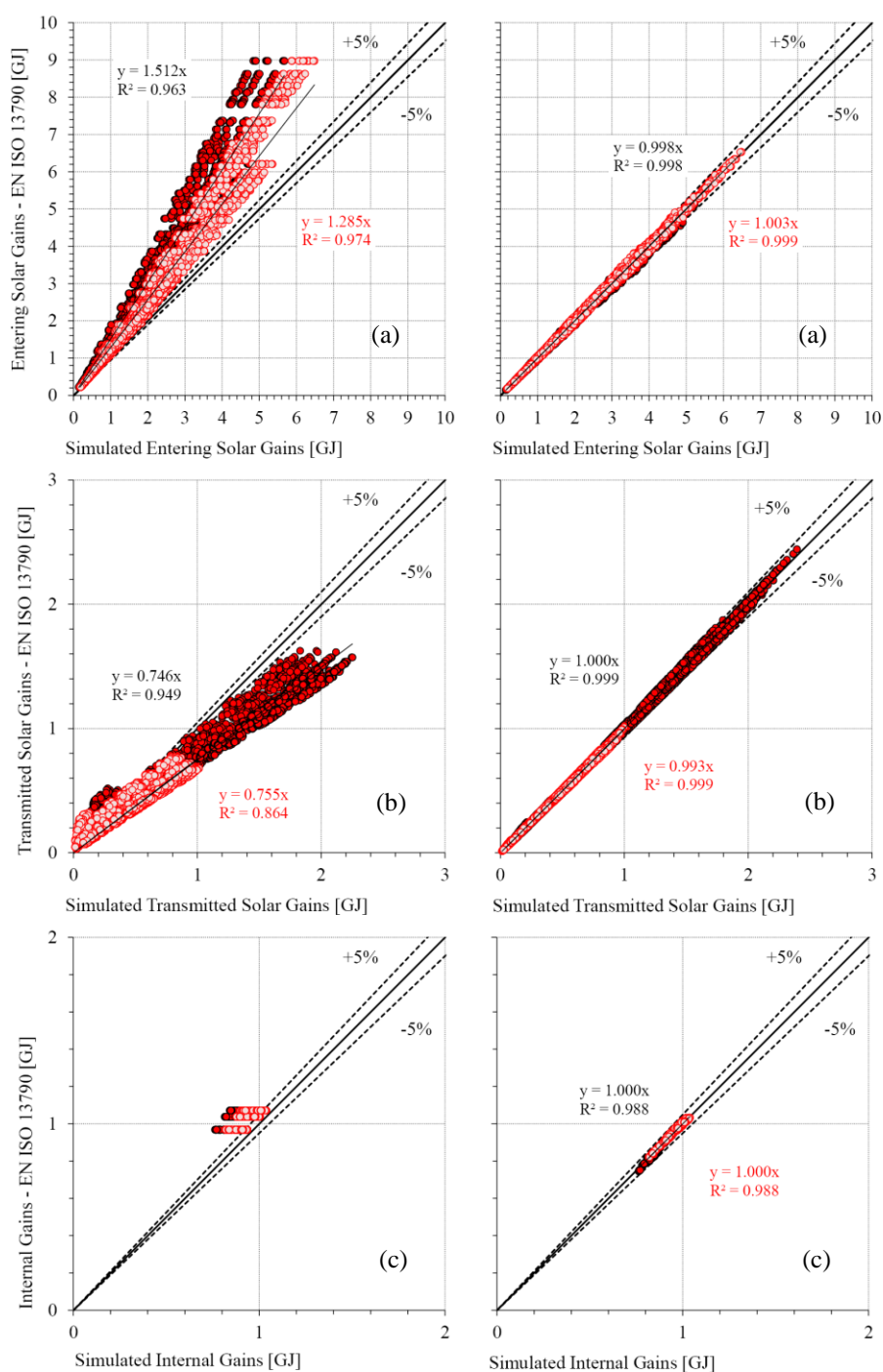


Figure 5c.1 - EN ISO 13790:2008 entering solar gains (a), transmitted solar gains (b) and internal gains (c), calculated according to the Standard (on the left) and using the correction coefficients (right) compared to the simulated gains. Insulated cases in lighter colours



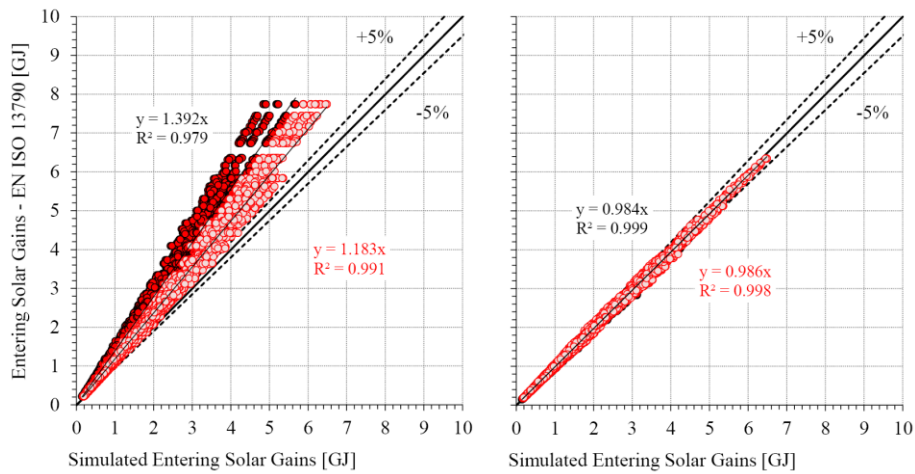


Figure 5c.2 - EN ISO 13790:2008 entering solar gains, calculated according to the Standard considering the procedure by Oliveti et al. for the evaluation of the effective solar heat gain coefficient (on the left) and using the correction coefficients (right) compared to the simulated gains. Insulated cases in lighter colours

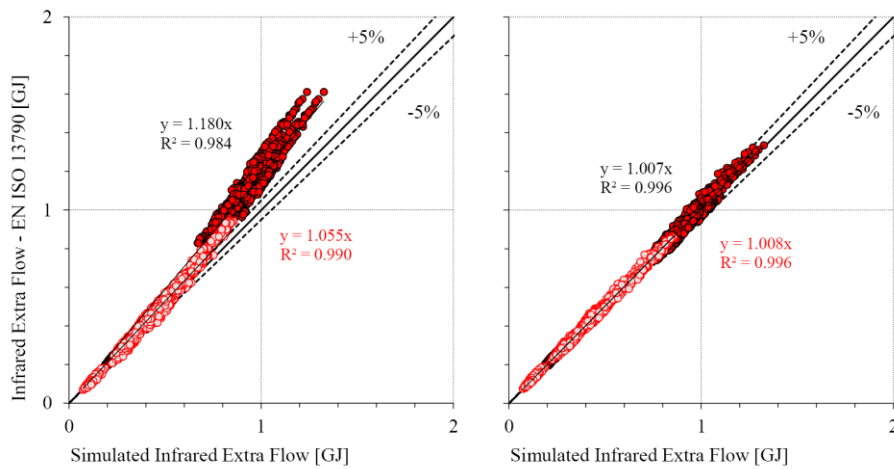


Figure 5c.3 - EN ISO 13790:2008 infrared extra flow towards the sky vault, calculated according to the Standard (on the left) and using the correction coefficients (right) compared to the simulated gains. Insulated cases in lighter colours

## 5c.3 Discussion

### 5c.3.1 Entering solar heat gains

The entering solar radiation gains are clearly overestimated by the EN ISO 13790:2008. As observed before, this is consistent with the lack of consideration for the re-dispersion of these gains by transmission or by radiation through the windows. The deviations are strongly dependent on the amount of dispersing surface (i.e., the S/V ratio) and, in particular, on the insulation level, which is also the variable considered in Figure 5c.1 to distinguish the result in two groups: insulated one in light red and uninsulated one in dark red. The spread of the points of these two groups around the trend line is mainly due to S/V ratio. As it can be seen, the trend line of the uninsulated cases demonstrates a general overestimation of +51.2% given by the EN ISO 13790:2008 method. In case of insulation, it is reduced to +28.5%. By using the correction factor  $f_{sol,gl}$  in Eq. (5c.22) the quasi-steady state results have been corrected, obtaining a percentage deviation within the 5% respect to the simulations.

Analysing the results of the quasi-steady state with the effective solar transmittance by Oliveti *et al.*, it can be noticed that, even with the agreement with the dynamic simulation is better, a large discrepancy is still present. The agreement is improved by the 10%: thus, the uninsulated cases present an overestimation of +39.2% and the insulated ones of +18.3% by the simplified method respect to the simulations. With the correction factor  $f_{sol,gl}'$  in Eq. (5c.23), also in this case the percentage deviation of the quasi-steady state results respect to the simulations is within the 5%.

### 5c.3.2 Solar heat gains by transmission

For the solar gains transmitted through the opaque envelope, the EN ISO 13790:2008 underestimates the results respect of the simulations. The trend is the same both for insulated and uninsulated cases and it is around -25%. The spreads of the results around the trend lines are similar in both cases (a little larger for the insulated ones).

By using Eq. (5c.24) and calculating the correction factor  $f_{sol,env}$  the quasi-steady state results have been corrected, and brought close to the 5% range of deviation respect of the simulations.

### **5c.3.3 Internal gains**

The convective internal gains are the same in both calculation methods and the deviations are due to the radiative part of the internal gains. The variability in the EN ISO 13790:2008 results is simply due to the different lengths of the months and a trend line cannot be defined. In simulation results, also the partially dispersion of the radiative part is considered. The overestimation provided by the Standard is between 10-20% for uninsulated cases and 5-10% for the insulated ones. Also the S/V ratios, as expected, are relevant.

### **5c.3.4 Infrared extra flow towards the sky vault**

In the calculation of the infrared extra flow towards the sky dome, it can be noticed a different behaviour from the insulated to the uninsulated cases: while for the insulated cases a good agreement is registered, for the uninsulated ones the EN ISO 13790:2008 overestimates (+18%). The difference is probably due to the estimation of the surface temperature for the calculation of  $h_{re}$ . Thus, the estimation of the extra flow for the insulated walls is quite good because the external surface temperature is close to the external environment temperature and, so, assuming this temperature for the estimation of the radiative heat transfer coefficient does not causes large errors as observed for the uninsulated walls.

### **5c.3.5 Assessment of the proposed correction factor with some BESTEST cases**

In Figure 5c.1, 5c.2 and 5c.3 the thermal gains components evaluated by means of the EN ISO 13790:2008 approach have been corrected by using the proposed correction factors. As observed in the previous paragraphs, the agreement with the heat gains determined by simulation is significantly improved and the percentage deviations are within a 5% range for most of the cases.

As done in part *b*, the proposed correction factors have been assessed with the BESTEST cases 600, 620, 900 and 920 with adiabatic floor. The results for the whole heat gains with the effective global solar heat gain coefficient by Oliveti *et al.* have been reported in Figure 5c.4.

A good agreement is registered and the thermal gains calculated pass from an overestimation of +17.6% to a light underestimation of -2.7% with respect to the simulated thermal gains.

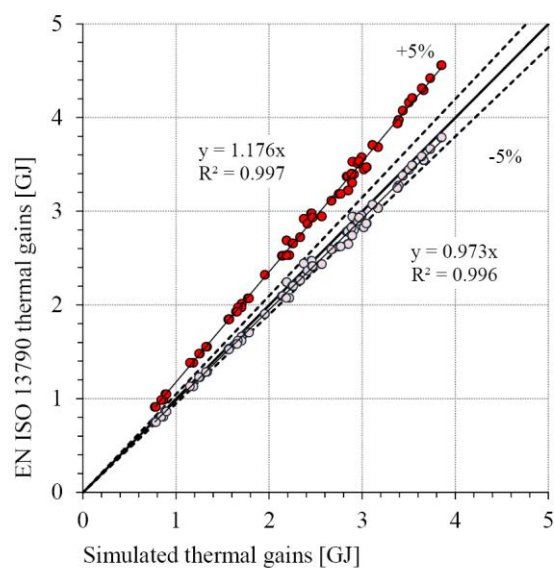


Figure 5c.4 - Thermal gains calculated by means of the EN ISO 13790:2008 method with the effective global solar heat gain coefficient (dark colour) and with the correction factor (light colour)

## 5c.4 Main findings

In the present part of chapter 5, the problem of the agreement between the thermal gains evaluated by means of the quasi-steady state method and BES tools is considered. The four different components of the heat gains have been distinguished and analysed separately.

For the entering solar radiation through the transparent envelope the quasi-steady state model completely neglects the amount of radiation reflected and dispersed through the windows (i.e., it assumes a black cavity hypothesis), as well as the amount absorbed by the opaque components but not involved in the air heat balance because redispersed by transmission. For the internal gains, the estimation of the contribution of the radiative component is affected by a similar problem and a fraction of it is lost by transmissions and does not participate in the air heat balance of the thermal zone. About the thermal gains components involving the external surface heat balance, the main problem is related to the determination of the surface heat transfer coefficient, which depends on the surface temperature that is not known in advance in the quasi-steady state methods and it is generally assumed equal to the external air temperature.

For each component of the thermal gains a correction factor has been proposed in order to make them closer to the ones estimated by BES tools in accordance with the EN ISO 13790:2008 prescriptions. In particular, these factors are statistically derived functions of the envelope characteristics (e.g., thermal transmittance or adiabatic surfaces amount). The improvements in the agreement between BES and simplified method have been assessed on the same cases used for their development and also on some BESTEST-based cases. In both ones, the percentage deviations have been reduced within a range of 5%.

## **Part d: Comparison between BES and EN ISO 13790:2008 quasi-steady state method**

### **5d.1 Methods**

In this last part, the final results (i.e., the monthly heating and cooling energy needs) have been calculated (according to the quasi-steady state method and the simulation) and compared.

The BESTEST cases presented in the first part of this chapter have been evaluated again with the use of the correction proposed. The simplified hypothesis about the floor, assumed adiabatic in the parts *b* and *c*, is not considered here, in order to have results comparable with the ones of part *a*.

As regards the comparison for the extensive simulation plan, the chosen cases are not all those considered in the previous parts of this chapter: in order to focus on the performance of the thermal zones with a residential use, all the alternatives proposed in part *c* for the study of the heat gains have been selected but only a ventilation of 0.3 ach/h, typical for dwellings, have been taken into account. As stated before, the imposed setpoints for the thermal losses calculation are those prescribed for this category. Both Messina and Milan have been considered in this last analysis.

#### ***5d.1.1 Methods: EN ISO 13790:2008 utilization factors***

In order to calculate the energy needs starting from the heat losses and gains, the technical Standard recurs to a dynamic coefficient, the utilization factor, which has to take into account of the dynamic effects occurring in the energy balance of the thermal zone. In particular, the aim of the utilization factor is to consider the effect of the building envelope thermal inertia and of the mismatch between thermal losses and thermal gains: by performing the evaluation on a monthly (or seasonal) basis, the integrals of the flows during the period are considered and, even if timestep by timestep the required energy need is given by the difference between heat losses and heat gains, the same concept cannot be extended to the monthly (or seasonal) integrals. Thus, because of the thermal inertia and, generally, of the different hourly profiles of the two thermal flows, there is a mismatch between their occurrences that cannot be detected by considering a long time-discretization period. For instance, as observed by van Dijk and Arkesteijn (1987) for the heating energy needs, the occurrence of heat gains when the heat

losses are low tends to reduce the heating needs and to lead to an overheating respect to the considered setpoint. To take into account of these phenomena, the EN ISO 13790:2008 proposes an utilization factor for the heating energy need calculation and another for the cooling one.

Referring to the heating problem, the gain utilization factor is used to weight the heat gains and to calculate the heating energy needs. This dimensionless variable is a function of the heat balance ratio  $\gamma_H$  between the gains and the losses and the parameter  $a_H$  which is statistically derived and considers the effect of the building inertia.

$$\gamma_H = \frac{Q_{H,gn}}{Q_{H,ht}} \quad (5d.1)$$

$$a_H = a_{H,0} + \frac{\tau}{\tau_{H,0}} \quad (5d.2)$$

where  $a_{H,0}$  is a dimensionless reference numerical parameter, which is equal to 1 for the monthly calculation and 0.8 for the seasonal one,  $\tau$  is the time constant of the building zone expressed in hours and  $\tau_{H,0}$  is the reference time constant, whose value is 15 h for the monthly calculation and 30 h for the seasonal ones.  $a_{H,0}$  and  $\tau_{H,0}$  can assume different values in the Member States, as consequence of specific empirical studies aim at better evaluating them. The time constant can be calculated with Eq. (5d.3):

$$\tau = \frac{C_m / 3600}{H_{tr} + H_{ve}} \quad (5d.3)$$

where  $C_m$  is the internal heat capacity of the building,  $H_{tr}$  and  $H_{ve}$  are the overall heat transfer coefficients, respectively by transmission and ventilation, presented in part *b*.  $C_m$  can be evaluated as the sum of the products between the internal heat capacity per area  $\kappa_i$  of each element  $k$  and its area. The area specific heat capacity can be determined by means of one of the methods described in EN ISO 13786:2007; in this context, the detailed approach described in chapter 4 has been implemented.

The gain utilization factor is defined as:

$$\text{If } \gamma_H > 0 \text{ and } \gamma_H \neq 1: \quad \eta_{H,gn} = \frac{1 - \gamma_H^{a_H}}{1 - \gamma_H^{a_H + 1}} \quad (5d.4)$$

$$\text{If } \gamma_H = 1: \quad \eta_{H,gn} = \frac{a_H}{a_H + 1} \quad (5d.5)$$

$$\text{If } \gamma_H < 0: \quad \eta_{H,gn} = \frac{1}{\gamma_H} \quad (5d.6)$$

For the cooling problem, the loss utilization factor is used to weight the heat losses and to calculate the cooling energy needs. The definition and used parameter are similar to the ones presented for the heating energy calculation: the loss utilization factor is a function of the heat balance ratio evaluated in the cooling conditions  $\gamma_C$  between the gains and the losses and the parameter  $a_C$  which, like  $a_H$ , is statistically derived and considers the effect of the building inertia.

$$\gamma_C = \frac{Q_{C,gn}}{Q_{C,ht}} \quad (5d.7)$$

$$a_C = a_{C,0} + \frac{\tau}{\tau_{C,0}} \quad (5d.8)$$

where  $a_{C,0}$  is a dimensionless reference numerical parameter and  $\tau_{C,0}$  is the reference time constant. Their values are the same of  $a_{H,0}$  and  $\tau_{H,0}$  but after specific empirical research, the Member States can decide to assume other reference values.

The loss utilization factor is defined as:

$$\text{If } \gamma_C > 0 \text{ and } \gamma_C \neq 1: \quad \eta_{C,ls} = \frac{1 - \gamma_C^{-a_C}}{1 - \gamma_C^{-(a_C+1)}} \quad (5d.9)$$

$$\text{If } \gamma_C = 1: \quad \eta_{C,ls} = \frac{a_C}{a_C + 1} \quad (5d.10)$$

$$\text{If } \gamma_C < 0: \quad \eta_{C,ls} = 1 \quad (5d.11)$$

For the implementation of the EN ISO 13790:2008 method for the estimation of the monthly energy needs, different thermal flows have been used: the ones calculated in accordance with the EN ISO 13790:2008 method, the corrected ones and, finally, the thermal flows evaluated by means of dynamic simulations. In this ways it has been possible to assess not only the heat flows but also the capability of the equations provided by the Standard to calculate the utilization factor.



## 5d.2 Results

### 5d.2.1 BESTEST cases

The annual energy results evaluated by means of the EN ISO 13790:2008 method with the proposed correction factors have been reported in Figure 5d.1 and 5d.2, for Milan and Messina, respectively.

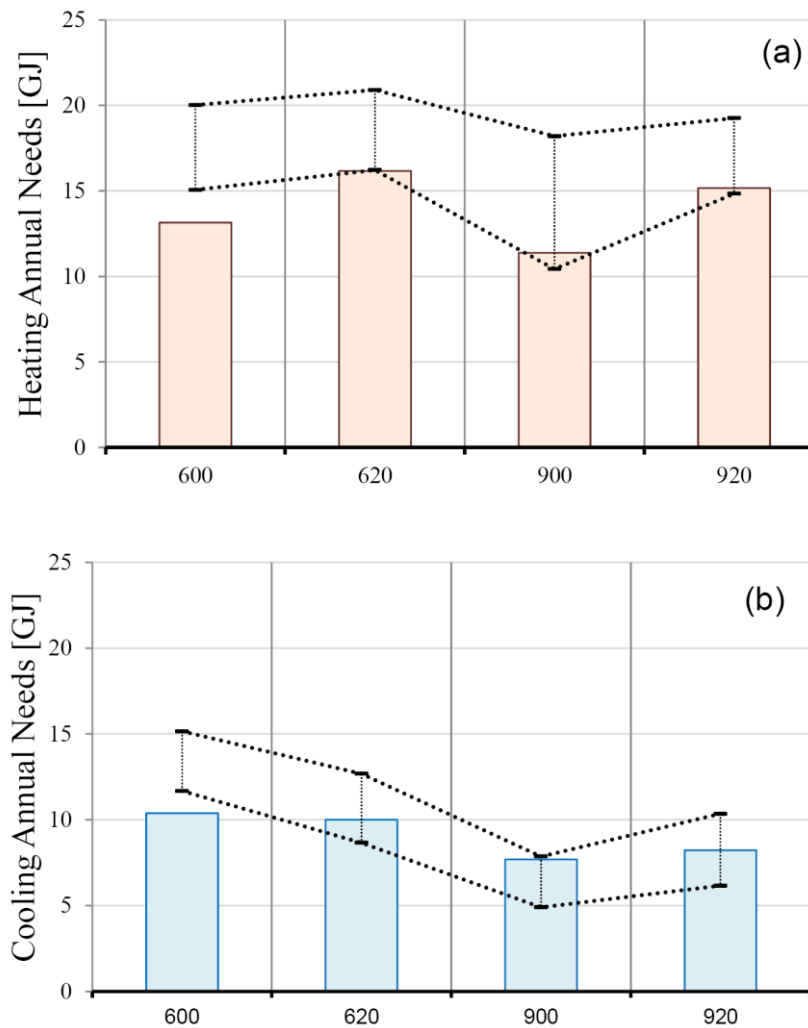


Figure 5d.1 - Quasi-steady state method with correction factor assessed with the BESTEST cases 600, 620, 900, 920 for the location of Milan: annual heating (a) and cooling (b) energy needs. The dotted lines delimitate the confidence interval

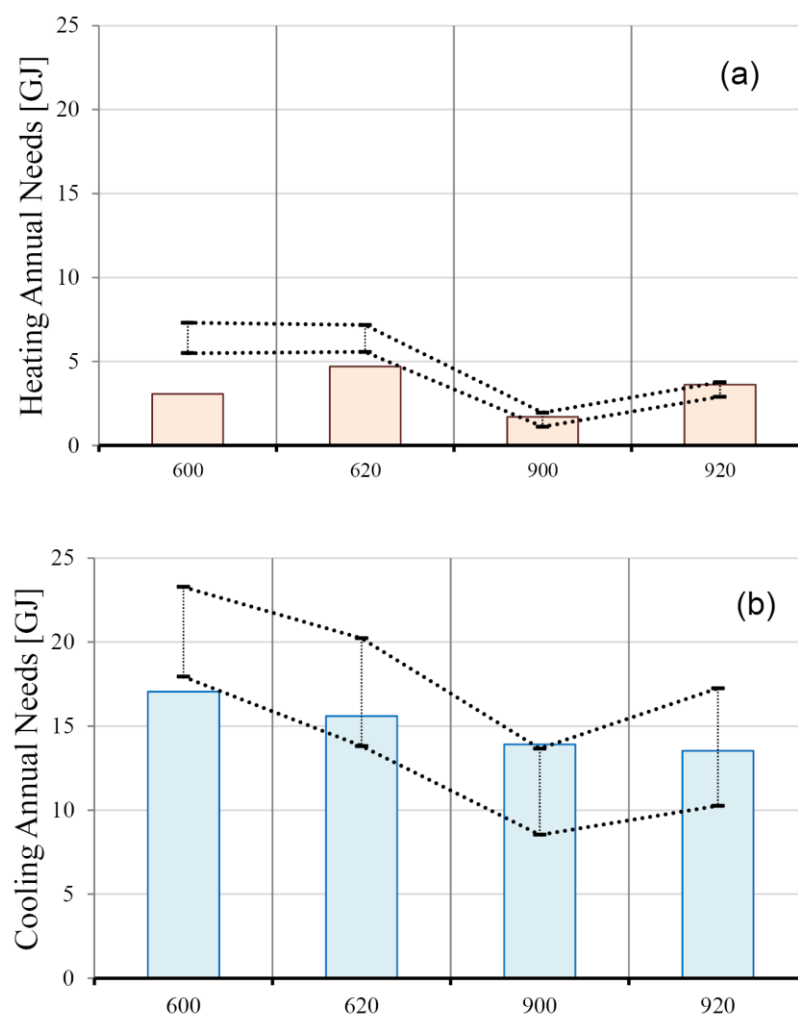


Figure 5d.2 - Quasi-steady state method with correction factor assessed with the BESTEST cases 600, 620, 900, 920 for the location of Messina: annual heating (a) and cooling (b) energy needs. The dotted lines delimitate the confidence interval

### 5d.2.2 Extensive simulation plan

The EN ISO 13790:2008 procedure has been implemented and the energy need results, both heating and cooling, have been compared with the ones provided by TRNSYS with air temperature setpoints (deadband 20 – 26 °C, for heating and cooling). The monthly heating energy needs have been compared in Figures 5d.3 and 5d.5 and the cooling ones in Figures 5d.4 and 5d.6.

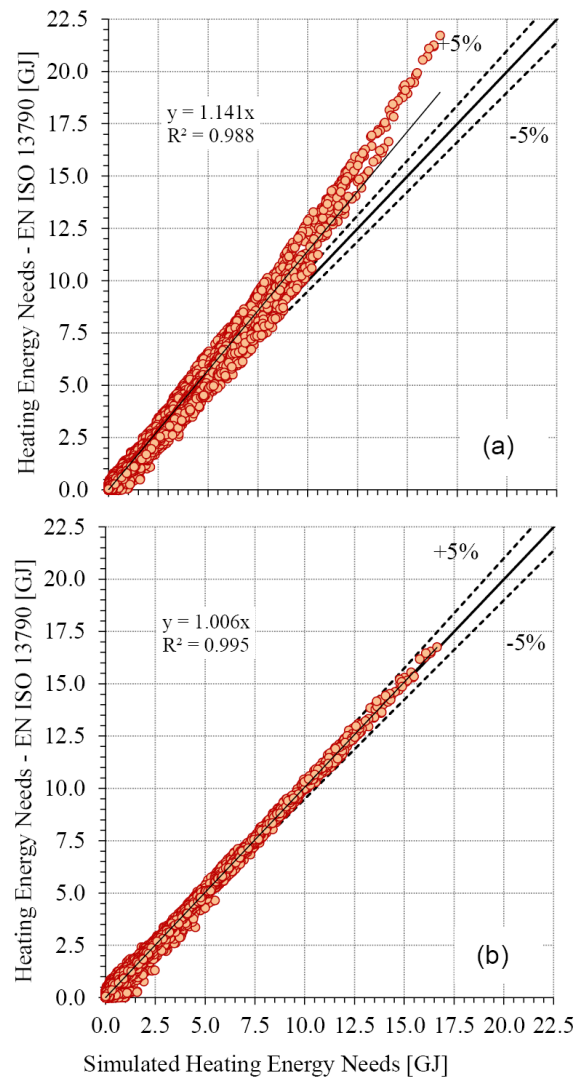
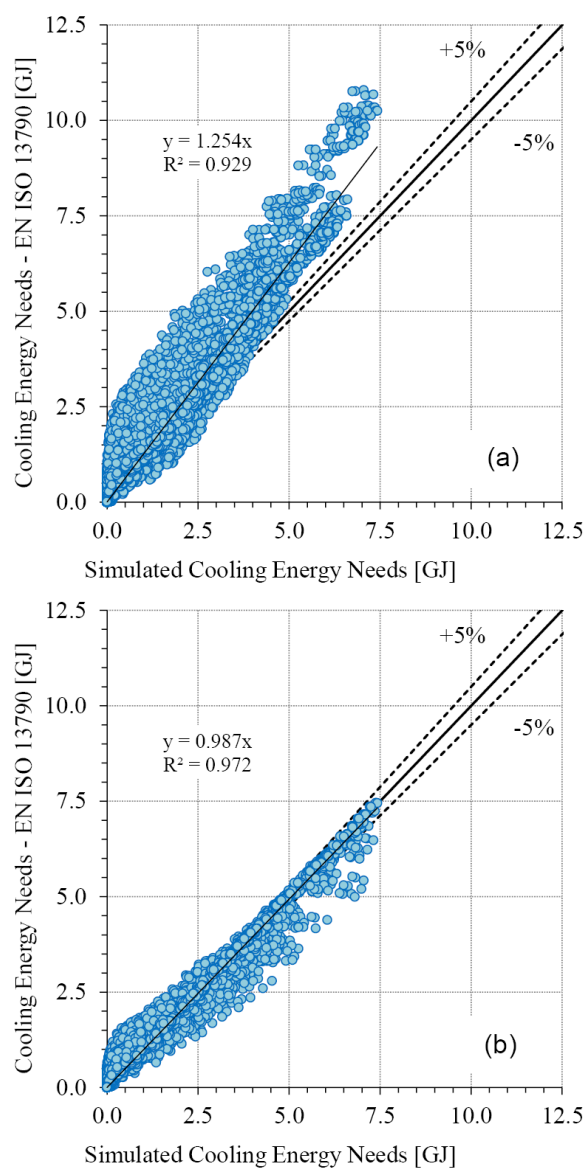


Figure 5d.3- EN ISO 13790:2008 monthly heating energy needs and TRNSYS heating energy needs considering the thermal flows according to the Standard (case a) and the corrected ones (case b)



*Figure 5d.4 - EN ISO 13790:2008 monthly cooling energy needs and TRNSYS cooling energy needs considering the thermal flows according to the Standard (case a) and the corrected ones (case b)*

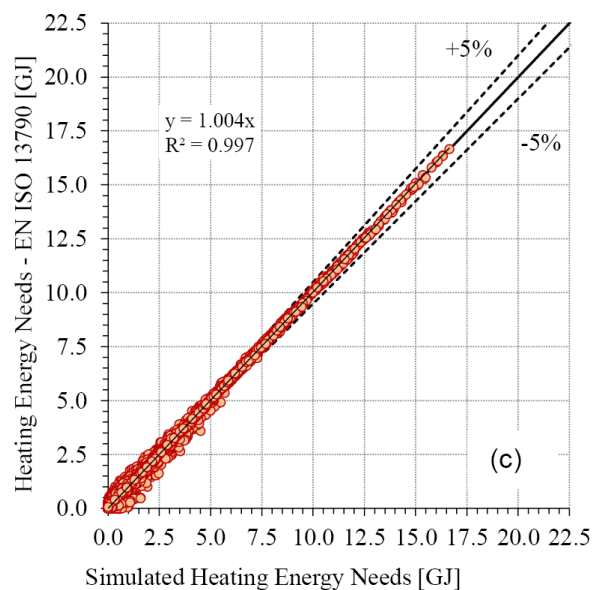


Figure 5d.5 -EN ISO 13790:2008 monthly heating energy needs and TRNSYS heating energy needs considering simulated heat gains and losses in the Standard calculation (case c)

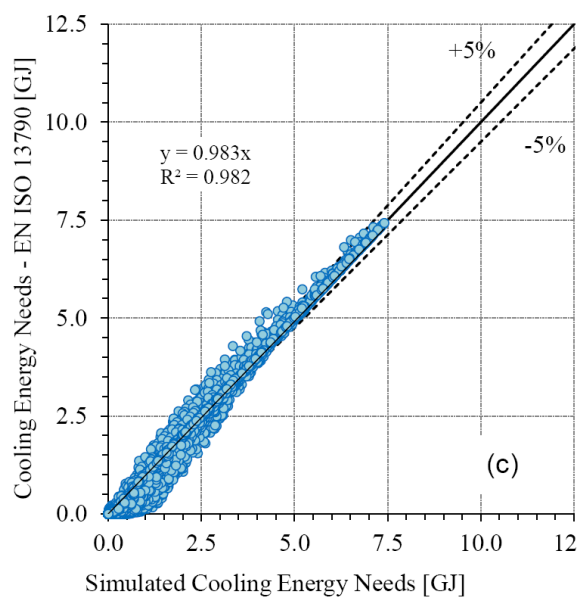


Figure 5d.6 - EN ISO 13790:2008 monthly cooling energy needs and TRNSYS cooling energy needs considering simulated heat gains and losses in the Standard calculation (case c)

### 5d.3 Discussion

After the calculation and the application of the developed correction factors to the thermal losses and gains, significant improvements have been registered in the assessment of the EN ISO 13790:2008 method with the BESTEST cases. For the annual heating energy needs there are not relevant changes but for the annual cooling energy needs the results are within or very close to the boundaries of the acceptability range.

As regards the monthly heating energy needs, without any correction to the heat losses and gains (case *a* in the Figures) there is an overestimation by the EN ISO 13790:2008 method of the 14.1%. Applying the correction coefficients elaborated in the previous paragraphs to the thermal losses and to the different components of the thermal gains (case *b*), the alignment between the simplified method and the dynamic simulation is improved and the overestimation by the first approach is reduced to 0.6%.

In case *c*, instead of the calculated thermal flows, directly the ones simulated with TRNSYS in parts *b* and *c* have been used in the quasi-steady state method. The trend remains the same with respect to the case *b* (+0.4% instead of +0.6%) but the spread of the results is reduced. This means that the residual deviations are most correlated to the inaccuracy of the correction factors and the gain utilization factor is well estimating the balance between heat losses and gains. Larger percentage discrepancies are encountered when the heating energy needs are lower than 2.5 GJ.

For the cooling energy needs, the results are similar. For what concerns the case *a*, a large overestimation is provided by using the EN ISO 13790:2008 approach with respect to the simulations. The trend is +25.4% and a large variability is encountered. For the monthly cooling energy needs the overestimation is larger than for the heating needs. Applying the correction coefficients (case *b*), the alignment between the simplified method and the dynamic simulation is improved and the discrepancy is reduced to -1.3%, even if the percentage deviations are larger than 5% for a large number of configurations.

In case *c*, the trend remains approximately the same with respect to the case *b* (-1.7%) but the spread of the results is reduced, as observed for the heating energy needs.

## **5d.4 Main findings**

In the last part of this chapter the quasi-steady state approach proposed by the technical Standard EN ISO 13790:2008 and detailed BES tools (TRNSYS in this case) have been compared.

The comparison of the monthly energy needs revealed a clear overestimation provided by the quasi-steady state approach respect to the dynamic simulation, especially for the cooling energy needs. For the monthly heating energy needs the overestimation is +14.1% while for the monthly cooling energy needs it is +25.4%.

Applying the correction factors to the thermal losses and gains, the results have been well aligned (+0.6% and -1.3% for the heating and the cooling needs, respectively). Moreover, this demonstrated that the utilization factor is well approximated by the Standard method and, in case, requires some further investigation for improving the estimation for those configurations and months with a low energy needs, both heating and cooling.

# **Chapter 6:**

# Conclusions





## Conclusions

This research work discussed both the possibilities and some issues related to the building energy simulation to characterize the building envelope energy performances. The research is focused on an extensive use of BES tools, aimed at investigating many alternatives according to the design of experiments approaches in the different topics discussed in the present work.

A first conclusion is about the methodology to manage the alternatives and to find out relationships between the different variables from a large number of results. The adopted statistical techniques have been useful in both tasks. In particular, the approach of the design of experiment has revealed a proper solution for assessment problems and it could be used also by professionals in their design activities. In many contexts, statistics is essential when using BES tools to simulate the building envelope, in particular if the final aim is to detect correlations and to develop simplified models. Nevertheless, the statistical approaches exploited in the present research basically are not comprehensive of the whole possible alternatives and other solutions can be more convenient according to the aims. For instance, in optimization analyses a partial factorial plan can be preferred because less time-consuming, especially if the higher rank interactions are known to be negligible. Whatever the context, coupling BES and statistical techniques allows to better use the simulation instruments.

### *Weather data and external conditions in BES*

As regards the weather files for BES, the TRY<sub>EN</sub> weather files have been developed in accordance with the EN ISO 15927-4:2005 procedure and compared to the original multi-year series of the data. The TRY<sub>EN</sub> monthly values for the climatic parameters (e.g., dry bulb temperature, solar radiation on horizontal surface, relative humidity) and the averages over the multi-year period are not in good agreement at the same time.

About the building energy performance results (i.e., annual heating and cooling energy needs and peak loads), estimated with the two weather file approaches, the deviations of TRY<sub>EN</sub> results from the averaged results of the multi-year series are within 10% but in some locations an overestimating/underestimating TRY<sub>EN</sub> trend can be identified. By increasing the number of years considered for the development of the TRY<sub>EN</sub>, this phenomenon is mitigated. To improve the representativeness when limited series are available, it is possible to modify the Standard procedure by introducing weighting coefficients for the different weather parameters, in order to develop different TRY<sub>EN</sub> to use for specific purposes.

The calculation method provided by the technical Standard EN ISO 13370:2007 to define the boundary temperature for walls and floors in touch with the ground, both for quasi-steady state and BES approaches, has been discussed. The Standard method has been compared to *FEM* simulations both in steady-state and dynamic conditions.

In the first ones, deviations lower than 1% have been registered. As concerns the dynamic problem, the forcing temperature period has been studied, finding that an annual-period forcing temperature should be considered in BES, as expected. Moreover, in order to evaluate accurately both flux and boundary temperature according to the EN ISO 13370:2007 method, the correct estimation of the time lag of the flux through the soil is crucial. In this case, the percentage deviation between FEM and Standard method are less than 3%.

As observed in chapter 2, the main problem in the accuracy of the proposed methods is the evaluation of the multi-dimensional heat flows and the time lag.

### ***BES validation and comparison***

The problem of the comparative validation between BES tools has been investigated, testing two well known simulation codes, TRNSYS 16.1 and EnergyPlus 7, both with the BESTEST cases and with the developed extensive comparative approach.

The monthly heating and cooling energy needs and hourly peak loads were considered, together with the hour of occurrence of the peaks. A building module composed by a single-storey thermal zone with 100 m<sup>2</sup> floor area has been used to develop a wide range of configurations, characterized by different opaque and transparent envelope compositions, expositions and windows orientations. The alignment done for the boundary conditions and the simulation hypotheses allowed to consider the relative performance of the two codes, pointing out the effects of the different algorithms and assumptions.

Beyond the comparative validation, the method can be useful when using simulation codes for particular aims, such as tuning simplified methods, doing energy diagnosis or performing calibration of the simulation.

### ***Building envelope characterization with BES***

In this part the comparison between different simulation tools has been focused on the modelling of single components of the building envelope instead of the whole thermal zone. About the dynamic behaviour of opaque components exposed to the external air, the Transfer Function Methods implemented in BES tools, in particular the Direct Root Finding in TRNSYS and the State Space in EnergyPlus, as well as an implicit finite difference scheme solution, have been assessed. The dynamic parameters proposed by the technical Standard EN ISO 13786:2007 (i.e., the periodic thermal transmittance, the time shift and the decrement factor) have been used for this purpose. Since these dynamic parameters are defined considering a sinusoidal forcing signal, the Fast Fourier Transform (*FFT*) analysis and the superposition of the effects have been used to evaluate the dynamic response of a sample of walls under more representative conditions.

The numerical methods result in agreement with the *FFT* outputs, with some small deviations for what concerns the time shift. The analysis allowed also to point out that under “real” forcing conditions, the dynamic parameters proposed by the EN ISO 13786:2007 are not representative of the actual behaviour.

In order to complete the comparison between EnergyPlus and TRNSYS, the surface temperature profiles of glazings and adiabatic surfaces have been analysed. For the peak surface temperatures, deviations of 2-4 °C between the two simulation codes are present, even if most of the cases the differences are lower than 1 °C and with a general overestimation of the surface temperatures calculated by EnergyPlus respect to TRNSYS values.

### ***BES and simplified models***

The quasi-steady state approach proposed by the technical Standard EN ISO 13790:2008 and detailed BES tools (TRNSYS in this case) have been compared. The simplified approach has been first assessed by means of the BESTEST methodology, finding that it is not within the acceptability ranges in most of the considered cases. A detailed analysis has been performed on the thermal losses and thermal gains in order to find where the two approaches differ and which are the causes.

As regards the thermal losses, the linearization of the radiative and convective heat exchanges and, consequently, the use of an operative temperature setpoint (due the modelling of the internal exchanges), are the main sources of discrepancy.

As concerns the thermal gains, the causes are different. For the entering solar radiation through the transparent envelope the quasi-steady state model assumes a black cavity hypothesis and so it completely neglects the amount of radiation reflected and dispersed through the windows, as well as the amount absorbed by the opaque components but not involved in the air heat balance because dispersed by transmission. For the internal gains, the estimation of the contribution of the radiative component is affected by a similar problem and it is partially lost by transmissions. About the thermal gains components involved in the external surface heat balance, the main problem is related to the determination of the surface heat transfer coefficient, which depends on the surface temperature that is not known in advance in the quasi-steady state methods and it is generally assumed equal to the external air temperature.

Both for the thermal losses and the thermal gains correction factors have been proposed in order to make them closer to the ones estimated by BES tools in accordance with the EN ISO 13790:2008 prescriptions.

The monthly energy needs have been finally compared, underling the overestimation by the quasi-steady state approach respect to the dynamic simulation, especially for the cooling energy needs. Applying the correction factors to the thermal losses and gains, the results have been well aligned. This demonstrated the validity of the proposed corrections and, moreover, that the utilization factor is well approximated by the Standard method and requires some further investigation for improving the estimation for those configurations and months with a low energy needs.

### ***Further developments***

For each topic developed in this research work, further developments have been considered.

As regards the study of the reference year weather files for BES, weighting factors for the weather parameters will be investigated in the construction of  $TRY_{EN}$  according to the EN ISO 15927-4:2005 procedure. The aim is to improve the representativeness of the  $TRY_{EN}$  with respect to the multi-year data series, especially when a limited number of complete years is available.

The analysis of the EN ISO 13370:2007 method for the evaluation of the heat flow through the walls and floors in thermal contact with the ground will be examined in depth by considering real annual sol-air forcing solicitations instead of the sinusoidal one and different kinds of configurations (aimed at assessing the other cases presented in the technical Standard and other aspect ratios of the floor). In this way, also the effects of the thermal bridges and the accuracy in the estimation of the external periodic heat transfer coefficient will be assessed.

The comparison between BES codes will be extended to other tools, analysing the latest release of TRNSYS (version 17) with 3-dimensional models for the distribution of the solar radiation entering through the glazings and the internal infrared exchanges. Moreover, also other widespread simulation software, such as ESP-r, could be tested. Particular attention will be paid to the internal infrared exchanges models implemented in the different BES tools and described in literature.

As regards the correction factors proposed for the thermal losses and gains evaluated according to the EN ISO 13790:2008 method, some further developments involve the assessment of the developed corrections. In particular, they are related to:

- the relationship between the surface temperature of the envelope and the correction of the thermal losses;
- the study of different distributions of the entering solar radiation and solar absorption coefficients of the opaque components for the assessment of the corrections of solar heat gains;
- the study of the correction for the internal gains in case of different ratio between the convective and the radiative parts.

In order to correlate the topic of the comparison of BES tools with the quasi-steady state method, the same thermal flows will be evaluated by means of another simulation software, such as EnergyPlus. Finally, the definition of the utilization factors, both of the thermal gains in the heating needs calculation and of the thermal losses in the cooling needs calculation, will be analysed.



# **Chapter 7:**

# Bibliography





## References

Anderson B.R., 1991. Calculation of the steady-state heat transfer through a slab-on-ground floor, *Building and Environment*, 26, 405-415.

URL: <http://www.sciencedirect.com/science/article/pii/036013239190067L>

American Society of Heating, Air-Conditioning and Refrigeration Engineers Inc (ASHRAE). 2011. *ANSI/ASHRAE Standard 140-2011 - Standard method of test for the evaluation of building energy analysis computer programs*. Atlanta, U.S.A..

Asan H. 2006. Numerical computation of time lags and decrement factors for different building materials, *Building and Environment*, 41, 615–620.

URL: <http://www.sciencedirect.com/science/article/pii/S0360132305001046>

Asan H. and Sancaktar Y.S. 1998. Effects of wall's thermophysical properties on time lag and decrement factor, *Energy and Buildings*, 28, 159–166.

URL: <http://www.sciencedirect.com/science/article/pii/S0378778898000073>

Baggio P., Corrado V., Murano G., and Riva G. 2010. Definizione degli anni tipo climatici delle province del Nord Italia. *La Termotecnica* 61 (11), 46-48.

Bradley D.E., Kummert M. and T.P. McDowell. 2004. Experiences with and interpretation of standard test methods of building energy analysis tools. *Proceedings of IBPSA-Canada Bi-Annual Conference eSIM*, Vancouver, Canada.

Claesson J., Hagentoft C.E. 1991. Heat loss to the ground from a building - I. General theory, *Building and Environment*, 26, 195-208.

URL: <http://www.sciencedirect.com/science/article/pii/0360132391900279>

Ceylan H.T. and Myers G.E. 1980. Long-time solutions to heat conduction transients with time-dependent inputs. *ASME Journal of Heat Transfer*, 102, 115–120.

Chatziangelidis K. and Bouris D. 2009. Calculation of the distribution of incoming solar radiation in enclosures. *Applied Thermal Engineering*, 29, 1096–1105.

URL: <http://www.sciencedirect.com/science/article/pii/S1359431108002585>

Ciulla G., Lo Brano V. and Orioli A. 2010. A criterion for the assessment of the reliability of ASHRAE conduction transfer function coefficients. *Energy and Buildings*, 42, 1426-1436.

URL: <http://www.sciencedirect.com/science/article/pii/S0378778810000897>

Confalonieri R., Bellocchi G., Bregaglio S. Donatelli M. and Acutis M. 2010. Comparison of sensitivity analysis techniques: A case study with the rice model WARM. *Ecological Modelling* 221, 1897–1906.

URL: <http://www.sciencedirect.com/science/article/pii/S0304380010002371>

Corrado V. and Fabrizio E. 2007. Assessment of building cooling energy need through a quasi-steady state model: Simplified correlation for gain-loss mismatch. *Energy and Buildings*, 39, 569-579. URL: <http://www.sciencedirect.com/science/article/pii/S0378778806002325>

Corrado V. and Paduos S. 2009. Prestazione Termica Dinamica dei Componenti Edilizi in Regime di Sollecitazione Dinamica: Modelli di Calcolo a Confronto (Thermal Dynamic Performance of Building Envelope Components under Dynamic Forcing Regime). *Proceedings of the 64<sup>th</sup> ATI National Congress*, L'Aquila, Italy.

Cucumo M., Kaliakatsos D. and Marinelli V. 1995. Estimating effective solar absorptance in rooms. *Energy and Buildings*, 23, 117-120.

URL: <http://www.sciencedirect.com/science/article/pii/0378778895009353>

Davies M.G., 1993. Heat loss from a solid ground floor, *Building and Environment*, 28, 405-415. URL: <http://www.sciencedirect.com/science/article/pii/0360132393900396>

Delsante A.E., 1988. Theoretical calculations of the steady-state heat losses through a slab-on-ground floor, *Building and Environment*, 23, 11-17.

URL: <http://www.sciencedirect.com/science/article/pii/0360132388900121>

Delsante A.E., 1989. Steady-state heat losses from the core and perimeter regions of a slab-on ground floor, *Building and Environment*, 24, 253-257.

URL: <http://www.sciencedirect.com/science/article/pii/0360132389900395>

Ente Nazionale Italiano di Normazione (UNI). 1994. *UNI 10349:1994 - Riscaldamento e raffrescamento degli edifici. Dati climatici (Heating and cooling of buildings. Climatic Data)*. Milan, Italy.

Ente Nazionale Italiano di Normazione (UNI). 2008. *UNI/TS 11300-1:2008 - Energy performance of buildings Part 1: Evaluation of energy need for space heating and cooling*. Milan, Italy.

Ente Nazionale Italiano di Normazione (UNI). 2012. *revUNI/TS 11300-1:2012 - Energy performance of buildings Part 1: Evaluation of energy need for space heating and cooling*. Draft. Milan, Italy.

Ente Nazionale Italiano di Normazione (UNI). 2008. *UNI/TS 11300-2:2008 - Energy performance of buildings Part 2: Evaluation of primary energy need and of system efficiencies for space heating and domestic hot water production*. Milan, Italy.

Ente Nazionale Italiano di Normazione (UNI). 2006. *UNI EN 12831:2006 - Heating systems in buildings. Method for calculation of the design heat load*. Milan, Italy.

Erbs D.G., Klein S.A. and Duffie J.A. 1982. Estimation of the diffuse radiation fraction of hourly, daily, and monthly-average global radiation. *Solar Energy*, 28, 293-302.

URL: <http://www.sciencedirect.com/science/article/pii/0038092X82903024>

European Committee for Standardization (CEN). 1998. *EN 410:1998 - Glass in building Determination of luminous and solar characteristics of glazing*. Brussels, Belgium.

European Committee for Standardization (CEN). 2007a. *EN ISO 6946:2007 - Building components and building elements. Thermal resistance and thermal transmittance. Calculation methods*. Brussels, Belgium.

European Committee for Standardization (CEN). 2007b. *EN ISO 10211:2007 - Thermal bridges in building construction - Heat flows and surface temperatures - Detailed calculations*. Brussels, Belgium.

European Committee for Standardization (CEN). 2007c. *EN ISO 13370:2007 - Thermal performance of buildings. Heat transfer via the ground. Calculation methods*. Brussels, Belgium.

European Committee for Standardization (CEN). 2007d. *EN ISO 13786:2007 Thermal performance of building components Dynamic thermal characteristics - Calculation methods*. Brussels, Belgium.

European Committee for Standardization (CEN). 2007e. *EN ISO 13789:2007 Thermal performance of buildings - Transmission and ventilation heat transfer coefficients - Calculation method (ISO 13789:2007)*. Brussels, Belgium.

European Committee for Standardization (CEN). 2008. *EN ISO 13790:2008 - Energy performance of buildings - Calculation of energy use for space heating and cooling*. Brussels, Belgium.

European Committee for Standardization (CEN). 2005. *EN ISO 13792:2005 - Thermal performance of buildings - Calculation of internal temperatures of a room in summer without mechanical cooling - Simplified methods*. Brussels, Belgium.

European Committee for Standardization (CEN). 2005. *EN ISO 15927-2:2009- Hygrothermal performance of buildings - Calculation and presentation of climatic data - Part 2: Hourly data for design cooling load*. Brussels, Belgium.

European Committee for Standardization (CEN). 2005. *EN ISO 15927-4:2005 - Hygrothermal performance of buildings - Calculation and presentation of climatic data - Part 4: Hourly data for assessing the annual energy use for heating and cooling*. Brussels, Belgium.

European Parliament and Council. 2002. *Directive 2002/91/EC on the energy performance of buildings*, Official Journal of the European Union. URL: <http://eur-lex.europa.eu/LexUriServ/LexUriServ.do?uri=OJ:L:2003:001:0065:0065:EN:PDF>

European Parliament and Council. 2010. *Directive 2010/31/EU on the energy performance of buildings (recast)*, Official Journal of the European Union. URL: <http://eur-lex.europa.eu/LexUriServ/LexUriServ.do?uri=OJ:L:2010:153:0013:0035:EN:PDF>

Fang K. T., Tang Y. and Yin J. 2008. Lower bounds of various criteria in experimental designs. *Journal of Statistical Planning and Inference* 138, 184-195.  
URL: <http://www.sciencedirect.com/science/article/pii/S037837580700208X>

Fürbringer J. M. and Roulet C. A. 1995. Comparison and combination of factorial and Monte-Carlo design in sensitivity analysis. *Building and Environment* 30(4), 505-519.  
URL: <http://www.sciencedirect.com/science/article/pii/036013239500013V>

Gansler R. A., Klein S. A. and Beckman W. A. 1994. Assessment of the accuracy of generated meteorological data for use in solar energy simulation studies. *Solar Energy* 53, 279-287.  
URL: <http://www.sciencedirect.com/science/article/pii/0038092X94906343>

Gasparella A., Pernigotto G., Cappelletti F., Romagnoni P. and Baggio P. 2011. Analysis and modelling of window and glazing systems energy performance for a well insulated residential building. *Energy and Buildings*, 43, 1030-1037.  
URL: <http://www.sciencedirect.com/science/article/pii/S0378778811000053>

Gasparella A., Pernigotto G., Baratieri M. and Baggio P. 2011b. Thermal dynamic transfer properties of the opaque envelope: Analytical and numerical tools for the assessment of the response to summer outdoor conditions. *Energy and Buildings*, 43, 2509–2517.

URL: <http://www.sciencedirect.com/science/article/pii/S0378778811002520>

Gasparella A., Cappelletti F., Pernigotto G. and Romagnoni P. 2012. Long-Term Evaluation of Internal Thermal Comfort with Different Kinds of Glazing Systems and Window Sizes: From Energetic Considerations to Users' Comfort. *ASHRAE Transactions*, 118-2.

URL: [http://www.techstreet.com/ashrae/cgi-bin/detail?product\\_id=1843649](http://www.techstreet.com/ashrae/cgi-bin/detail?product_id=1843649)

Giaconia C. and Orioli A. 2000. On the reliability of ASHRAE conduction transfer function coefficients of walls. *Applied Thermal Engineering*, 20,21–47.

URL: <http://www.sciencedirect.com/science/article/pii/S1359431199000058>

Guan L. 2009. Preparation of future weather data to study the impact of climate change on buildings. *Building and Environment*, 44(4), 793-800.

URL: <http://www.sciencedirect.com/science/article/pii/S0360132308001376>

Hagentoft C.E. 1988. Temperature under a house with variable insulation, *Building and Environment*, 23, 225-231.

URL: <http://www.sciencedirect.com/science/article/pii/0360132388900078>

Hagentoft C.E. and Claesson J., 1991. Heat loss to the ground from a building - II. Slab on the ground, *Building and Environment*, 26, 395-403.

URL: <http://www.sciencedirect.com/science/article/pii/036013239190066K>

Hagentoft C.E., 1996a. Heat losses and temperature in the ground under a building with and without ground water flow - I. Infinite ground water flow rate, *Building and Environment*, 31, 3-11.

URL: <http://www.sciencedirect.com/science/article/pii/0360132395000283>

Hagentoft C.E., 1996b. Heat losses and temperature in the ground under a building with and without ground water flow - II. Finite ground water flow rate, *Building and Environment*, 31, 13-19.

URL: <http://www.sciencedirect.com/science/article/pii/0360132395000291>

Hagentoft C.E. 2002a. Steady-state heat loss for an edge-insulated slab: Part I, *Building and Environment*, 37, 19-25.

URL: <http://www.sciencedirect.com/science/article/pii/S0360132300000925>

Hagentoft C.E. 2002b. Periodic heat loss for an edge insulated slab: Part II: A mixed boundary value problem, *Building and Environment*, 37, 27-34.

URL: <http://www.sciencedirect.com/science/article/pii/S0360132300000937>

Hall I., Prairie R., Anferson H. and Boes E. 1978. Generation of a typical meteorological year for 26 SOLMET stations. Technical Report SAND -78- 1601, Sandia Laboratories, Albuquerque, New Mexico.

Harriman L.G., Colliver D.G. and Quinn H.K. 1999. New weather data for energy calculations. *ASHRAE Journal*, 41, 31-38.

URL: [http://www.techstreet.com/ashrae/cgi-bin/detail?product\\_id=1711792](http://www.techstreet.com/ashrae/cgi-bin/detail?product_id=1711792)

Henninger R.H. and Witte M.J. 2010. Energyplus testing with building thermal envelope and fabric load tests from ANSI/ASHRAE Standard 140-2007. U.S. Department of Energy Energy Efficiency and Renewable Energy Office of Building Technologies Washington, D.C.

URL: [http://apps1.eere.energy.gov/buildings/energyplus/pdfs/energyplus\\_ashrae\\_140\\_envelope.pdf](http://apps1.eere.energy.gov/buildings/energyplus/pdfs/energyplus_ashrae_140_envelope.pdf)

Hensen J. 1999. Simulation of building energy and indoor environmental quality - some weather data issues. *Proceedings of the International Workshop on Climate data and their applications in engineering*, Prague, Czech Republic, 1-15.

URL: [http://www.bwk.tue.nl/bps/hensen/publications/99\\_climate\\_prague.pdf](http://www.bwk.tue.nl/bps/hensen/publications/99_climate_prague.pdf)

Hottel H.C. and Sarofim A.F. 2007. *Radiative Transfer*. New York, U.S.A..

Hwang R. L. and Shu S.Y. 2011. Building envelope regulations on thermal comfort in glass facade buildings and energy-saving potential for PMV-based comfort control. *Building and Environment*, 46, 824–834.

URL: <http://www.sciencedirect.com/science/article/pii/S036013231000301X>

Jensen S.O. 1995. Validation of building energy simulation programs: a methodology. *Energy and Buildings*, 22, 133-144.

URL: <http://www.sciencedirect.com/science/article/pii/037877889400910C>

Jokisalo J. and Kurnitski J. 2007. Performance of EN ISO 13790 utilisation factor heat demand calculation method in a cold climate. *Energy and Buildings*, 39, 236-247.

URL: <http://www.sciencedirect.com/science/article/pii/S0378778806001861>

Judkoff R.D. 1988. Validation of building energy analysis simulation programs at the solar energy research institute. *Energy and Buildings*, 10, 221-239.

URL: <http://www.sciencedirect.com/science/article/pii/0378778888900084>

Judkoff R.D. and Neymark J. 1995. International Energy Agency Building Energy Simulation Test (BESTEST) and Diagnostic Method. IEA SHC Task 12/IEA BCS Annex 21.

URL: <http://www.nrel.gov/docs/legosti/old/6231.pdf>

Judkoff R.D. and Neymark J. with Beausoleil-Morrison I., Ben-Nakhi A., Crowley M., Deru M., Henninger R., Ribberink H., Thornton J., Wijsman A. and Witte M. 2008. Testing and validation of building energy simulation tools. IEA SHC Task 34/IEA ECBCS Annex 43.

URL: <http://www.nrel.gov/docs/fy08osti/43388.pdf>

Judkoff R.D., Wortman D., O'Doherty B. and Burch J. 2008. A methodology for validating building energy analysis simulations. Technical Report NREL/TP-550-42059.

URL: <http://www.nrel.gov/docs/fy08osti/42059.pdf>

Kang D. H., Mo P. H., Choi D. H., Song S Y., Yeo M. S. and Kim K. W. 2010. Effect of MRT variation on the energy consumption in a PMV-controlled office. *Building and Environment*, 45, 1914–1922.

URL: <http://www.sciencedirect.com/science/article/pii/S0360132310000788>

Keeble E. 1990. Availability of UK climatic data for use in simulation. BEPAC Technical Note 1, Building Research Establishment.

Kontoleon K.J. and Bikas D.K. 2007. The effect of south wall's outdoor absorption coefficient on time lag, decrement factor and temperature variations. *Energy and Buildings*, 39,1011–1018.

URL: <http://www.sciencedirect.com/science/article/pii/S0378778806002775>

Kontoleon K.J and Eumorfopoulou E.A. 2008. The influence of wall orientation and exterior surface solar absorptivity on time lag and decrement factor in the Greek region. *Renewable Energy*, 33,1652–1664.

URL: <http://www.sciencedirect.com/science/article/pii/S0960148107002844>

Levine D. M., Krehbiel T. C., Berenson M. L. and Stephan D. F. 2012. *Business Statistics*, 6<sup>th</sup> Edition.



Lomas K.J. and Eppel H. 1992. Sensitivity analysis techniques for building thermal simulation programs. *Energy and Buildings*, 19, 21-44.

URL: <http://www.sciencedirect.com/science/article/pii/037877889290033D>

Lomas K.J., Eppel H., Martin C.J. and Bloomfield D.P. 1997. Empirical validation of building simulation programs. *Energy and Buildings*, 26, 253-275.

URL: <http://www.sciencedirect.com/science/article/pii/S0378778897000078>

Lund H. 1974. The reference year a set of climate data for environmental engineering. *Second Symposium on the use of computers for environmental engineering*, Paris, France.

Lund H. 1991. The design reference year. *Third IBPSA Conference*, Nice, France, 600-606.

URL: [http://www.ibpsa.org/proceedings/BS1991/BS91\\_600\\_606.pdf](http://www.ibpsa.org/proceedings/BS1991/BS91_600_606.pdf)

Lund H. and Eidorff S. 1980. Selection methods for a production of test reference year. Technical Report ES DK - 248-77, Technical University of Denmark, Copenhagen, Denmark.

Luo C., Moghtaderi B., Sugo H. and Page A. 2007. Time lags and decrement factors under air-conditioned and free-floating conditions for multi-layer materials. *Proceedings of the Building Simulation 2007 Conference*, Beijing, China, 95-100.

URL: [http://www.ibpsa.org/proceedings/BS2007/p098\\_final.pdf](http://www.ibpsa.org/proceedings/BS2007/p098_final.pdf)

McClellan T.M. and Pedersen C.O. 1997. Investigation of Outside Heat Balance Models for Use in a Heat Balance Cooling Load Calculation. *ASHRAE Transactions*, 103-2, 469-484.

URL: [http://www.techstreet.com/ashrae/cgi-bin/detail?product\\_id=1715994](http://www.techstreet.com/ashrae/cgi-bin/detail?product_id=1715994)

Melo A.P., Cóstola D., Lamberts R. and Hensen J.L.M. 2012. Assessing the accuracy of a simplified building energy simulation model using BESTEST: The case study of Brazilian regulation. *Energy and Buildings*, 45, 219-228.

URL: <http://www.sciencedirect.com/science/article/pii/S0378778811005470>

Mihalakakou G., Santamouris M., Asimakopoulos D. and Argiriou A. 1995. On the ground temperature below buildings. *Solar Energy*, 55, 355-362.

URL: <http://www.sciencedirect.com/science/article/pii/0038092X95000605>

Mitalas G.P. and Arseneault J.G. 1971. Fortran IV Program to calculate z-transfer functions for the calculations of transient heat transfer through walls and roofs. *NBS Building Science Series*, 39.

Moinard S. and Guyon G. 1999. Empirical Validation of EDF ETNA and GENEC test-cell models. Final Report, IEA SHC Task 22 Building Energy Analysis Tools Project A.3.

Montgomery D. C. and Runger G. C. 2003. *Applied Statistics and Probability for Engineers*, 3<sup>rd</sup> Edition.

Neymark J., Girault P., Guyon G., Judkoff R., LeBerre R., Ojalvo J. and Reimer P. 2005. The “ETNA BESTEST” empirical validation data set. *Proceedings of Building Simulation 2005*, Montréal, Canada, 839-846.

URL: [http://www.ibpsa.org/proceedings/BS2005/BS05\\_0839\\_846.pdf](http://www.ibpsa.org/proceedings/BS2005/BS05_0839_846.pdf)

Neymark J. and Judkoff R., with Beausoleil-Morrison I., Ben-Nakhi A., Crowley M., Deru M., Henninger R., Ribberink H., Thornton J., Wijsman A. and Witte M. 2009. IEA BESTEST in-depth diagnostic cases for ground coupled heat transfer related to slab-on –grade construction. *Proceedings of Building Simulation 2009*, Glasgow, Scotland, 1099-1106.

URL: [http://www.ibpsa.org/proceedings/BS2009/BS09\\_1099\\_1106.pdf](http://www.ibpsa.org/proceedings/BS2009/BS09_1099_1106.pdf)

Neymark J., Judkoff R., Knabe G., Le H.-T., Dürig M., Glass A. and Zweifel G. 2002. Applying the building energy simulation test (BESTEST) diagnostic method to verification of space conditioning equipment models used in whole-building energy simulation programs. *Energy and Buildings*, 34, 917-931.

URL: <http://www.sciencedirect.com/science/article/pii/S0378778802000725>

Oliveira Panão M.J.N., Camelo S.M.L. and Gonçalves, H.J.P. 2011. Assessment of the Portuguese building thermal code: Newly revised requirements for cooling energy needs used to prevent the overheating of buildings in the summer. *Energy*, 36, 3262-3271.

URL: <http://www.sciencedirect.com/science/article/pii/S0360544211001745>

Oliveira Panão M.J.N., Camelo S.M.L. and Gonçalves, H.J.P. 2012. Solar Load Ratio and ISO 13790 methodologies: Indirect gains from sunspaces. *Energy and Buildings*, 51, 212-222.

URL: <http://www.sciencedirect.com/science/article/pii/S0378778812002745>

Oliveti G., Arcuri N., Bruno R. and De Simone M. 2011 An accurate calculation model of solar heat gain through glazed surfaces. *Energy and Buildings*, 43, 269-274.

URL: <http://www.sciencedirect.com/science/article/pii/S0378778810004068>

Oliveti G., Arcuri N., De Simone M. and Bruno R. 2012a. Solar heat gains and operative temperature in attached sunspaces. *Renewable Energy*, 39, 241-249.

URL: <http://www.sciencedirect.com/science/article/pii/S0960148111004538>

Oliveti G., Arcuri N., De Simone M. and Bruno R. 2012b. Experimental evaluations of the building shell radiant exchange in clear sky conditions. *Solar Energy*, 86, 1785-1795.

URL: <http://www.sciencedirect.com/science/article/pii/S0038092X12001144>

Orosa J.A. and Oliveira, A.C. 2010. Implementation of a method in EN ISO 13790 for calculating the utilisation factor taking into account different permeability levels of internal coverings. *Energy and Buildings*, 42, 598-604.

URL: <http://www.sciencedirect.com/science/article/pii/S0378778809002795>

Orosa J.A. and Oliveira, A.C. 2012. A field study on building inertia and its effects on indoor thermal environment. *Renewable Energy*, 37, 89-96.

URL: <http://www.sciencedirect.com/science/article/pii/S0960148111003016>

Ouyang K. and Haghighat F. 1991. A procedure for calculating thermal response factors of multi-layered walls – state space method. *Building and Environment*, 26, 173–177.

URL: <http://www.sciencedirect.com/science/article/pii/0360132391900246>

Palomo Del Barrio E. and Guyon G. 2003. Theoretical basis for empirical model validation using parameters space analysis tools. *Energy and Buildings*, 35, 985-996.

URL: <http://www.sciencedirect.com/science/article/pii/S0378778803000380>

Palomo Del Barrio E. and Guyon G. 2004. Application of parameters space analysis tools for empirical model validation. *Energy and Buildings*, 36, 23-33.

URL: <http://www.sciencedirect.com/science/article/pii/S0378778803000392>

Perez R., Ineichen P., Seals R., Michalsky J. and Stewart P.. 1990. Modeling daylight availability and irradiance components from direct and global irradiance. *Solar Energy*, 44, 271-289. URL: <http://www.sciencedirect.com/science/article/pii/0038092X9090055H>

Pietrzyk K. 2010. Thermal Performance of a Building Envelope - A Probabilistic Approach. *Journal of Building Physics*, 34, 77-96. URL: <http://jen.sagepub.com/content/34/1/77.full.pdf+html>

Prada A. 2012. *Energy performance of buildings: modeling of dynamic summer behavior*. Ph.D. Thesis, University of Trento, Trento, Italy.

URL: [http://eprints-phd.biblio.unitn.it/770/1/Prada\\_Alessandro.pdf](http://eprints-phd.biblio.unitn.it/770/1/Prada_Alessandro.pdf)

Press W.H., Teukolsky S.A., Vetterling W.T. and Flannery B.P. 2007. Numerical recipes. In: *The Art of Scientific Computing*, 3<sup>rd</sup> edition, Cambridge University Press, Cambridge, U.K.

Rantala J. 2005. A new method to estimate the periodic temperature distribution underneath a slab-on-ground structure. *Building and Environment*, 40, 832-840.

URL: <http://www.sciencedirect.com/science/article/pii/S0360132304002537>

Seem J.E. 1987. *Modeling of Heat in Buildings*. PhD Thesis, Madison, University of Wisconsin, U.S.A.. URL: <http://minds.wisconsin.edu/handle/1793/7916>

Soleimani-Mohseni M., Thomas, B. and Fahlén P. 2006. Estimation of operative temperature in buildings using artificial neural networks. *Energy and Buildings*, 38, 635-640.

URL: <http://www.sciencedirect.com/science/article/pii/S0378778805002069>

Solar Energy Laboratory. 2005. University of Wisconsin, Madison, TRNSYS 16 Documentation.

Sorrentino G., Scaccianoce G., Morale M. and Franzitta V. 2012. The importance of reliable climatic data in the energy evaluation. *Energy* 48, 74-79.

URL: <http://www.sciencedirect.com/science/article/pii/S0360544212002952>

Struck C., de Wilde P., Evers J. E. J., Hensen J. and Plokker W. 2009. On selecting weather data sets to estimate a building design's robustness to climate variations. *Proceedings of the 11<sup>th</sup> IBPSA Building Simulation Conference*. Glasgow, U.K, 513-520. URL: [http://www.ibpsa.org/proceedings/BS2009/BS09\\_0513\\_520.pdf](http://www.ibpsa.org/proceedings/BS2009/BS09_0513_520.pdf)

Suehrcke H., Peterson E.L. and Selby N. 2008. Effect of roof solar reflectance on the building heat gain in a hot climate. *Energy and Buildings*, 40, 2224-2235.

URL: <http://www.sciencedirect.com/science/article/pii/S0378778808001485>.

Tronchin L. and Fabbri K. 2008. Energy performance building evaluation in Mediterranean countries: Comparison between software simulations and operating rating simulation. *Energy and Buildings*, 40, 1176-1187.

URL: <http://www.sciencedirect.com/science/article/pii/S0378778807002447>

Ulgen K. 2002. Experimental and theoretical investigation of effects of wall's thermophysical properties on time lag and decrement factor. *Energy and Buildings*, 34, 273-278.

URL: <http://www.sciencedirect.com/science/article/pii/S0378778801000871>

U.S. Department of Energy. 2012. EnergyPlus Documentation.

URL: <http://apps1.eere.energy.gov/buildings/energyplus/pdfs/engineeringreference.pdf>

Van der Veken J., Saelens D., Verbeeck G. and Hens H. 2004. Comparison of steady-state and dynamic building energy simulation programs. *Proceedings of the international Buildings IX ASHRAE conference on the performance of exterior envelopes of whole buildings*. Clearwater Beach, Florida, U.S.A..

URL: [http://www.techstreet.com/ashrae/cgi-bin/detail?product\\_id=1724713](http://www.techstreet.com/ashrae/cgi-bin/detail?product_id=1724713)

van Dijk H.A.L. and Arkesteijn C.A.M. 1987. Windows and space heating requirements; Parameter studies leading to a simplified calculation method. The Netherland national report on activities within step 5, TNO Institute of Applied Physics.

Yohanis Y. G. and Norton B. 1999. Utilization factor for building solar-heat gain for use in a simplified energy model. *Applied Energy*, 63, 227-239.

URL: <http://www.sciencedirect.com/science/article/pii/S030626199900032X>

Yumrutaş R., Kaşka Ö and Yildirim E. 2007. Estimation of total equivalent temperature difference values for multilayer walls and flat roofs by using periodic solution. *Building and Environment*, 42, 1878–1885.

URL: <http://www.sciencedirect.com/science/article/pii/S0360132306000667>

Walton G.N. 1983. Thermal Analysis Research Program Reference Manual. NBSSIR 83-2655. National Bureau of Standards, U.S.A..

Zhou J., Zhang G., Lin Y. and Li Y. 2008. Coupling of thermal mass and natural ventilation in buildings. *Energy and Buildings*, 40, 979-986.

URL: <http://www.sciencedirect.com/science/article/pii/S0378778807002083>

Jensen S.O. 1989. The PASSYS Project Phase 1: Subgroup Model Validation and Development : Final Report 1986-1989.

# Annexes

---

## Annex A

In this Annex, the statistical techniques considered in this work are described and their main advantages and limitations underlined, as well as the context of their application.

### A.1 *Factorial Experiment*

In a factorial experimental design, the independent variables controlled are called factors and the values they can assume, levels. The main characteristic of a factorial experiment is that experimental trials (or runs) are performed at all combinations of factor levels. This is particularly important because it allows to investigate all the possible interaction effects among the investigated factors. The factorial approach can yield more information respect to other statistical methods, such as the Monte-Carlo method, as observed by Fürbringer and Roulet (1995). Many typologies of factorial designs are present in literature, as indicated for instance by Fang *et al.* (2008) and in this chapter only the ones implemented in this research have been discussed, according to the models presented by Montgomery and Runger (2003) and Levine *et al.* (2012).

The effect of a factor (called *main effect*) is the change in response originated by a change in its level. For instance, if we want to assess the response of the numerical algorithms implemented in BES tools for the heat transfer by conduction through the opaque components, the thermal mass of the wall can be a factor and changing its value from low (e.g., timber structure) to high (e.g., concrete structure) its main effect can be assessed. In many situations, the only main effects are not able to characterize the response and also the interactions have to be taken into account. An interaction between two factors is present when the difference in response between the levels of one factor is not the same at all levels of the other factors, as can be easily seen in Figure A.1.

In this example it is possible to see that there are not interactions between the internal convective gains and the average thermal transmittance of the envelope in the simulation of the heating energy needs while an interaction between the thermal transmittance and the amount of dispersing surface is obviously present. From this representation, it is possible to detect an interaction when the two lines are not parallel, as in Figure A.1 on the right.



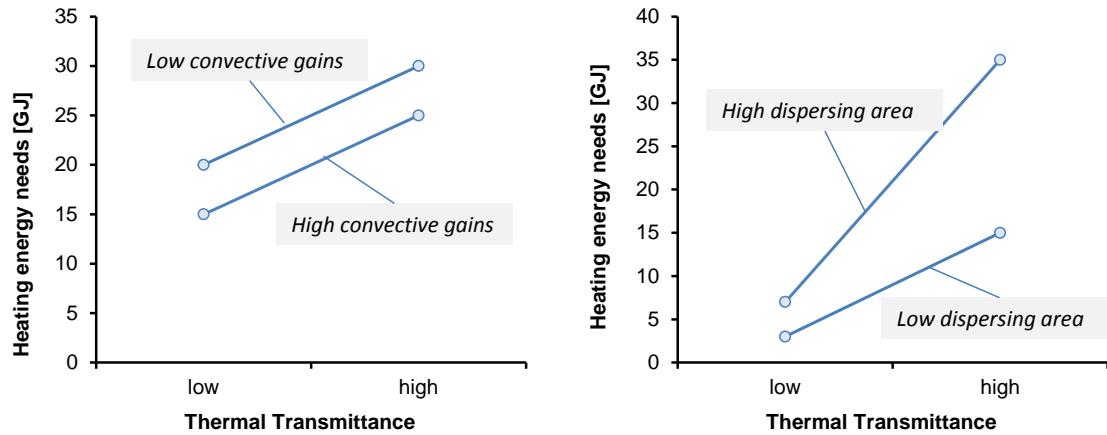


Figure A.1 – Absence of interaction between the thermal transmittance of the envelope and the convective internal gains (left) and presence of interaction between the thermal transmittance of the envelope and its dispersing area (right) for the determination of the heating energy needs by BES

The factorial experiments are the only way to detect and analyse the interactions between the assessed variables. Other techniques, such as the *one factor at a time (OFAT)*, vary one single factor and not all the factors simultaneously. In many applications, in particular for those where the interaction between the variables is relevant, the *OFAT* is not able to recognize the interactions and it is generally inefficient because it requires more experiments than a factorial approach and there is no assurance of a correct estimation (Montgomery and Runger, 2003).

### A.1.2 Fixed-Effects Model

In this research work, most of the considered variables are fixed factors (i.e., specific values have been chosen for them, without considering a probability function). In this paragraph the fixed model for 2 factors will be discussed.

Considering two fixed factors  $F_1$  and  $F_2$  with  $f_1$  and  $f_2$  levels and  $n$  replicates for each  $ij$  combination, the main effects,  $\beta_{1,i}$  and  $\beta_{2,j}$  respectively, and interaction  $(\beta_1\beta_2)_{ij}$ , are generally defined as deviations from the mean:

$$\begin{cases} \sum_{i=1}^{f_1} \beta_{1,i} = 0 \\ \sum_{j=1}^{f_2} \beta_{2,j} = 0 \\ \sum_{i=1}^{f_1} (\beta_1 \beta_2)_{ij} = 0 \\ \sum_{j=1}^{f_2} (\beta_1 \beta_2)_{ij} = 0 \end{cases} \quad (\text{A.1})$$

The total of the observations taken at the  $i^{th}$  level of  $F_1$  is indicated with  $y_{i..}$ , the total of the observations taken at the  $j^{th}$  level of  $F_2$  is  $y_{.j.}$ , the observations at the  $i^{th}$  level of  $F_1$  and the  $j^{th}$  level of  $F_2$  are  $y_{ij.}$  and  $y_{...}$  is the total of all observations.  $\bar{y}$  indicates an average.

$$y_{i..} = \sum_{j=1}^{f_2} \sum_{k=1}^n y_{ijk} \quad \bar{y}_{i..} = \frac{y_{i..}}{f_2 n} \quad i = 1 \dots f_1 \quad (\text{A.2})$$

$$y_{.j.} = \sum_{i=1}^{f_1} \sum_{k=1}^n y_{ijk} \quad \bar{y}_{.j.} = \frac{y_{.j.}}{f_1 n} \quad j = 1 \dots f_2 \quad (\text{A.3})$$

$$y_{ij.} = \sum_{k=1}^n y_{ijk} \quad \bar{y}_{ij.} = \frac{y_{ij.}}{n} \quad \begin{matrix} i = 1 \dots f_1 \\ j = 1 \dots f_2 \end{matrix} \quad (\text{A.4})$$

$$y_{...} = \sum_{i=1}^{f_1} \sum_{j=1}^{f_2} \sum_{k=1}^n y_{ijk} \quad \bar{y}_{...} = \frac{y_{...}}{f_1 f_2 n} \quad (\text{A.5})$$

Each observation  $y_{ijk}$  is run in a random order so that the plan is completely randomized. A statistical model can be defined:

$$Y_{ijk} = \mu + \beta_{1,i} + \beta_{2,j} + (\beta_1 \beta_2)_{ij} + \varepsilon_{ijk} \quad (\text{A.6})$$

Where  $\mu$  is the overall mean effect and  $\varepsilon_{ijk}$  is the random error component, whose distribution is normal with a mean equal to 0 and a variance of  $\sigma^2$ .

As often in statistics, the adopted approach is the tests of the hypotheses:

- the main effect for the factor  $F_1$ :
  - $H_0: \beta_{1,1} = \beta_{1,2} = \dots = \beta_{1,f_1} = 0$
  - $H_1$ : at least one  $\beta_{1,i} \neq 0$
- the main effect for the factor  $F_2$ :
  - $H_0: \beta_{2,1} = \beta_{2,2} = \dots = \beta_{2,f_2} = 0$
  - $H_1$ : at least one  $\beta_{2,j} \neq 0$
- the interaction between the factors:
  - $H_0: (\beta_1\beta_2)_{11} = (\beta_1\beta_2)_{12} = \dots = (\beta_1\beta_2)_{ij} = 0$
  - $H_1$ : at least one  $(\beta_1\beta_2)_{ij} \neq 0$

The assessment of these hypotheses can be done by means of the ANOVA technique which requires that the total variability is decomposed:

$$\begin{aligned} \sum_{i=1}^{f_1} \sum_{j=1}^{f_2} \sum_{k=1}^n (y_{ijk} - \bar{y}_{...})^2 &= f_2 n \sum_{i=1}^{f_1} (\bar{y}_{i.} - \bar{y}_{...})^2 + f_1 n \sum_{j=1}^{f_2} (\bar{y}_{.j} - \bar{y}_{...})^2 + \\ &+ n \sum_{i=1}^{f_1} \sum_{j=1}^{f_2} (\bar{y}_{ij.} - \bar{y}_{i.} - \bar{y}_{.j} + \bar{y}_{...})^2 + \sum_{i=1}^{f_1} \sum_{j=1}^{f_2} \sum_{k=1}^n (y_{ijk} - \bar{y}_{ij.})^2 \end{aligned} \quad (\text{A.7})$$

Or, in symbols:

$$SS_T = SS_{F_1} + SS_{F_2} + SS_{F_1 F_2} + SS_E \quad (\text{A.8})$$

The total variability can be decomposed in the part due to the factors, the part due to the interactions and the errors. The degrees of freedom can be partitioned in the following way:

$$f_1 f_2 n - 1 = (f_1 - 1) + (f_2 - 1) + (f_1 - 1)(f_2 - 1) + f_1 f_2 (n - 1) \quad (\text{A.9})$$

The mean squares can be calculated dividing each variability component by its degrees of freedom.

$$\frac{SS_T}{f_1 f_2 n - 1} = \frac{SS_{F_1}}{f_1 - 1} + \frac{SS_{F_2}}{f_2 - 1} + \frac{SS_{F_1 F_2}}{(f_1 - 1)(f_2 - 1)} + \frac{SS_E}{f_1 f_2 (n - 1)} \quad (\text{A.10})$$

$$MS_T = MS_{F_1} + MS_{F_2} + MS_{F_1 F_2} + MS_E \quad (\text{A.11})$$

Evaluating the expected values of the means squares are:

$$\begin{aligned}
 E(MS_{F_1}) &= E\left(\frac{SS_{F_1}}{f_1 - 1}\right) = \sigma^2 + \frac{f_2 n \sum_{i=1}^{f_1} \beta_{1,i}^2}{f_1 - 1} \\
 E(MS_{F_2}) &= E\left(\frac{SS_{F_2}}{f_2 - 1}\right) = \sigma^2 + \frac{f_1 n \sum_{j=1}^{f_2} \beta_{2,j}^2}{f_2 - 1} \\
 E(MS_{F_1 F_2}) &= E\left(\frac{SS_{F_1 F_2}}{(f_1 - 1)(f_2 - 1)}\right) = \sigma^2 + \frac{n \sum_{i=1}^{f_1} \sum_{j=1}^{f_2} (\beta_1 \beta_2)_{ij}^2}{(f_1 - 1)(f_2 - 1)} \\
 E(MS_E) &= E\left(\frac{SS_E}{f_1 f_2 (n - 1)}\right) = \sigma^2
 \end{aligned} \tag{A.12}$$

If the null hypotheses are true the expected values are all equal to  $\sigma^2$ . For this reason the hypotheses are tested by means of the following ratios:

$$F_0 = \frac{MS_{F_1}}{MS_E} \quad \begin{array}{l} F\text{-distribution with } (f_1 - 1) \text{ and } (f_1 f_2 (n - 1)) \\ \text{degrees of freedom} \end{array} \tag{A.13}$$

$$F_0 = \frac{MS_{F_2}}{MS_E} \quad \begin{array}{l} F\text{-distribution with } (f_2 - 1) \text{ and } (f_1 f_2 (n - 1)) \\ \text{degrees of freedom} \end{array} \tag{A.14}$$

$$F_0 = \frac{MS_{F_1 F_2}}{MS_E} \quad \begin{array}{l} F\text{-distribution with } (f_1 - 1) (f_2 - 1) \text{ and } (f_1 f_2 (n - 1)) \\ \text{degrees of freedom} \end{array} \tag{A.15}$$

Once decided the level of significance  $\alpha$ , each  $F_0$  is compared to the correspondent  $F$ -distribution value. When  $F_0$  is larger, the null hypothesis is rejected and the alternative hypothesis is assumed as true. A true null hypothesis means that a factor (or an interaction) has not influence at all while a true alternative hypothesis means that at least there is a level which is significant. When the ANOVA analysis is completed, the residuals, which are the deviations between the observations and their averages for each combination of levels of the different factors, have to be checked in order to assess the adequacy and the integrity of the model.

The discussed model has only 2 factors but it can be easily extended for a general number of factors. In that case, also the interactions between more than 2 factors have to be considered. In some cases a factor has a large number of possible levels and in order to generalize the results, its levels are randomly extracted. In this case the factor is called random factor and the resulting model random-effects model. If some factors are fixed and other not, the model is called mixed-model.

### A.1.2 $2^k$ plans

Among the factorial plan, we have some special cases involving  $k$  factors, each one with just two possible levels (e.g., low and high levels or factor present or absent). This kind of factorial plan is particularly useful for starting screening analyses, when the number of factor to test is high.

In this work, generally  $2^k$  plans have not been followed because for some variables related to the buildings geometry or thermo physical properties are difficult to describe by means of binary factors (e.g., the orientation of the windows). Anyway, they have been the basis for the development of the factorial plans considered in this research and, when possible, some variables have been connoted with high and low values (e.g., the solar heat gain coefficient) or with the absence or presence of the factor itself (e.g., the internal gains).

The simplest  $2^k$  design plan has just 2 factors and it is called  $2^2$  plan. It is generally represented with a square, whose sides represent the two factors and whose corners are the combinations of levels. The low level is indicated with a negative sign while the high level with a positive one.

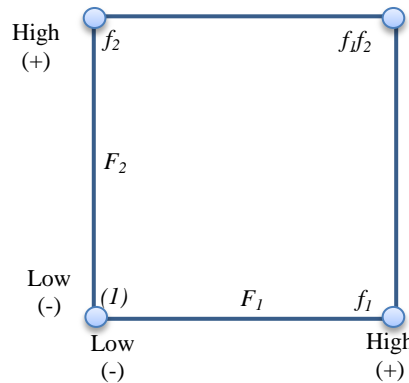


Figure A.2 -  $2^2$  Plan

In this plan, the effects can be estimated as *contrasts* (e.g., calculating the difference between the results at the high and at the low levels):

$$F_1 = \frac{1}{2n} [f_1 + f_1f_2 - f_2 - (1)] \quad (\text{A.16})$$

$$F_2 = \frac{1}{2n} [f_2 + f_1f_2 - f_1 - (1)] \quad (\text{A.17})$$

$$F_1F_2 = \frac{1}{2n} [f_1f_2 + (1) - f_1 - f_2] \quad (\text{A.18})$$

## A.2 Correlation indexes

In some cases the correlation present between two variables is investigated. The simplest index which can be used for this aim is the correlation index  $r$  by Pearson. This index is useful in particular to detect the level of linear correlation between two variables and it is defined as the covariance of the two variables divided by the product of their standard deviations:

$$r = \frac{\sum_{i=1}^n (x_i - \bar{x})(y_i - \bar{y})}{\sqrt{\sum_{i=1}^n (x_i - \bar{x})^2} \sqrt{\sum_{i=1}^n (y_i - \bar{y})^2}} \quad (\text{A.19})$$

The index can vary from -1 to +1, according to its definition. A unitary value means a perfect linear correlation between the tested variables while a null value means that there is not a linear correlation but other kind of correlations, which this index cannot detect, could be identified. Thus, a very low or null  $r$  index does not indicate that there is no correlation at all but just that, in case, it is not linear. A positive value refers to a direct linear correlation, while a negative one to an inverse linear correlation. Generally absolute values lower than 0.1 means that there is no linear correlation, between 0.1 and 0.3 that the linear correlation is small, from 0.3 to 0.5 medium and, only when larger than 0.5, strong.

The index is not considered a robust statistical indicator and so it can easily lead to misleading results in presence of outliers. As it is defined to investigate a linear correlation, the relationship between the two studied variables has to be monotonic over the investigate domain.

The main limitation of Pearson's index is the focus on the linear correlations, which are generally the first kind of correlations researched between two variables in particular in a starting screening analysis. In order to deepen the relationship among variables, other indexes have been developed, such as the rank correlation index  $\rho$  by Spearman, that belongs to the non-parametric measures of statistical dependence between variables. Like Pearson's index, Spearman's index is defined in the range between -1 and +1 and it able to assess the monotonic correlations in the studied domain but without the limitation of the linear relationship.

This index can be calculated with different types of variables (e.g., ordinal numeric or continuous numeric ones) and the main requirement is that they are ranked variables. Starting from the raw scores (i.e., the original collected data for the two considered variables),  $X_i$  and  $Y_i$ , the ranks  $x_i$  and  $y_i$  are calculated and then the index:

$$\rho = \frac{\sum_{i=1}^n (x_i - \bar{x})(y_i - \bar{y})}{\sqrt{\sum_{i=1}^n (x_i - \bar{x})^2} \sqrt{\sum_{i=1}^n (y_i - \bar{y})^2}} \quad (\text{A.20})$$

As it can be noticed, Eq. (A.20) is exactly the same as Eq. (A.19) but the ranks are considered instead of the original values. Differently from Pearson's index, Spearman's index is a robust statistical correlation index in case of outliers.

In Figure A.3 an example of the different results provided by the two correlation indexes is reported.

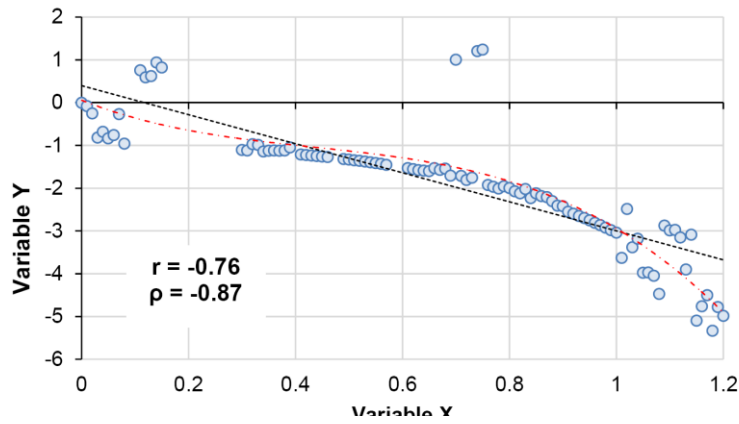


*Figure A.3 - Pearson's and Spearman's indexes*

### A.3 Multiple linear regression

The ANOVA reported in the paragraph A.1 for the analysis of the factorial experimental plans, as well as the correlation indexes described in A.2, have as main aims to identify if an effect is present (e.g., if there is at least one level of a considered factor which is statistically relevant in influencing a response variable) and if a correlation between two variables can be expressed, respectively. Even if in some particular factorial plans, the  $2^k$  plans, it is possible to easily estimate the effects by contrast, generally we have to use other techniques to estimate the entity of correlation between one of the factors and the dependent variable. In this research, the chosen statistical technique is the multiple linear regression.

This technique differs from the simple linear regression because of the number of independent variables (or regressors) considered, which are more than one both for the independent and the dependent ones. As in the simple regression model, the adjective “linear” is referred to the relationship between a regressor and a response variable and the independent one can be also a complex function far away to have a linear trend. For instance, Eq. (A.21) can be a linear regression but Eq. (1.22) not.

$$Y = \mu + \beta \ln x + \varepsilon \quad (\text{A.21})$$

$$Y = \mu + \beta^x + \varepsilon \quad (\text{A.22})$$

In many cases, anyway, even if the relationship is not linear, it is possible to properly redefine the variables; for example Eq. (A.22) can be redefine as Eq. (A.23) and the regression coefficients estimated by means of this technique.

$$Y^I = \ln Y = \mu^I + \beta^I \cdot x + \varepsilon \quad (\text{A.23})$$

The general regression model with  $k$  independent variables can be written as:

$$Y = \mu + \beta_1 \cdot x_1 + \beta_2 \cdot x_2 + \dots + \beta_k \cdot x_k + \varepsilon \quad (\text{A.24})$$

The interactions seen in A.1.2 can be included in the model. For example, if the interaction  $x_1 x_2$  is called  $x_3$ , the model in Eq. (A.25) can be rewritten as the one in Eq. (A.26).

$$Y = \mu + \beta_1 \cdot x_1 + \beta_2 \cdot x_2 + \beta_3 \cdot x_1 x_2 + \varepsilon \quad (\text{A.25})$$

$$Y = \mu + \beta_1 \cdot x_1 + \beta_2 \cdot x_2 + \beta_3 \cdot x_3 + \varepsilon \quad (\text{A.26})$$

Since the independent variables have generally different units of measurements, it is difficult to see which is the most influent and so to perform a sensitivity analysis (Confalonieri



*et al.*, 2010). For this reason, often standardized coefficients are represented, together with the common unstandardized ones. These regression coefficients are defined as the product between the unstandardized coefficient of a considered independent variable and the ratio between the standard deviation of the response variable and the one of the independent one.

### A.3.1 Least squares method

The most frequently used method to estimate the regression coefficients  $\beta_k$  is the method of least squares.  $n$  observations ( $x_{i1}, x_{i2}, \dots, x_{ik}, y_i$  with  $i=1, 2, \dots, n$ ) are required and they have to be larger than the number of the  $k$  regressors. The observations satisfy the Eq. (A.27):

$$y_i = \mu + \sum_{j=1}^k \beta_j x_{ij} + \varepsilon_i \quad (\text{A.27})$$

The least square function  $L$  is:

$$L = \sum_{i=1}^n \varepsilon_i^2 = \sum_{i=1}^n \left( y_i - \mu - \sum_{j=1}^k \beta_j x_{ij} \right)^2 \quad (\text{A.28})$$

And it has to be minimized respect to them, to obtain  $p = k+1$  equations for the estimators  $\hat{\beta}_j$  of the regression coefficients:

$$\left\{ \begin{array}{l} n\hat{\mu} + \hat{\beta}_1 \sum_{i=1}^n x_{i1} + \hat{\beta}_2 \sum_{i=1}^n x_{i2} + \dots + \hat{\beta}_k \sum_{i=1}^n x_{ik} = \sum_{i=1}^n y_i \\ \hat{\mu} \sum_{i=1}^n x_{i1} + \hat{\beta}_1 \sum_{i=1}^n x_{i1}^2 + \hat{\beta}_2 \sum_{i=1}^n x_{i1}x_{i2} + \dots + \hat{\beta}_k \sum_{i=1}^n x_{i1}x_{ik} = \sum_{i=1}^n x_{i1}y_i \\ \vdots \\ \hat{\mu} \sum_{i=1}^n x_{ik} + \hat{\beta}_1 \sum_{i=1}^n x_{i1}x_{ik} + \hat{\beta}_2 \sum_{i=1}^n x_{ik}x_{i2} + \dots + \hat{\beta}_k \sum_{i=1}^n x_{ik}^2 = \sum_{i=1}^n x_{ik}y_i \end{array} \right. \quad (\text{A.29})$$

The equations can be represented in a more compact way by means of matrixes and vectors. Eq. (A.27) becomes:

$$\mathbf{y} = \mathbf{X}\boldsymbol{\beta} + \boldsymbol{\varepsilon} \quad (\text{A.30})$$

Where:

$$\mathbf{y} = \begin{bmatrix} y_1 \\ y_2 \\ \vdots \\ y_n \end{bmatrix} \quad \mathbf{X} = \begin{bmatrix} 1 & x_{11} & \cdots & x_{1k} \\ 1 & x_{21} & \cdots & x_{2k} \\ \vdots & \vdots & & \vdots \\ 1 & x_{n1} & \cdots & x_{nk} \end{bmatrix} \quad \boldsymbol{\beta} = \begin{bmatrix} \mu \\ \beta_1 \\ \vdots \\ \beta_k \end{bmatrix} \quad \boldsymbol{\varepsilon} = \begin{bmatrix} \varepsilon_1 \\ \varepsilon_2 \\ \vdots \\ \varepsilon_n \end{bmatrix}$$

$\mathbf{y}$  is the  $(n \times 1)$  vector of the observations,  $\mathbf{X}$  the  $(n \times p)$  matrix of the levels of the independent variables,  $\boldsymbol{\beta}$  the  $(p \times 1)$  vector of regression coefficients and  $\boldsymbol{\varepsilon}$  the  $(n \times 1)$  vector of the random errors.

Eq. (A.28) can be written as:

$$L = \sum_{i=1}^n \varepsilon_i^2 = \boldsymbol{\varepsilon}' \boldsymbol{\varepsilon} = (\mathbf{y} - \mathbf{X}\boldsymbol{\beta})'(\mathbf{y} - \mathbf{X}\boldsymbol{\beta}) \quad (\text{A.31})$$

The estimators of the regression coefficients are:

$$\hat{\boldsymbol{\beta}} = (\mathbf{X}' \mathbf{X})^{-1} \mathbf{X}' \mathbf{y} \quad (\text{A.32})$$

The estimated model is:

$$\hat{\mathbf{y}} = \hat{\boldsymbol{\beta}} \mathbf{X} \quad (\text{A.33})$$

The residuals (i.e., the difference between each observation and the one estimated by means of the regression model) can also be expressed by means of a matrix notation as a  $(n \times 1)$  vector.

$$\mathbf{e} = \mathbf{y} - \hat{\mathbf{y}} \quad (\text{A.34})$$

The residuals have to be analysed to assess the adequacy of the estimated model, in particular for what concerns the hypothesis of constant variance and normal distribution.

### A.3.2 Hypotheses tests for the multiple regression model

As seen in the section A.1, a statistical test can be adopted to assess the significance of the developed model:

- $H_0: \beta_1 = \beta_2 = \dots = \beta_k = 0$
- $H_1: \text{at least one } \beta_j \neq 0$

The total variance can be decomposed into the part explained by the regressors and the part due to the errors:

$$SS_T = SS_R + SS_E \quad (\text{A.35})$$

And a statistical test  $F_0$  can be defined:

$$F_0 = \frac{\left( \frac{SS_R}{k} \right)}{\left( \frac{SS_E}{n-p} \right)} = \frac{MS_R}{MS_E} \quad (\text{A.36})$$

After choosing a level of significance  $\alpha$ ,  $F_0$  is compared to the correspondent  $F$ -distribution value. When  $F_0$  is larger, the null hypothesis is rejected and the alternative hypothesis is assumed as true (i.e., at least one regression coefficient is different from zero).

Similarly, each single regression coefficient can be tested:

- $H_0: \beta_j = 0$
- $H_1: \beta_j \neq 0$

### A.3.3 Determination coefficient and selection of the regressors

From the sums of squares, it is possible to evaluate a global statistic which assesses the fit of the model. Its name is determination coefficient  $R^2$  and its value can be between 0 and 1: when it is very low the model is not descriptive of the correlation between the variables while if it is close to 1 it is well representative and the model can also be used for forecasting aims.

$$R^2 = \frac{SS_R}{SS_T} \quad (\text{A.37})$$

If the number of regressors increases, also the determination coefficient gets higher. This could lead to include in the model also variables not related in a significant way with the response. In order to avoid misleading indications by the determination coefficients, an adjusted  $R^2$  has been defined:

$$R_{adj}^2 = 1 - \frac{\left( \frac{SS_E}{n-p} \right)}{\left( \frac{SS_T}{n-1} \right)} \quad (\text{A.38})$$

$R^2_{adj}$  increases just if a variable added to the model reduces the error mean square.

Different strategies are available to determine which regressors have to be included in the model. One of the most used is the *stepwise algorithm*, which has also been adopted in this study. According to this method, several regression models are built by adding or removing independent variables at each step. A variable is included or removed according to the variation of a partial  $F$  statistical test. The probabilities for the inclusion (alpha-to-enter) of the exclusion (alpha-to-remove) in this research have been set to 5% and 10%, respectively: if the probability of  $F$  is less or equal to 5% the variable is included and if it is larger of equal to 10% removed.

The stepwise regression starts with a model with a single independent variable, which is the one with the highest correlation with the response. At the further steps, the other variables are examined and the one with the maximum value of  $F$  is compared to the limit selected to be included.

$$F_j = \frac{SS_R(\beta_j | \beta_1, \mu)}{MS_E(x_j, x_1)} \quad (\text{A.39})$$

$MS_E$  is the error mean square for the model containing both  $x_i$  and  $x_j$ . In the same step, the variables previously added are examined to find if one of them can be removed. The  $F$  values are calculated for each variable present in the model at the  $i^{th}$  step and the one with the highest value is compared to the limit for the exclusion. The procedure finishes when no other variables can be added or removed.

In some cases there are correlations between the independent variables, such as when the interactions are assessed. Two or more regressors which are correlated should not be included in the model at the same time, in order to avoid *multicollinearity* problem: indeed, strong dependencies can affect the correct estimation of the regression coefficients. A specific statistical index has been derived for taking under control the multicollinearity problem, the *variable inflation factor VIF*.

$$VIF(\beta_j) = \frac{1}{(1 - R_j^2)} \quad (\text{A.40})$$

Where  $R_j^2$  is the determination coefficient of the regression model with  $\beta_j$  as response variable and the other  $(k-1)$  regressors as independent variables. A value larger than 10 for the

*VIF* means that there is a multicollineary problem. In some cases a limit of 5 is considered, in order to be surer to avoid the problem.

## **Annex B**

In this Annex, the graphs with the monthly average dry bulb temperature, daily solar radiation on the horizontal surface and relative humidity have been reported for the locations examined in chapter 2a (Aosta, Bergamo, Monza, Trento, Varese, De Bilt).

## Aosta

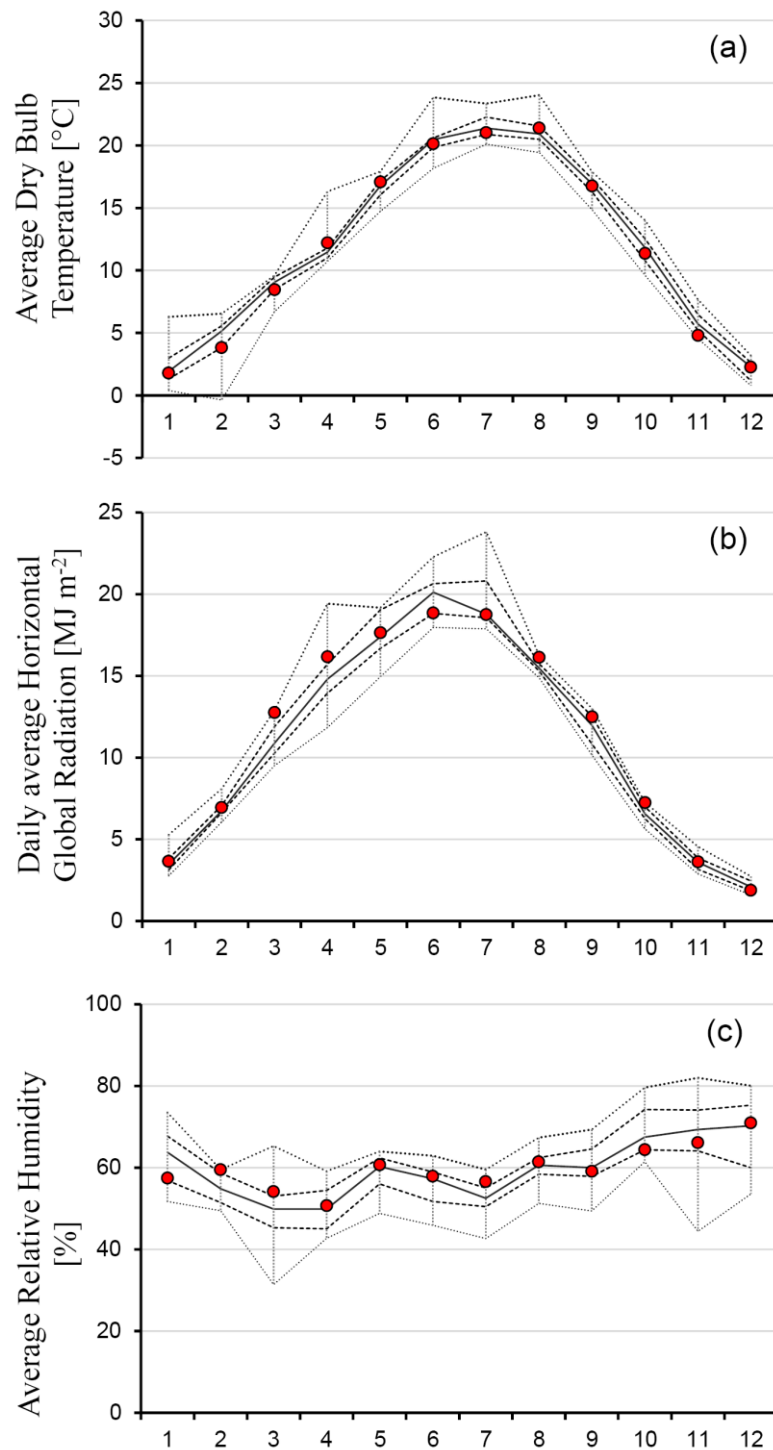


Figure B.1 - (a) Average monthly temperature (b) average daily horizontal global radiation and (c) average monthly relative humidity for Aosta. The red dots represent the  $TRY_{EN}$  monthly values, the external dotted lines represent the maximum and the minimum for the multi-year series, the internal dotted lines the first and the third quartile ( $Q_1$  and  $Q_3$ ), while the continuous line is the median

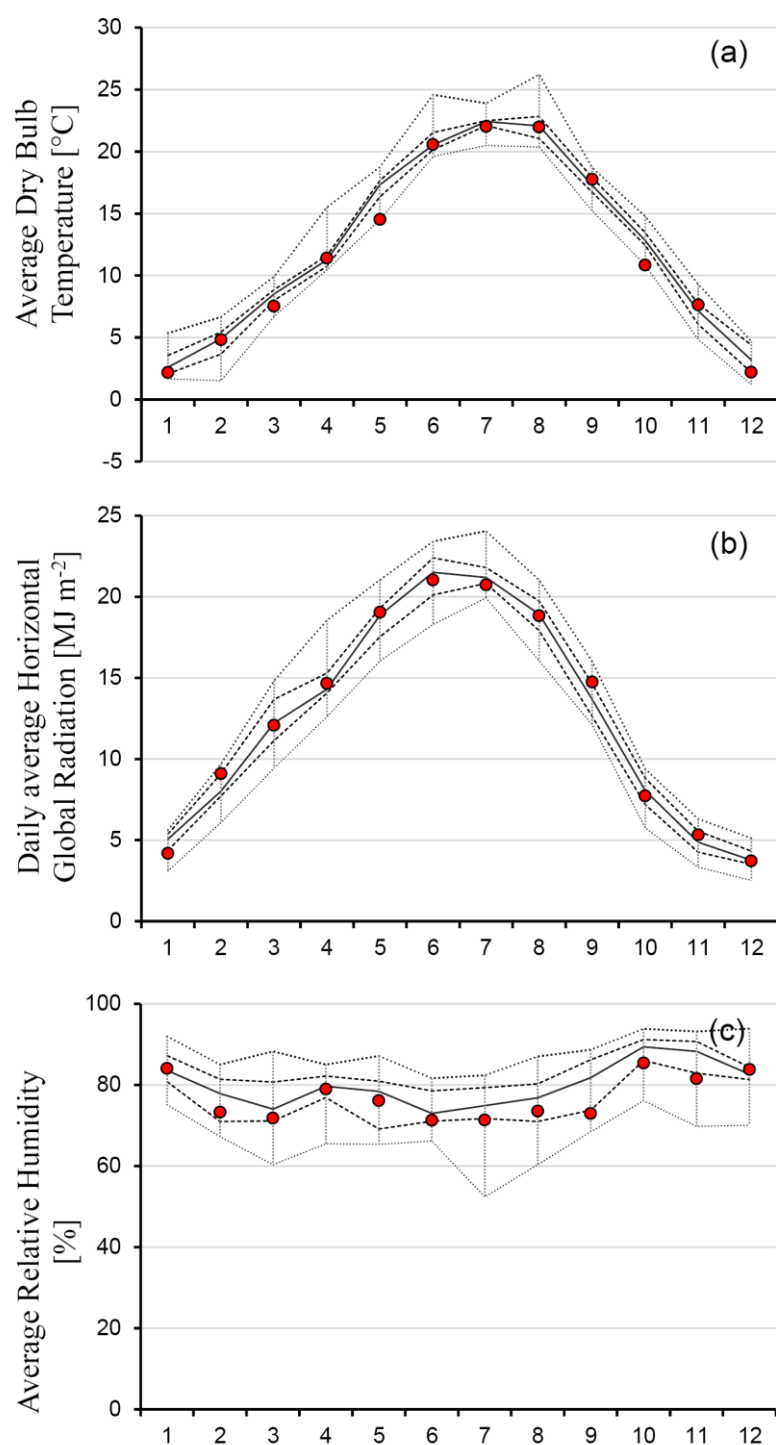
**Bergamo**

Figure B.2 - (a) Average monthly temperature (b) average daily horizontal global radiation and (c) average monthly relative humidity for Bergamo. The red dots represent the  $TRY_{EN}$  monthly values, the external dotted lines represent the maximum and the minimum for the multi-year series, the internal dotted lines the first and the third quartile ( $Q_1$  and  $Q_3$ ), while the continuous line is the median



## Monza

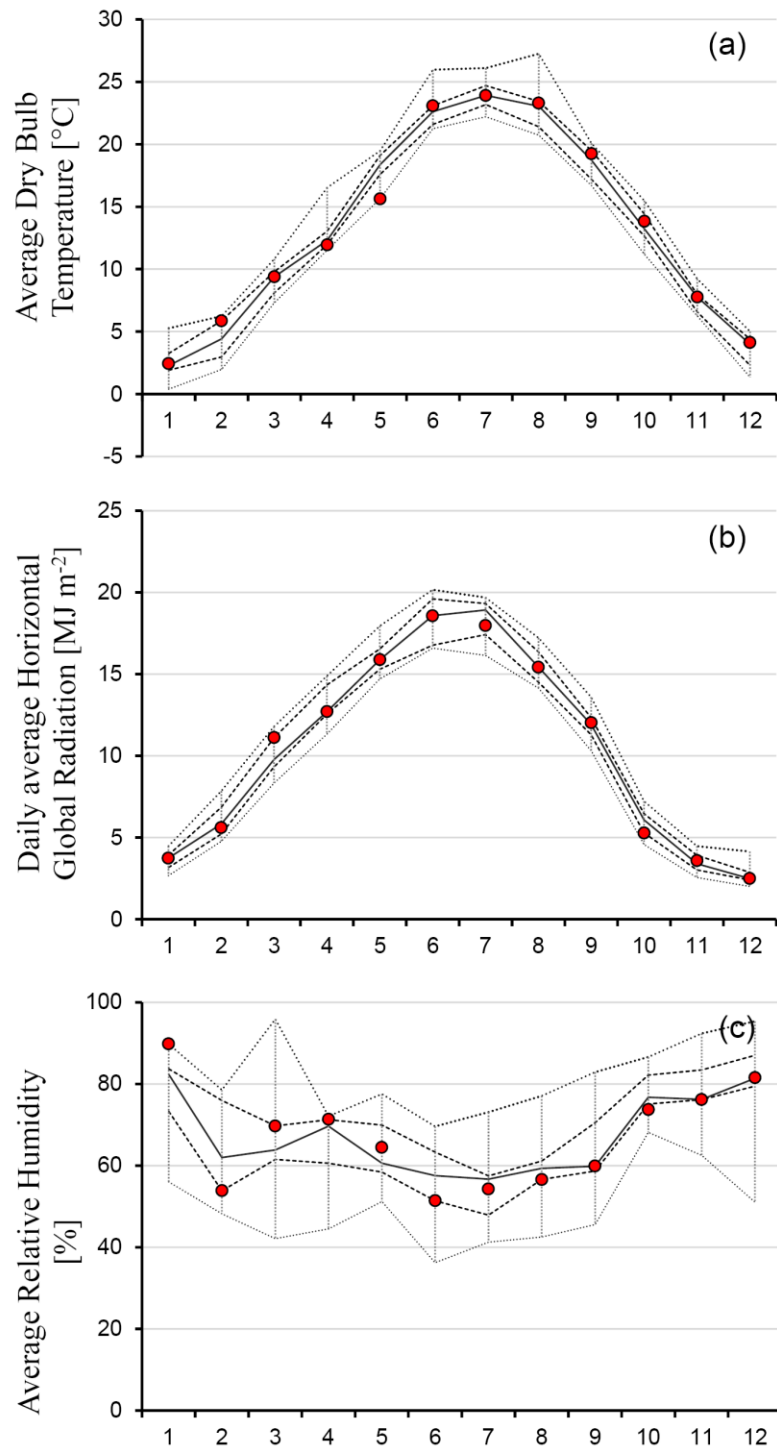


Figure B.3 - (a) Average monthly temperature (b) average daily horizontal global radiation and (c) average monthly relative humidity for Monza. The red dots represent the  $TRY_{EN}$  monthly values, the external dotted lines represent the maximum and the minimum for the multi-year series, the internal dotted lines the first and the third quartile ( $Q_1$  and  $Q_3$ ), while the continuous line is the median

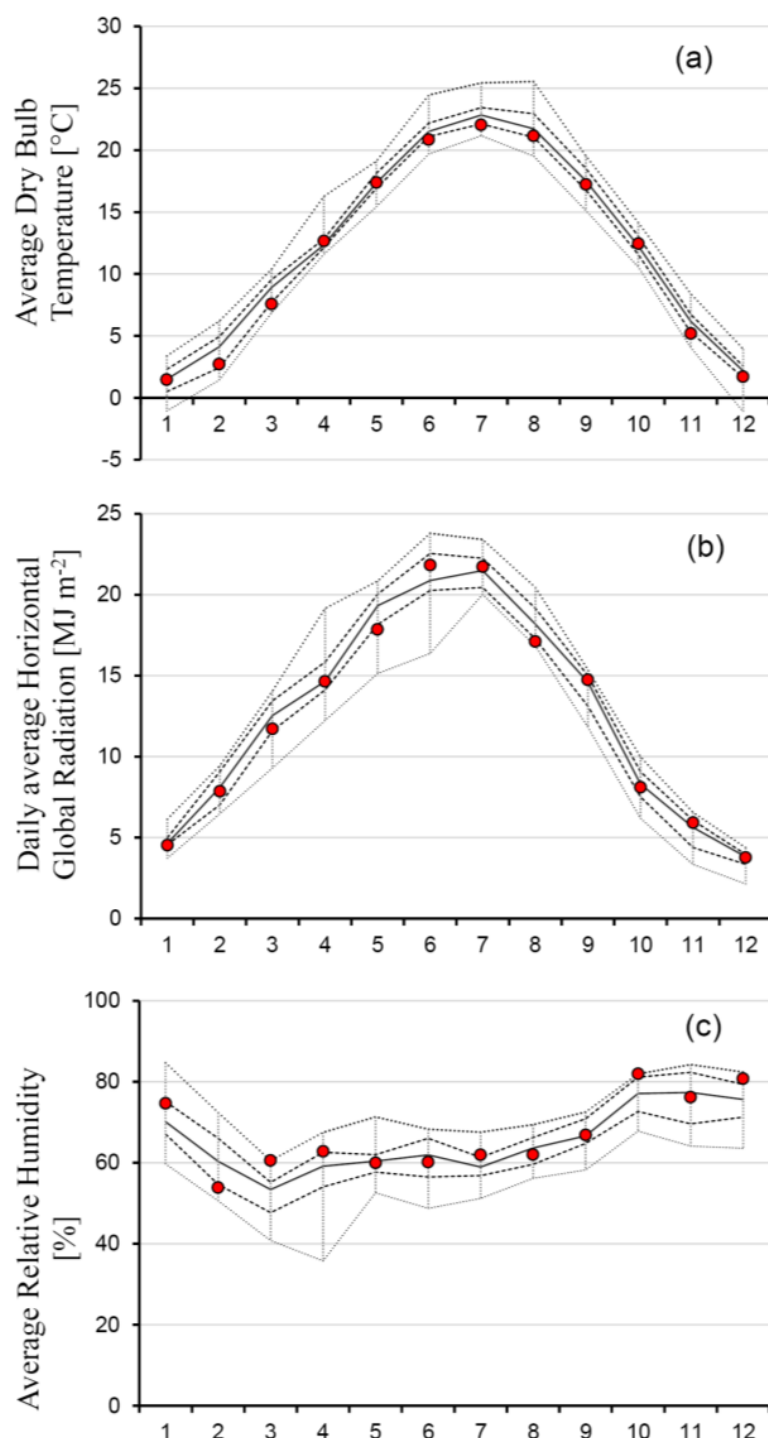
*Trento*

Figure B.4 - (a) Average monthly temperature (b) average daily horizontal global radiation and (c) average monthly relative humidity for Trento. The red dots represent the TRY<sub>EN</sub> monthly values, the external dotted lines represent the maximum and the minimum for the multi-year series, the internal dotted lines the first and the third quartile (Q<sub>1</sub> and Q<sub>3</sub>), while the continuous line is the median

**Varese**

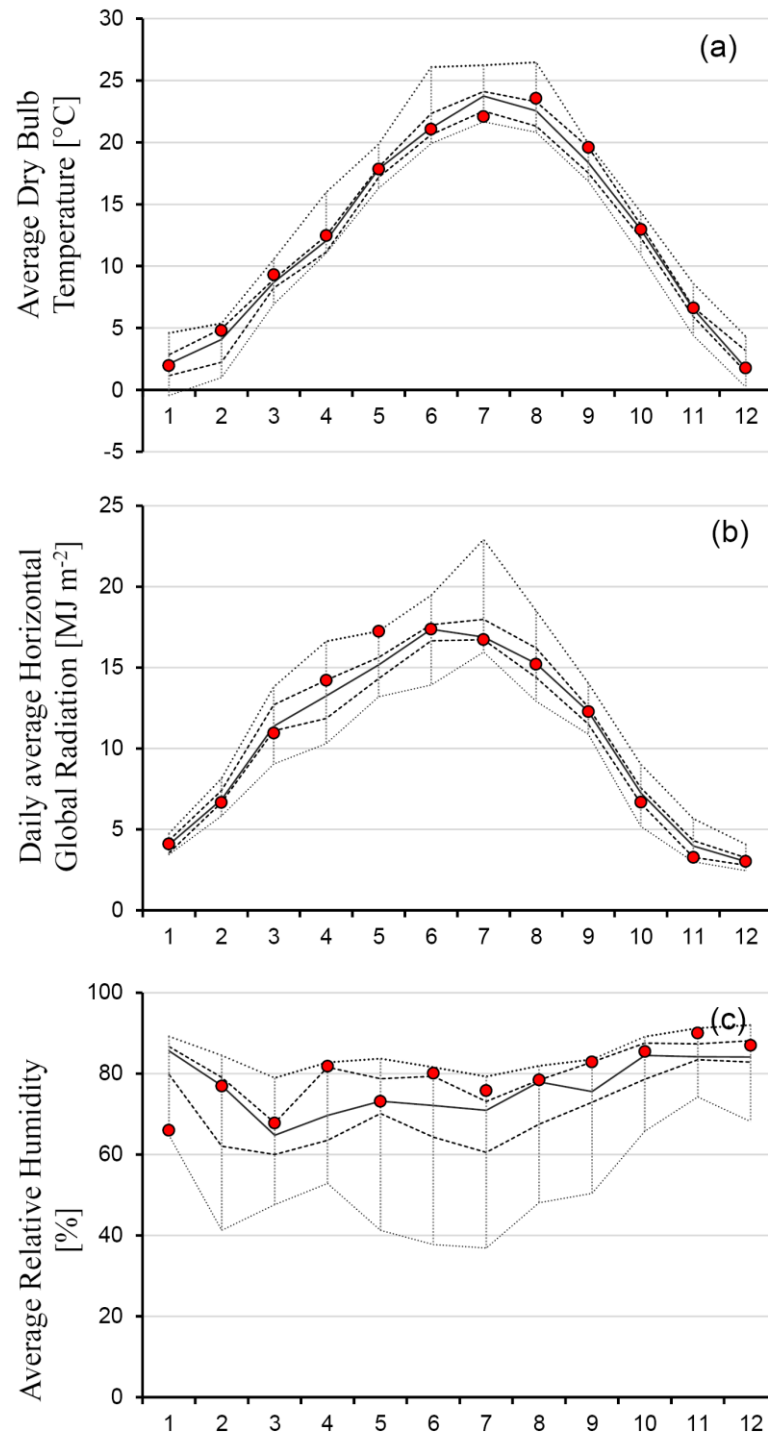


Figure B.5 - (a) Average monthly temperature (b) average daily horizontal global radiation and (c) average monthly relative humidity for Varese. The red dots represent the TRY<sub>EN</sub> monthly values, the external dotted lines represent the maximum and the minimum for the multi-year series, the internal dotted lines the first and the third quartile ( $Q_1$  and  $Q_3$ ), while the continuous line is the median

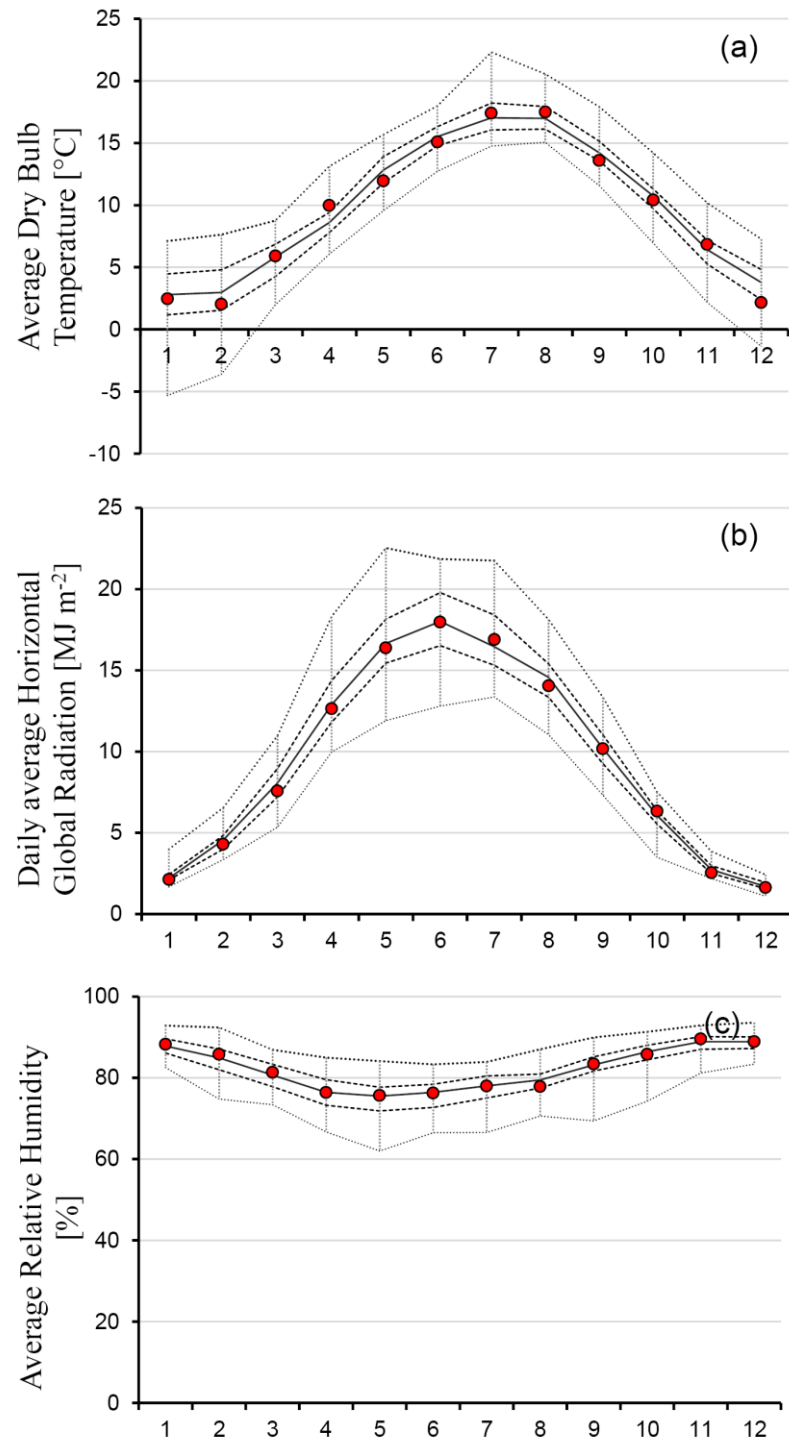
*De Bilt*

Figure B.6 - (a) Average monthly temperature (b) average daily horizontal global radiation and (c) average monthly relative humidity for De Bilt. The red dots represent the  $TRY_{EN}$  monthly values, the external dotted lines represent the maximum and the minimum for the multi-year series, the internal dotted lines the first and the third quartile ( $Q_1$  and  $Q_3$ ), while the continuous line is the median



## **Annex C**

In this Annex, the tables and the graphs with the periodic thermal transmittances and time shifts for the walls studied in chapter 4a have been reported for the locations of Milan, Rome and Palermo.

# Milan

Table C.1 - Periodic thermal transmittance according to the conventional EN ISO 13786, the FFT and the DRF approaches, with percentage differences between DRF and FFT values for the different orientations in the case of Milan. All values in  $[W m^{-2} K^{-1}]$

	EN 13786	NORTH			EAST			WEST			SOUTH			HORIZONTAL		
		FFT	DRF	$\Delta\%$	FFT	DRF	$\Delta\%$	FFT	DRF	$\Delta\%$	FFT	DRF	$\Delta\%$	FFT	DRF	$\Delta\%$
A5	<b>0.084</b>	0.086	0.085	-1.45%	0.066	0.065	-1.57%	0.070	0.069	-1.03%	0.079	0.078	-1.03%	0.086	0.085	-1.43%
A10	<b>0.045</b>	0.046	0.046	-0.45%	0.035	0.035	-0.75%	0.037	0.037	-0.05%	0.042	0.042	-0.40%	0.046	0.046	-0.18%
A15	<b>0.030</b>	0.030	0.031	2.16%	0.023	0.024	2.84%	0.025	0.025	2.78%	0.028	0.028	3.00%	0.030	0.031	1.81%
B5	<b>0.129</b>	0.133	0.133	-0.29%	0.100	0.099	-0.51%	0.109	0.109	0.09%	0.120	0.120	0.26%	0.132	0.132	-0.07%
B10	<b>0.074</b>	0.076	0.077	0.84%	0.058	0.058	0.90%	0.062	0.063	1.40%	0.069	0.070	1.51%	0.076	0.077	1.30%
B15	<b>0.050</b>	0.051	0.053	4.25%	0.039	0.040	3.43%	0.042	0.044	4.81%	0.046	0.049	4.79%	0.051	0.053	4.25%
C5	<b>0.049</b>	0.050	0.050	-0.69%	0.038	0.037	-0.89%	0.041	0.041	-0.41%	0.046	0.045	-0.62%	0.049	0.049	-0.45%
C10	<b>0.028</b>	0.028	0.028	0.63%	0.021	0.021	0.88%	0.023	0.023	1.17%	0.026	0.026	1.12%	0.028	0.028	1.26%
C15	<b>0.019</b>	0.019	0.020	4.25%	0.014	0.015	4.19%	0.015	0.016	3.82%	0.017	0.018	4.30%	0.018	0.019	4.86%
D5	<b>0.050</b>	0.050	0.050	-0.43%	0.038	0.038	-0.48%	0.041	0.041	-0.23%	0.046	0.046	-0.25%	0.050	0.050	-0.27%
D10	<b>0.028</b>	0.028	0.029	1.74%	0.021	0.021	2.01%	0.023	0.024	2.24%	0.026	0.026	2.12%	0.028	0.028	1.68%
D15	<b>0.018</b>	0.019	0.019	4.96%	0.014	0.015	5.72%	0.015	0.016	5.62%	0.017	0.018	5.86%	0.018	0.019	4.85%
M10	<b>1.126</b>	1.161	1.142	-1.67%	0.982	0.940	-4.26%	1.060	1.039	-1.96%	1.086	1.066	-1.84%	1.140	1.121	-1.63%
M20	<b>0.419</b>	0.435	0.425	-2.44%	0.317	0.311	-2.10%	0.363	0.354	-2.34%	0.391	0.383	-2.04%	0.429	0.419	-2.17%
M30	<b>0.150</b>	0.152	0.150	-1.84%	0.115	0.113	-1.73%	0.124	0.122	-1.53%	0.139	0.137	-1.49%	0.152	0.149	-1.67%

Table C.2 - Time shift (in the range -24 to 0 hours) according to the conventional EN ISO 13786, the FFT and the DRF approaches, with absolute differences between DRF and FFT values for the different orientations in the case of Milan. All values in [h]

	EN 13786	NORTH			EAST			WEST			SOUTH			HORIZONTAL		
		FFT	DRF	$\Delta$	FFT	DRF	$\Delta$	FFT	DRF	$\Delta$	FFT	DRF	$\Delta$	FFT	DRF	$\Delta$
A5	<b>-9.1</b>	-6.0	-5.0	1.0	-12.0	-11.0	1.0	-8.0	-7.0	1.0	-10.0	-9.0	1.0	-9.0	-8.0	1.0
A10	<b>-9.9</b>	-7.0	-6.0	1.0	-13.0	-12.0	1.0	-9.0	-8.0	1.0	-11.0	-10.0	1.0	-10.0	-9.0	1.0
A15	<b>-10.9</b>	-8.0	-6.0	2.0	-14.0	-12.0	2.0	-10.0	-8.0	2.0	-12.0	-10.0	2.0	-11.0	-9.0	2.0
B5	<b>-8.1</b>	-5.0	-4.0	1.0	-11.0	-10.0	1.0	-7.0	-6.0	1.0	-9.0	-8.0	1.0	-8.0	-7.0	1.0
B10	<b>-8.9</b>	-6.0	-5.0	1.0	-12.0	-11.0	1.0	-8.0	-6.0	2.0	-9.0	-8.0	1.0	-9.0	-8.0	1.0
B15	<b>-9.9</b>	-7.0	-5.0	2.0	-13.0	-11.0	2.0	-9.0	-7.0	2.0	-11.0	-9.0	2.0	-10.0	-8.0	2.0
C5	<b>-12.9</b>	-10.0	-9.0	1.0	-16.0	-15.0	1.0	-12.0	-11.0	1.0	-14.0	-13.0	1.0	-13.0	-12.0	1.0
C10	<b>-13.9</b>	-11.0	-10.0	1.0	-17.0	-16.0	1.0	-13.0	-12.0	1.0	-15.0	-14.0	1.0	-14.0	-13.0	1.0
C15	<b>-14.9</b>	-12.0	-10.0	2.0	-18.0	-16.0	2.0	-14.0	-12.0	2.0	-16.0	-14.0	2.0	-15.0	-14.0	1.0
D5	<b>-13.3</b>	-10.0	-9.0	1.0	-16.0	-15.0	1.0	-12.0	-11.0	1.0	-14.0	-13.0	1.0	-14.0	-13.0	1.0
D10	<b>-14.3</b>	-11.0	-10.0	1.0	-17.0	-16.0	1.0	-13.0	-12.0	1.0	-15.0	-14.0	1.0	-15.0	-13.0	2.0
D15	<b>-15.3</b>	-12.0	-11.0	1.0	-18.0	-17.0	1.0	-15.0	-13.0	2.0	-16.0	-15.0	1.0	-16.0	-14.0	2.0
M10	<b>-2.8</b>	-1.0	0.0	1.0	-2.0	-2.0	-	-3.0	-2.0	1.0	-3.0	-2.0	1.0	-3.0	-2.0	1.0
M20	<b>-6.8</b>	-4.0	-3.0	1.0	-9.0	-8.0	1.0	-6.0	-5.0	1.0	-7.0	-6.0	1.0	-7.0	-6.0	1.0
M30	<b>-10.7</b>	-8.0	-7.0	1.0	-14.0	-13.0	1.0	-10.0	-9.0	1.0	-11.0	-11.0	-	-11.0	-10.0	1.0

*Table C.3 - Periodic thermal transmittance according to the conventional EN ISO 13786, the FFT and the SS approaches, with percentage differences between SS and FFT values for the different orientations in the case of Milan. All values in  $[W m^{-2} K^{-1}]$*

	EN 13786	NORTH			EAST			WEST			SOUTH			HORIZONTAL		
		FFT	SS	$\Delta\%$	FFT	SS	$\Delta\%$	FFT	SS	$\Delta\%$	FFT	SS	$\Delta\%$	FFT	SS	$\Delta\%$
A5	<b>0.084</b>	0.086	0.083	-3.89%	0.066	0.064	-2.58%	0.070	0.068	-3.13%	0.079	0.078	-0.56%	0.086	0.083	-2.71%
A10	<b>0.045</b>	0.046	0.044	-4.38%	0.035	0.034	-3.41%	0.037	0.036	-3.70%	0.042	0.042	-1.10%	0.046	0.044	-4.41%
A15	<b>0.030</b>	0.030	0.029	-5.10%	0.023	0.022	-4.03%	0.025	0.024	-4.31%	0.028	0.027	-2.09%	0.030	0.029	-5.15%
B5	<b>0.129</b>	0.133	0.128	-4.37%	0.100	0.097	-2.89%	0.109	0.105	-3.39%	0.120	0.120	-0.32%	0.132	0.127	-3.85%
B10	<b>0.074</b>	0.076	0.073	-4.72%	0.058	0.056	-3.55%	0.062	0.060	-3.46%	0.069	0.068	-0.90%	0.076	0.073	-4.02%
B15	<b>0.050</b>	0.051	0.048	-5.68%	0.039	0.037	-4.30%	0.042	0.040	-4.56%	0.046	0.046	-1.57%	0.051	0.048	-5.52%
C5	<b>0.049</b>	0.050	0.047	-5.00%	0.038	0.036	-4.10%	0.041	0.039	-4.14%	0.046	0.045	-2.05%	0.049	0.047	-4.83%
C10	<b>0.028</b>	0.028	0.027	-5.49%	0.021	0.020	-4.35%	0.023	0.022	-4.59%	0.026	0.025	-1.40%	0.028	0.026	-5.25%
C15	<b>0.019</b>	0.019	0.018	-6.31%	0.014	0.014	-2.17%	0.015	0.015	-4.87%	0.017	0.016	-4.47%	0.018	0.017	-5.57%
D5	<b>0.050</b>	0.050	0.048	-5.71%	0.038	0.036	-4.37%	0.041	0.039	-4.44%	0.046	0.045	-2.38%	0.050	0.047	-5.06%
D10	<b>0.028</b>	0.028	0.026	-6.38%	0.021	0.020	-5.07%	0.023	0.022	-4.82%	0.026	0.025	-1.72%	0.028	0.026	-5.56%
D15	<b>0.018</b>	0.019	0.017	-7.97%	0.014	0.013	-2.45%	0.015	0.014	-5.26%	0.017	0.016	-4.75%	0.018	0.017	-6.00%
M10	<b>1.126</b>	1.161	1.140	-1.80%	0.982	0.961	-2.09%	1.060	1.042	-1.62%	1.086	1.098	1.17%	1.140	1.131	-0.78%
M20	<b>0.419</b>	0.435	0.406	-6.67%	0.317	0.300	-5.29%	0.363	0.339	-6.59%	0.391	0.379	-3.16%	0.429	0.406	-5.36%
M30	<b>0.150</b>	0.152	0.143	-6.30%	0.115	0.109	-5.11%	0.124	0.117	-5.52%	0.139	0.135	-3.02%	0.152	0.144	-5.34%

*Table C.4 - Time shift (in the range -24 to 0 hours) according to the conventional EN ISO 13786, the FFT and the SS approaches, with absolute differences between SS and FFT values for the different orientations in the case of Milan. All values in [h]*

	EN 13786	NORTH			EAST			WEST			SOUTH			HORIZONTAL		
		FFT	SS	$\Delta$	FFT	SS	$\Delta$	FFT	SS	$\Delta$	FFT	SS	$\Delta$	FFT	SS	$\Delta$
A5	<b>-9.1</b>	-6.0	-6.0	-	-12.0	-12.0	-	-8.0	-8.0	-	-10.0	-10.0	-	-9.0	-9.0	-
A10	<b>-9.9</b>	-7.0	-7.0	-	-13.0	-13.0	-	-9.0	-9.0	-	-11.0	-11.0	-	-10.0	-10.0	-
A15	<b>-10.9</b>	-8.0	-8.0	-	-14.0	-14.0	-	-10.0	-10.0	-	-12.0	-12.0	-	-11.0	-11.0	-
B5	<b>-8.1</b>	-5.0	-5.0	-	-11.0	-11.0	-	-7.0	-7.0	-	-9.0	-9.0	-	-8.0	-8.0	-
B10	<b>-8.9</b>	-6.0	-6.0	-	-12.0	-12.0	-	-8.0	-8.0	-	-9.0	-10.0	-1.0	-9.0	-9.0	-
B15	<b>-9.9</b>	-7.0	-7.0	-	-13.0	-13.0	-	-9.0	-9.0	-	-11.0	-11.0	-	-10.0	-10.0	-
C5	<b>-12.9</b>	-10.0	-10.0	-	-16.0	-16.0	-	-12.0	-12.0	-	-14.0	-14.0	-	-13.0	-13.0	-
C10	<b>-13.9</b>	-11.0	-11.0	-	-17.0	-17.0	-	-13.0	-13.0	-	-15.0	-15.0	-	-14.0	-14.0	-
C15	<b>-14.9</b>	-12.0	-12.0	-	-18.0	-18.0	-	-14.0	-14.0	-	-16.0	-16.0	-	-15.0	-15.0	-
D5	<b>-13.3</b>	-10.0	-10.0	-	-16.0	-16.0	-	-12.0	-12.0	-	-14.0	-14.0	-	-14.0	-14.0	-
D10	<b>-14.3</b>	-11.0	-11.0	-	-17.0	-17.0	-	-13.0	-14.0	-1.0	-15.0	-16.0	-1.0	-15.0	-15.0	-
D15	<b>-15.3</b>	-12.0	-12.0	-	-18.0	-19.0	-1.0	-15.0	-15.0	-	-16.0	-17.0	-1.0	-16.0	-16.0	-
M10	<b>-2.8</b>	-1.0	-1.0	-	-2.0	-2.0	-	-3.0	-3.0	-	-3.0	-3.0	-	-3.0	-3.0	-
M20	<b>-6.8</b>	-4.0	-4.0	-	-9.0	-9.0	-	-6.0	-6.0	-	-7.0	-7.0	-	-7.0	-7.0	-
M30	<b>-10.7</b>	-8.0	-8.0	-	-14.0	-14.0	-	-10.0	-10.0	-	-11.0	-11.0	-	-11.0	-11.0	-



*Table C.5 - Periodic thermal transmittance according to the conventional EN ISO 13786, the FFT and the FDM approaches, with percentage differences between FDM and FFT values for the different orientations in the case of Milan. All values in  $[W m^{-2} K^{-1}]$*

	EN 13786	NORTH			EAST			WEST			SOUTH			HORIZONTAL		
		FFT	FDM	$\Delta\%$	FFT	FDM	$\Delta\%$	FFT	FDM	$\Delta\%$	FFT	FDM	$\Delta\%$	FFT	FDM	$\Delta\%$
A5	<b>0.084</b>	0.086	0.083	-3.76%	0.066	0.064	-3.09%	0.070	0.068	-3.19%	0.079	0.078	-0.96%	0.086	0.082	-4.07%
A10	<b>0.045</b>	0.046	0.044	-4.31%	0.035	0.034	-4.27%	0.037	0.036	-3.57%	0.042	0.041	-1.74%	0.046	0.044	-4.72%
A15	<b>0.030</b>	0.030	0.029	-4.93%	0.023	0.022	-4.28%	0.025	0.024	-4.06%	0.028	0.027	-2.14%	0.030	0.028	-5.40%
B5	<b>0.129</b>	0.133	0.128	-3.94%	0.100	0.097	-2.39%	0.109	0.105	-3.78%	0.120	0.120	-0.44%	0.132	0.126	-4.04%
B10	<b>0.074</b>	0.076	0.073	-4.52%	0.058	0.055	-3.73%	0.062	0.059	-4.06%	0.069	0.068	-1.19%	0.076	0.072	-4.76%
B15	<b>0.050</b>	0.051	0.048	-5.12%	0.039	0.037	-4.69%	0.042	0.040	-4.62%	0.046	0.045	-2.02%	0.051	0.048	-5.44%
C5	<b>0.049</b>	0.050	0.047	-6.03%	0.038	0.036	-5.14%	0.041	0.039	-5.10%	0.046	0.044	-2.92%	0.049	0.046	-6.45%
C10	<b>0.028</b>	0.028	0.026	-6.44%	0.021	0.020	-5.73%	0.023	0.022	-5.60%	0.026	0.025	-3.45%	0.028	0.026	-6.52%
C15	<b>0.019</b>	0.019	0.017	-6.91%	0.014	0.013	-6.22%	0.015	0.014	-6.16%	0.017	0.016	-3.97%	0.018	0.017	-6.99%
D5	<b>0.050</b>	0.050	0.048	-5.16%	0.038	0.036	-4.14%	0.041	0.039	-4.31%	0.046	0.045	-2.36%	0.050	0.047	-5.81%
D10	<b>0.028</b>	0.028	0.027	-5.35%	0.021	0.020	-4.51%	0.023	0.022	-4.49%	0.026	0.025	-2.36%	0.028	0.026	-6.26%
D15	<b>0.018</b>	0.019	0.017	-5.73%	0.014	0.013	-4.89%	0.015	0.014	-5.15%	0.017	0.016	-2.81%	0.018	0.017	-6.96%
M10	<b>1.126</b>	1.161	1.138	-1.98%	0.982	0.955	-2.73%	1.060	1.029	-2.92%	1.086	1.092	0.62%	1.140	1.112	-2.39%
M20	<b>0.419</b>	0.435	0.417	-4.26%	0.317	0.309	-2.70%	0.363	0.347	-4.38%	0.391	0.389	-0.58%	0.429	0.411	-4.16%
M30	<b>0.150</b>	0.152	0.144	-5.59%	0.115	0.110	-4.00%	0.124	0.118	-4.74%	0.139	0.136	-1.67%	0.152	0.142	-6.11%

*Table C.6 - Time shift (in the range -24 to 0 hours) according to the conventional EN ISO 13786, the FFT and the FDM approaches, with absolute differences between FDM and FFT values for the different orientations in the case of Milan. All values in [h]*

	EN 13786	NORTH			EAST			WEST			SOUTH			HORIZONTAL		
		FFT	FDM	$\Delta$	FFT	FDM	$\Delta$	FFT	FDM	$\Delta$	FFT	FDM	$\Delta$	FFT	FDM	$\Delta$
A5	<b>-9.1</b>	-6.0	-6.0	-	-12.0	-12.0	-	-8.0	-8.0	-	-10.0	-10.0	-	-9.0	-9.0	-
A10	<b>-9.9</b>	-7.0	-7.0	-	-13.0	-13.0	-	-9.0	-9.0	-	-11.0	-10.0	1.0	-10.0	-10.0	-
A15	<b>-10.9</b>	-8.0	-8.0	-	-14.0	-14.0	-	-10.0	-10.0	-	-12.0	-11.0	1.0	-11.0	-11.0	-
B5	<b>-8.1</b>	-5.0	-5.0	-	-11.0	-11.0	-	-7.0	-7.0	-	-9.0	-8.0	1.0	-8.0	-8.0	-
B10	<b>-8.9</b>	-6.0	-6.0	-	-12.0	-12.0	-	-8.0	-8.0	-	-9.0	-9.0	-	-9.0	-9.0	-
B15	<b>-9.9</b>	-7.0	-7.0	-	-13.0	-13.0	-	-9.0	-9.0	-	-11.0	-10.0	1.0	-10.0	-10.0	-
C5	<b>-12.9</b>	-10.0	-10.0	-	-16.0	-16.0	-	-12.0	-12.0	-	-14.0	-14.0	-	-13.0	-13.0	-
C10	<b>-13.9</b>	-11.0	-11.0	-	-17.0	-16.0	1.0	-13.0	-13.0	-	-15.0	-15.0	-	-14.0	-14.0	-
C15	<b>-14.9</b>	-12.0	-12.0	-	-18.0	-18.0	-	-14.0	-14.0	-	-16.0	-16.0	-	-15.0	-15.0	-
D5	<b>-13.3</b>	-10.0	-10.0	-	-16.0	-16.0	-	-12.0	-12.0	-	-14.0	-14.0	-	-14.0	-13.0	1.0
D10	<b>-14.3</b>	-11.0	-11.0	-	-17.0	-17.0	-	-13.0	-13.0	-	-15.0	-15.0	-	-15.0	-14.0	1.0
D15	<b>-15.3</b>	-12.0	-12.0	-	-18.0	-18.0	-	-15.0	-14.0	1.0	-16.0	-16.0	-	-16.0	-15.0	1.0
M10	<b>-2.8</b>	-1.0	-1.0	-	-2.0	-2.0	-	-3.0	-3.0	-	-3.0	-3.0	-	-3.0	-3.0	-
M20	<b>-6.8</b>	-4.0	-4.0	-	-9.0	-9.0	-	-6.0	-6.0	-	-7.0	-7.0	-	-7.0	-7.0	-
M30	<b>-10.7</b>	-8.0	-8.0	-	-14.0	-13.0	1.0	-10.0	-9.0	1.0	-11.0	-11.0	-	-11.0	-11.0	-

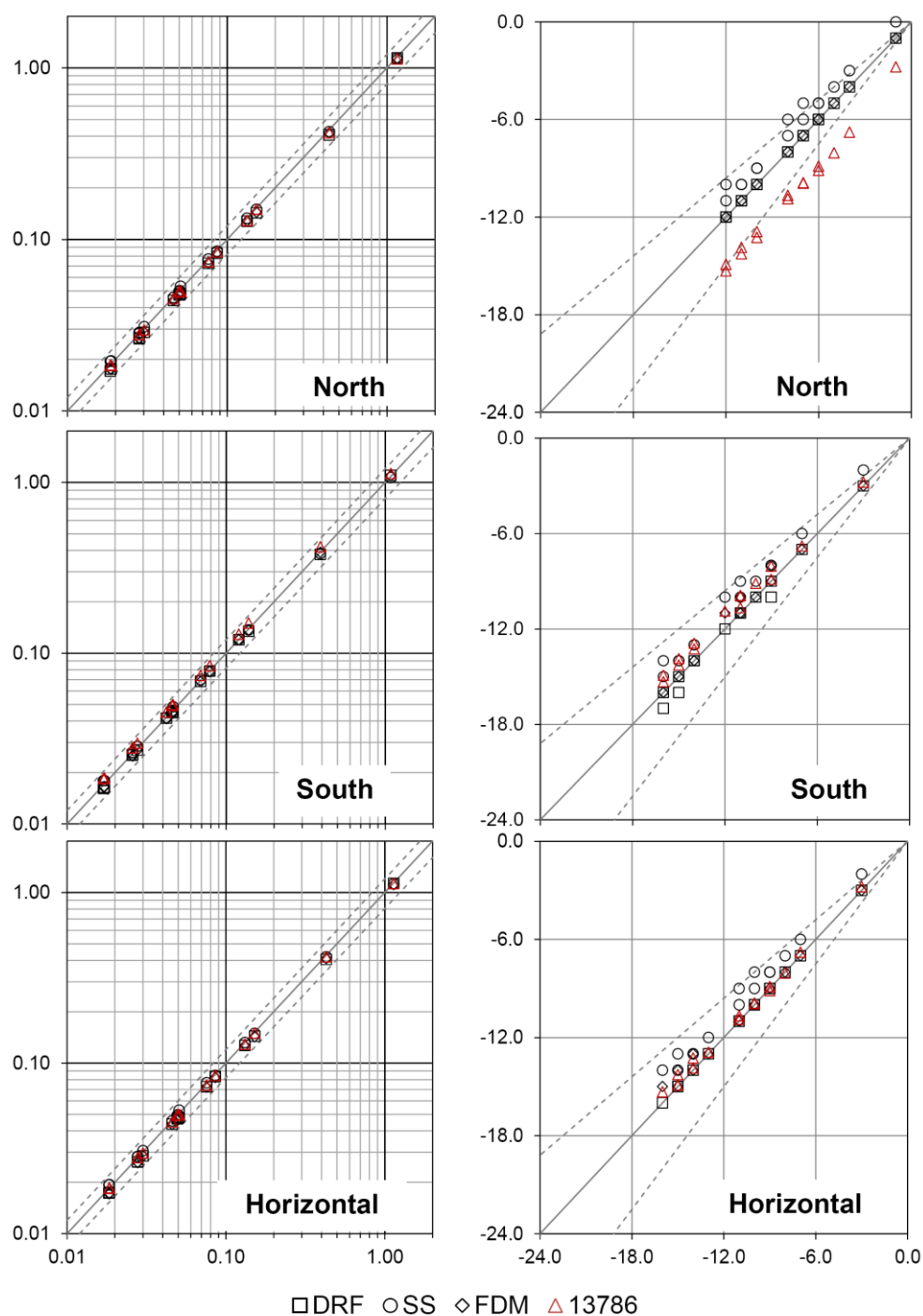


Figure C.1 - Periodic thermal transmittances in  $[W m^{-2} K^{-1}]$  (left) and time shifts in  $[h]$  (right) for the conditions of Milan for the South, North and Horizontal walls respect to the reference FFT parameters. Dotted lines represent the  $\pm 20\%$  range

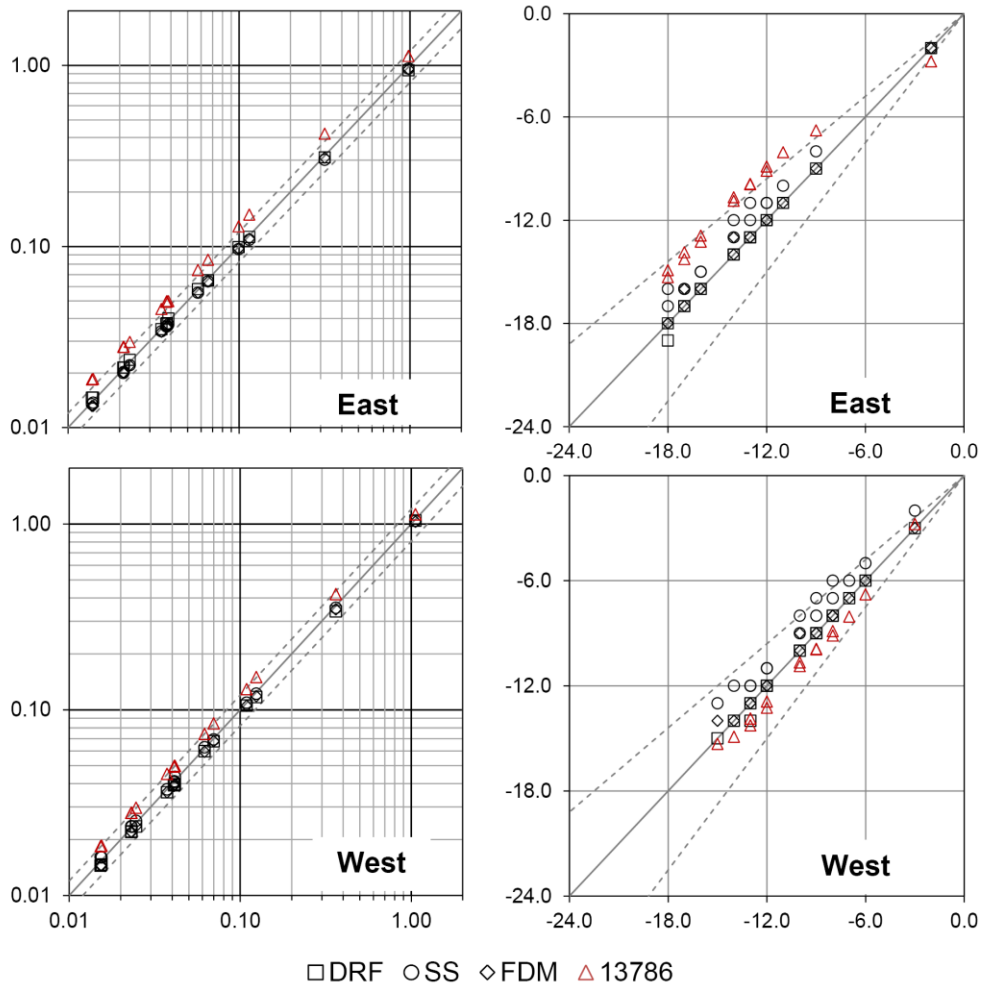


Figure C.2 - Periodic thermal transmittances in  $[W m^{-2} K^{-1}]$  (left) and time shifts in  $[h]$  (right) for the conditions of Milan for the East and West-oriented walls respect to the reference FFT parameters. Dotted lines represent the  $\pm 20\%$  range

**Rome**

*Table C.7 - Periodic thermal transmittance according to the conventional EN ISO 13786, the FFT and the DRF approaches, with percentage differences between DRF and FFT values for the different orientations in the case of Rome. All values in  $[W m^{-2} K^{-1}]$*

	EN 13786	NORTH			EAST			WEST			SOUTH			HORIZONTAL		
		FFT	DRF	$\Delta\%$	FFT	DRF	$\Delta\%$	FFT	DRF	$\Delta\%$	FFT	DRF	$\Delta\%$	FFT	DRF	$\Delta\%$
A5	<b>0.084</b>	0.085	0.083	-1.77%	0.060	0.058	-3.73%	0.066	0.065	-1.81%	0.076	0.075	-2.17%	0.085	0.082	-2.81%
A10	<b>0.045</b>	0.045	0.045	-1.07%	0.032	0.030	-4.93%	0.035	0.035	-0.96%	0.041	0.040	-1.19%	0.045	0.044	-2.29%
A15	<b>0.030</b>	0.030	0.031	4.59%	0.021	0.020	-5.53%	0.023	0.024	3.56%	0.027	0.027	0.71%	0.030	0.030	0.24%
B5	<b>0.129</b>	0.131	0.132	0.15%	0.091	0.088	-2.89%	0.104	0.104	-0.52%	0.118	0.117	-0.25%	0.130	0.130	-0.73%
B10	<b>0.074</b>	0.075	0.076	1.72%	0.052	0.050	-3.47%	0.059	0.060	1.46%	0.067	0.068	0.62%	0.075	0.075	0.59%
B15	<b>0.050</b>	0.050	0.053	5.00%	0.035	0.033	-4.41%	0.039	0.041	4.85%	0.045	0.047	4.61%	0.050	0.052	3.53%
C5	<b>0.049</b>	0.049	0.050	3.66%	0.034	0.034	-0.52%	0.039	0.040	3.20%	0.044	0.045	3.18%	0.048	0.050	3.82%
C10	<b>0.028</b>	0.027	0.029	7.07%	0.019	0.019	0.15%	0.022	0.023	6.05%	0.025	0.026	6.11%	0.027	0.029	7.81%
C15	<b>0.019</b>	0.018	0.020	11.06%	0.013	0.013	0.26%	0.015	0.016	10.25%	0.016	0.018	10.29%	0.018	0.020	12.41%
D5	<b>0.050</b>	0.049	0.051	3.53%	0.034	0.034	-1.28%	0.039	0.040	3.24%	0.045	0.046	2.69%	0.049	0.051	4.03%
D10	<b>0.028</b>	0.027	0.029	6.57%	0.019	0.019	-0.75%	0.022	0.023	6.29%	0.025	0.026	5.79%	0.027	0.029	7.31%
D15	<b>0.018</b>	0.018	0.020	11.45%	0.013	0.012	-1.12%	0.015	0.016	10.15%	0.016	0.018	10.18%	0.018	0.020	12.59%
M10	<b>1.126</b>	1.140	1.130	-0.83%	0.965	0.947	-1.81%	1.038	1.007	-2.99%	1.080	1.058	-2.06%	1.126	1.107	-1.68%
M20	<b>0.419</b>	0.429	0.421	-1.98%	0.296	0.279	-5.47%	0.351	0.338	-3.59%	0.384	0.375	-2.32%	0.425	0.412	-2.91%
M30	<b>0.150</b>	0.150	0.149	-0.77%	0.104	0.119	13.90%	0.117	0.117	-0.51%	0.135	0.132	-2.48%	0.149	0.145	-2.96%

*Table C.8 - Time shift (in the range -24 to 0 hours) according to the conventional EN ISO 13786, the FFT and the DRF approaches, with absolute differences between DRF and FFT values for the different orientations in the case of Rome. All values in [h]*

	EN 13786	NORTH			EAST			WEST			SOUTH			HORIZONTAL		
		FFT	DRF	$\Delta$	FFT	DRF	$\Delta$	FFT	DRF	$\Delta$	FFT	DRF	$\Delta$	FFT	DRF	$\Delta$
A5	<b>-9.1</b>	-6.0	-5.0	1.0	-11.0	-10.0	1.0	-7.0	-7.0	-	-9.0	-8.0	1.0	-9.0	-8.0	1.0
A10	<b>-9.9</b>	-6.0	-5.0	1.0	-12.0	-11.0	1.0	-8.0	-7.0	1.0	-10.0	-9.0	1.0	-9.0	-8.0	1.0
A15	<b>-10.9</b>	-8.0	-7.0	1.0	-13.0	-11.0	2.0	-9.0	-9.0	-	-11.0	-10.0	1.0	-10.0	-9.0	1.0
B5	<b>-8.1</b>	-5.0	-4.0	1.0	-9.0	-8.0	1.0	-6.0	-5.0	1.0	-8.0	-7.0	1.0	-8.0	-7.0	1.0
B10	<b>-8.9</b>	-5.0	-4.0	1.0	-10.0	-9.0	1.0	-7.0	-6.0	1.0	-9.0	-8.0	1.0	-8.0	-7.0	1.0
B15	<b>-9.9</b>	-6.0	-5.0	1.0	-12.0	-10.0	2.0	-8.0	-7.0	1.0	-10.0	-8.0	2.0	-9.0	-8.0	1.0
C5	<b>-12.9</b>	-10.0	-8.0	2.0	-15.0	-15.0	-	-12.0	-11.0	1.0	-13.0	-12.0	1.0	-13.0	-12.0	1.0
C10	<b>-13.9</b>	-11.0	-9.0	2.0	-16.0	-15.0	1.0	-13.0	-11.0	2.0	-14.0	-13.0	1.0	-14.0	-12.0	2.0
C15	<b>-14.9</b>	-12.0	-10.0	2.0	-17.0	-15.0	2.0	-14.0	-12.0	2.0	-16.0	-14.0	2.0	-15.0	-13.0	2.0
D5	<b>-13.3</b>	-10.0	-9.0	1.0	-15.0	-15.0	-	-12.0	-11.0	1.0	-14.0	-13.0	1.0	-13.0	-12.0	1.0
D10	<b>-14.3</b>	-11.0	-9.0	2.0	-17.0	-15.0	2.0	-13.0	-12.0	1.0	-15.0	-13.0	2.0	-14.0	-13.0	1.0
D15	<b>-15.3</b>	-12.0	-10.0	2.0	-18.0	-16.0	2.0	-14.0	-12.0	2.0	-16.0	-14.0	2.0	-15.0	-13.0	2.0
M10	<b>-2.8</b>	-1.0	0.0	1.0	-2.0	-1.0	1.0	-2.0	-1.0	1.0	-2.0	-2.0	-	-3.0	-2.0	1.0
M20	<b>-6.8</b>	-4.0	-3.0	1.0	-6.0	-6.0	-	-5.0	-4.0	1.0	-6.0	-6.0	-	-6.0	-6.0	-
M30	<b>-10.7</b>	-7.0	-7.0	-	-12.0	-12.0	-	-9.0	-9.0	-	-11.0	-10.0	1.0	-10.0	-9.0	1.0

*Table C.9 - Periodic thermal transmittance according to the conventional EN ISO 13786, the FFT and the SS approaches, with percentage differences between SS and FFT values for the different orientations in the case of Rome. All values in  $[W m^{-2} K^{-1}]$*

	EN 13786	NORTH			EAST			WEST			SOUTH			HORIZONTAL		
		FFT	SS	$\Delta\%$	FFT	SS	$\Delta\%$	FFT	SS	$\Delta\%$	FFT	SS	$\Delta\%$	FFT	SS	$\Delta\%$
A5	<b>0.084</b>	0.085	0.081	-4.32%	0.060	0.058	-2.52%	0.066	0.064	-4.00%	0.076	0.076	-1.01%	0.085	0.080	-5.93%
A10	<b>0.045</b>	0.045	0.045	-1.48%	0.032	0.031	-1.80%	0.035	0.035	-1.36%	0.041	0.040	-2.11%	0.045	0.042	-6.61%
A15	<b>0.030</b>	0.030	0.029	-1.79%	0.021	0.021	1.29%	0.023	0.023	-0.62%	0.027	0.027	1.05%	0.030	0.028	-3.94%
B5	<b>0.129</b>	0.131	0.127	-3.61%	0.091	0.090	-0.78%	0.104	0.100	-3.93%	0.118	0.117	-0.26%	0.130	0.125	-4.51%
B10	<b>0.074</b>	0.075	0.072	-4.64%	0.052	0.052	0.44%	0.059	0.057	-4.65%	0.067	0.067	-0.71%	0.075	0.071	-5.07%
B15	<b>0.050</b>	0.050	0.049	-3.35%	0.035	0.036	3.74%	0.039	0.038	-3.03%	0.045	0.044	-1.76%	0.050	0.047	-6.21%
C5	<b>0.049</b>	0.049	0.048	-1.11%	0.034	0.034	0.86%	0.039	0.038	-0.51%	0.044	0.045	2.43%	0.048	0.048	-0.36%
C10	<b>0.028</b>	0.027	0.027	-0.69%	0.019	0.020	5.02%	0.022	0.022	0.12%	0.025	0.026	3.18%	0.027	0.028	0.52%
C15	<b>0.019</b>	0.018	0.018	-0.29%	0.013	0.014	10.12%	0.015	0.015	0.27%	0.016	0.017	3.27%	0.018	0.018	1.37%
D5	<b>0.050</b>	0.049	0.048	-1.50%	0.034	0.035	1.96%	0.039	0.039	-1.28%	0.045	0.045	1.26%	0.049	0.049	-0.86%
D10	<b>0.028</b>	0.027	0.027	-1.27%	0.019	0.020	5.93%	0.022	0.022	-0.56%	0.025	0.025	1.79%	0.027	0.027	0.53%
D15	<b>0.018</b>	0.018	0.018	-0.77%	0.013	0.014	9.75%	0.015	0.014	-0.38%	0.016	0.017	2.09%	0.018	0.018	1.67%
M10	<b>1.126</b>	1.140	1.120	-1.75%	0.965	0.921	-4.56%	1.038	1.022	-1.54%	1.080	1.093	1.17%	1.126	1.104	-1.96%
M20	<b>0.419</b>	0.429	0.401	-6.58%	0.296	0.288	-2.63%	0.351	0.327	-6.83%	0.384	0.372	-3.02%	0.425	0.395	-6.98%
M30	<b>0.150</b>	0.150	0.143	-4.61%	0.104	0.101	-2.85%	0.117	0.113	-3.86%	0.135	0.131	-2.83%	0.149	0.140	-6.31%

*Table C.10 - Time shift (in the range -24 to 0 hours) according to the conventional EN ISO 13786, the FFT and the SS approaches, with absolute differences between SS and FFT values for the different orientations in the case of Rome. All values in [h]*

	EN 13786	NORTH			EAST			WEST			SOUTH			HORIZONTAL		
		FFT	SS	$\Delta$	FFT	SS	$\Delta$	FFT	SS	$\Delta$	FFT	SS	$\Delta$	FFT	SS	$\Delta$
A5	<b>-9.1</b>	-6.0	-7.0	-1.0	-11.0	-11.0	-	-7.0	-7.0	-	-9.0	-9.0	-	-9.0	-9.0	-
A10	<b>-9.9</b>	-6.0	-7.0	-1.0	-12.0	-12.0	-	-8.0	-9.0	-1.0	-10.0	-10.0	-	-9.0	-9.0	-
A15	<b>-10.9</b>	-8.0	-7.0	1.0	-13.0	-15.0	-2.0	-9.0	-9.0	-	-11.0	-12.0	-1.0	-10.0	-12.0	-2.0
B5	<b>-8.1</b>	-5.0	-5.0	-	-9.0	-10.0	-1.0	-6.0	-7.0	-1.0	-8.0	-8.0	-	-8.0	-8.0	-
B10	<b>-8.9</b>	-5.0	-6.0	-1.0	-10.0	-11.0	-1.0	-7.0	-8.0	-1.0	-9.0	-9.0	-	-8.0	-9.0	-1.0
B15	<b>-9.9</b>	-6.0	-7.0	-1.0	-12.0	-12.0	-	-8.0	-9.0	-1.0	-10.0	-10.0	-	-9.0	-10.0	-1.0
C5	<b>-12.9</b>	-10.0	-9.0	1.0	-15.0	-15.0	-	-12.0	-12.0	-	-13.0	-13.0	-	-13.0	-12.0	1.0
C10	<b>-13.9</b>	-11.0	-10.0	1.0	-16.0	-16.0	-	-13.0	-13.0	-	-14.0	-14.0	-	-14.0	-13.0	1.0
C15	<b>-14.9</b>	-12.0	-11.0	1.0	-17.0	-17.0	-	-14.0	-14.0	-	-16.0	-15.0	1.0	-15.0	-15.0	-
D5	<b>-13.3</b>	-10.0	-10.0	-	-15.0	-15.0	-	-12.0	-12.0	-	-14.0	-14.0	-	-13.0	-13.0	-
D10	<b>-14.3</b>	-11.0	-11.0	-	-17.0	-16.0	1.0	-13.0	-13.0	-	-15.0	-15.0	-	-14.0	-14.0	-
D15	<b>-15.3</b>	-12.0	-12.0	-	-18.0	-17.0	1.0	-14.0	-14.0	-	-16.0	-16.0	-	-15.0	-15.0	-
M10	<b>-2.8</b>	-1.0	-1.0	-	-2.0	-2.0	-	-2.0	-2.0	-	-2.0	-3.0	-1.0	-3.0	-3.0	-
M20	<b>-6.8</b>	-4.0	-3.0	1.0	-6.0	-7.0	-1.0	-5.0	-5.0	-	-6.0	-6.0	-	-6.0	-6.0	-
M30	<b>-10.7</b>	-7.0	-7.0	-	-12.0	-14.0	-2.0	-9.0	-9.0	-	-11.0	-12.0	-1.0	-10.0	-12.0	-2.0

*Table C.11 - Periodic thermal transmittance according to the conventional EN ISO 13786, the FFT and the FDM approaches, with percentage differences between FDM and FFT values for the different orientations in the case of Rome. All values in  $[W m^{-2} K^{-1}]$*

	EN 13786	NORTH			EAST			WEST			SOUTH			HORIZONTAL		
		FFT	FDM	$\Delta\%$	FFT	FDM	$\Delta\%$	FFT	FDM	$\Delta\%$	FFT	FDM	$\Delta\%$	FFT	FDM	$\Delta\%$
A5	<b>0.084</b>	0.085	0.082	-3.55%	0.060	0.058	-3.54%	0.066	0.064	-3.26%	0.076	0.076	-0.55%	0.085	0.081	-4.87%
A10	<b>0.045</b>	0.045	0.044	-3.66%	0.032	0.031	-3.27%	0.035	0.034	-3.49%	0.041	0.041	-0.22%	0.045	0.043	-5.25%
A15	<b>0.030</b>	0.030	0.028	-4.21%	0.021	0.020	-3.69%	0.023	0.022	-3.78%	0.027	0.026	-1.06%	0.030	0.028	-5.98%
B5	<b>0.129</b>	0.131	0.126	-3.81%	0.091	0.088	-2.53%	0.104	0.100	-3.91%	0.118	0.117	-0.41%	0.130	0.125	-4.53%
B10	<b>0.074</b>	0.075	0.072	-3.86%	0.052	0.050	-3.83%	0.059	0.057	-4.07%	0.067	0.067	-0.82%	0.075	0.071	-5.18%
B15	<b>0.050</b>	0.050	0.048	-4.45%	0.035	0.033	-4.68%	0.039	0.038	-4.55%	0.045	0.044	-1.07%	0.050	0.047	-5.93%
C5	<b>0.049</b>	0.049	0.046	-5.03%	0.034	0.032	-5.61%	0.039	0.037	-5.18%	0.044	0.043	-2.37%	0.048	0.045	-6.34%
C10	<b>0.028</b>	0.027	0.026	-5.35%	0.019	0.018	-5.94%	0.022	0.021	-5.61%	0.025	0.024	-2.88%	0.027	0.025	-6.86%
C15	<b>0.019</b>	0.018	0.017	-5.95%	0.013	0.012	-6.27%	0.015	0.014	-6.30%	0.016	0.016	-3.56%	0.018	0.017	-7.45%
D5	<b>0.050</b>	0.049	0.047	-4.92%	0.034	0.033	-4.68%	0.039	0.037	-4.62%	0.045	0.044	-2.24%	0.049	0.046	-6.52%
D10	<b>0.028</b>	0.027	0.026	-5.15%	0.019	0.018	-5.14%	0.022	0.021	-4.91%	0.025	0.024	-2.53%	0.027	0.026	-6.49%
D15	<b>0.018</b>	0.018	0.017	-5.80%	0.013	0.012	-5.75%	0.015	0.014	-5.43%	0.016	0.016	-2.95%	0.018	0.017	-6.90%
M10	<b>1.126</b>	1.140	1.115	-2.18%	0.965	0.938	-2.78%	1.038	1.013	-2.37%	1.080	1.086	0.52%	1.126	1.094	-2.87%
M20	<b>0.419</b>	0.429	0.414	-3.57%	0.296	0.287	-2.75%	0.351	0.336	-4.07%	0.384	0.382	-0.37%	0.425	0.406	-4.37%
M30	<b>0.150</b>	0.150	0.143	-4.87%	0.104	0.100	-4.03%	0.117	0.112	-4.31%	0.135	0.133	-1.84%	0.149	0.140	-5.92%

*Table C.12 - Time shift (in the range -24 to 0 hours) according to the conventional EN ISO 13786, the FFT and the FDM approaches, with absolute differences between FDM and FFT values for the different orientations in the case of Rome. All values in [h]*

	EN 13786	NORTH			EAST			WEST			SOUTH			HORIZONTAL		
		FFT	FDM	$\Delta$	FFT	FDM	$\Delta$	FFT	FDM	$\Delta$	FFT	FDM	$\Delta$	FFT	FDM	$\Delta$
A5	<b>-9.1</b>	-6.0	-5.0	1.0	-11.0	-11.0	-	-7.0	-7.0	-	-9.0	-9.0	-	-9.0	-9.0	-
A10	<b>-9.9</b>	-6.0	-6.0	-	-12.0	-12.0	-	-8.0	-8.0	-	-10.0	-10.0	-	-9.0	-9.0	-
A15	<b>-10.9</b>	-8.0	-7.0	1.0	-13.0	-13.0	-	-9.0	-9.0	-	-11.0	-11.0	-	-10.0	-10.0	-
B5	<b>-8.1</b>	-5.0	-4.0	1.0	-9.0	-9.0	-	-6.0	-6.0	-	-8.0	-8.0	-	-8.0	-7.0	1.0
B10	<b>-8.9</b>	-5.0	-5.0	-	-10.0	-10.0	-	-7.0	-7.0	-	-9.0	-9.0	-	-8.0	-8.0	-
B15	<b>-9.9</b>	-6.0	-6.0	-	-12.0	-11.0	1.0	-8.0	-8.0	-	-10.0	-10.0	-	-9.0	-9.0	-
C5	<b>-12.9</b>	-10.0	-9.0	1.0	-15.0	-15.0	-	-12.0	-11.0	1.0	-13.0	-13.0	-	-13.0	-12.0	1.0
C10	<b>-13.9</b>	-11.0	-10.0	1.0	-16.0	-16.0	-	-13.0	-12.0	1.0	-14.0	-14.0	-	-14.0	-13.0	1.0
C15	<b>-14.9</b>	-12.0	-11.0	1.0	-17.0	-17.0	-	-14.0	-14.0	-	-16.0	-15.0	1.0	-15.0	-15.0	-
D5	<b>-13.3</b>	-10.0	-10.0	-	-15.0	-15.0	-	-12.0	-12.0	-	-14.0	-14.0	-	-13.0	-13.0	-
D10	<b>-14.3</b>	-11.0	-11.0	-	-17.0	-16.0	1.0	-13.0	-13.0	-	-15.0	-15.0	-	-14.0	-14.0	-
D15	<b>-15.3</b>	-12.0	-12.0	-	-18.0	-17.0	1.0	-14.0	-14.0	-	-16.0	-16.0	-	-15.0	-15.0	-
M10	<b>-2.8</b>	-1.0	-1.0	-	-2.0	-2.0	-	-2.0	-2.0	-	-2.0	-2.0	-	-3.0	-3.0	-
M20	<b>-6.8</b>	-4.0	-3.0	1.0	-6.0	-7.0	-1.0	-5.0	-5.0	-	-6.0	-6.0	-	-6.0	-6.0	-
M30	<b>-10.7</b>	-7.0	-7.0	-	-12.0	-12.0	-	-9.0	-9.0	-	-11.0	-11.0	-	-10.0	-10.0	-

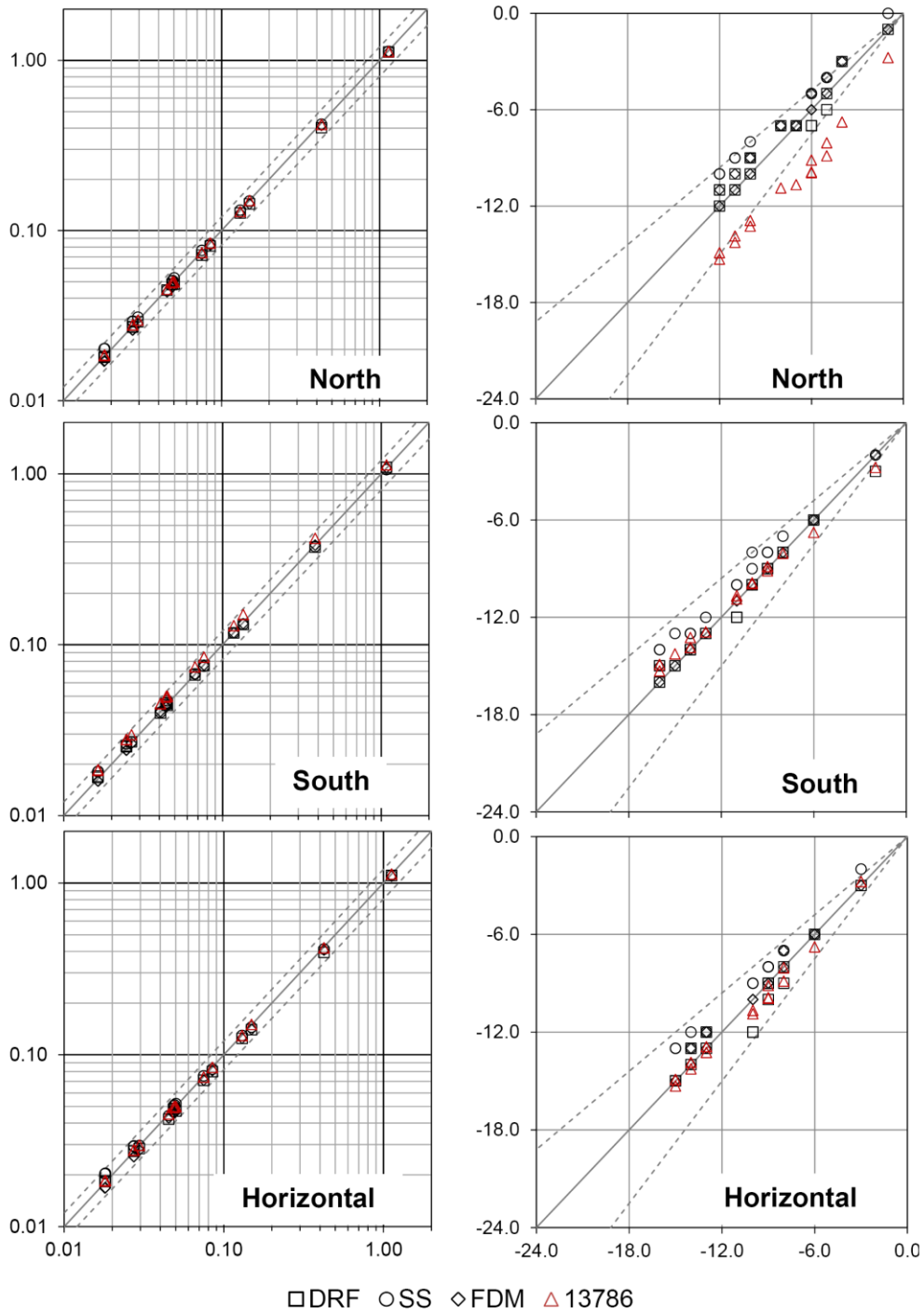


Figure C.3 - Periodic thermal transmittances in  $[W m^{-2} K^{-1}]$  (left) and time shifts in  $[h]$  (right) for the conditions of Rome for the South, North and Horizontal walls respect to the reference FFT parameters. Dotted lines represent the  $\pm 20\%$  range

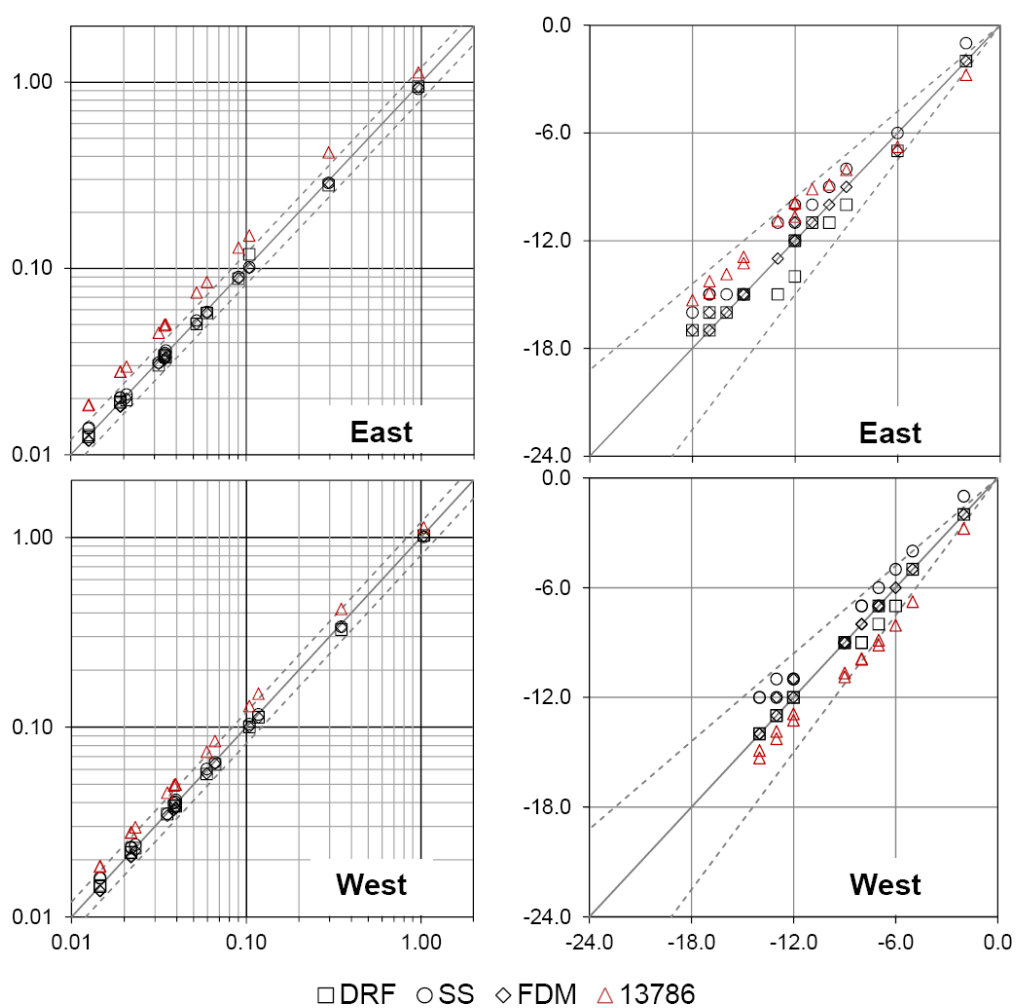


Figure C.4 - Periodic thermal transmittances in  $[W m^{-2} K^{-1}]$  (left) and time shifts in  $[h]$  (right) for the conditions of Rome for the East and West-oriented walls respect to the reference FFT parameters. Dotted lines represent the  $\pm 20\%$  range



**Palermo**

*Table C.13 - Periodic thermal transmittance according to the conventional EN ISO 13786, the FFT and the DRF approaches, with percentage differences between DRF and FFT values for the different orientations in the case of Palermo. All values in  $[W m^{-2} K^{-1}]$*

	EN 13786	NORTH			EAST			WEST			SOUTH			HORIZONTAL		
		FFT	DRF	$\Delta\%$	FFT	DRF	$\Delta\%$	FFT	DRF	$\Delta\%$	FFT	DRF	$\Delta\%$	FFT	DRF	$\Delta\%$
A5	<b>0.084</b>	0.083	0.082	-0.69%	0.058	0.057	-2.30%	0.063	0.062	-1.43%	0.076	0.072	-5.47%	0.087	0.086	-1.01%
A10	<b>0.045</b>	0.044	0.044	0.68%	0.031	0.031	-1.33%	0.034	0.034	0.01%	0.041	0.039	-4.41%	0.046	0.046	0.39%
A15	<b>0.030</b>	0.029	0.030	3.67%	0.021	0.021	0.65%	0.022	0.023	1.95%	0.027	0.026	-2.03%	0.030	0.031	3.34%
B5	<b>0.129</b>	0.130	0.131	0.43%	0.090	0.089	-1.51%	0.099	0.099	-0.36%	0.116	0.111	-4.28%	0.134	0.134	0.19%
B10	<b>0.074</b>	0.074	0.075	2.41%	0.051	0.051	0.22%	0.056	0.057	1.46%	0.067	0.065	-2.86%	0.077	0.078	1.63%
B15	<b>0.050</b>	0.049	0.052	6.12%	0.034	0.036	3.71%	0.037	0.039	4.69%	0.045	0.045	0.15%	0.051	0.054	5.03%
C5	<b>0.049</b>	0.047	0.047	0.43%	0.034	0.033	-1.92%	0.037	0.037	-0.46%	0.044	0.042	-4.79%	0.050	0.050	0.12%
C10	<b>0.028</b>	0.026	0.027	2.05%	0.019	0.019	0.10%	0.021	0.021	1.28%	0.025	0.024	-3.00%	0.028	0.029	2.17%
C15	<b>0.019</b>	0.018	0.019	5.52%	0.013	0.013	3.08%	0.014	0.014	4.89%	0.016	0.016	0.39%	0.019	0.019	5.19%
D5	<b>0.050</b>	0.047	0.048	0.60%	0.034	0.034	-1.49%	0.037	0.037	-0.17%	0.044	0.042	-4.69%	0.050	0.050	0.42%
D10	<b>0.028</b>	0.026	0.027	2.74%	0.019	0.019	0.99%	0.021	0.021	1.51%	0.025	0.024	-2.80%	0.028	0.028	2.48%
D15	<b>0.018</b>	0.017	0.018	5.95%	0.012	0.013	4.67%	0.014	0.014	4.45%	0.016	0.016	0.74%	0.018	0.019	6.19%
M10	<b>1.126</b>	1.137	1.144	0.58%	0.960	0.920	-4.15%	1.023	0.986	-3.63%	1.076	1.005	-6.61%	1.138	1.127	-0.96%
M20	<b>0.419</b>	0.430	0.420	-2.25%	0.301	0.289	-3.96%	0.336	0.324	-3.68%	0.382	0.356	-6.85%	0.435	0.427	-1.90%
M30	<b>0.150</b>	0.145	0.144	-1.24%	0.104	0.100	-3.15%	0.112	0.110	-1.55%	0.134	0.126	-6.11%	0.153	0.150	-1.44%

*Table C.14 - Time shift (in the range -24 to 0 hours) according to the conventional EN ISO 13786, the FFT and the DRF approaches, with absolute differences between DRF and FFT values for the different orientations in the case of Palermo. All values in [h]*

	EN 13786	NORTH			EAST			WEST			SOUTH			HORIZONTAL		
		FFT	DRF	$\Delta$	FFT	DRF	$\Delta$	FFT	DRF	$\Delta$	FFT	DRF	$\Delta$	FFT	DRF	$\Delta$
A5	<b>-9.1</b>	-6.0	-5.0	1.0	-11.0	-10.0	1.0	-7.0	-6.0	1.0	-9.0	-8.0	1.0	-8.0	-7.0	1.0
A10	<b>-9.9</b>	-7.0	-6.0	1.0	-12.0	-11.0	1.0	-8.0	-7.0	1.0	-9.0	-8.0	1.0	-9.0	-8.0	1.0
A15	<b>-10.9</b>	-8.0	-6.0	2.0	-13.0	-11.0	2.0	-9.0	-8.0	1.0	-10.0	-9.0	1.0	-10.0	-9.0	1.0
B5	<b>-8.1</b>	-5.0	-4.0	1.0	-8.0	-8.0	-	-6.0	-5.0	1.0	-7.0	-7.0	-	-7.0	-6.0	1.0
B10	<b>-8.9</b>	-6.0	-5.0	1.0	-10.0	-8.0	2.0	-7.0	-6.0	1.0	-8.0	-7.0	1.0	-8.0	-7.0	1.0
B15	<b>-9.9</b>	-7.0	-5.0	2.0	-11.0	-9.0	2.0	-8.0	-6.0	2.0	-9.0	-8.0	1.0	-9.0	-7.0	2.0
C5	<b>-12.9</b>	-10.0	-9.0	1.0	-15.0	-14.0	1.0	-11.0	-10.0	1.0	-13.0	-12.0	1.0	-12.0	-11.0	1.0
C10	<b>-13.9</b>	-11.0	-10.0	1.0	-16.0	-15.0	1.0	-12.0	-11.0	1.0	-14.0	-13.0	1.0	-13.0	-12.0	1.0
C15	<b>-14.9</b>	-12.0	-10.0	2.0	-17.0	-15.0	2.0	-13.0	-12.0	1.0	-15.0	-13.0	2.0	-14.0	-13.0	1.0
D5	<b>-13.3</b>	-10.0	-9.0	1.0	-15.0	-14.0	1.0	-12.0	-11.0	1.0	-13.0	-12.0	1.0	-13.0	-12.0	1.0
D10	<b>-14.3</b>	-11.0	-10.0	1.0	-16.0	-15.0	1.0	-13.0	-12.0	1.0	-14.0	-13.0	1.0	-14.0	-13.0	1.0
D15	<b>-15.3</b>	-12.0	-11.0	1.0	-18.0	-16.0	2.0	-14.0	-12.0	2.0	-16.0	-14.0	2.0	-15.0	-13.0	2.0
M10	<b>-2.8</b>	-2.0	-1.0	1.0	-3.0	-2.0	1.0	-2.0	-1.0	1.0	-2.0	-1.0	1.0	-2.0	-2.0	-
M20	<b>-6.8</b>	-4.0	-3.0	1.0	-6.0	-6.0	-	-5.0	-4.0	1.0	-6.0	-5.0	1.0	-6.0	-5.0	1.0
M30	<b>-10.7</b>	-8.0	-7.0	1.0	-12.0	-12.0	-	-9.0	-8.0	1.0	-10.0	-10.0	-	-10.0	-9.0	1.0

*Table C.15 - Periodic thermal transmittance according to the conventional EN ISO 13786, the FFT and the SS approaches, with percentage differences between SS and FFT values for the different orientations in the case of Palermo. All values in  $[W m^{-2} K^{-1}]$*

	EN 13786	NORTH			EAST			WEST			SOUTH			HORIZONTAL		
		FFT	SS	$\Delta\%$	FFT	SS	$\Delta\%$	FFT	SS	$\Delta\%$	FFT	SS	$\Delta\%$	FFT	SS	$\Delta\%$
A5	<b>0.084</b>	0.083	0.080	-4.13%	0.058	0.057	-2.92%	0.063	0.061	-3.53%	0.076	0.073	-3.29%	0.087	0.085	-2.48%
A10	<b>0.045</b>	0.044	0.042	-4.42%	0.031	0.030	-3.90%	0.034	0.032	-3.90%	0.041	0.039	-3.73%	0.046	0.044	-3.82%
A15	<b>0.030</b>	0.029	0.028	-2.84%	0.021	0.020	-4.68%	0.022	0.021	-4.68%	0.027	0.025	-5.63%	0.030	0.029	-4.59%
B5	<b>0.129</b>	0.130	0.124	-4.79%	0.090	0.087	-3.60%	0.099	0.095	-4.06%	0.116	0.113	-2.92%	0.134	0.129	-3.62%
B10	<b>0.074</b>	0.074	0.070	-4.68%	0.051	0.049	-3.53%	0.056	0.053	-5.35%	0.067	0.064	-4.08%	0.077	0.074	-3.31%
B15	<b>0.050</b>	0.049	0.046	-5.63%	0.034	0.032	-6.55%	0.037	0.036	-5.14%	0.045	0.043	-4.88%	0.051	0.049	-4.61%
C5	<b>0.049</b>	0.047	0.045	-4.69%	0.034	0.032	-4.63%	0.037	0.035	-4.33%	0.044	0.041	-6.09%	0.050	0.048	-4.14%
C10	<b>0.028</b>	0.026	0.025	-6.07%	0.019	0.018	-5.35%	0.021	0.020	-4.84%	0.025	0.023	-5.16%	0.028	0.027	-4.62%
C15	<b>0.019</b>	0.018	0.016	-11.0%	0.013	0.012	-6.11%	0.014	0.013	-5.14%	0.016	0.015	-6.09%	0.019	0.018	-4.90%
D5	<b>0.050</b>	0.047	0.045	-5.69%	0.034	0.032	-5.08%	0.037	0.035	-4.69%	0.044	0.042	-6.28%	0.050	0.048	-4.32%
D10	<b>0.028</b>	0.026	0.025	-7.21%	0.019	0.018	-5.70%	0.021	0.020	-5.23%	0.025	0.023	-5.71%	0.028	0.026	-4.98%
D15	<b>0.018</b>	0.017	0.015	-13.0%	0.012	0.012	-6.87%	0.014	0.013	-6.04%	0.016	0.015	-6.64%	0.018	0.017	-5.34%
M10	<b>1.126</b>	1.137	1.122	-1.33%	0.960	0.938	-2.26%	1.023	1.000	-2.25%	1.076	1.057	-1.84%	1.138	1.133	-0.41%
M20	<b>0.419</b>	0.430	0.400	-7.02%	0.301	0.280	-6.70%	0.336	0.311	-7.33%	0.382	0.358	-6.31%	0.435	0.413	-4.99%
M30	<b>0.150</b>	0.145	0.136	-6.52%	0.104	0.097	-6.11%	0.112	0.105	-5.61%	0.134	0.126	-6.06%	0.153	0.145	-4.71%

*Table C.16 - Time shift (in the range -24 to 0 hours) according to the conventional EN ISO 13786, the FFT and the SS approaches, with absolute differences between SS and FFT values for the different orientations in the case of Palermo. All values in [h]*

	EN 13786	NORTH			EAST			WEST			SOUTH			HORIZONTAL		
		FFT	SS	$\Delta$	FFT	SS	$\Delta$	FFT	SS	$\Delta$	FFT	SS	$\Delta$	FFT	SS	$\Delta$
A5	<b>-9.1</b>	-6.0	-6.0	-	-11.0	-11.0	-	-7.0	-7.0	-	-9.0	-9.0	-	-8.0	-8.0	-
A10	<b>-9.9</b>	-7.0	-7.0	-	-12.0	-12.0	-	-8.0	-8.0	-	-9.0	-10.0	-1.0	-9.0	-9.0	-
A15	<b>-10.9</b>	-8.0	-8.0	-	-13.0	-13.0	-	-9.0	-9.0	-	-10.0	-11.0	-1.0	-10.0	-10.0	-
B5	<b>-8.1</b>	-5.0	-5.0	-	-8.0	-9.0	-1.0	-6.0	-6.0	-	-7.0	-8.0	-1.0	-7.0	-7.0	-
B10	<b>-8.9</b>	-6.0	-6.0	-	-10.0	-10.0	-	-7.0	-7.0	-	-8.0	-9.0	-1.0	-8.0	-8.0	-
B15	<b>-9.9</b>	-7.0	-7.0	-	-11.0	-12.0	-1.0	-8.0	-8.0	-	-9.0	-10.0	-1.0	-9.0	-9.0	-
C5	<b>-12.9</b>	-10.0	-10.0	-	-15.0	-15.0	-	-11.0	-11.0	-	-13.0	-13.0	-	-12.0	-12.0	-
C10	<b>-13.9</b>	-11.0	-11.0	-	-16.0	-16.0	-	-12.0	-12.0	-	-14.0	-14.0	-	-13.0	-13.0	-
C15	<b>-14.9</b>	-12.0	-12.0	-	-17.0	-17.0	-	-13.0	-14.0	-1.0	-15.0	-15.0	-	-14.0	-14.0	-
D5	<b>-13.3</b>	-10.0	-10.0	-	-15.0	-15.0	-	-12.0	-12.0	-	-13.0	-13.0	-	-13.0	-13.0	-
D10	<b>-14.3</b>	-11.0	-12.0	-1.0	-16.0	-17.0	-1.0	-13.0	-13.0	-	-14.0	-15.0	-1.0	-14.0	-14.0	-
D15	<b>-15.3</b>	-12.0	-13.0	-1.0	-18.0	-18.0	-	-14.0	-14.0	-	-16.0	-16.0	-	-15.0	-15.0	-
M10	<b>-2.8</b>	-2.0	-2.0	-	-3.0	-3.0	-	-2.0	-2.0	-	-2.0	-2.0	-	-2.0	-2.0	-
M20	<b>-6.8</b>	-4.0	-4.0	-	-6.0	-7.0	-1.0	-5.0	-5.0	-	-6.0	-6.0	-	-6.0	-6.0	-
M30	<b>-10.7</b>	-8.0	-8.0	-	-12.0	-12.0	-	-9.0	-9.0	-	-10.0	-10.0	-	-10.0	-10.0	-

*Table C.17 - Periodic thermal transmittance according to the conventional EN ISO 13786, the FFT and the FDM approaches, with percentage differences between FDM and FFT values for the different orientations in the case of Palermo. All values in  $[W m^{-2} K^{-1}]$*

	EN 13786	NORTH			EAST			WEST			SOUTH			HORIZONTAL		
		FFT	FDM	$\Delta\%$	FFT	FDM	$\Delta\%$	FFT	FDM	$\Delta\%$	FFT	FDM	$\Delta\%$	FFT	FDM	$\Delta\%$
A5	<b>0.084</b>	0.083	0.080	-4.01%	0.058	0.057	-3.03%	0.063	0.061	-3.53%	0.076	0.073	-3.32%	0.087	0.083	-3.96%
A10	<b>0.045</b>	0.044	0.042	-4.21%	0.031	0.030	-4.31%	0.034	0.032	-3.66%	0.041	0.039	-3.89%	0.046	0.044	-4.10%
A15	<b>0.030</b>	0.029	0.027	-4.82%	0.021	0.020	-5.38%	0.022	0.021	-4.17%	0.027	0.025	-4.65%	0.030	0.029	-4.46%
B5	<b>0.129</b>	0.130	0.124	-4.48%	0.090	0.086	-4.53%	0.099	0.095	-4.23%	0.116	0.112	-3.45%	0.134	0.129	-3.89%
B10	<b>0.074</b>	0.074	0.070	-4.65%	0.051	0.049	-3.74%	0.056	0.054	-4.45%	0.067	0.064	-3.86%	0.077	0.073	-4.64%
B15	<b>0.050</b>	0.049	0.046	-5.25%	0.034	0.033	-4.44%	0.037	0.036	-4.78%	0.045	0.043	-4.60%	0.051	0.049	-5.10%
C5	<b>0.049</b>	0.047	0.044	-5.58%	0.034	0.032	-5.59%	0.037	0.035	-5.22%	0.044	0.041	-5.69%	0.050	0.047	-5.49%
C10	<b>0.028</b>	0.026	0.025	-5.88%	0.019	0.018	-6.37%	0.021	0.020	-5.77%	0.025	0.023	-5.63%	0.028	0.026	-5.92%
C15	<b>0.019</b>	0.018	0.016	-6.55%	0.013	0.012	-6.96%	0.014	0.013	-6.21%	0.016	0.015	-6.09%	0.019	0.017	-6.39%
D5	<b>0.050</b>	0.047	0.045	-5.01%	0.034	0.032	-5.30%	0.037	0.035	-5.04%	0.044	0.042	-5.41%	0.050	0.047	-5.04%
D10	<b>0.028</b>	0.026	0.025	-5.13%	0.019	0.018	-5.37%	0.021	0.020	-5.41%	0.025	0.023	-5.68%	0.028	0.026	-5.51%
D15	<b>0.018</b>	0.017	0.016	-5.50%	0.012	0.012	-6.09%	0.014	0.013	-5.99%	0.016	0.015	-6.18%	0.018	0.017	-5.92%
M10	<b>1.126</b>	1.137	1.112	-2.20%	0.960	0.925	-3.61%	1.023	0.991	-3.16%	1.076	1.052	-2.25%	1.138	1.117	-1.84%
M20	<b>0.419</b>	0.430	0.409	-4.76%	0.301	0.287	-4.47%	0.336	0.320	-4.89%	0.382	0.368	-3.59%	0.435	0.418	-3.83%
M30	<b>0.150</b>	0.145	0.138	-5.32%	0.104	0.098	-5.86%	0.112	0.106	-4.91%	0.134	0.127	-5.28%	0.153	0.145	-5.08%

*Table C.18 - Time shift (in the range -24 to 0 hours) according to the conventional EN ISO 13786, the FFT and the FDM approaches, with absolute differences between FDM and FFT values for the different orientations in the case of Palermo. All values in [h]*

	EN 13786	NORTH			EAST			WEST			SOUTH			HORIZONTAL		
		FFT	FDM	$\Delta$	FFT	FDM	$\Delta$	FFT	FDM	$\Delta$	FFT	FDM	$\Delta$	FFT	FDM	$\Delta$
A5	<b>-9.1</b>	-6.0	-6.0	-	-11.0	-11.0	-	-7.0	-7.0	-	-9.0	-9.0	-	-8.0	-8.0	-
A10	<b>-9.9</b>	-7.0	-7.0	-	-12.0	-12.0	-	-8.0	-8.0	-	-9.0	-9.0	-	-9.0	-9.0	-
A15	<b>-10.9</b>	-8.0	-8.0	-	-13.0	-13.0	-	-9.0	-9.0	-	-10.0	-10.0	-	-10.0	-10.0	-
B5	<b>-8.1</b>	-5.0	-5.0	-	-8.0	-9.0	-1.0	-6.0	-6.0	-	-7.0	-7.0	-	-7.0	-7.0	-
B10	<b>-8.9</b>	-6.0	-6.0	-	-10.0	-10.0	-	-7.0	-7.0	-	-8.0	-8.0	-	-8.0	-8.0	-
B15	<b>-9.9</b>	-7.0	-7.0	-	-11.0	-11.0	-	-8.0	-8.0	-	-9.0	-9.0	-	-9.0	-9.0	-
C5	<b>-12.9</b>	-10.0	-10.0	-	-15.0	-15.0	-	-11.0	-11.0	-	-13.0	-13.0	-	-12.0	-12.0	-
C10	<b>-13.9</b>	-11.0	-11.0	-	-16.0	-16.0	-	-12.0	-12.0	-	-14.0	-14.0	-	-13.0	-13.0	-
C15	<b>-14.9</b>	-12.0	-12.0	-	-17.0	-17.0	-	-13.0	-13.0	-	-15.0	-15.0	-	-14.0	-14.0	-
D5	<b>-13.3</b>	-10.0	-10.0	-	-15.0	-15.0	-	-12.0	-12.0	-	-13.0	-13.0	-	-13.0	-12.0	1.0
D10	<b>-14.3</b>	-11.0	-11.0	-	-16.0	-16.0	-	-13.0	-13.0	-	-14.0	-14.0	-	-14.0	-14.0	-
D15	<b>-15.3</b>	-12.0	-12.0	-	-18.0	-17.0	1.0	-14.0	-14.0	-	-16.0	-15.0	1.0	-15.0	-15.0	-
M10	<b>-2.8</b>	-2.0	-2.0	-	-3.0	-3.0	-	-2.0	-2.0	-	-2.0	-2.0	-	-2.0	-2.0	-
M20	<b>-6.8</b>	-4.0	-4.0	-	-6.0	-7.0	-1.0	-5.0	-5.0	-	-6.0	-6.0	-	-6.0	-6.0	-
M30	<b>-10.7</b>	-8.0	-8.0	-	-12.0	-12.0	-	-9.0	-9.0	-	-10.0	-10.0	-	-10.0	-10.0	-

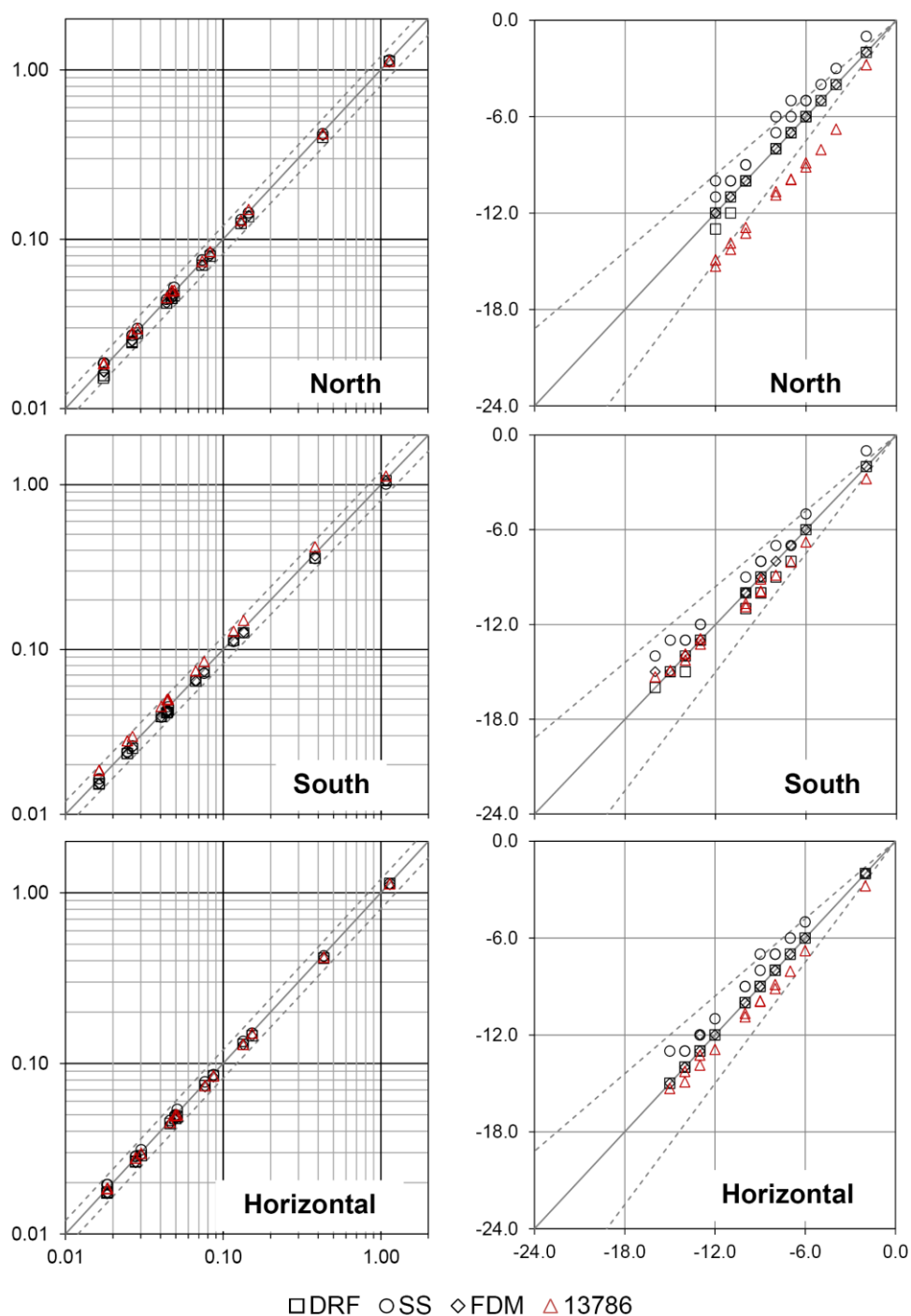


Figure C.5 - Periodic thermal transmittances in  $[W m^{-2} K^{-1}]$  (left) and time shifts in  $[h]$  (right) for the conditions of Palermo for the South, North and Horizontal walls respect to the reference FFT parameters. Dotted lines represent the  $\pm 20\%$  range

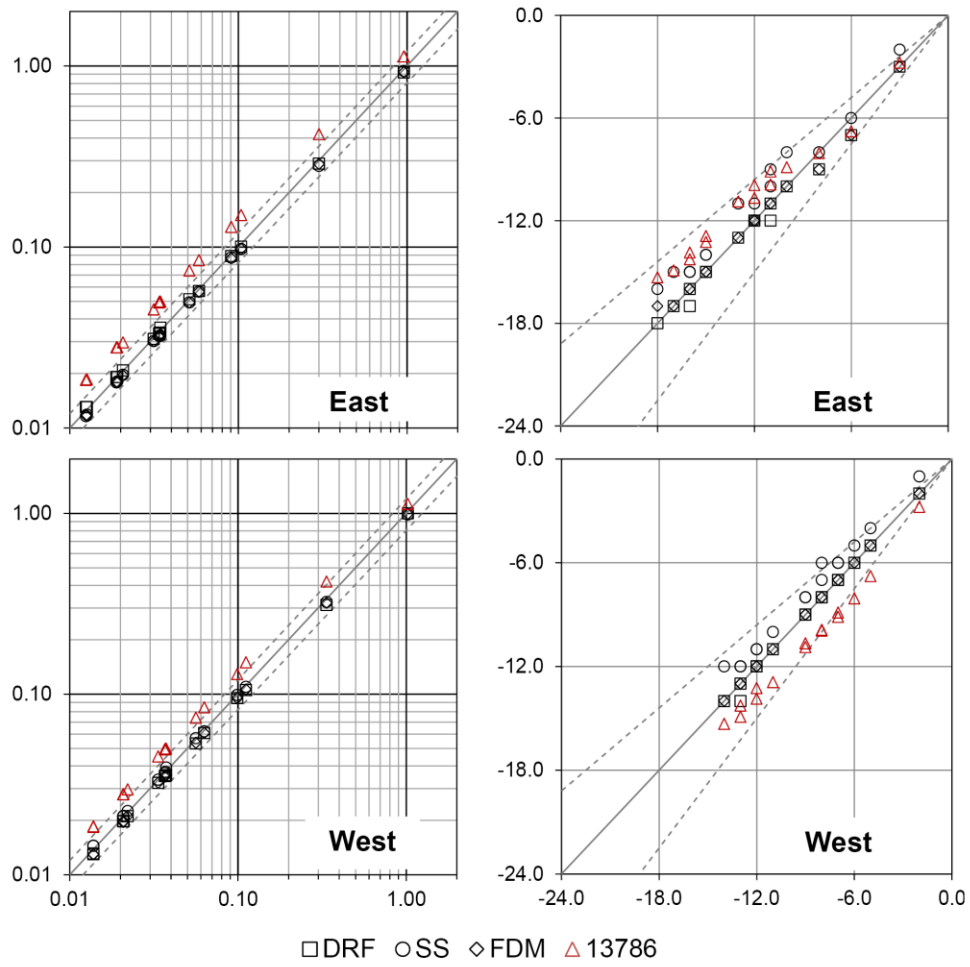


Figure C.6 - Periodic thermal transmittances in  $[W m^{-2} K^{-1}]$  (left) and time shifts in  $[h]$  (right) for the conditions of Palermo for the East and West-oriented walls respect to the reference FFT parameters. Dotted lines represent the  $\pm 20\%$  range

## **Annex D**

In this Annex, the graphs with the comparison between the thermal losses calculated in accordance with the EN ISO 13790:2008 method and the simulated ones are represented.

## 20 °C temperature setpoints

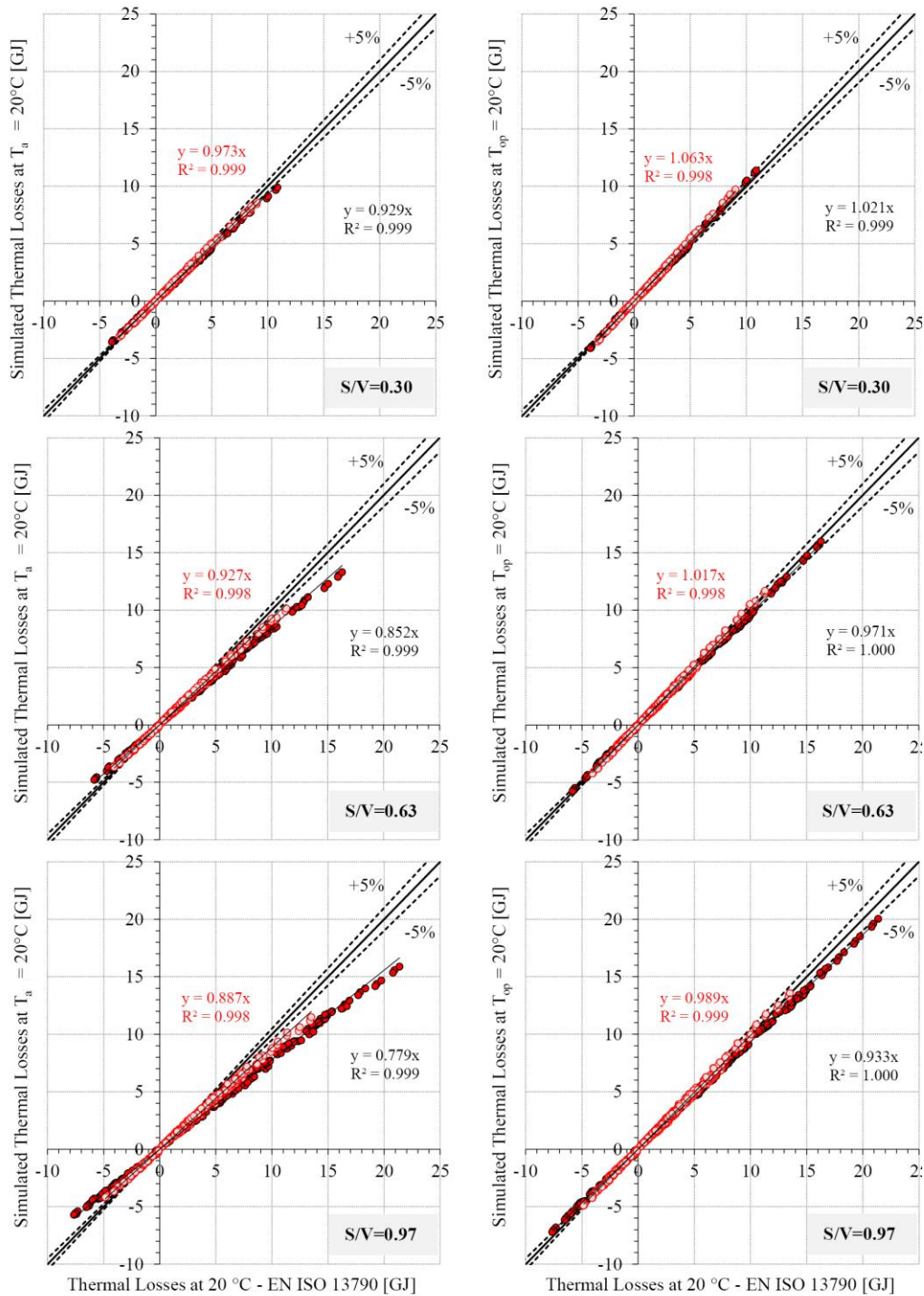


Figure D.1 - Simulated thermal losses with 20 °C air temperature setpoint (on the left) and 20 °C operative setpoint (on the right), without ventilation for the different S/V. Insulated cases in lighter colours

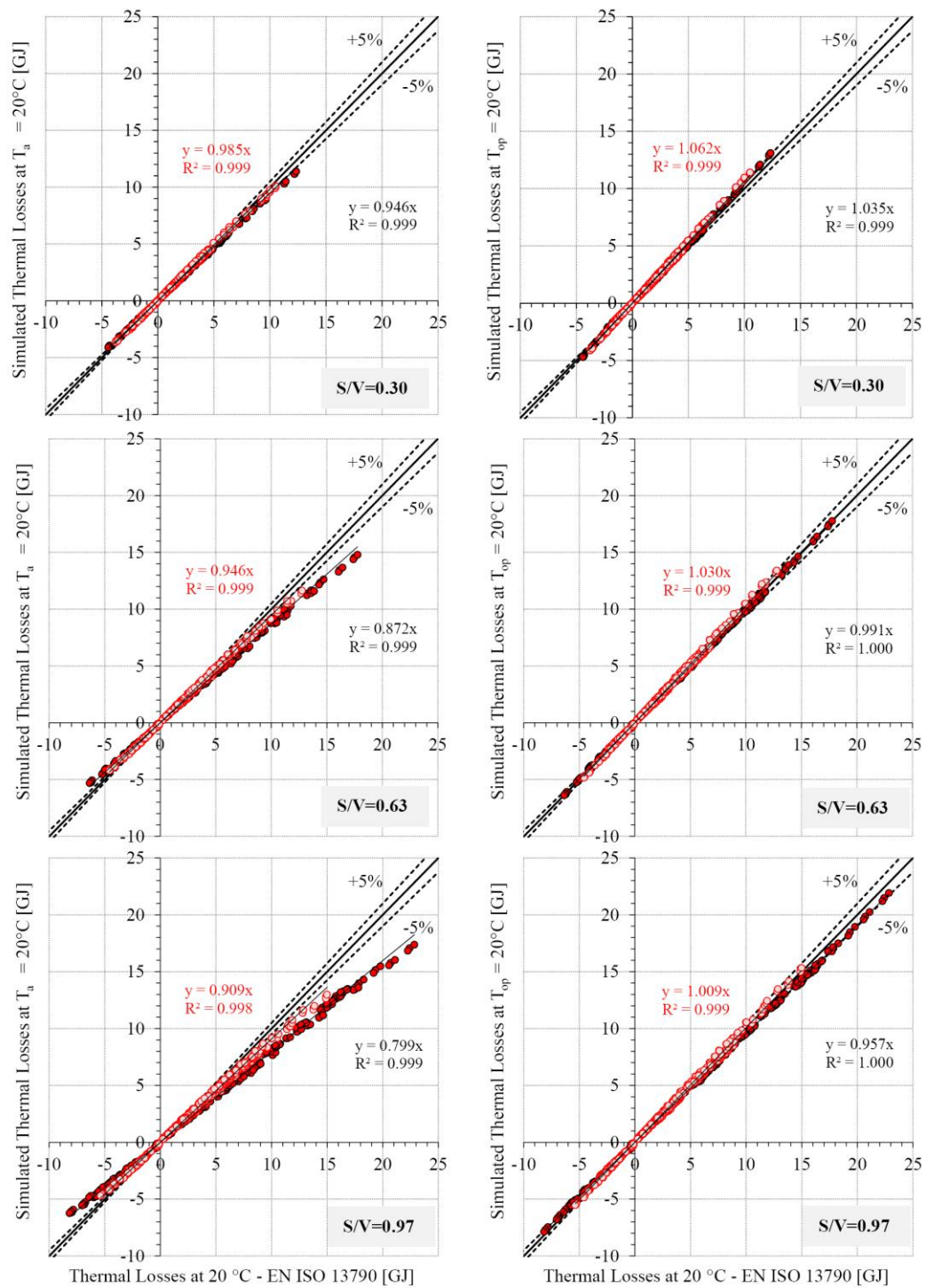


Figure D.2 - Simulated thermal losses with 20 °C air temperature setpoint (on the left) and 20 °C operative setpoint (on the right), with 0.3 ach/h of ventilation rate for the different S/V. Insulated cases in lighter colours



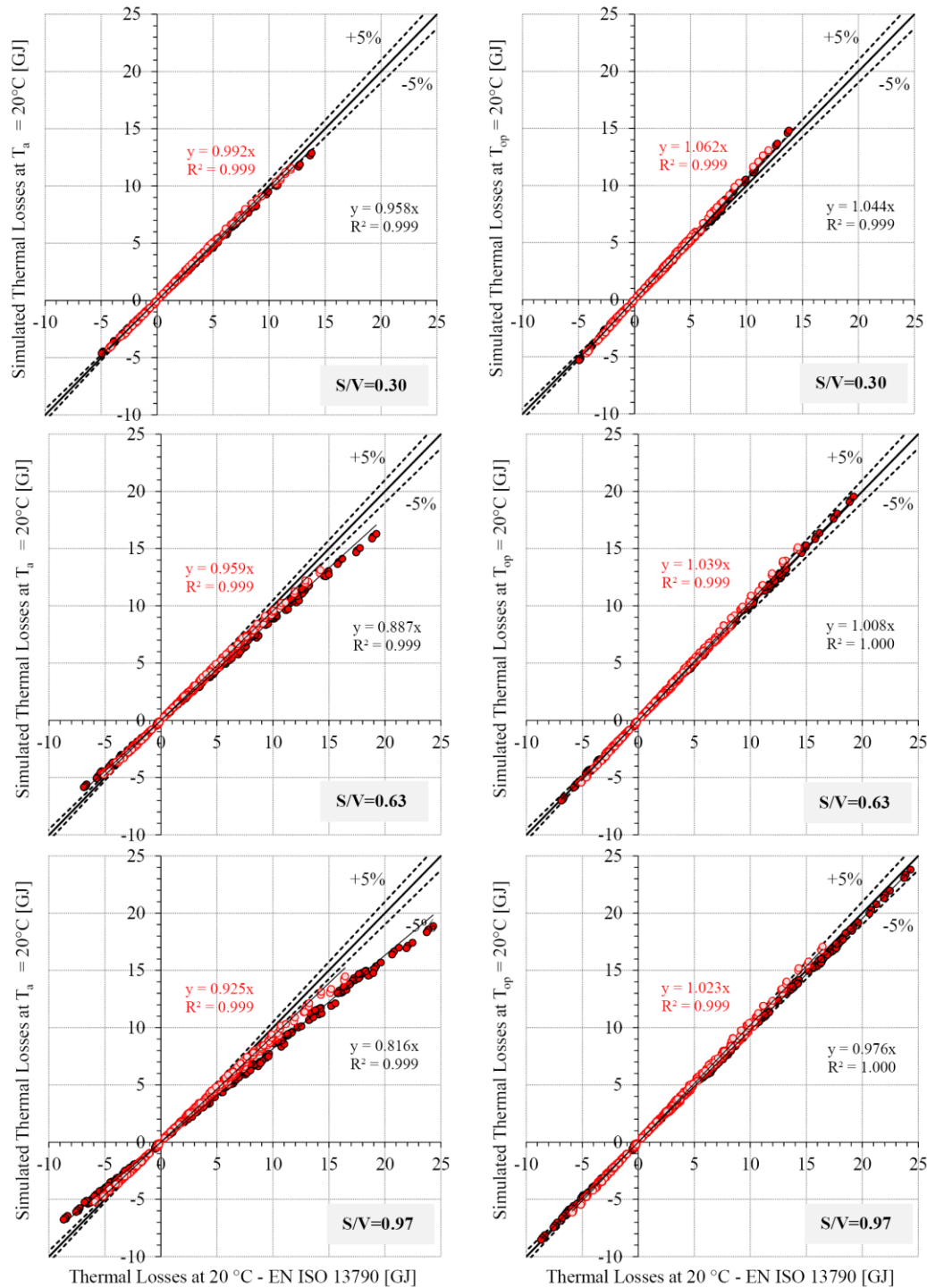


Figure D.3 - Simulated thermal losses with 20 °C air temperature setpoint (on the left) and 20 °C operative setpoint (on the right), with 0.6 ach/h of ventilation rate for the different S/V.  
Insulated cases in lighter colours

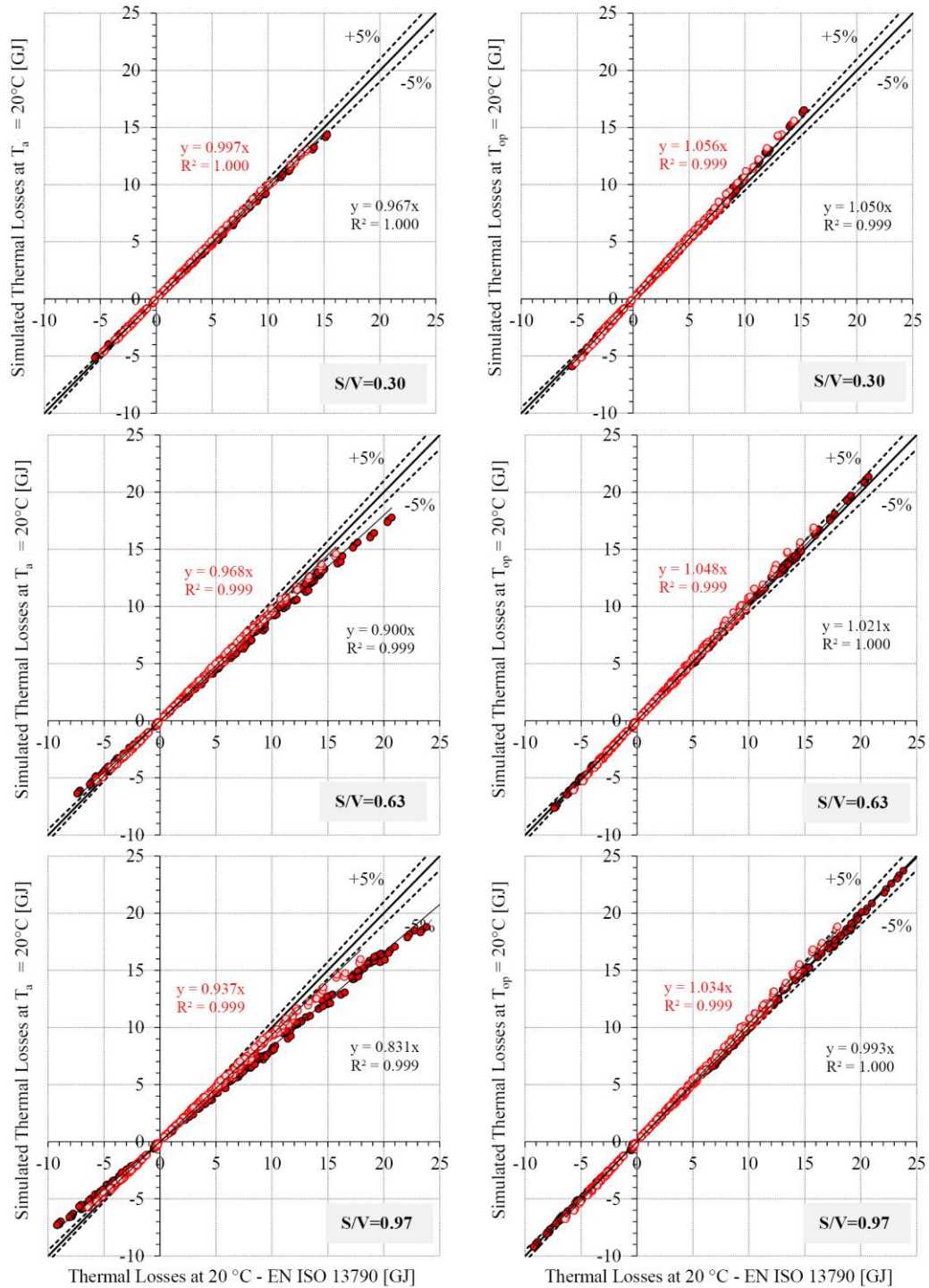


Figure D.4 - Simulated thermal losses with 20 °C air temperature setpoint (on the left) and 20 °C operative setpoint (on the right), with 0.9 ach/h of ventilation rate for the different S/V. Insulated cases in lighter colours

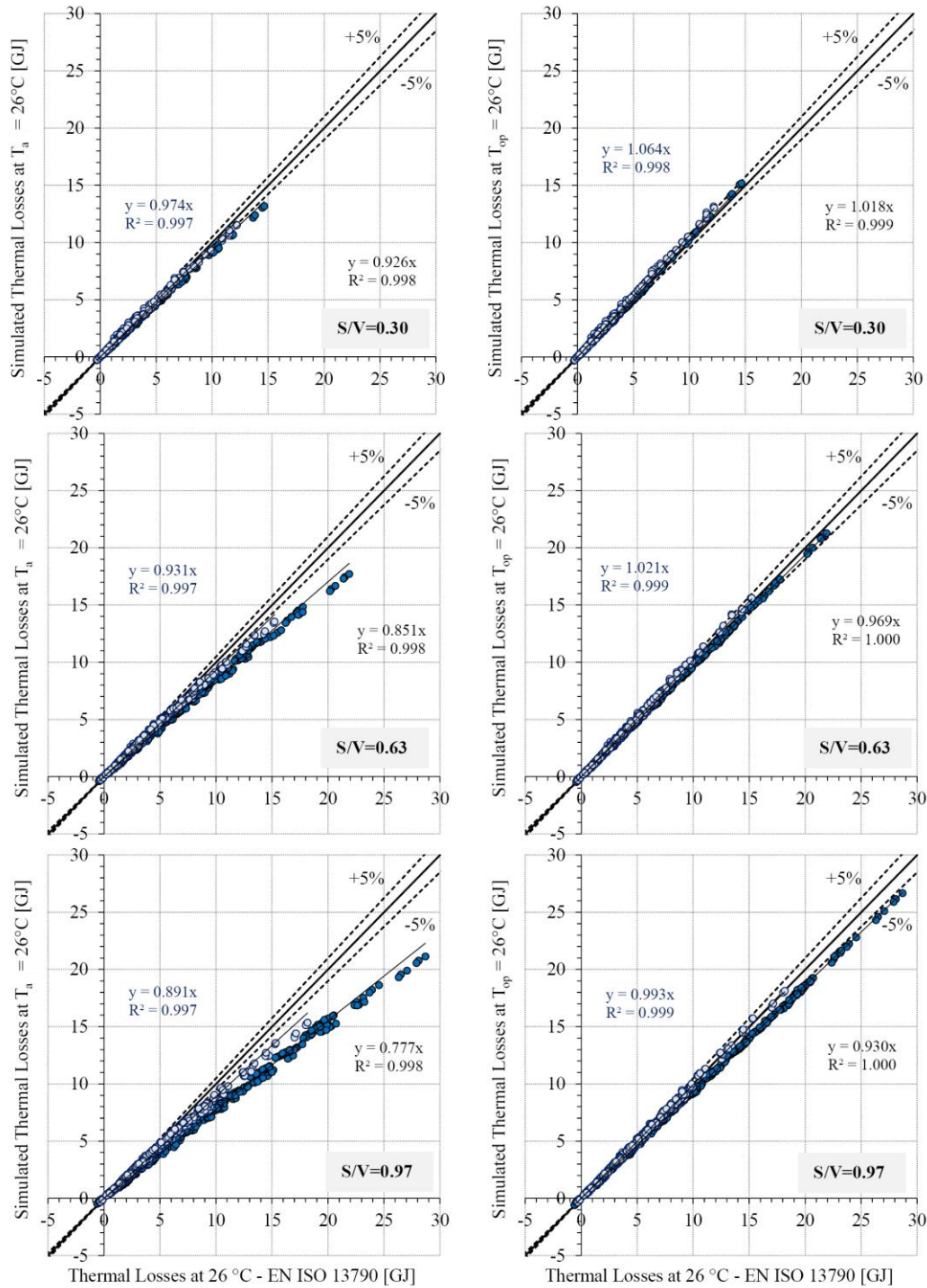
**26 °C temperature setpoints**

Figure D.5 - Simulated thermal losses with 26 °C air temperature setpoint (on the left) and 26 °C operative setpoint (on the right), without ventilation for the different  $S/V$ . Insulated cases in lighter colours

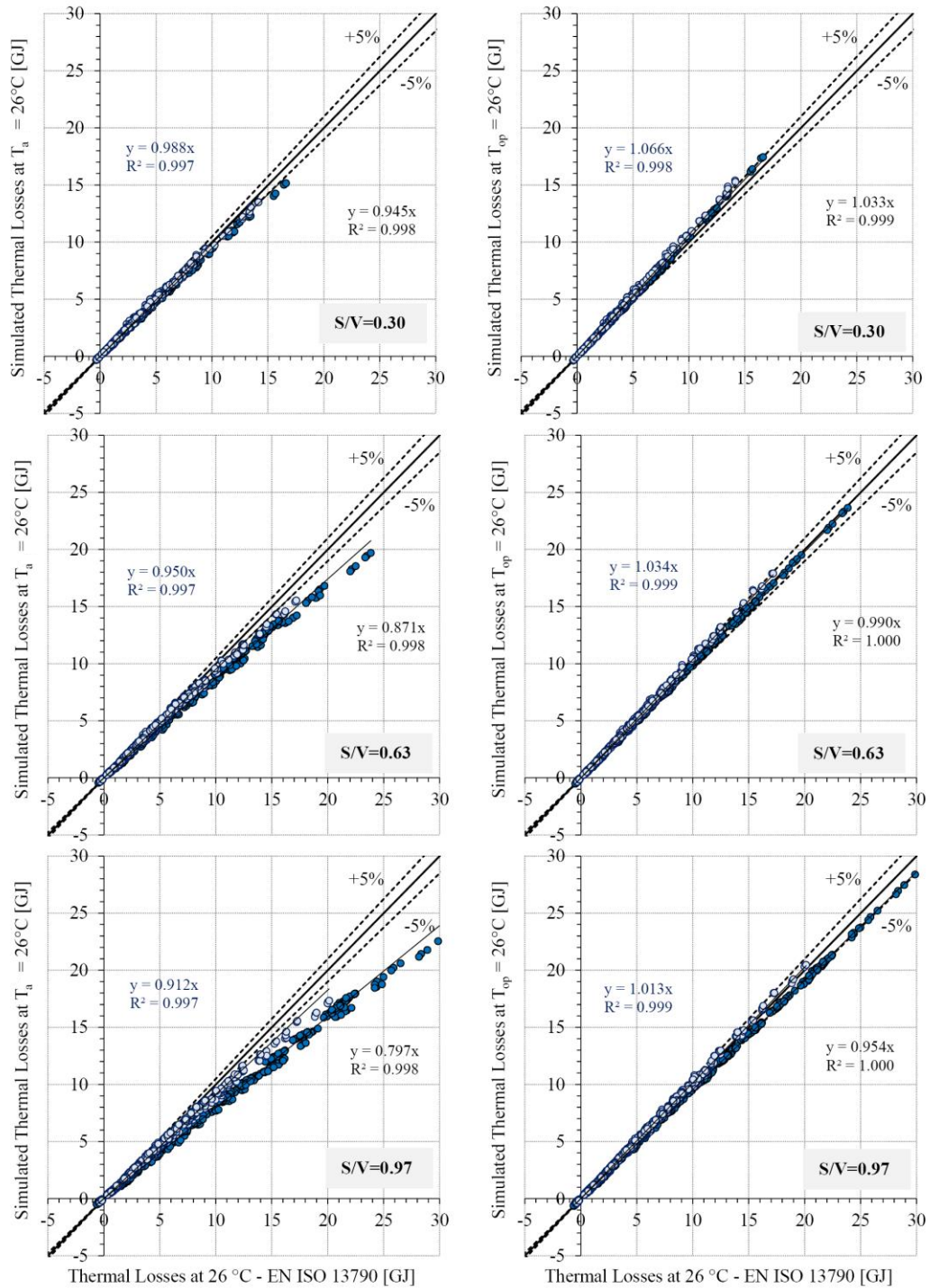


Figure D.6 - Simulated thermal losses with 26 °C air temperature setpoint (on the left) and 26 °C operative setpoint (on the right), with 0.3 ach/h of ventilation rate for the different S/V. Insulated cases in lighter colours



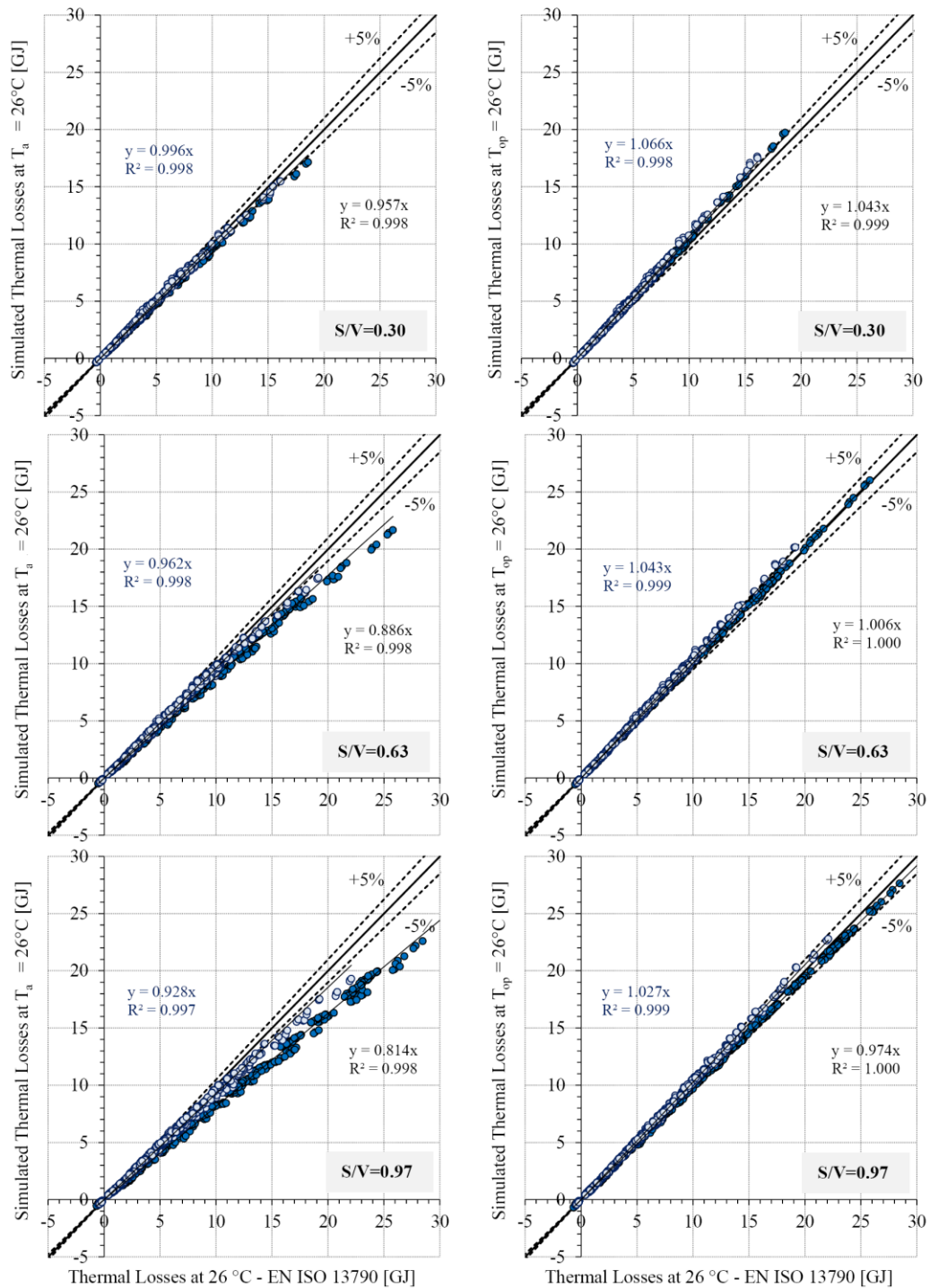


Figure D.7 - Simulated thermal losses with  $26^\circ\text{C}$  air temperature setpoint (on the left) and  $26^\circ\text{C}$  operative setpoint (on the right), with 0.6 ach/h of ventilation rate for the different S/V. Insulated cases in lighter colours

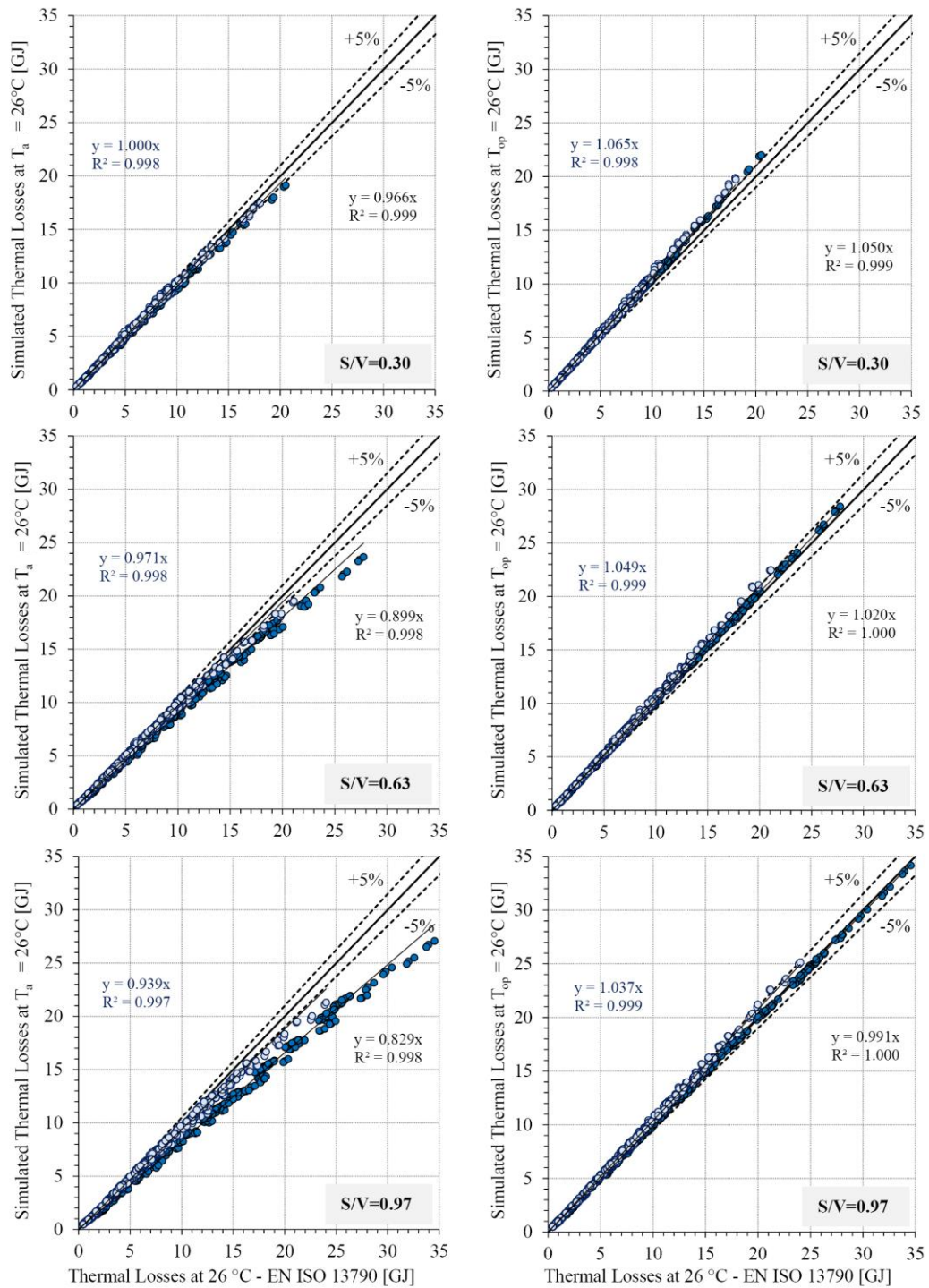


Figure D.8 - Simulated thermal losses with 26 °C air temperature setpoint (on the left) and 26 °C operative setpoint (on the right), with 0.9 ach/h of ventilation rate for the different S/V. Insulated cases in lighter colours